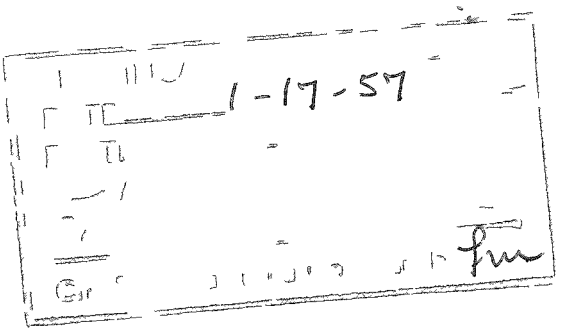

ANL-5511
Reactors - Power

ARGONNE NATIONAL LABORATORY
P. O. Box 299
Lemont, Illinois

REACTOR ENGINEERING DIVISION QUARTERLY REPORT

SECTION II

July, August, September, 1955

Compiled by

Members of the Reactor Engineering Division

Published January, 1956

Previous Reports:

ANL-5471 April 1, 1955 through June 30, 1955
ANL-5461 January 1, 1955 through March 31, 1955
ANL-5371 October 1, 1954 through December 31, 1954

Operated by the University of Chicago
under
Contract W-31-109-eng-38

DISCLAIMER

This report was prepared as an account of work sponsored by an agency of the United States Government. Neither the United States Government nor any agency Thereof, nor any of their employees, makes any warranty, express or implied, or assumes any legal liability or responsibility for the accuracy, completeness, or usefulness of any information, apparatus, product, or process disclosed, or represents that its use would not infringe privately owned rights. Reference herein to any specific commercial product, process, or service by trade name, trademark, manufacturer, or otherwise does not necessarily constitute or imply its endorsement, recommendation, or favoring by the United States Government or any agency thereof. The views and opinions of authors expressed herein do not necessarily state or reflect those of the United States Government or any agency thereof.

DISCLAIMER

Portions of this document may be illegible in electronic image products. Images are produced from the best available original document.

TABLE OF CONTENTS

Page

PART A. ADVANCED WATER REACTOR PROGRAM

SUMMARY 13

I. EXPERIMENTAL BOILING WATER REACTOR (EBWR) 17

A. Reactor 17

1. Core 17

a. Corrosion of EBWR - Type Fuel Plates 17
b. Boiling Water Corrosion of Zircaloy 2 17

2. Control Rods and Drive Mechanisms 18

a. Design and Prototype Testing 18
b. Zircaloy 2 - Stainless Steel Contact Corrosion . . . 25

3. Pressure Vessel 25

a. Vessel 25
b. Thermal Shield 27
c. Support and Containment Structure 31

4. Biological Shielding 39

a. Calculations for D_2O Operation 39
b. Physical Arrangement 45

5. High-Pressure Emergency Boron Injection System . . . 46

6. Reactor Water Purification System 48

7. Feed Water Make-up System 51

8. Retention Tanks 51

B. Steam Plant 52

1. Carry-over of Radioactive Material in Steam 52

2. Air Drying and Fluid Recovery System 52

UNCLASSIFIED

TABLE OF CONTENTS

Page

C. Instrumentation, Control and Electrical Power System. . . 59

1. Nuclear Instrumentation Facilities 59

2. Electrical Power System 59

D. Building 63

1. General 63

2. Emergency Air-Lock Doors 65

II. SUPPORTING AND ALTERNATE DESIGN RESEARCH AND DEVELOPMENT 67

A. Alternate Methods of Operation of EBWR 67

1. Forced Circulation - H_2O 67

2. Heavy Water Design 68

B. Boiling Heat Transfer Studies 70

1. Multi-channel Natural Circulation Boiling Density at 600 psig 70

2. Single Channel Unrestricted Circulation Boiling Studies 74

3. Single Channel Forced and Natural Circulation Boiling Density at 150 and 250 psig 82

C. Fuel Elements 88

1. Corrosion Tests on Fuel and Cladding Materials 88

a. Zircaloy 2-Clad, Uranium - 5% Zirconium Plates . 88
b. Aluminum Clad Natural Uranium Plates 91
c. Fuel Plate End Closures 91
d. Aluminum Alloys 91
e. Urania-Thoria Bodies 100

2. Detection and Location of Fuel Element Ruptures . . . 106

TABLE OF CONTENTS

Page

D. Control and Thermal Shield Materials 107

1. Alternate Control Rods for EBWR 107

2. Boron-Stainless Steel Development 108

a. Fabrication 108
b. Corrosion 111

3 Corrosion of Aluminum-Boron-Nickel Alloy 111

4. Soluble Poisons 111

E. Control Rod Drive Mechanism 117

1. Hydraulically Operated Drive Mechanism 117

2. Magnetic Jack Drive Mechanism 118

PART B. FAST POWER BREEDER REACTOR PROGRAM

SUMMARY 119

I. EXPERIMENTAL BREEDER REACTOR-I (EBR-I) 121

A. Conversion Ratio Measurements 121

B. Activation Cross Sections in the Outer Blanket 127

II. EXPERIMENTAL BREEDER REACTOR-II (EBR-II) 132

A. Decay Heat Cooling Requirements of Spent EBR-II Fuel Subassemblies 132

B. Water Pressure Drop Tests of EBR-II Core Subassembly 133

C. Irradiation of EBR-II Pin-Type Fuel Elements 141

III. EBR-II WORKING MODEL 145

System Performance Tests 145

1. Control Rod and the Cover Raising and Rotating Mechanism 145

DECLASSIFIED

TABLE OF CONTENTS

Page

2. Fuel Unloading System 146

3. d-c Electromagnetic Pump 146

4. Sodium Purification 148

IV. SUPPORTING AND ALTERNATE DESIGN RESEARCH AND DEVELOPMENT 151

A. Thermal Cycling of Molybdenum-Uranium and Zirconium-Uranium Alloys 151

B. Induction Heating of a Four-Inch IPS Sodium Test Loop . . 154

C. Inspection of 1472F Sodium Loop Welds 156

PART C. REACTOR TECHNOLOGY - RESEARCH AND DEVELOPMENT

I. REACTOR SAFETY AND KINETICS 160

A. ZPR-III 160

B. Machine Solution of Kinetics Equation 160

1. Solution of the Kinetics Equations, given k_{ex} 161

2. Solution of the Kinetics Equations, given n 163

C. Analytical Solutions of Kinetics Equations 166

1. Solution for n, given k_{ex} 166

2. Solution for k_{ex}, given n 168

D. Kinetic Studies 171

E. Thermal Inertia 174

1. Temperature Distribution in Two-Region Cylindrical Geometry with Experimentally Rising Heat Source in Control Region 174

DECLASSIFIED

TABLE OF CONTENTS

Page

2. Time Variation of Stored Heat in Sodium-Cooled Uranium Rod During Transient 176

II. FUEL AND STRUCTURAL MATERIAL 180

A. Export-Type Fuel Plates 180

B. Borax III Fuel Plates 180

C. Examinations of Heat Exchanges from ANL Water Loop at MTR. 180

III. INSTRUMENTATION 184

Neutron-Sensitive Electron Photomultiplier Tubes 184

DECLASSIFIED

LIST OF FIGURES

No.	Title	Page
1	Boiling Water Corrosion of Zircaloy 2-Clad Type 430 Thimble Tested for 129 hr in 500F Degassed Distilled Water	19
2	EBWR Control Rod	20
3	EBWR Control Rod Drive Mechanism	21
4	Control Rod Scram Time	24
5	Test Facility for EBWR Control Rod and Drive Mechanism	26
6	EBWR Pressure Vessel	28
7	EBWR Pressure Vessel Containment Structure	32
8	Blast Shield Assembly	37
9	Calculated Fast Neutron Flux in the EBWR Shield	40
10	Calculated Radial Thermal Neutron Flux in the EBWR Shield	41
11	Calculated Axial Thermal Neutron Flux Above the EBWR Core	42
12	Calculated Axial Thermal Neutron Flux Below the EBWR Core	43
13	Air-Drying and Fluid Recovery System	53
14	Estimated Recovery System Flows (Air and Vapor)	55
15	Emergency Condenser Water Box Drain	57
16	Schematic Plan View of EBWR Power Plant and Control Areas	60
17	Simplified Line Diagram of EBWR Electrical System	62
18	Connected H.P. and 1-hr kw Loads - EBWR Facility	64
19	Schematic of Emergency Air-Lock Doors for EBWR	66

DECLASSIFIED

LIST OF FIGURES

No.	Title	Page
20	Isometric Plot of $(C_s/C_\ell)_{avg} = \phi \frac{L_B}{L}, \frac{W_T h_{fg}}{Q_T}$ for Multichannel Section at 600 psi.	71
21	$(C_s/C_\ell)_{avg}$ as $(W_T h_{fg}/Q_T)$ for $L_B/L = 0.65$	72
22	Effect of Subcooling on Exit (C_s/C_ℓ) for Various Power Levels	72
23	Effect of Inlet Velocity on $(C_s/C_\ell)_{exit}$ for 10F Subcooling with Curve for Saturated Data	73
24	Effect of Pressure on $(C_s/C_\ell)_{exit}$ as a Function of Inlet Velocity	73
25	600 psi Unrestricted Single Channel Circulation Loop (Armadilla)	75
26	Schematic of Armadilla Test Loop	77
27	Comparison of Calculated with Actual Performance of Armadilla	80
28	Modified Martinelli-Nelson Boiling Friction Factor Ratio As a Function of Exit Voids and Slip Ratio	81
29	Modified Martinelli-Nelson Two-Phase Friction Factor Ratio As a Function of Local Voids and Slip Ratio	81
30	Slip Ratio As a Function of Inlet Velocity at 150 psig (1/2 x 3-1/2 x 60 in. Vertical Channel)	86
31	Slip Ratio As a Function of Inlet Velocity at 250 psig (1/2 x 3-1/2 x 60 in. Vertical Channel)	87
32	Zircaloy 2-Clad, Uranium-5% Zirconium Alloy Plates Tested for 70 hr in 550F Degassed Water	89
33	Corrosion Behavior of EBWR Reference Alloy Plate and Aluminum-Clad Natural Uranium Plate After Addition of Known Defect	90
34	Corrosion of Aluminum-Nickel Alloy (M-388) in 500F Water (pH = 5.0)	93

DECLASSIFIED

LIST OF FIGURES

No.	Title	Page
35	As-Removed Samples of Stainless Steel and Aluminum-Nickel Alloy M-388 After Exposure for 2 Weeks in 500F Water (pH = 5.0; Resistivity = 300,000 ohm-cm)	94
36	Corrosion of Aluminum-Nickel Alloy (M-388) in 500F Demineralized Water (pH = 6.5)	95
37	As-Removed Samples After Exposure for 2 Weeks in 500F Water at 16 fps (pH = 6.5; Resistivity = 1,500,000 ohm-cm)	97
38	Variation in Corrosion Rates of Aluminum-Nickel Alloys	98
39	As-Removed Samples After Exposure for 4 Weeks in 500F Water (pH = 5.0; Resistivity = 300,000 ohm-cm) . . .	99
40	Corrosion of Austenitic Stainless Steel as a Function of Test Conditions	101
41	Miniature End Box Fuel Element Core after Exposure for 7 days in Static Water at 414F	102
42	Urania-Thoria Bodies Irradiated in CP-5 Autoclave Test Facility	105
43	Removal of H_3BO_3 Using Amberlite IRA-400 Resin (Run No. 4)	115
44	Removal of H_3BO_3 Using Amberlite IRA-400 Resin	116
45	U^{238} Capture Distribution Along Vertical Axis of the EBR	123
46	U^{238} Capture Distribution Along Midplane of the EBR . . .	123
47	U^{235} Fission Distribution Along Vertical Axis of the EBR	124
48	U^{235} Fission Distribution Along Midplane of the EBR. . . .	124
49	Computed vs Measured Foil Activations in the Outer Blanket of the EBR	129
50	Measured vs Computed Cross Section Ratios in Outer Blanket of EBR	130

DECLASSIFIED

LIST OF FIGURES

No.	Title	Page
51	Dissipation of Simulated Decay Heat Generated in EBR-II Core Subassembly	134
52	Water Pressure Drop in EBR-II Core Subassembly (120F Water)	135
53	Schematic of Hold-down Test Facility	136
54	Resultant Hold-Down Forces for Modified EBR-II Core Subassembly in Water at 120F and 103 psig	136
55	Calculated Hold-Down Forces and Pressure Drops for Modified Design EBR-II Core Subassembly in Sodium at 900F	142
56	Enlarged Sections of EBR-II Pin-Type Fuel Elements Irradiated in CP-5 Test No. 2	144
57	Fuel Unloading System - EBR-II Working Model	147
58	Performance Characteristics of Model Tank Pump in Sodium at 370C	149
59	Molybdenum-Uranium and Zirconium-Uranium Alloy Pins Thermal Cycled in NaK	152
60	Surface Condition of Molybdenum-Uranium and Zirconium-Uranium Alloy Pins Thermal Cycled in NaK. Magnification: X4	153
61	Sequence of Insulating Induction Heated Sodium Test Loop	155
62	Induction Heating Time for 4-inch Sodium Loop	157
63	Spherodized Carbide and Sigma Phase Formation	157
64	Heat-Affected Zone Crack	157
65	Cracking Along Carbides at Grain Boundaries	157
66	Decarburization of Sodium-Wetted Surface	159

DECLASSIFIED

LIST OF FIGURES

No.	Title	Page
67	Oscillatory Response of Neutron Population to Sinusoidal Reactivity Input at ~Zero Power	172
68	Response to an Impressed Periodic Variation in Reactivity on a Reactor at Zero Power Having an Effective Lifetime of 4×10^{-8} Seconds.	173
69	Fraction of Heat Remaining in Fuel Rod (sodium stagnant) for Exponentially Rising Heat Source of Period $1/\alpha$	179
70	Tube Assembly for MTR Water to Water Heat Exchange Showing Area of Failure	181
71	Stress Corrosion Crack Starting at Outside of Heat Exchanger Tube	183
72	Pulse Height Distribution in B^{10} and in Al-U-Al Sensitized Photomultiplier Tubes	185
73	Neutron-Sensitive Electron Photomultiplier Tube Covers and Assemblies	186

REACTOR ENGINEERING DIVISION QUARTERLY REPORT

SECTION II

PART A. ADVANCED WATER REACTOR PROGRAM

SUMMARY - J. M. West

The boiling reactor being built at Argonne will hereafter be referred to as the Experimental Boiling Water Reactor (EBWR). Discontinuance of the BER designation will avoid further confusion resulting from different names being used by Argonne and Washington AEC personnel.

Since the EBWR plant design is now essentially complete, this report contains more detailed information than heretofore. A summary of all pertinent physics calculations is included. Semi-detailed descriptions of some nonstandard parts of the plant which were either inadequately described in previous reports or which have undergone significant changes are also given.

The steel cylinder (400,000 cu ft) in which the EBWR is to be housed will be completed about November 1. Tests will then be made to verify that the specification of 500 cu ft maximum leakage at a pressure of 15 psig has been met. After leak and pressure testing, openings will be cut in the steel shell for temporary access and for installation of the permanent air locks.

The equipment being supplied by Allis-Chalmers for the power plant has begun to arrive and is being stored at Argonne until the EBWR building reaches the stage where this equipment can be installed. Major transformers and switchgear are already on hand. The turbine and condenser will be shipped in November. All Allis-Chalmers equipment is expected to be available prior to the time when it is needed.

The design of support and containment features for the reactor has been completed. Very heavy vertical steel columns imbedded in the concrete base and biological shield, and tied together by cross beams above the reactor, are used to prevent the pressure vessel from being blown upward as a result of the enormous forces which could conceivably result from a chemical reaction between molten core metal and water. Shock absorbers consisting of alternate layers of steel and wood sheets are placed between the reactor and the vertical columns to protect these tension members from excessive bending forces. The maximum explosion would relieve itself by rupturing the lower part of the pressure vessel and shattering the concrete shield at the sides and bottom of the reactor. The gas-tight steel building would be protected from damage by its 2-ft thick concrete lining.

DECLASSIFIED

A complete control rod and mechanical drive mechanism combination is being tested under geometrical, temperature, and pressure conditions anticipated in the EBWR. Although some sticking of the control rod, due to foreign particles in the small clearance between ring seals and shaft, has been observed, this type of drive mechanism is expected to be satisfactory after minor modifications. Other types of rod drives are being vigorously investigated, however, including: (1) mechanical drives with rotating rather than sliding seals; (2) hydraulic, floating piston-type; and (3) magnetic jack drives. The EBWR design is such that different rod drives can be substituted after the reactor has been operated, if this proves to be desirable.

The flexibility being built into EBWR to permit future operation with forced circulation and conversion to a D_2O reactor has required changes and additions to the pressure vessel and shield. A borated steel thermal shield inside the pressure vessel is a necessity for operation with D_2O. Without such a thermal shield the secondary gamma radiation created by capture of leakage thermal neutrons in the walls of the pressure vessel would create excessive thermal stresses. Experimental batches of stainless steel containing one per cent or more of boron have been prepared by a number of industrial concerns. Corrosion resistance is good, and ductility is adequate for use in the thermal shield.

Two 12-in. diameter pipes are to be provided for exhausting cooling water in forced circulation operation, instead of the four 8-in. diameter pipes described previously. The complexity of the shielding and the piping underneath the reactor is thereby reduced.

The reactor shield has been finalized and materials are being ordered. A one-half-inch thick layer of ferroboron-cement plaster is applied to the outside surface of the lead thermal shield. This will reduce radioactivation of structural materials and of the air surrounding the pressure vessel. In the radial direction, the ferroboron is followed by a 5-foot thickness of magnetite concrete and by 3 ft of ordinary concrete. Dense concrete containing steel punchings is used below the reactor. A combination of steel and water is used above the reactor. Removable magnetite concrete blocks are placed in those portions of the biological shield traversed by piping. This feature will be a convenience during initial construction and will make subsequent removal of the pressure vessel mechanically feasible. No cooling will be provided for the concrete blocks. The estimated maximum temperature of 250F is not expected to be unduly detrimental.

Inasmuch as the heat treatments required for the 1.5% niobium - 5% zirconium - 93.5% uranium fuel alloy to achieve dimensional stability and corrosion resistance appear to be incompatible, emphasis is being placed on dimensional stability and clad integrity. This introduced the possibility of eliminating the niobium constituent. It was found, however, that the decreased hardness of the uranium-zirconium alloy aggravated plate-rolling problems. The corrosion rate is also increased enormously. Niobium appears to be a worth-while, even though expensive, ingredient of the EBWR fuel.

Sample natural uranium plates have been made to EBWR specifications by the Argonne Metallurgy Division. No defects were found in corrosion tests in 550F water. The techniques for making fuel plates and mounting them in assemblies appear to be satisfactory, and production can begin when Zircaloy 2 supplies arrive.

Cost estimates by industrial concerns for fabricating enriched uranium "spike" plates for EBWR are much higher than anticipated. As a result, slightly enriched fuel is being reconsidered. A final decision will not be made until all factors including relative flexibility of the two types of core have been thoroughly evaluated. A small number of spikes and natural uranium assemblies would be required to take care of uncertainties in the required enrichment even for the slightly enriched case.

The problem of detecting cladding failures in EBWR fuel plates continues to be a formidable one. Calculations indicate that the existence of a failure somewhere in the core can be detected by radiation monitoring of the exhaust gases from the main power plant condenser. No simple method for quickly determining which fuel plate has failed is yet evident. Mock-up tests have shown that radioactivity quickly disperses throughout the core, thereby making it difficult, if not impossible, to determine by radioactivity measurements the cooling channel from which the fission products originated.

In view of the scarcity and high cost of hafnium, alternate materials for control rods are under development. One type of control cross has a mixture of sintered gadolinium and samarium oxides packed in a hollow stainless steel can. Boron-stainless steel alloys also show promise.

Further corrosion tests on aluminum-nickel alloys show low corrosion rates in stagnant neutral water. At high water velocities the corrosion-erosion increases markedly, but the rate is reduced in slightly acidic water. Some evidence exists that excess hydrogen inhibits corrosion. This will be studied further.

Tests are being performed to determine the influence of boiling heat transfer on the corrosion rates of Zircaloy 2 and aluminum-nickel surfaces. No conclusive results are yet available.

Clad specimens of thorium oxide containing 10% of enriched UO_2 have been irradiated in 500F water to burnups between 0.05 and 0.3 atomic-%. Post-irradiation examinations showed varying degrees of fracturing of the cylindrical ceramic specimens, perhaps indicating excessive thermal stresses. No damage to the cladding was observed.

DECLASSIFIED

Boiling heat transfer tests continue. Both single and multiple cooling channels are used. The range of data is extended by using both forced and natural circulation. Results for any given set of conditions are considered reliable, but many additional variables must be explored and correlated before the performance of different boiling heat transfer channels can be predicted in advance.

DECLASSIFIED

I. EXPERIMENTAL BOILING WATER REACTOR (EBWR)

A. Reactor

1. Core

a. Corrosion of EBWR-Type Fuel Plates - C. R. Breden

EBWR-type fuel plates, made by the modified picture frame technique, are being corrosion tested to evaluate fabrication techniques. All of the plates contain uranium-5% zirconium-1-1/2% niobium and are clad with Zircaloy 2. The plates have not been given the heat treatment now considered best for dimensional stability.

The previous test history of the plates has been reported in ANL-5471.[1] After additional exposure in degassed water for 142 hr at 420F and 692 hr at 550F, warpage has occurred in plates No. 123, 127, 129, 133, and 134. These plates are about 55 in. long. The balance of the test plates, each of which is about 30 in. long, show no significant changes.

Eight roll-clad plates, each containing uranium-5% zirconium-1-1/2% niobium and clad with 0.022-in. Zircaloy 2, were tested for 145 hr in 550F degassed water. Three plates (Nos. 175, 178, and 179) were heat treated (to impart dimensional stability) in salt at 800C for 20 min, isothermally quenched in salt at 650C, and held at 650C for 24 hr. The remaining plates (Nos. 176, 181, 183, 184, 185) were not heat treated. No significant changes were noted.

b. Boiling Water Corrosion of Zircaloy 2 - C. Wohlberg

A boiling corrosion test apparatus has been constructed to determine the corrosion effect of water on test materials with boiling occurring at the surface of the material. The test apparatus consists essentially of a thermal siphon loop into which is inserted a ferromagnetic thimble clad with the material to be tested. This thimble is heated by an induction coil placed within the thimble; the exterior, clad surface of the thimble is exposed to the water in the loop. A steam space above the loop is cooled by radiation from a large closure flange and by a cooling coil. In operation the entire system is brought to a steady state by means of immersion heaters. The radio-frequency generator supplying the induction coil is then turned on and adjusted to give the maximum possible heat throughput without overheating the cooling water and shutting off the generator.

---

[1] Reactor Engineering Division Quarterly Report - Section II, (September, 1955), Table IV, p. 101.

DECLASSIFIED

In the current test, a Type 430 stainless steel thimble, clad with Zircaloy 2 (0.015 in. thick), was exposed for 129 hr in degassed, distilled water at 500F. It is estimated by observation of the deposit of corrosion product on the outside of the thimble, that a cylindrical area 5 in. long by 1.56 in. diameter (area 0.17 sq ft) acted as the major heat throughput surface. The estimated heat throughput for the test was 30,000 Btu/(hr)(sq ft).

The Zircaloy 2 - clad showed the dark greenish discoloration characteristic of this metal. Some powdery corrosion product, as well as metallic chips, were observed on the surface of the heat transfer zone (see Fig. 1). The bulge or buckling was caused by the surrounding water (under pressure) squeezing the jacket tightly around the thimble and forcing excess metal into a bulge at a weak spot.

2. Control Rods and Drive Mechanism

a. Design and Prototype Testing - C. F. Bullinger

The EBWR reference control rod (Fig. 2) is a cross-shaped unit of hafnium with a Zircaloy 2 follower and a Type 304 stainless steel extension shaft.

The entire unit is built up from 0.062-in. thick sheet hafnium, Zircaloy 2, and stainless steel, the sheets being fastened either by spot welding or riveting. The joint between the hafnium rod and the Zircaloy follower is a butt weld, whereas the Zircaloy to stainless steel connection is a riveted lap joint.

The basic philosophy of the design is flexibility. The unit is designed so that any warping which may occur cannot exert enough lateral pressure to cause severe binding in the 1/2-in. wide channel guide.

The EBWR Model II reference design control rod drive mechanism (Fig. 3) is of the external mechanical type featuring a lead screw, driven nut, and scram latch mechanism operating outside the reactor pressure shell, with the drive shaft entering the reactor through a floating ring sliding seal.

The Model II drive is the evolutionary design of Model I described in ANL-5371[2] and is built to meet the following requirements:-

---

[2]Reactor Engineering Division Quarterly Report, (January 15, 1955), p. 211.

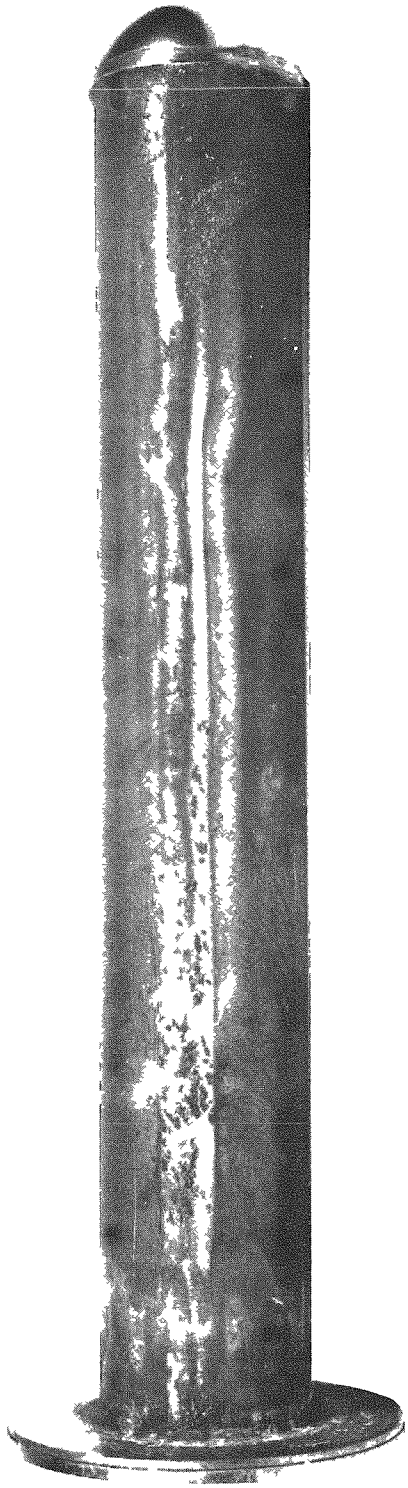

FIG. 1
BOILING WATER CORROSION OF ZIRCALOY 2-CLAD
TYPE 430 THIMBLE TESTED FOR 129 hr
IN 500 F DEGASSED DISTILLED WATER

DECLASSIFIED

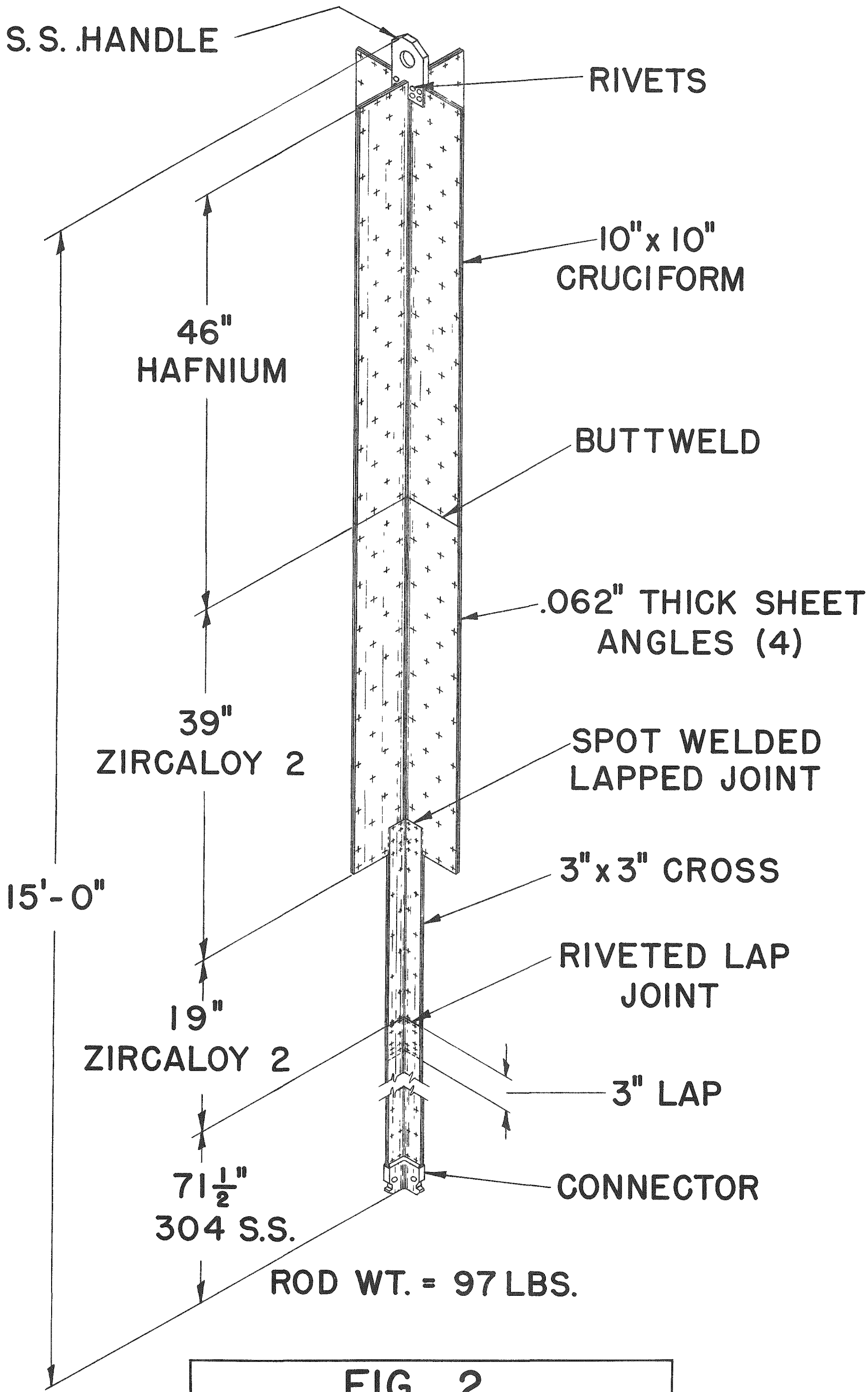

FIG. 2

EBWR CONTROL ROD

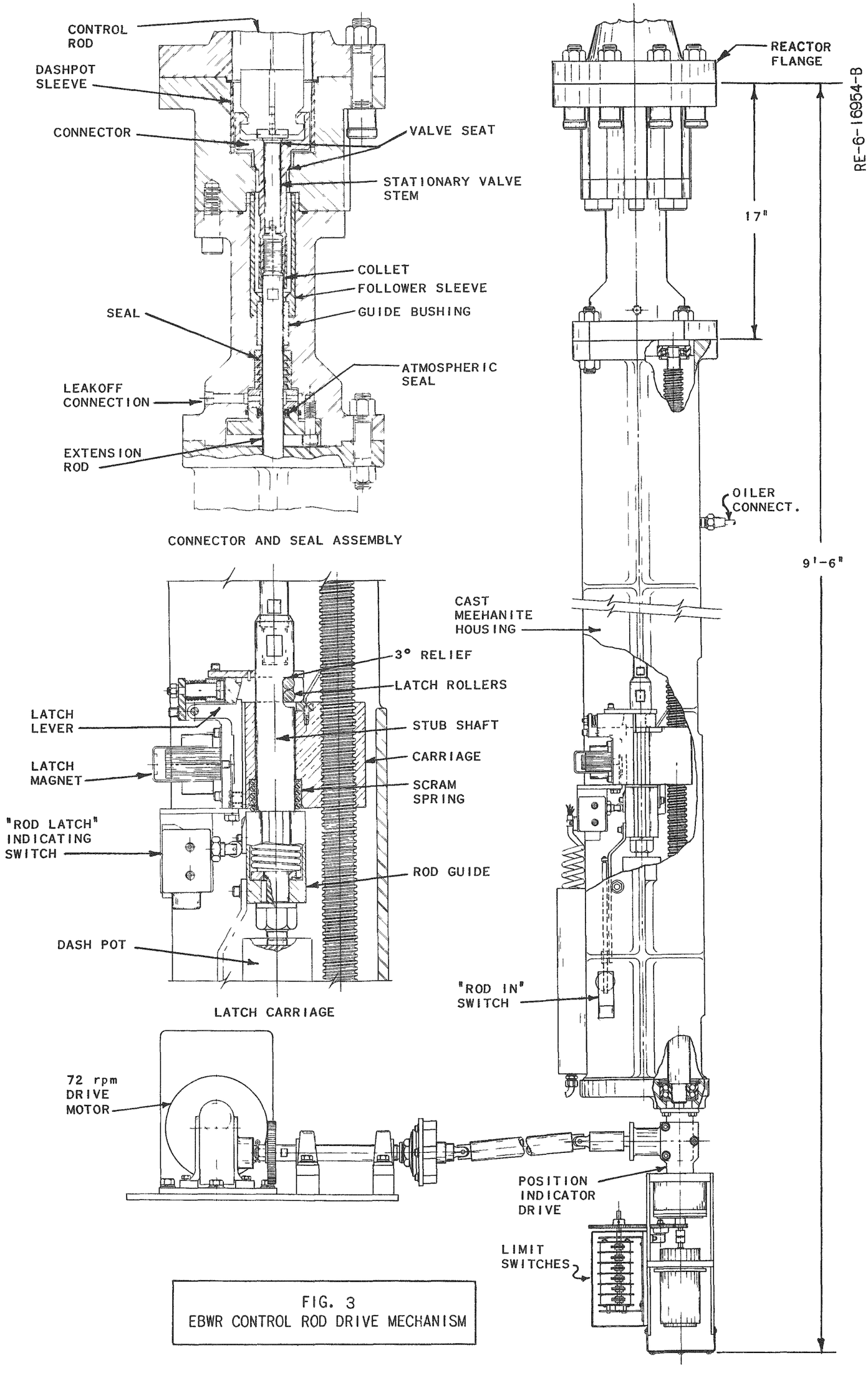

FIG. 3
EBWR CONTROL ROD DRIVE MECHANISM

DECLASSIFIED

(1)	Operating pressure	600 psig
(2)	Operating temperature	160F
(3)	Number of control rods	9
(4)	Control rod center-line distance	12-3/4 in.
(5)	Control rod travel	48 in.
(6)	Rate of travel (max.)	28.8 in./min
(7)	Rod scram time	0.5 sec at 200 psi
(8)	Positionability	± 0.025 in.
(9)	Control rod weight	97 lb
(10)	Dash pot (primary)	external
(11)	Dash pot stroke	6 in
(12)	Dash pot reaction (constant force)	1700 lb
(13)	Leakage rate (max.)	750 cc/min/rod
(14)	Complete "fail safe" characteristics	
(15)	Control rod and drive unit separately removable from reactor without draining reactor vessel.	

In order to meet requirements (5) and (10), the overall length of the complete mechanism has been increased by approximately 22 in. to 9 ft 6 in.

The increased length requirement has resulted in a redesign of the latch arrangement. Because of the high column loading of the 1 in. diameter x 60 in. long drive shaft in scramming, the unit was made into a three-piece assembly consisting of the control rod connector, the drive shaft, and the stub shaft containing the scram latch groove. This permits the Armco 17-4 PH shaft to be heat treated to 45 Rockwell "C" before being centerless ground to 0.995 -0.996 in. diameter for chrome plating. The finished diameter is 1.0001-0.997 in. Ends are threaded before chrome plating.

The maximum hardness condition of the shaft is required to prevent scoring and sticking of the shaft in the floating seal rings. Use of 30-35 Rockwell "C" hardness chrome-plated shafts has resulted in immediate sticking due to small particles and fine chips. When a shaft of proper hardness is used only a slight burnished effect is noticed from such action. Any jamming which could occur can be overpowered by the 2900-lb force available in the lead screw drive.

DECLASSIFIED

The Type 309 control rod connector (Fig. 3) is threaded to the drive shaft. Slight adjustments in over-all length may be made and the two parts locked together with the threaded collet. The connector also serves as the velocity-limiting piston and auxiliary dashpot piston. The control rod may be released by rotating the connector 45 degrees after the safety pin is removed. This function may be performed without draining the reactor vessel.

The 4340 heat treated, chrome-plated stub shaft threads on to the lower end of the drive shaft and contains the scram latch groove. The supporting face of the latch is relieved at a 3-degree angle to assure release. The latch roller carriage is spring-actuated to release and is held closed by the energized solenoid coil. Interruption of the current releases the latch.

The column loading limitations of the drive shaft, in deceleration during the scram stop, dictated the necessity for a 6-in. long dashpot travel at a constant force of 1700 lb. The deceleration curve for 600-psig operation is shown in Fig. 4.

The switches of the control rod drive are all adjustable-cam operated. The rod latch indicating switch shown in Fig. 3 energizes the motor control circuit to drive the latch carriage nut downward when the latch is released. Thus the rod drive follows the shaft extension downward after a scram. The switch also actuates a board pilot light to indicate whether or not the rod is latched to the drive. The switch is actuated by the roller leaf striking an adjustable cam face on the rod guide.

The scram timing and position indicator switch shown in Fig. 3 is actuated by the adjustable probe attached to the rod guide and actuates the timer circuit and a pilot light to indicate that the control rod is completely inserted in the core.

The four-switch multiple circuit timer unit is gear driven off the position indicator drive. The two-piece sheet metal cams are adjustable over 350 degrees of operation.

Switch No. 1 actuates a pilot light to indicate the "full out" position.

Switches No. 2 and No. 3 are operating sequence switches and, although adjustable, are intended for normal operation at the 10% level. Each rod may be raised to a 10% elevation where switch No. 2 prevents further upward movement until all other rods are raised to the same position. Switch No. 3 of each rod partially completes the safety release circuit when the rod is raised to the 10% level. When all rods have reached the 10% level, the release circuit is fully completed, and from this location, any rod may be raised to any elevation at the operator's discretion.

DECLASSIFIED

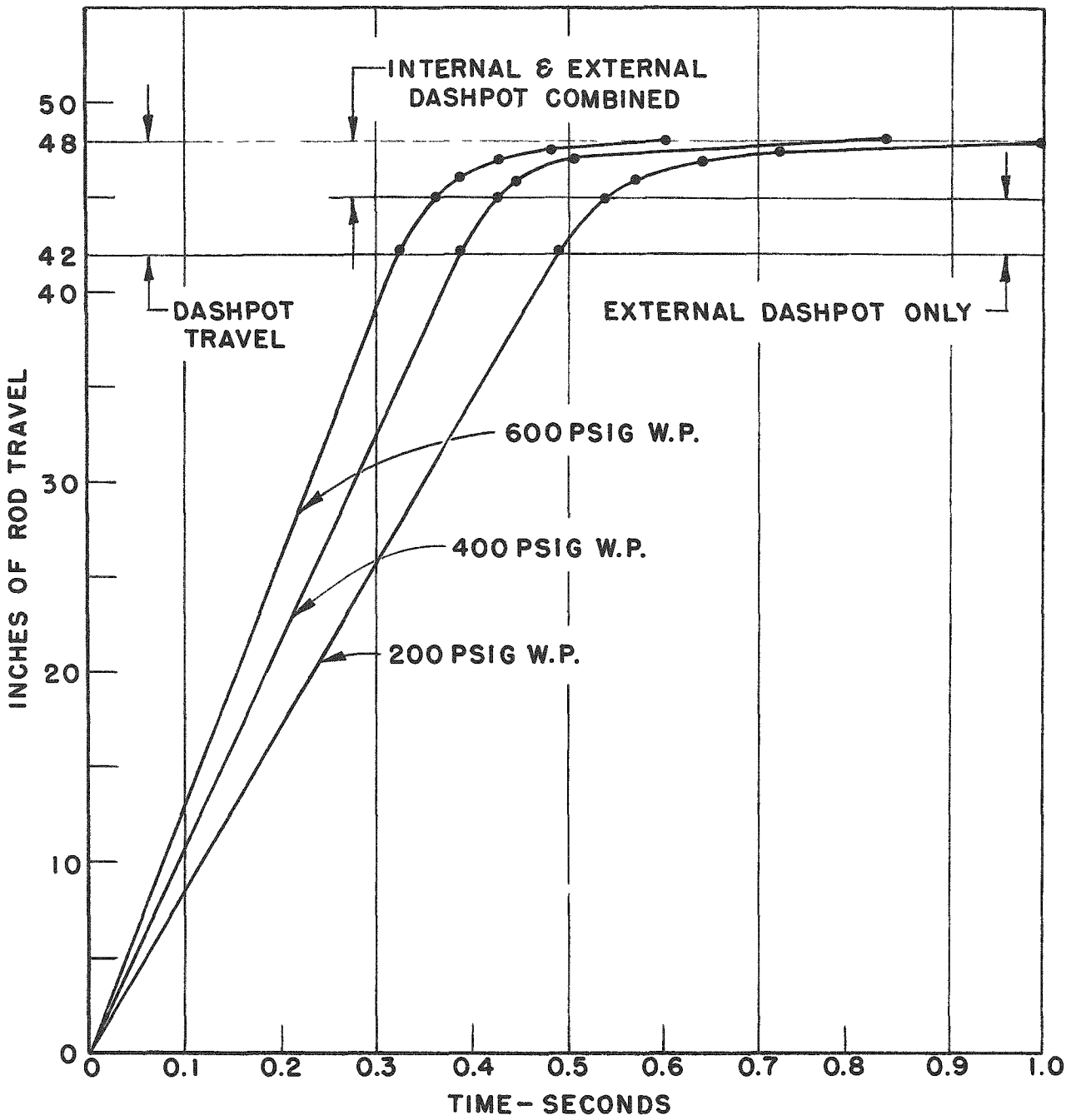

FIG. 4
CONTROL ROD SCRAM TIME

DECLASSIFIED

Position indication is achieved through individual Telesyn generator transmitter and receiver circuits driven through a 50:1 high precision gear box.

The control rod drive is powered by a 1/3-hp, 200-inch-lb torque, 72-rpm, 3-phase, 60-cycle, 220-volt gear motor with brake. An external gear train provides for speed variation.

A test facility, shown in Fig. 5, has been constructed to test both the control rod in its guide and the control rod drive mechanism under simulated EBWR conditions. At present, a test of a reference control drive mechanism is under way, using a mocked-up stainless steel control rod and guide. The latter will be replaced by a reference material control rod and guide (Zircaloy 2) as soon as the proper materials become available for fabrication.

b. Zircaloy 2 - Stainless Steel Contact Corrosion - C. R. Breden

Contact-corrosion test specimens of Zircaloy 2 bolted to Types 304 and 347 stainless steels have accumulated a total of 5672 hr in dynamic (~10 fps), degassed, demineralized water (1470 hr at 500F and 4202 hr at 600F). Static corrosion tests on duplicate specimens in air-saturated and in degassed water have accumulated a total of 5212 hr at 500F and 5850 hr at 600F. No contact or crevice effects are detectable.

3. Pressure Vessel

a. Vessel - N. Balai, L. C. Livesey, A. H. Heineman

Several modifications have been made in the vessel closure design:

(1) The upper ring forging has been revised to provide a continuous shoulder support for the indexing plugs, in lieu of intermittent brackets welded to the vessel walls (interim design). This revision was deemed necessary for the solution of the impact problem associated with the hazard of dropping the indexing plugs.

(2) The plug support bearings have been eliminated to avoid the difficulties involved with bearings exposed to boiling water. This change also allows a narrower support shoulder, with resulting improvement in thermal stress conditions.

(3) Excess metal from the forging was trimmed further in order to meet a three-hour shutdown and heating-up time specification.

DECLASSIFIED

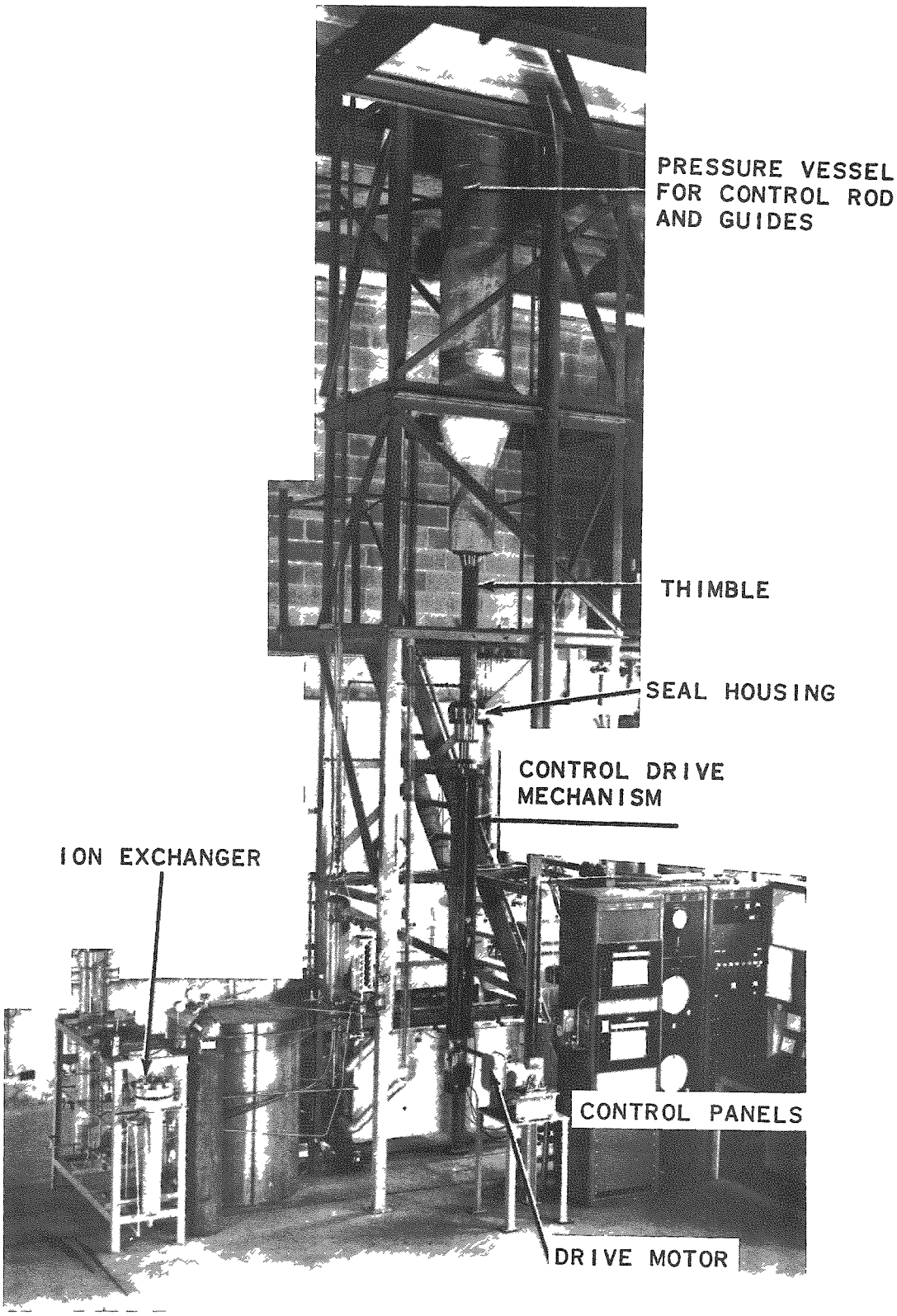

FIG. 5
TEST FACILITY FOR EBWR CONTROL
ROD AND DRIVE MECHANISM

DECLASSIFIED

Calculations for the new ring forging dimensions and consideration of the venting arrangement provided in the closure design show that at a constant heat input rate, the vessel, including the heavy closure cover, can be heated from 70F to 488F in three hours. The maximum cooling down rate is 185F per hour. These heating and cooling rates meet the specifications for the vessel and have been confirmed by Babcock and Wilcox Company, the fabricator of the unit.

The modified design (Fig. 6) features an external removable turntable to which the plugs are lifted and affixed (by bolting) during indexing operation.

Erection and fabrication problems associated with the installation of biological shielding around the control rod thimbles at the bottom of the vessel have necessitated a redesign of the flange connections. The revised design utilizes loose threaded flanges which can be removed for installation of shielding, then reinstalled and tack welded in place in the field after vessel and shielding erection.

Nozzle connections to the vessel have been changed in that the four 8-inch pump suction connections for future forced circulation operation have been replaced by two 12-inch connections.

b. Thermal Shield - R. J. Rickert

The projected use of the EBWR facility with D_2O as the moderator and coolant magnifies the shielding problems considerably since D_2O is a very poor neutron absorber. The design of the biological shielding provides for future operation with D_2O. The D_2O core has also dictated the thermal shield requirements to protect the pressure vessel from excessive thermal stresses due to gamma heating.

Table I shows the calculated heat generation in the pressure vessel wall for each type of thermal shielding. These heating values decay exponentially through the wall with the slopes given. All values are based on the same neutron fluxes which were determined in the biological shielding calculations reported on page 39. This represents the most extreme condition expected in the EBWR.

The solution of the differential equation for thermal stress yields the following equation for an axially unrestrained, insulated cylinder with exponentially decaying heat generation through the wall. Axial temperature variations are assumed to be negligible from the thermal stress standpoint. The radial gamma-ray heating is at a point far enough removed from the ends of the vessel so that the bending stresses produced at the knuckles of the heads are negligible. The maximum stress occurs at the inside surface and is tangential tensile stress.

DECLASSIFIED

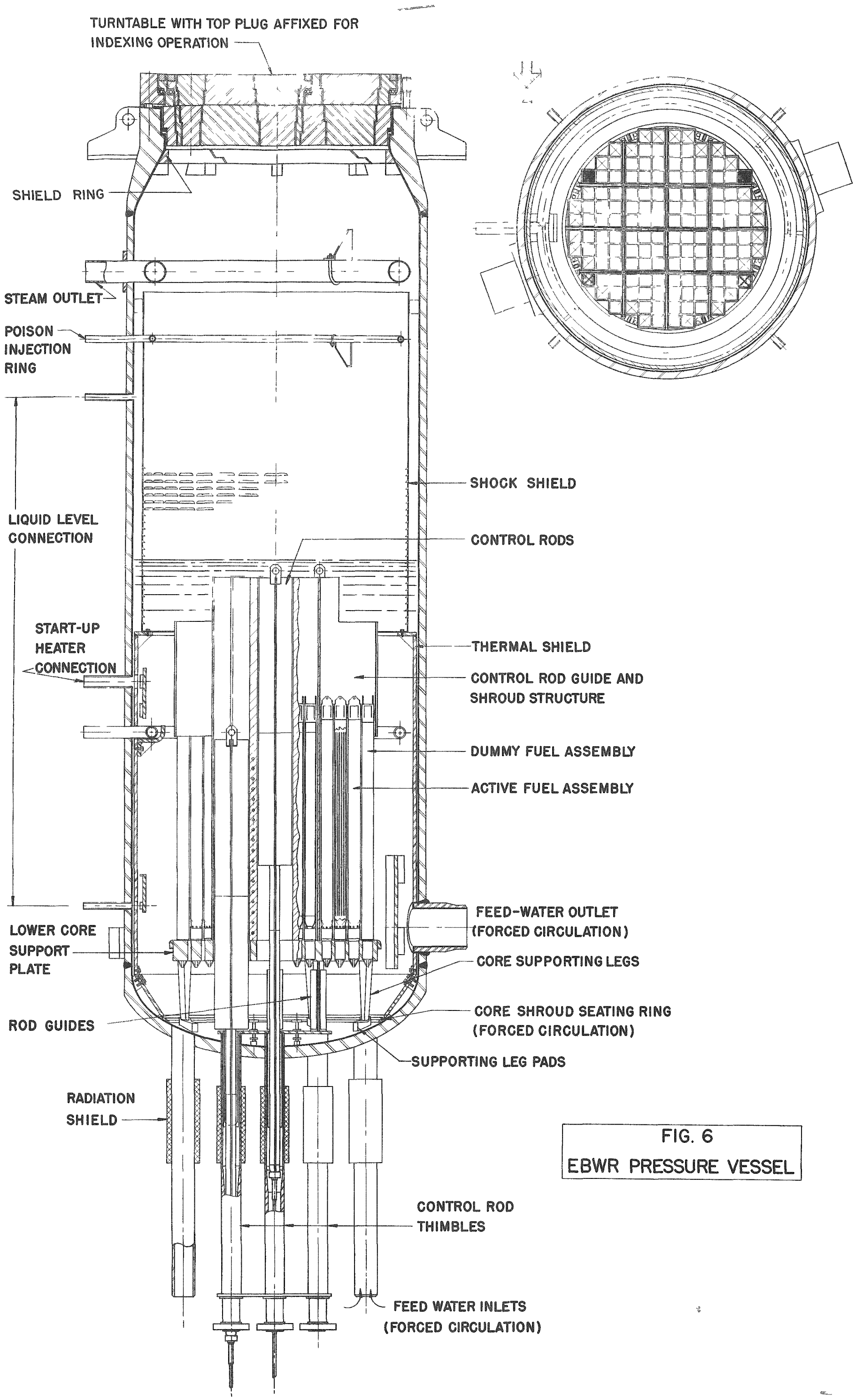

FIG. 6
EBWR PRESSURE VESSEL

Table I

RADIATION HEATING IN PRESSURE VESSEL WALL

Thermal Shielding		Heat, watts/cm^3		Exponential Slope, $\frac{1}{cm}$
Stainless Steel, in.	Boron, %	Inside Surface	Outside Surface	
-	None -	>1	-	-
1	-	>1	-	-
1	1/2	0.31	0.075	0.2235
1/2	1	~0.34	-	-
1	1	0.24	0.0675	0.20
1	2	0.185	0.0663	0.162
5	-	~0.36	~0.077	0.243
6	-	~0.2	~0.043	0.242

$$\sigma_t(R_1) = \frac{E\,\alpha\,H}{(1-\mu)A^2k}\left[1 + \frac{2(AR_1+1)}{A^2(R_1)^2} + \frac{AR_1}{3}e^{-At} + \frac{2(R_2)^2}{(R_2)^2-(R_1)^2}\left(\frac{AR_2+1}{A^2(R_2)^2}e^{-At} - \frac{AR_1+1}{A^2(R_1)^2} - \frac{At}{3}e^{-At}\right)\right] \quad (1)$$

where

$\sigma_t(R_1)$ = tangential stress at R_1, psi

E = Young's Modulus, psi

α = Linear coefficient of thermal expansion, 1/F

H = heating at R_1, Btu/(hr)(cu ft)

μ = Poisson's Ratio

A = exponential slope of heating curve, 1/ft (absolute value)

k = thermal conductivity of wall, Btu/(hr)(ft)(F)

R_1 = inside radius of vessel, ft

R_2 = outside radius of vessel, ft

DECLASSIFIED

Equation (1) indicates that the thermal stress is not affected by the heat transfer conditions at the inside surface, but only by the rate of heat generation and the thermal conductivity of the wall. Since the cladding on the inside of the vessel is not considered in calculating the strength of the vessel, it is ignored here. The heating at the inside surface is attenuated through the clad by e^{-At} clad to obtain H.

The calculated stresses in the vessel wall for the various thermal shielding conditions are listed in Table II. The following constants were used in the calculations:

$$E = 29 \times 10^6 \text{ psi}$$

$$\alpha = 7 \times 10^{-6}/F$$

$$\mu = 0.3$$

$$k = 24 \text{ Btu/(hr)(ft)(F)}$$

$$R_1 = 3.51 \text{ ft}$$

$$R_2 = 3.70 \text{ ft}$$

Table II

THERMAL STRESSES IN PRESSURE VESSEL WALL

Thermal Shielding			
Stainless Steel, in.	Boron, %	Heating - $H(R_1)$, watts/cm^3	Thermal Stress - $\sigma_t(R_1)$, psi
-	None -	>1	Excessive
1	-	>1	Excessive
1	1/2	0.289	1800
1/2	1	~0.32	~2300
1	1	0.222	1600
1	2	0.176	1400
5	-	~0.33	~2100
6	-	~0.185	~1200

The ASME Code (Section I - Power Boilers) infers that all stresses other than the pressure stress whose sum does not exceed 10% of the allowable working stress of the material at design conditions can be ignored. The allowable stress for SA-212B steel of 17,500 psi for the EBWR temperature range is the working stress at the design pressure of 800 psi; therefore, the thermal stresses must be held to less than 1750 psi.

As shown in Table II, a stainless steel - 1 wt-% boron thermal shield (1 in. thick) will keep the thermal stress to 1600 psi. Recent development work by steel suppliers indicates that 1% boron-containing stainless steel will be available at a lower cost than the required thickness of ordinary stainless steel (6 in.). The samples received thus far are strong and ductile; however, irradiation and corrosion data are not yet available.

The mechanical arrangement of the thermal shield is shown in Fig. 6. The cylindrical portion of the shield is 9 ft high with a horizontal ring around the top which projects inward to a point 6 in. from the vessel wall. The D_2O core will have an upper fuel element support consisting of a horizontal flat plate of boron-stainless steel (1 in. thick x 5 ft-10 in. dia.) about 2 ft above the core surface. This plate will act in combination with the ring as a shadow thermal shield for the upper portion of the vessel. This combination is necessary to prevent serious restriction of the downcomer annulus. The lower portion of the vessel is shielded by a conical section of boron-stainless steel (1 in. thick) and by the lower core support plate.

c. Support and Containment Structure - N. Balai, A H. Heineman L. C. Livesey, E. H. van Zylstra

The pressure vessel support structure must serve the dual purpose of supporting the vessel under both normal static and abnormal impact conditions (resulting from accidental dropping of pieces of heavy equipment on the vessel) and of containing any missiles which might be launched as the result of a violent metal-water chemical reaction within the reactor core.

Figure 7 shows the structure designed to meet the above requirements. Two sets of three parallel Carilloy T-1 columns are anchored in the reinforced concrete below the reactor and extend upward to the top of the pressure vessel. Three parallel Carilloy T-1 hold-down beams span a 6-in thick missile (and biological) shield and are connected to the two sets of vertical columns with removable wedges. The columns are protected from the full lateral force of an explosion of the core by two blast shields made up of 1-in steel plates and 3-in. layers of redwood and Celotex. The pressure vessel is supported from the top of the columns on a flexible structure made up from Carilloy T-1 beams. C-shaped springs have been placed between the pressure vessel mounting lugs and the support structure as added insurance against damage in case a piece of heavy equipment is dropped on the pressure vessel.

DECLASSIFIED

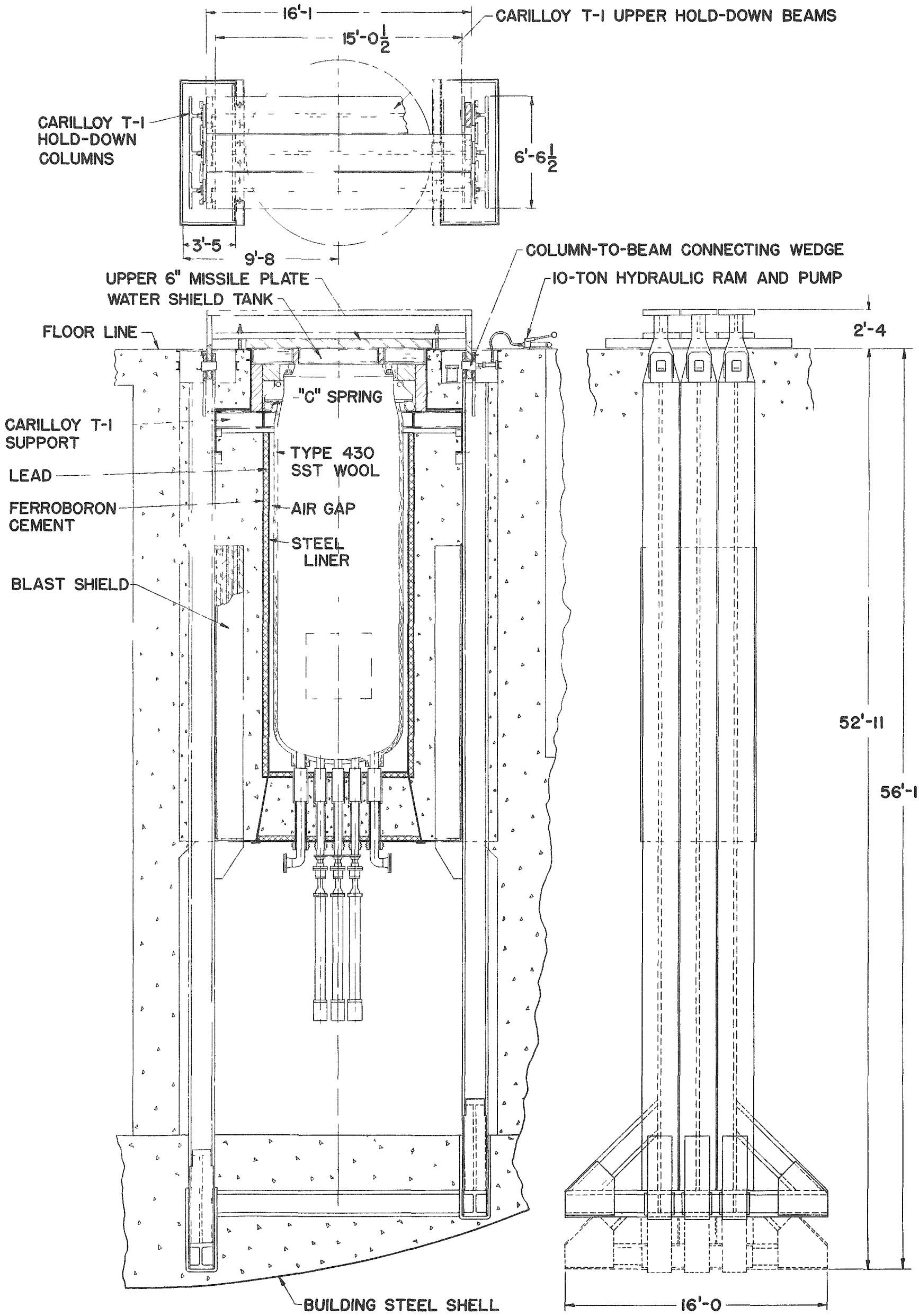

FIG. 7
EBWR PRESSURE VESSEL CONTAINMENT STRUCTURE

Vessel Support under Impact Loading

The vertical location of the support structure with respect to the building floor is dictated by the water level requirements of the turbine and condenser. The top of the pressure vessel closure flange has been fixed at 24 in. below the floor line. The establishment of this dimension introduces a number of probable impact loadings on the vessel and its support structure. The maximum free fall, assuming a drop height from 6 in. above the floor line, and the masses involved are as follows:

Component	Weight, tons	Maximum fall, in.
Unloading coffin	15.0	18
Vessel cover	8.5	30
Indexing plugs	6.0	42
Indexing plug carrier plate	10.0	30

The support was calculated, first, for a static loading condition and checked for the impact loading condition as outlined by Roark.[3] The stress intensification for dynamic loading is given by (Article 84):

$$\frac{d_i}{d} = \frac{s_i}{s} = 1 + \sqrt{1 + 2\frac{h}{d}K}$$

where

d_i = deflection on impact, in.

s_i = stress on impact, psi

d = static deflection of beam by impacting mass, in.

s = static stress in beam by impacting mass, in.

h = height of fall, in.

K = a function of the interacting masses and is, by Case 4 (Article 85),

$$K = \frac{1 + \frac{13}{35}\frac{M_1}{M} + \frac{M_2}{M}}{\left(1 + \frac{1}{2}\frac{M_1}{M} + \frac{M_2}{M}\right)^2}$$

[3] R. J. Roark, Formulas for Stress and Strain, (2nd ed.; New York: McGraw-Hill Book Co., Inc., 1943), Articles 84 and 85, pp. 318-321

DECLASSIFIED

M = impacting mass

M_1 = mass of beam struck

M_2 = mass attached to beam and receiving the impact by mass M.

Results of calculations for the various impact conditions considered are summarized in Table III. It is apparent from Table III that the use of ordinary structural steel shapes (A-7) is risky under impact conditions, inasmuch as impact stresses are very close to or exceed the ultimate strength of the material and, in all cases, exceed the yield strength. The reason for this is that the A-7 sections are very stiff when sized to support the maximum static load for the short span length required. The deflection of a stiff beam is very low and results in high stress intensification ratios during impact. Since the large calculated stresses suggest the use of high-strength structural alloys, the most severe impact condition [No. (5), Table III] was recalculated for the U. S. Steel Corporation alloy Carilloy T-1. It was found that the T-1 alloy will sustain the impact loading but at a low factor of safety (F.S. = 1.25 based on the ultimate tensile strength). To raise the factor of safety, springs are interposed between the lug supports of the vessel and the structural frame beams, as shown in Fig. 7.

An eight-point vessel support system has been adopted to simplify the framing of the high-strength alloy steel support structure. A detailed structural design by the Architect-Engineer (Sargent and Lundy of Chicago) indicates that a heavier member, i.e., a 12 WF 133, is necessary to obtain the necessary rotational flange stiffness under impact.

Vessel Containment

The design of the structure for vessel containment is based upon the assumption that 25% of the metal in the EBWR core will react with the water present so that a high-order detonation results.

The Armour Research Foundation was given a subcontract to evaluate the force system for such a high-order detonation. The energy release used was 0.8×10^9 calories. Experimental data used to verify calculations were obtained by Armour for the Office of Naval Research. Calculations were based on the conservation of mass, energy and momentum. In this particular case, the energy release was assumed to be the same as from a spherical block of TNT the size of the EBWR core. A final Phase I report was issued, listing the following results:

(1) The lower section of the vessel (in contact with the water phase) will fail under a reflected shock wave pressure of 40,700 atmospheres at the sides and 13,800 atmospheres at the bottom.

DECLASSIFIED

Table III

SUMMARY OF CALCULATED IMPACT LOADING STRESSES

Reactor Type	Impact Conditions	Masses, tons			Free Fall, in.	Intensification Ratio	Material*	Stresses, psi		
		M	M_1	M_2				Allowable Bending (Static)	Impact	Total
H_2O	(1) Coffin dropped on vessel; shell full of water; cover in place.	15	1.7	114	18	14.8	A-7	20,000	36,800	56,800
H_2O	(2) Coffin dropped on vessel; water at operating level; cover in place.	15	1.7	102	18	15.5	A-7	20,000	38,300	58,300
D_2O	(3) Vessel cover dropped; water at operating level.	8.5	1.7	88.5	30	21.5	A-7	20,000	30,100	50,100
D_2O	(4) Indexing plugs dropped; water at operating level.	6.0	1.7	82.5	42	26.1	A-7	20,000	26,100	46,100
D_2O	(5) Assembly of indexing plugs and carrier plate dropped; water at operating level.	16.0	1.7	82.5	30	21.2	A-7	20,000	56,700	76,700
D_2O	(6) Same as (5) except for material in support structure.	16.0	1.7	82.5	30	12.4	T-1	35,000	49,800	84,800

*A-7 = Ordinary Structural Steel (24 WF 76)

T-1 = U. S. Steel Alloy Carilloy T-1 (12 WF 79)

(2) The top of the vessel will not fail, since the maximum shock wave pressure is 260 atmospheres (3800 psi). (Although the static strength of the vessel is 3200 psi, the actual strength under impulse loads of short duration is much greater because of a large increase in strength at high strain rates.)

(3) The transmission of the shock wave through the concrete biological shield in the radial direction and through the lower shielding plug in the axial direction will reduce these masses to rubble.

(4) The durations of the applied forces are very low, i.e., 10 milliseconds maximum.

Armour free field pressure calculations indicated that an unprotected column could not withstand the outward shock wave pressures. After high-pressure crushing tests on pine, oak and redwood had been run, it was decided that redwood had the best energy-absorbing properties. Later tests indicated that once the shock wave pressure had been somewhat reduced by a combination of redwood and steel layers, several layers of Celotex would further reduce the load transmitted to the hold-down columns. Accordingly a blast shield was designed so that the shock wave must pass through 3 in. of redwood and 1 in. of steel repeated three times, then through 3 in. of Celotex and 1 in. of steel repeated two times.

The theory of the composite blast shield is to absorb successively the shock energy in the compressible wood medium, transforming shock energy into heat energy. The steel transforms the material velocity component back into a shock wave which is then partially absorbed by the next compressible layer. Details of the blast shield are shown in Fig. 8. A thin sheet steel cover has been placed over the assembly and caulked to keep water from the shielding concrete out of the redwood and Celotex.

The sequence of loading as determined by the Armour force-time calculations[4] is as follows:

Member	Time Scale, milliseconds	Duration, milliseconds	Type of Loading
Column	+1	2 (max.)	Bending
Column	+5	6	Axial Extension
Upper Beam	+5	6	Bending
Column Anchor	+1	2	Couple
Column Anchor	+5	6	Axial Extension & Bending

[4]Design Evaluation of EBWR (Boiling Experimental Reactor) in Regard to Internal Explosions, Phase Report No. 1 ARF No. MO73, (May 10, 1955)

DECLASSIFIED

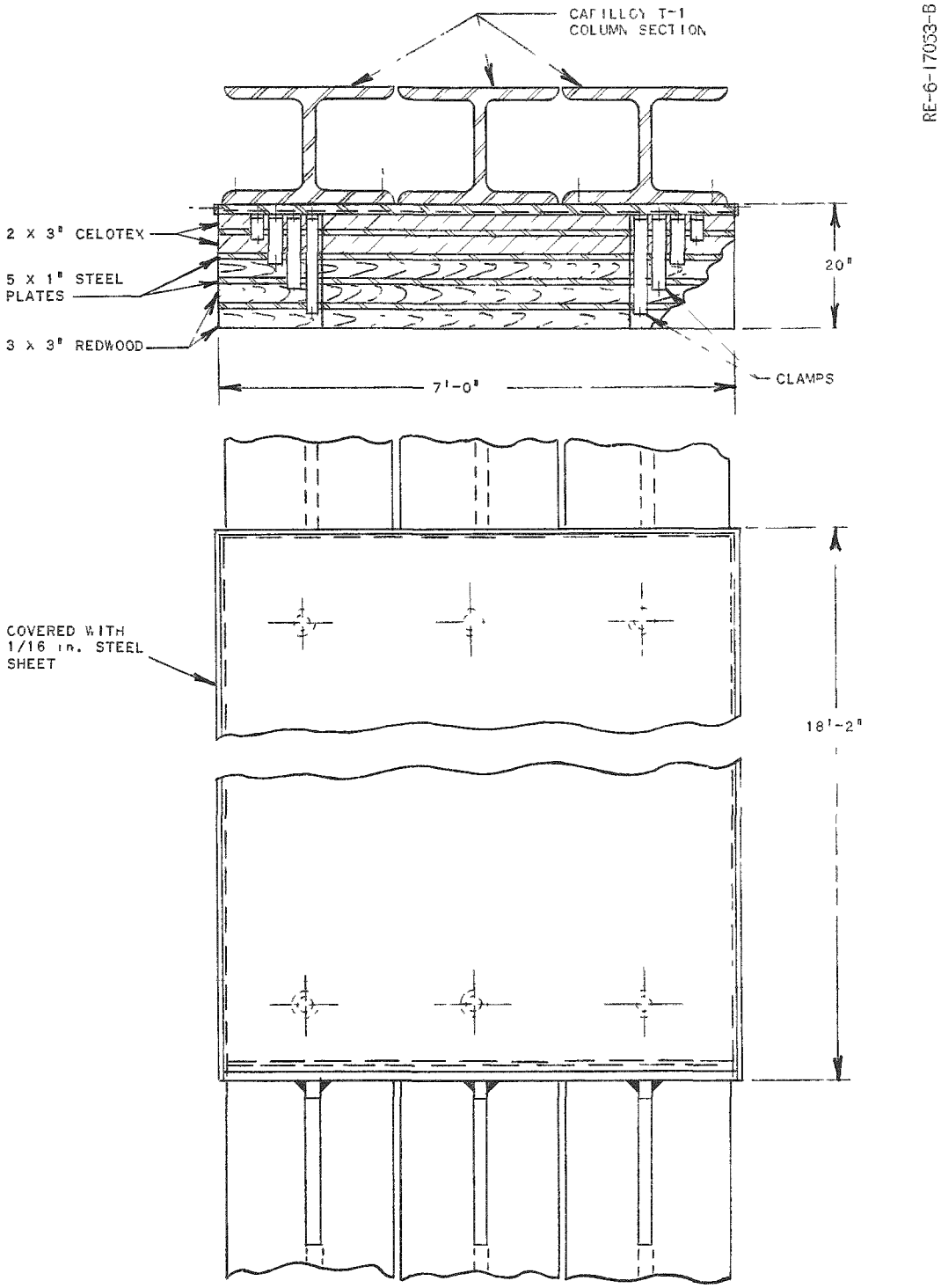

FIG. 8
BLAST SHIELD ASSEMBLY

DECLASSIFIED

Selection of proportions for the structural members was made by successive approximations and corrections of the static design with applicable dynamic-loading factors. The dynamic load factor is defined as the dynamic deflection divided by the static deflection.

The constants for the dynamic-loading factors were obtained from Armour unpublished data.

From the earliest calculations, it was immediately apparent that the conventional structural steel design was inappropriate. The calculated section sizes (with the conventional factor of safety of 3) were extremely heavy and bulky. Accordingly, the conventional design criterion was abandoned, along with conventional structural steel (ASTM A-7) materials, in favor of a low factor of safety, taking into account the inherent increase in strength of metals as a function of strain rate and the use of the high-strength, quenched and tempered alloy steel, Carilloy T-1. With this criterion, beam and column sections were determined, using the static ultimate tensile strength of the alloy as the allowable stress with static loads reduced by the dynamic load factors obtained from Armour. The sections required are much larger than any listed conventional rolled sections and must be fabricated from plates.

The factors of safety in the present design are between 1 and 2, and further reductions may be possible. This is not recommended at this time because of: (1) the uncertainties in the assumptions concerning restraint of the various sections at points of attachment; (2) uncertainties in loading of the members as a function of the assumed type of explosion; and (3) uncertainties in the effectiveness of the final layer of the blast shield.

In order to provide anchor beam subassemblies which can be installed in the building at the proper time in the construction sequence, the columns are made in two pieces. The bottom of stub columns will be welded in place on the two anchor beam subassemblies. These subassemblies will then be placed in the building shell. The tops of the columns will then be welded to the stub columns.

Reinforcing rods will be welded to the anchor beams so that the upward force of 21,000,000 lb will be resisted by the shear strength of the concrete along a 45-degree line beginning at the edges of the bottom flange of each of the anchor beams. Since the building shell has a semielliptical bottom, the outboard anchor beam cannot be buried as deep as the inboard anchor beam; therefore two cross anchor beams have been provided to keep the outboard anchor beam from pulling out from under the mass of concrete below the fuel storage well.

DECLASSIFIED

It should be pointed out that the assumption of a metal-water reaction occurring in the form of a high-order detonation is very pessimistic and is used for design in EBWR only because of lack of sufficient experimental evidence and because of the dire effects of such an explosion if not properly contained. Metal-water reaction tests were made by Aerojet-General Corporation on the EBWR reference fuel alloy during June. The alloy was melted in an induction furnace and then dropped into a container of water; only 5% of the alloy reacted with the water, with no destructive effects. A black oxide coating, 0.0005 in. thick, was formed on the remaining metal. When a blasting cap, set off under water by the falling metal, was used to disperse the molten metal, all of the metal reacted with the water in a quiet, non-destructive manner. It is estimated that particle size was 200 mesh. The pressure rise was only slightly greater than that due to the blasting cap alone. Other tests carried out by Knolls Atomic Power Laboratory indicate that the reaction of Zircaloy 2 and water can be sustained only above the melting point of the metal and proceeds in the manner of a pressure surge rather than as a detonation.

4. Biological Shielding

a. Calculations for Heavy Water Operation - M. Grotenhuis, R. J. Rickert, A. E. McArthy, S. A. Bernsen, C. K. Soppet

The flux distributions of both neutrons and gamma-rays in the light water-reflected EBWR[5] are completely outmoded by the possibility of using heavy water in the reflector. The higher thermal neutron flux in the reflector necessitates the use of a borated stainless steel thermal shield as well as heavier, or a thicker, layer of concrete.

The neutron flux calculations for the heavy water-reflected EBWR in the adjusted shield have been completed and the results are presented in Figs. 9 to 12. While the gamma-ray flux distributions are not complete, sufficient work has been done to indicate that the heating in the vessel is not prohibitive and that the biological shield is adequate.

The methods of calculating the flux distributions are outlined in ANL-5233.[6] The fast neutron attenuation in heavy water was obtained by using the removal cross section as reported in ORNL-1843.[7]

---

[5]Reactor Engineering Division Quarterly Report, ANL-5461 (April 15, 1955) p. 69.

[6]M. Grotenhuis, J. W. Butler, "Submarine Advanced Reactor Shield Design," ANL-5233 (February 24, 1954)

[7]G. T. Chapman, C. L. Storrs, "Effective Neutron Removable Cross Sections for Shielding," ORNL-1843 (September 19, 1955) p. 23.

DECLASSIFIED

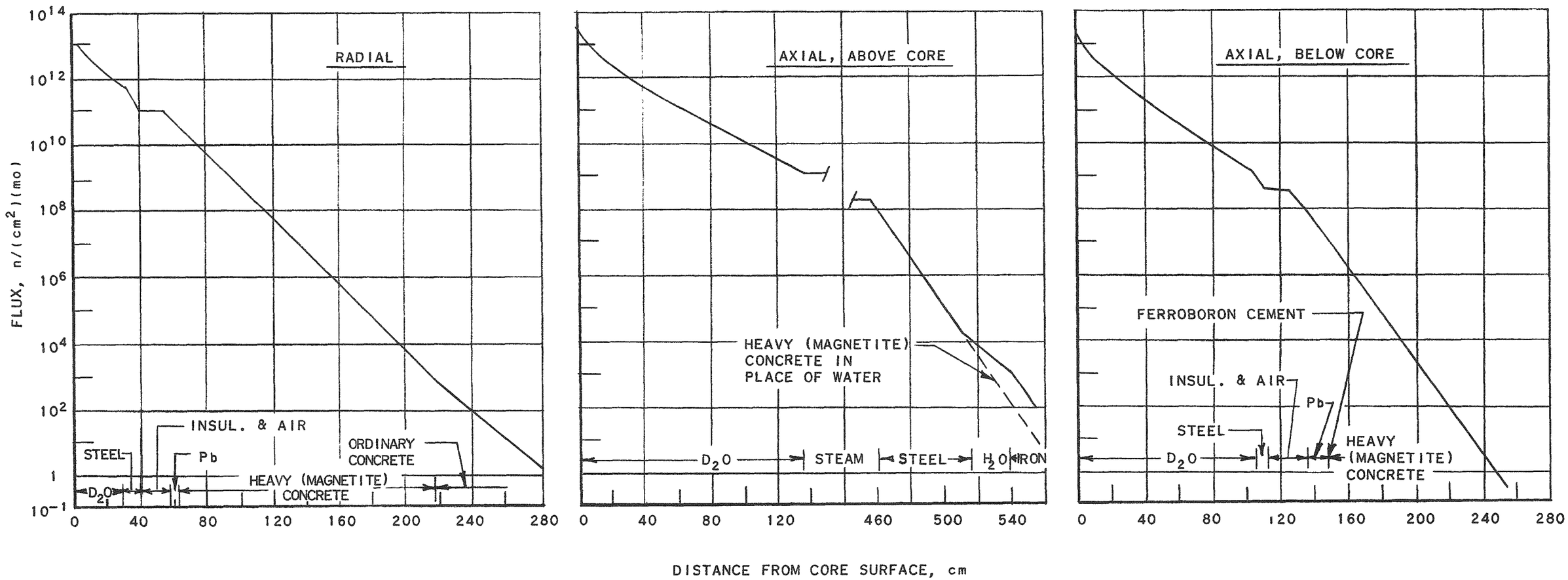

FIG. 9
CALCULATED FAST NEUTRON FLUX IN THE EBWR SHIELD

RE-7-17025-B

DECLASSIFIED
DECLASSIFIED

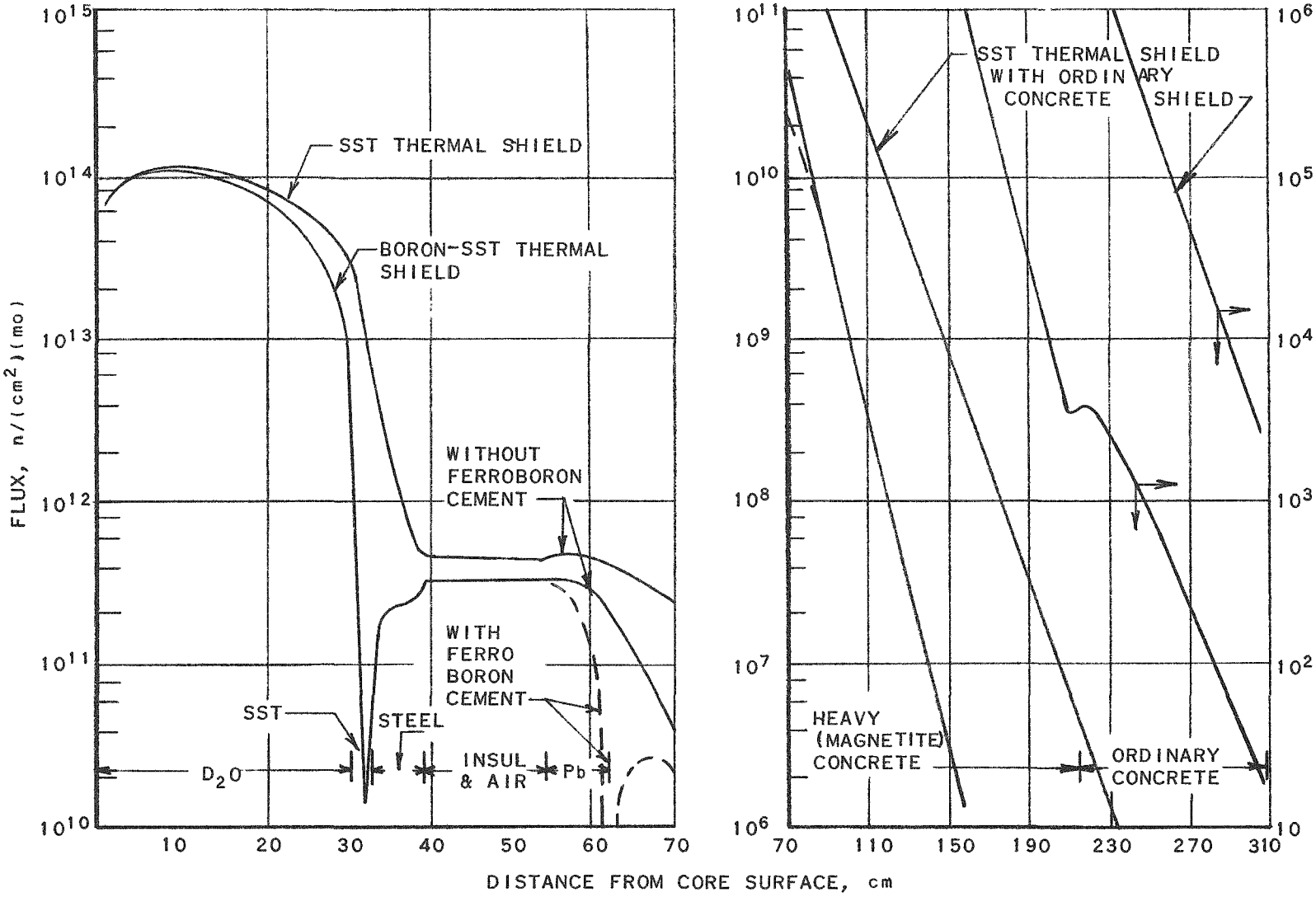

FIG. 10
CALCULATED RADIAL THERMAL NEUTRON FLUX IN THE EBWR SHIELD

RE-7-17015-A

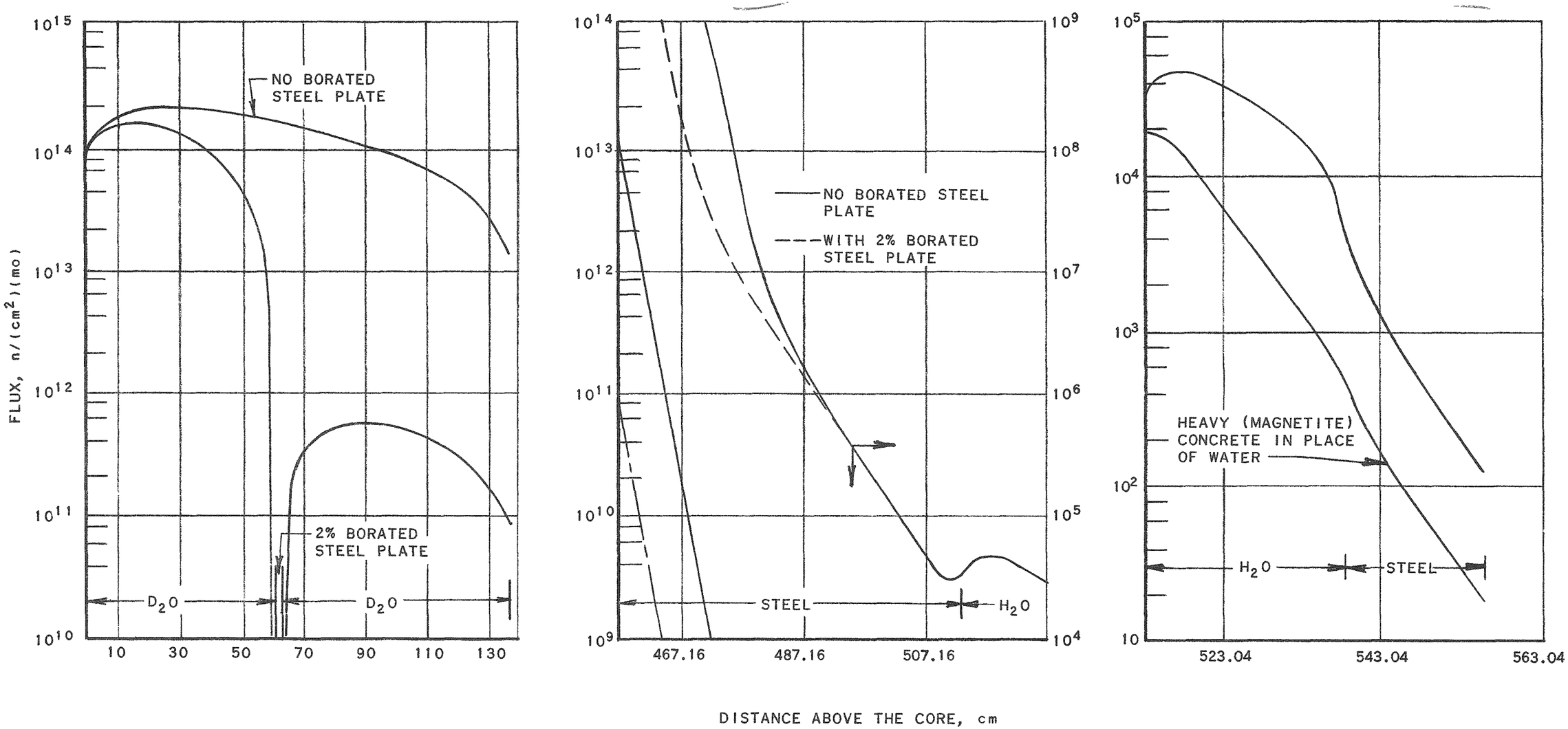

FIG. 11
CALCULATED AXIAL THERMAL NEUTRON FLUX ABOVE THE EBWR CORE

RE-7-17016-B

DECLASSIFIED
DECLASSIFIED

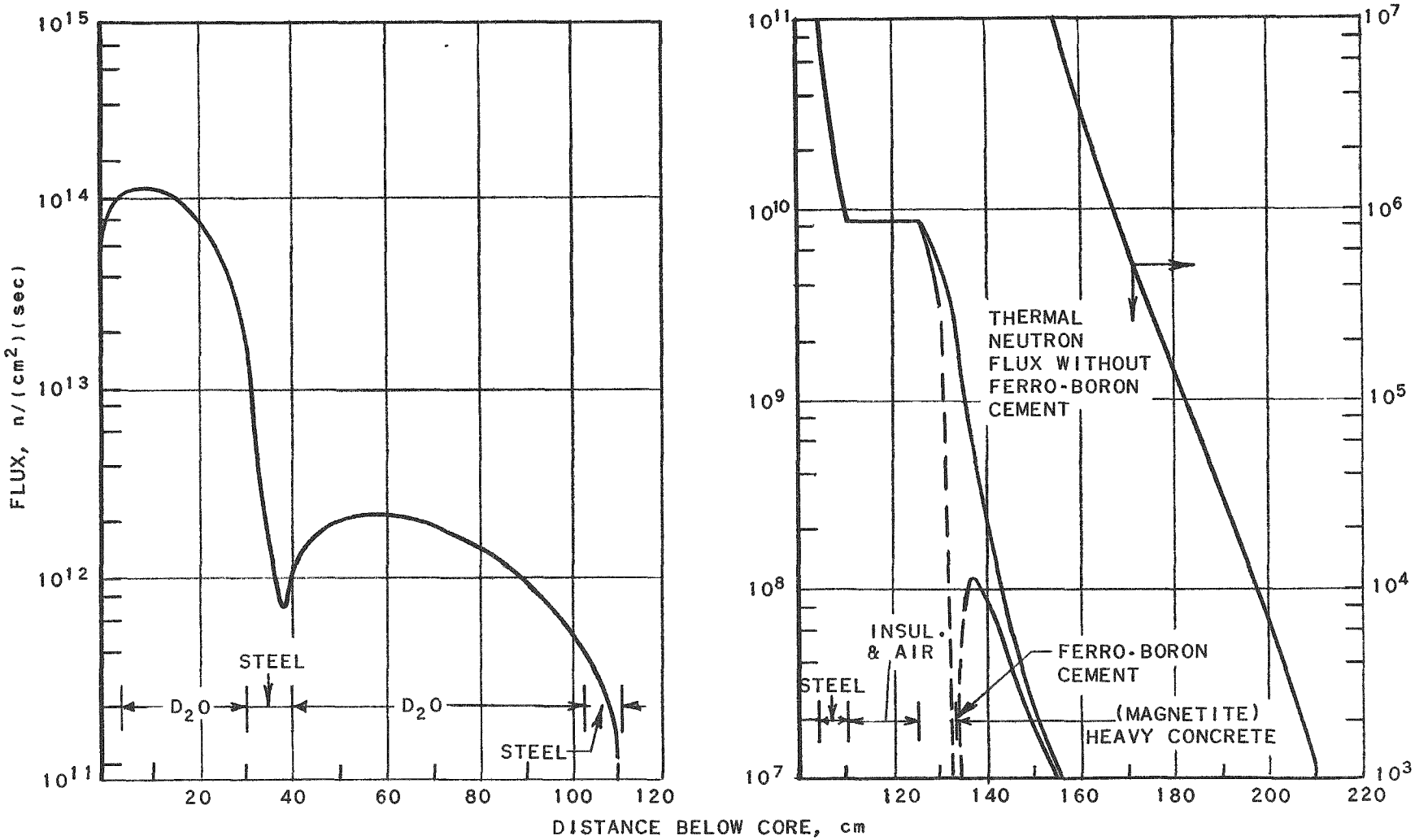

FIG. 12
CALCULATED AXIAL THERMAL NEUTRON FLUX BELOW THE EBWR CORE

RE-7-17023-A

Indications are that the thermal neutron flux distributions are less than the calculated values. The slab geometry employed would indicate this as well as other pessimistic assumptions in the determination of the source term of the thermal neutrons. Future calculations in spherical geometry are contemplated when an AVIDAC program is completed.

The flux distributions are based on a 4-ft diameter core operating at 40 mw. The vessel is designed to hold a 5-ft diameter core retaining a 1-ft thick reflector; however, the 1-foot reflector was retained with the 4-foot core as an extreme case.

The core composition assumed is given in Table IV. The shield composition along the core centerlines in the three directions is given in Table V.

Table IV

CORE COMPOSITION

(in vol-fraction)

D_2O ($\rho = 0.8$)	0.9226
$U^{235} - U^{238}$	0.03936
Zr	0.03665
Nb	0.00141

Table V

SHIELD THICKNESSES ON CORE CENTERLINES

(in inches)

	Radial	Axial Up	Axial Down
D_2O	12 ($\rho = 0.8$)	24 ($\rho = 0.66$)	12($\rho = 0.8$)
Stainless Steel	-	1 (2% B)	4
D_2O	-	29	25
Steam	-	126	-
Stainless Steel (2%B)	1	-	-
Steel	2-1/2	22	2-1/2
Insulation and air	6	-	6
Lead	3	-	3
Ferroboron Cement	1/2	-	1
Heavy (Magnetite) Concrete	60	10 (or H_2O)	48
Ordinary Concrete	36	-	-
Steel	-	7	-

DECLASSIFIED

b. Physical Arrangement - E. E. Hamer, J. H. Monaweck

The biological shielding is built up around a 3/4-in. thick carbon steel tank surrounding the pressure vessel. There is a 6-in. thick annular space between this tank and the pressure vessel, 3 in. of which is occupied by stainless steel wool insulation; the remaining 3 in. is air space. Horizontal cooling coils are attached to the outer surface of the steel tank on approximately 12-inch centers, in order to maintain the reactor shielding at reasonably low temperatures. Lead bricks, some with grooves to receive the cooling coils, are stacked around the shield tank, and molten lead is poured into the grooves to surround the cooling coils. Lead bricks (3 in. thick) are used in the lower part of the structure surrounding the reactor core; 2-in. thick bricks are used in the upper portion. A 1/2-in. thick layer of ferroboron cement is placed around the lead brick structure.

The remainder of the shielding space, between the ferroboron cement and the outer octagonal concrete (2 ft-10 in. thick) shield retaining wall, is filled with either heavy concrete or ordinary concrete, depending upon vertical elevation. At the bottom of the reactor (where it is necessary to minimize the thickness of the shielding in order to keep the control rod nozzles, which must penetrate the shielding, to a reasonable length) heavy concrete utilizing steel punchings and fine magnetite ore as the coarse and fine aggregate, respectively, is used. This formulation corresponds to a final density of 290 lb/cu ft. From an elevation corresponding approximately to the bottom of the reactor vessel itself to a point several feet above the top of the core, concrete utilizing coarse and fine magnetite ore as the coarse and fine aggregate (density 220 lb/cu ft) is used. Ordinary concrete is used for the upper part of the bulk shielding.

The shielding above the core includes the heavy steel vessel cover, and a composite shield consisting of a water tank (~11 in. thick) attached to a 6-in. thick steel plate. Above this steel plate, the heavy beams comprising the reactor containment structure also serve as shielding. All shielding above the reactor vessel is removable for access to the vessel for refueling operations.

At points up the side of the reactor vessel, where pipes must penetrate the shielding and attach to the vessel, stepped rectangular holes are left in the bulk shielding by inserting permanent forms made up of 1/4-in. thick carbon steel plate prior to pouring the bulk shielding. These permanent forms are welded at their inner end to the steel tank surrounding the vessel. Pipes are brought out from the vessel through holes in the steel tank, and after going through a triple offset to eliminate direct paths for neutron streaming, the pipes pass through the outer concrete retaining wall through larger pipes set in the concrete. The larger pipes are welded at one end to the 1/4-in. thick permanent forms and at the other end (through bellows) to the process piping. The space within the stepped

DECLASSIFIED

rectangular holes surrounding the process piping is filled with removable lead, heavy concrete, and ordinary concrete blocks. The filled holes are sealed with gasketed steel plate closures at the other face of the reactor shield.

Ferroboron cement has been incorporated in the shielding design as an inexpensive material to attenuate slow neutrons escaping from the lead gamma shield. Experiments have been carried out to determine the optimum formula for such a cement to enable it to be applied in a 1/2-in. thick vertical wall around the lead shield.

A steel support consisting of standard fence manufactured from interwoven wire (~0.11 in. dia.) was fastened to a flat vertical surface and several cement formulations containing various proportions of sharp building sand, crushed ferroboron (100 mesh), mortar cement, portland cement, and water, were applied. The following formulation appeared to give the most satisfactory result:

Building Sand (sharp)	2 lb
Crushed Ferroboron (100 mesh; 17-1/2% B, min.)	1 lb
Mortar Cement	1 lb
Water	0.151 lb.

The quick-setting property of mortar cement enabled application of a 2-foot high test area without sagging. Thorough wetting at least once after initial set was found to improve hardness materially.

5. High-Pressure Boric Acid Injection System - V. C. Hall

The high-pressure boric acid injection system is a standby emergency system to reduce the reactor core activity below criticality. The boron solution is injected if, after a scram signal, two adjacent control rods do not fully enter the core. A two-second delay is allowed for the complete insertion of control rods after a scram signal. The amount of boric acid solution which can be injected is sufficient to overcome 12-1/2% reactivity. This amounts to 4740 gm H_3BO_3 for the EBWR core.

The high-pressure tank location is inside the reinforced shield on the main floor. The injection will be through one of the four 6-in. forced recirculation inlet lines on the bottom of the reactor. The connecting lines will be 2-1/2-in. Schedule 40S stainless pipe (approximately 75 ft. long). There will be two 2-1/2-in. solenoid trip valves (RA12) and a check valve in the line at the exit of the high-pressure tank. The trip valves may actuate automatically or manually by a mechanical trip lever located inside the service building. The equivalent length of straight pipe to account for pressure drops in the valves, elbows, etc., is approximately 225 ft.

DECLASSIFIED

In order to inject the solution into the reactor, the high-pressure tank will have an air volume maintained at 1600 psig, above the liquid. During the injection this air will expand as the liquid level drops, reducing the over-all head pressure. It is assumed that the air expansion will be adiabatic, following the relationshop

$$\frac{P_1}{P_2} = \left(\frac{V_2}{V_1}\right)^k ,$$

where k = 1.56 for air at 75 atmospheres.

Assumptions which have been made to calculate the time required for solution injection are as follows:

(1)	Valves open instantaneously	
(2)	Total tank volume:	60 cu ft (450 gal)
(3)	Volume of boric acid solution:	22 cu ft (165 gal)
(4)	Volume of air:	38 cu ft (285 gal)
(5)	Initial tank pressure:	1600 psig
(6)	Pipe coefficient of friction:	0.02
(7)	Volume of pipe from boric acid tank to reactor vessel:	3.5 cu ft

In calculating the amount of boric acid required to shut down the reactor it was assumed that 3% reactivity was tied up in voids, but that sufficient boric acid should be injected to overcome a reactivity of 12-1/2%. A reduction of 3% reactivity would require approximately 4-1/2 cu ft of concentrated boric acid solution. A reduction of 12-1/2% reactivity would require approximately 18-1/2 cu ft of boric acid solution.

The following tabulation lists the amount of poison, injection time, and reactivity control effected for various operating pressures.

Operating Pressure, psi	Reactivity Control, %	H_3BO_3 Volume, cu ft			Injection Time, sec
		For Reactivity	Piping	Total	
650	3	4-1/2	3-1/2	8	4.6
650	12-1/2	18-1/2		22	26
700	3	4-1/2		8	4.8
700	12-1/2	12-1/2		22	31
800	3	4-1/2		8	5.3
800	12-1/2	18-1/2	3-1/2	22	50

DECLASSIFIED

6. Reactor Water Purification System - C. J. Zitek

After an extensive study of the water systems of various operating reactors, it was decided that no water treatment as such would be applied to the reactor water, at least for the initial operation. Operational performance and experience may indicate the need for some type of treatment to minimize corrosion and entrainment in the steam.

The reactor system will be initially filled with deionized water (not deaerated) having a specific resistance of 6 megohms (total solids about 0.2 ppm). It is imperative that the total solids (both soluble and insoluble) of the reactor water be kept at a minimum to prevent: (1) deposition of soluble and insoluble constituents from reactor water to heat transfer surfaces; and (2) excessive radioactivity build-up in the turbine and condenser system and reactor auxiliary components, i.e., steam drier, start-up heater, feed-water pumps, valves, and the piping. The preventive measures include: (a) full-flow filtration of condensate and (b) a continuous by-pass purification loop.

a. Full-flow Filtration of Condensate

Two "Fulflo" filters of 180-gpm capacity each are in parallel between the reactor feed-water pumps and the reactor vessel. Each unit contains 75 cotton thread filter cartridges, which result in a moderate loading of 2.4 gpm per cartridge. Laboratory tests have indicated that at this loading no difficulty should arise from excessive pressure drop due to packing of the cotton threads. Normally only one unit will be in operation. The second unit will be a stand-by which will be switched into the system when the differential pressure across the operating unit reaches a predetermined value indicating clogging of the filter surfaces.

The cotton thread filter cartridges are capable of removing particulate matter down to 2 to 5-micron size. It is difficult to predict what percentage of the corrosion-erosion products from the turbine-condenser system will be retained in the filter. Utility power plant operation indicates between 25 to 50% of the iron in the condensate is in the insoluble form. However, the particle size distribution is not known and the greater percentage probably is in colloidal form or constitutes particles less than one micron. There is the possibility that the cotton fibers will adsorb or exchange colloidal corrosion products and metallic ions such as Fe^{++} and Fe^{+++}; thus the effectiveness of these filter units may be greater than expected.

No attempt has been made to determine the radioactivity level that will be attained in the filter units, but it should not be high. Because of the expected low activity level these units will not have integral shielding. If the activity level does increase to a high level (10 to 20 r/hr), temporary shielding will be installed.

Removal of the "hot" filter cartridges is facilitated by having the filter cartridges in a removable cage assembly. The entire assembly will be lifted from the vessel and placed in a container for removal and ultimate disposal.

b. By-pass Purification Loop

The by-pass purification loop has a three-fold purpose: (1) maintain reactor water quality of 1-megohm specific resistance (equivalent to 0.5 to 1.0 ppm total solids); (2) afford primary clean up of reactor system after a fuel plate failure; and (3) supply normal shutdown cooling facility.

The quality of the reactor water will be maintained at 1-megohm specific resistance by continuous recirculation of a maximum of 10 gpm through the purification loop. The flow rate necessary to maintain the above water quality was calculated to be less than 5 gpm, using the corrosion data supplied by Allis-Chalmers. This corrosion data was for an Admiralty Metal-tubed condenser. Because of the change to aluminum condenser tubes - subsequent to the sizing of the loop - the 5 gpm value is probably high and the actual flow rate through the loop will probably be less than 5 gpm.

The loop will be operated at a maximum flow rate following a fuel plate failure in an attempt to remove the major portion of the contamination - uranium, plutonium, and fission product oxides and soluble compounds.

Over-all Description

Two complete systems (10 gpm each) are to be installed in parallel to afford continuous cleanup operation during renewal of components. Each loop consists of a regenerative heat exchanger, secondary cooler, pre-filter, mixed-bed ion exchange unit, after-filter and circulating pump.

Both systems can be operated simultaneously, and by proper valving, the regenerative heat exchanger, filters, and ion exchange column are by-passed, leaving only the secondary coolers and circulating pumps in the system. The secondary coolers and pumps are designed for 50-gpm capacity each and when operating at this capacity will fulfill the normal shutdown cooling requirement - dissipate 1% of full reactor power (682,600 Btu/hr). Seven hours after a normal shutdown the core decay heat amounts to 1% of full power. During the first seven hours the reactor steam will be condensed in the condenser and the reactor water temperature should drop to 212F. At that time, the above-mentioned cooling facility will be put into effect and the reactor water temperature brought down and maintained at 120F.

DECLASSIFIED

Filter Units

"Fulflo" filter units of 10-gpm capacity are used in the purification loop. Each unit contains 12 cotton thread cartridges (2-micron size) in a removable cage assembly. The loading is low - 0.84 gpm/cartridge - to prevent packing and subsequent increase in differential pressure across the unit.

The pre-filter units are expected to remove about 90% of the insoluble "crud" and to prevent plugging of the ion exchange columns during normal service. The 90% efficiency value was determined by laboratory testing using synthetic "crud" (Fe_3O_4). The ultimate size was between 0.02 and 0.04 micron but the agglomerate size was from 5 to 10 microns. During cleanup of the reactor water after a fuel plate failure, these units are expected to remove about 40% of the total corrosion products.

The after-filters are intended to remove any resin particles which may be flushed out of the ion exchange columns.

During normal service, the radioactivity level of the prefilter is expected to be as high as 30 to 40 r/hr. However, rough calculations indicate that the activity level may be as high as 400 r/hr at one meter one week after fuel plate failure. Because of the possibly high activity level, the two pre-filters are designed to have 4 in. of lead shielding as an integral part of the units. The activity level of the after-filters is not expected to be high and no shielding is planned.

Mixed-Bed Ion Exchange Unit

Two mixed-bed ion exchange units are the main components of the purification loop. Each bed is made up of 6 cu ft of highly basic anion resin (IRA-400 or equivalent) and 3 cu ft of cation resin (IRA-120 or equivalent). The mixed resins are to be contained in a removable basket assembly for ease of loading and unloading. The pressure vessel is not designed for back-flushing or regeneration of resins in place. (At the present time, regeneration of the loaded resins is not being considered.) The resin volume of these units was scaled down (by ratio of flow rates) from those being used on the production reactors at the AEC Savannah River site.

The ion exchange beds will take out all ionic impurities in the reactor water and possibly some of the finer insoluble and colloidal material which gets past the pre-filters. The effluent flow from these units is expected to have a specific resistance of 12 megohms and a pH about 7.0. No estimate can be made of the life expectancy of these units because of the variables involved. Break-through of the column will be determined by strip chart conductivity readings in the control room.

DECLASSIFIED

During normal service the activity level in these units will increase gradually to possibly 30 to 40 r/hr. Calculations indicate an increase in activity of about 10 r/hr at one meter after one week of decay due to cleanup after a fuel plate failure, assuming only 1% of the fission products are soluble and would be picked up by the resins. There is a possibility that these units will become considerably "hotter" due to filtration or adsorption of colloidal particles which pass through the pre-filter. Because of the possible high radiation level these units are designed with 4 in. of lead shielding.

Disposal of "Hot" Filter Assemblies and Resin Beds

Both the pre-filters and ion exchange units will be removed from the EBWR building for replacement of the removable assemblies. Because these units are heavy, due to the integral shielding, they are mounted on mobile carriers on rails for ease of installation and maintenance.

After a reasonable decay period, the shielded unit will be transported to the Site burial ground where the filter or resin bed will be removed and stored. The shielding vessel will be decontaminated and returned to the EBWR for reloading.

7. Feed Water Make-up System - C. J. Zitek

Two mixed-bed ion exchange units (10-gpm, 6000-gallon capacity) will supply demineralized water (not deaerated) having a specific resistance of 6 megohms and a pH of 7.0. The total solids will be below 0.2 ppm. A "Fulflo" filter unit (10 gpm) is in each of the effluent discharge pipes to protect against carry-over of resin fines or extraneous material into the reactor water system. The quality of the water from the operating unit will be recorded in the control room.

This water will be used for the initial filling of the reactor system, make-up water requirements, shield cooling system, and reactor shield flooding.

The ion exchange units are to be located in the service building basement and the effluent will be piped to a 200-gallon storage tank located on the turbine floor of the reactor building. Because of the expected low make-up water requirement, the 200-gallon storage tank will be ample. The water level in the tank will be indicated in the control room.

8. Retention Tanks - C. J. Zitek

Two 3000-gallon storage tanks, located in the reactor building basement, will be used to collect all the drainage from the

UNCLASSIFIED

various system components. The laboratory sink drainage will be collected in a 1500-gallon tank located in the basement of the service building.

When any of these tanks are full, the contents will be monitored for activity. If non-radioactive the contents will be pumped to the site sewer system. If radioactive (and depending upon the activity level) the contents will either be pumped through a portable ion exchange bed to reduce the activity level, or pumped directly into Dempster tank trucks for transport to a decontamination area for ultimate disposal.

B. Steam Plant

1. Carry-over of Radioactive Material in Steam - C. J. Zitek

The amount of activity carried over to the turbine and condenser system depends on the extent of entrainment in the steam of soluble and insoluble solids and volatile constituents in the reactor water. An extensive entrainment study was made by the Argonne Chemical Engineering Division at conditions approximating those of full-power operation of EBWR. This work was done using a nonvolatile constituent Cs^{137} Cl as the tracer. The decontamination factor (ratio of concentration of the tracer in boiler to that in the steam) varied between 1×10^4 and 4×10^4.

Calculations of the activity that will be carried over into the turbine during normal operation were made, using a decontamination factor of 1×10^3 to be on the pessimistic side; the results indicated that shielding of turbine or condenser will not be necessary.

Conditions will be entirely different after a fuel plate failure. No attempt has been made to calculate the resulting activity levels in the external steam system. All of the fission product gases and 50% of the iodine released by the fuel during corrosion will be carried over into the turbine by the steam. Most or all of the iodine is expected to condense somewhere in the turbine and either "plate" out on the turbine internals or be dissolved by the wet steam and returned to the reactor vessel in the condensate. The fission product gases are expected to be drawn out of the system through the air ejector and be discharged to the atmosphere through the reactor building vent. An AEC filter will be placed in the exhaust line to trap any particulate matter which may be inadvertently carried over.

2. Air-Drying and Fluid Recovery System - V. C. Hall, E. A. Wimunc

The system shown schematically in Fig. 13 is designed (1) to minimize in-leakage and to recover most out-leakage of radioactive gases and vapors and return this leakage to the steam system; and (2) to minimize contamination and loss of D_2O during the possible use of heavy

1. AIR & POSSIBLE VAPOR FROM HORIZONTAL TURBINE CASING SEAL
2. AIR & VAPOR FROM TURBINE SEALS & PRESSURE CONTROL VALVE
3. AIR & VAPOR FROM AIR EJECTOR AFTER-COOLER
4. AIR FROM REACTOR FEED PUMPS
5. CONDENSATE FROM AIR EJECTOR AFTER-COOLER
6. WATER FROM CONTROL ROD THIMBLE SEALS
7. WATER FROM REACTOR FEED PUMPS

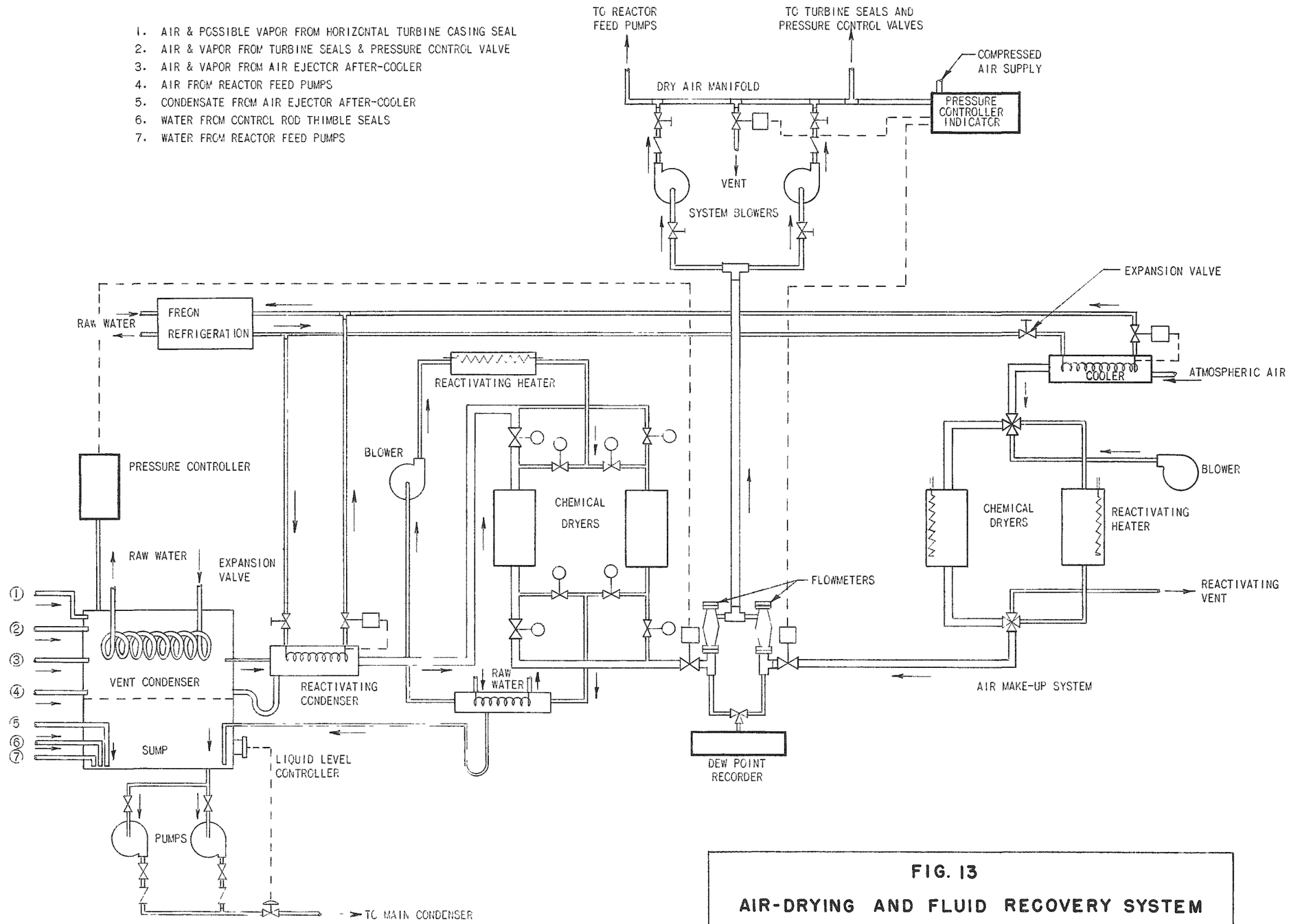

FIG. 13

AIR-DRYING AND FLUID RECOVERY SYSTEM

DECLASSIFIED

DECLASSIFIED

water as the EBWR working fluid. The system consists of two sections, one for drying atmospheric make-up air and the other for separating and recovering the working fluid and sealing air.

a. Equipment to be Sealed

Table VI shows the components that are to be sealed; Fig. 14 shows the estimated flows under normal operating conditions.

Table VI

ESTIMATED GLAND SEAL FLOWS

Item and Supplier	Air Required to Seal, lb/hr	Air to Recovery System, lb/hr	Steam to Recovery System, lb/hr
HP Turbine Gland (Allis Chalmers)	36.4	18.2	32.7
LP Turbine Gland (Allis Chalmers)	36.4	18.2	32.7
Turbine Lift Rods (2) (Allis Chalmers)	1.2	1.0	2.6
Reactor Feed Pumps (2) (Allis Chalmers)	30.0	15.0	-
Pressure Control Valves:			
By-pass Valve (Schutte and Koerting)	0.6	0.4	0.8
Relief and Regulating Valve (Foster Engineering)	0.5	0.4	0.7
Throttle Valve (Gimpel Machine Works)	1.6	1.0	7.0
TOTAL	106.7	54.2	76.5

The turbine is equipped with a shaft seal which minimizes leakage of radioactive steam to the surrounding atmosphere. The seal will consist of a labyrinth containing three annuli surrounding the shaft at the high pressure and low pressure ends. The outer annulus will be supplied with dry air at + 6 in. H_2O pressure; the inner will be supplied with system steam at 2 psig, and the center annulus will exhaust to a vacuum of - 6 in. H_2O which will collect leakage from the adjoining grooves and return it to the recovery system.

DECLASSIFIED

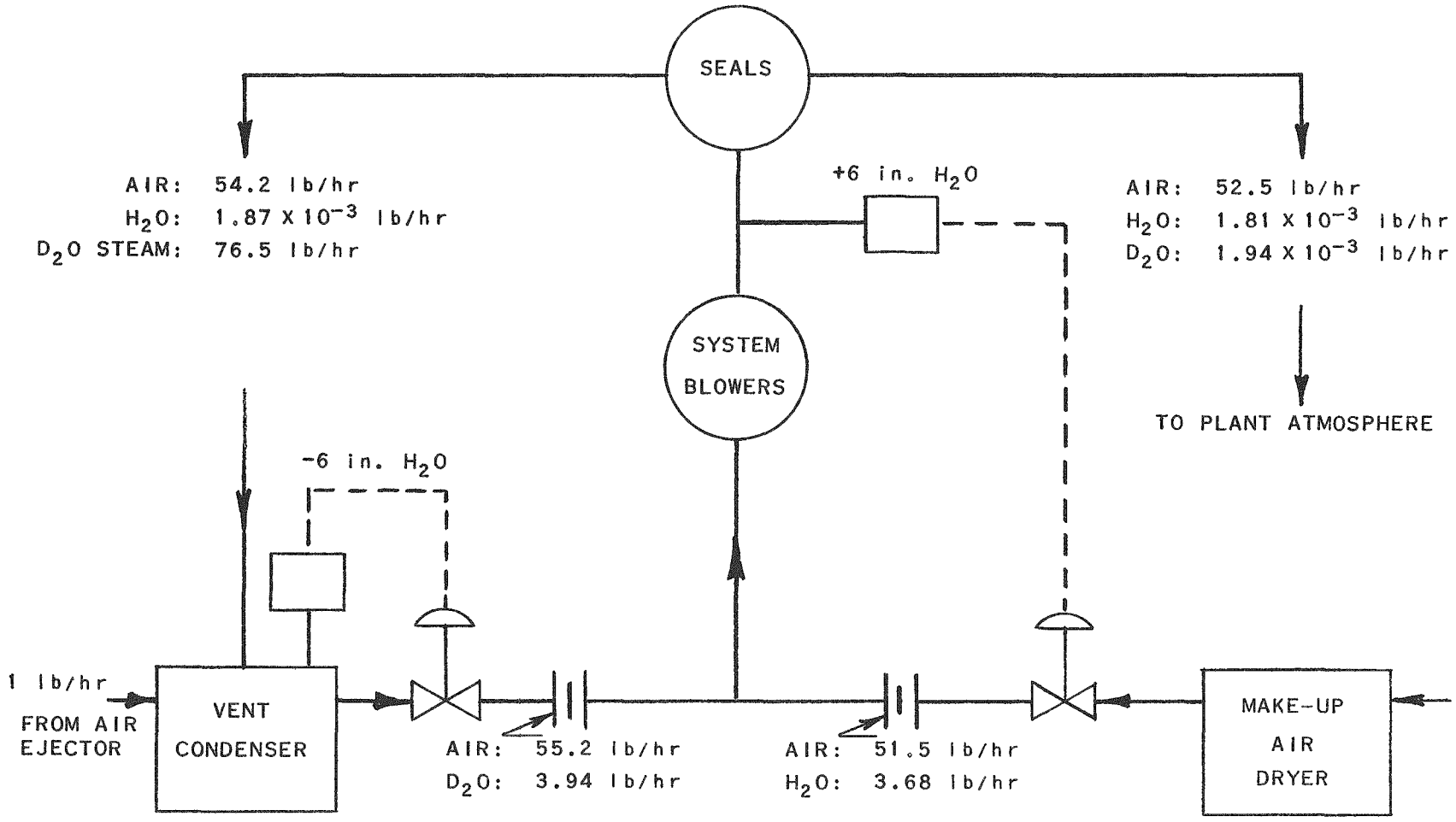

FIG. 14
ESTIMATED RECOVERY SYSTEM FLOWS
(AIR AND VAPOR)

RE-8-16932-A

In addition to these seals, the turbine is equipped with light-gage welded housings covering all flanged-and-bolted joints. A small recess cut circumferentially into the upper horizontal joint flange face is evacuated by the recovery system (-6 in. H_2O) to collect leakage. The interior of the housing flange is held at + 6 in. H_2O pressure as in the case of the shaft seals.

In addition to a mechanical seal, the reactor feed pumps are equipped with a labyrinth fluid recovery seal.

With the exception of the few special valves, pressure relief and regulating valve, the turbine throttle valve and the steam by-pass valve, all valves in the steam power plant system are of the conventional globe or gate design with welded or pressure sealed bonnets slightly modified for deep packing glands, lantern rings, and bleed-off openings. Teflon or Teflon-impregnated asbestos packing will be used in most of the valves. Although packing will be installed above and below the lantern rings initially, the bleed-off openings will not be used unless operation dictates the necessity for a collection or alarm system. Past experience indicates that packing glands hold leakage to a very low value under normal circumstances and only a careful maintenance program should be necessary.

Stem packing is used on the pressure-regulating valve and the steam by-pass valve; however, three connections are made on the gland for tying this seal to fluid recovery system.

Leakage of circulating water in the condenser around tube joints into the reactor system is prevented by providing a double tube sheet with tubes rolled into each sheet and an evacuated space between the sheets to trap and by-pass leakage. This leakage will be drained to a 6-in. pipe tank inside the 1200-gallon vacuum tank which is maintained at condenser vacuum by the air ejectors (see Fig. 15). The 6-in. pipe tank is used to collect and indicate small amounts of leakage which would be difficult to detect in the larger tank.

If the condenser tube should rupture, circulating water would mix with the system water. This leakage can be detected by checking the conductivity of the condensate in the hot well (two sides); increasing conductivity would indicate leakage. In this event the operator would close the circulating water inlet and outlet butterfly valves on the side which had indicated high conductivity. The closure of the butterfly valves will actuate a 6-in. Hills McCanna valve to dump the condenser circulating water in that half of the condenser to the 1200-gallon vacuum tank. The condenser can continue to operate; however, the condenser pressure will rise due to the decrease in cooling area. The vacuum tank can be drained to a 3,000-gallon retention tank when necessary.

DECLASSIFIED

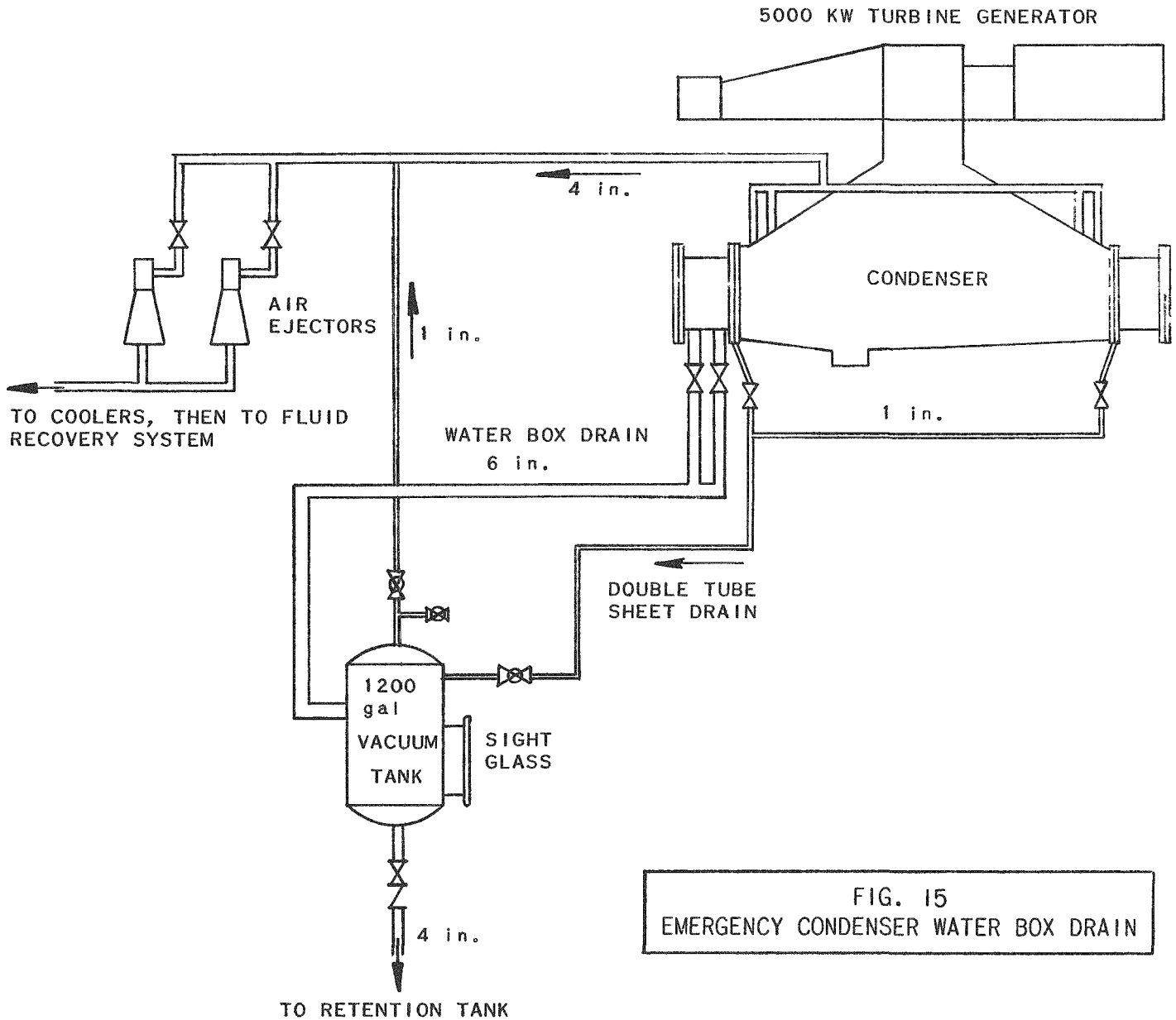

FIG. 15
EMERGENCY CONDENSER WATER BOX DRAIN

RE-8-16931-A

The conditions for the steam plant performance were set forth as maximum tolerable out-leakage of working fluid and minimum tolerable in-leakage of contamination to the working fluid:

Total loss of working fluid (D_2O) <1 lb/day;
Total intake of water from atmosphere <0.5 lb/day.

The moisture content of the circulating air or make-up air was set at 0.5 grain of water vapor per pound of dry air, which corresponds to a dew point of -40F.

The air-drying system was designed to be a tight over-all steam system. Sources of in-leakage and fluid loss are acknowledged; therefore the following measurements will be made when the system is in operation:

(1) Air in-leakage 1 lb/hr (estimated).
(2) Loss of fluid through condensation of steam in the vacuum tank.
(3) Contamination of fluid by water vapor from vacuum tank entering air ejector.
(4) Steam and fluid loss through valve stems, control rods, etc.

b. Operation

The system will deliver air at a controlled pressure of 6 in. water gage above atmosphere. It will take an air vapor mixture from the seals at a controlled vacuum of 6 in. water gage below atmosphere. These pressures will be controlled automatically, except where the total air at the suction of the working fluid recovery section exceeds the amount of air necessary to maintain the set system pressure. This condition will occur when the air-ejection rate from the power facilities exceeds the air leakage rate from the seals and glands (initial hogging). An automatic relief valve will prevent over-pressure during this time.

A vent condenser consisting of a primary section cooled by raw water will be capable of condensing and cooling a 250F water vapor and air mixture (150 lb/hr of vapor and 150 lb/hr of air) to a final saturated condition of 120F, and a secondary section cooled by mechanical refrigeration that will further cool and dehumidify to a saturated temperature of 40F. The vent condenser is equipped with a system sump capacity of 50 gallons to which all condensate from the "fluid recovery" portion of the system will drain.

A sump pump will be required to return the condensate to the main condenser during startup and shutdown, at which time the main condenser is not under operating vacuum conditions. However, it may be possible to turn off the sump pump during normal operation to take advantage

of the free flow of the working fluid due to the pressure differential between the sump tank (- 6 in. H_2O) and the main condenser (2.5 in. Hg abs.). A selector switch starts either of the two sump pumps in the system. The normal level in the sump tank is controlled by a Fisher Governor Type 2500-259 Level-Trol column-type liquid level controller. This unit would control a 1-1/2-in. Fisher-type 555T diaphragm motor valve. The level control is independent of the operation of either sump pump.

A high-level Magnetrol float switch is provided to start both sump pumps should the level rise too high above the normal level position. These pumps will cycle until one pump is selected by the operator for continuous operation. Actuation of the high-level switch will signal an alarm in the control room to warn the operator of an abnormal condition.

C Instrumentation, Control, and Electrical Power System.

1. Nuclear Instrumentation Facilities - E. E. Hamer

Six facilities for nuclear instrumentation are provided in the EBWR structure. Four of these facilities (for ion chambers) are through holes (6 in. dia.) tangent to the lead shield surrounding the reactor vessel. Two holes are located on the north side of the vessel at elevations 1 ft above and 1 ft below the core midplane. The other two holes are located on the south side at identical elevations. The holes are stepped at each end to accommodate stepped shield plugs, and are sloped downward slightly toward the east face for drainage.

Two blind radial holes (for fission chambers) are located on the west side at an elevation paralleling the core midplane. The holes are 4 in. in diameter, with provision for stepped shield plugs, and are sloped toward the reactor face for drainage.

A chain hoist support structure is provided above the holes on both east and west faces of the reactor to facilitate removal of the shielding plugs as circumstances warrant.

2. Electrical Power System - F. Verber

Figure 16 is a schematic plan view of the EBWR power plant and control areas. The electrical distribution and control equipment are located in the basement of the service building. Adjacent to this building is the outdoor-type substation which houses the 4160-volt switchgear, the Main Power Transformer, and the Reserve Auxiliaries Supply Transformer.

DECLASSIFIED

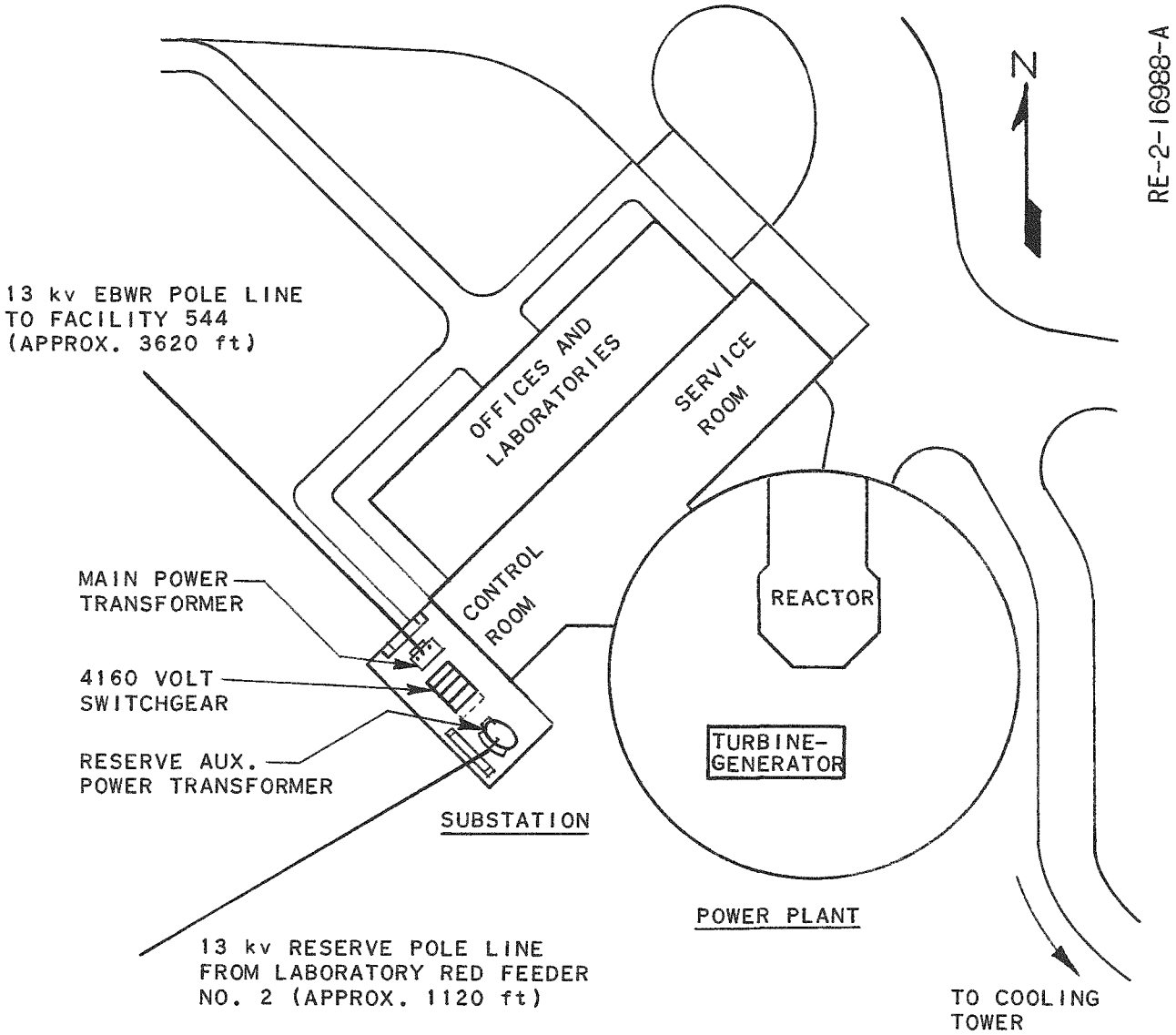

FIG. 16
SCHEMATIC PLAN VIEW OF EBWR POWER
PLANT AND CONTROL AREAS

DECLASSIFIED

a. 4160-volt Circuits

With reference to the simplified line diagram in Fig. 17, the 5,000-kw generator output is brought directly to the 4160-volt, 3-phase, 60-cycle main bus of the outdoor substation switchgear through a 1200-ampere, 3 P.S.T. generator air circuit breaker. A 1200-ampere circuit breaker is provided for the main power transformer (5000/6250 kva) for delivery of the generator output (minus the EBWR auxiliary power demand) to the Laboratory 13-kv power distribution system.

The auxiliary power requirements of EBWR are served from the 4160-volt bus through a 1200-ampere breaker and 750/1000-kva main auxiliary power transformer.

It should be noted that the Laboratory power distribution system (13 kv) is used to provide power for the various auxiliary circuits when the generator is not in operation.

b. 4160-volt Switchgear

The 4160-volt switchgear is of the outdoor, metal-clad type with vertical lift air circuit breakers, equipped with solenoid operators and shunt trip coils for 125-volt, d-c operation. The 3-phase interrupting capacity of the circuit breakers is 150,000 kva at 4160 volts. The 3-phase short circuit kva at the 4160-volt bus is approximately 92,500 when the EBWR facility is connected to the north bus section of Facility 544.

c. Reserve and Emergency Auxiliary Power Supplies

To provide power supply for the various auxiliary drives in the event of loss of the 13-kv pole line circuit to Facility 544 (when the generator is not operating) and/or loss of the 750/1000-kva main auxiliary transformer circuit, a 750/862-kva reserve auxiliary transformer is incorporated in the design. The transformer will furnish power to the 480-volt, 3-phase, 60-cycle bus via the south bus section of Facility 544.

In normal operation the 480-volt bus will be fed from the 750/1000-kva main auxiliary transformer. Loss of voltage on the bus will initiate operation of under-voltage relays on the 480-volt switchgear bus to effect automatic tripping of the circuit breaker designated "M" in Fig. 17 and, after a delay of approximately one second, will initiate closure of circuit breaker "R" and restore power to the 480-volt bus. A selector switch is included on the Electrical Auxiliaries control panel (in the Control Room) to interchange the function of the main and reserve power supplies.

DECLASSIFIED

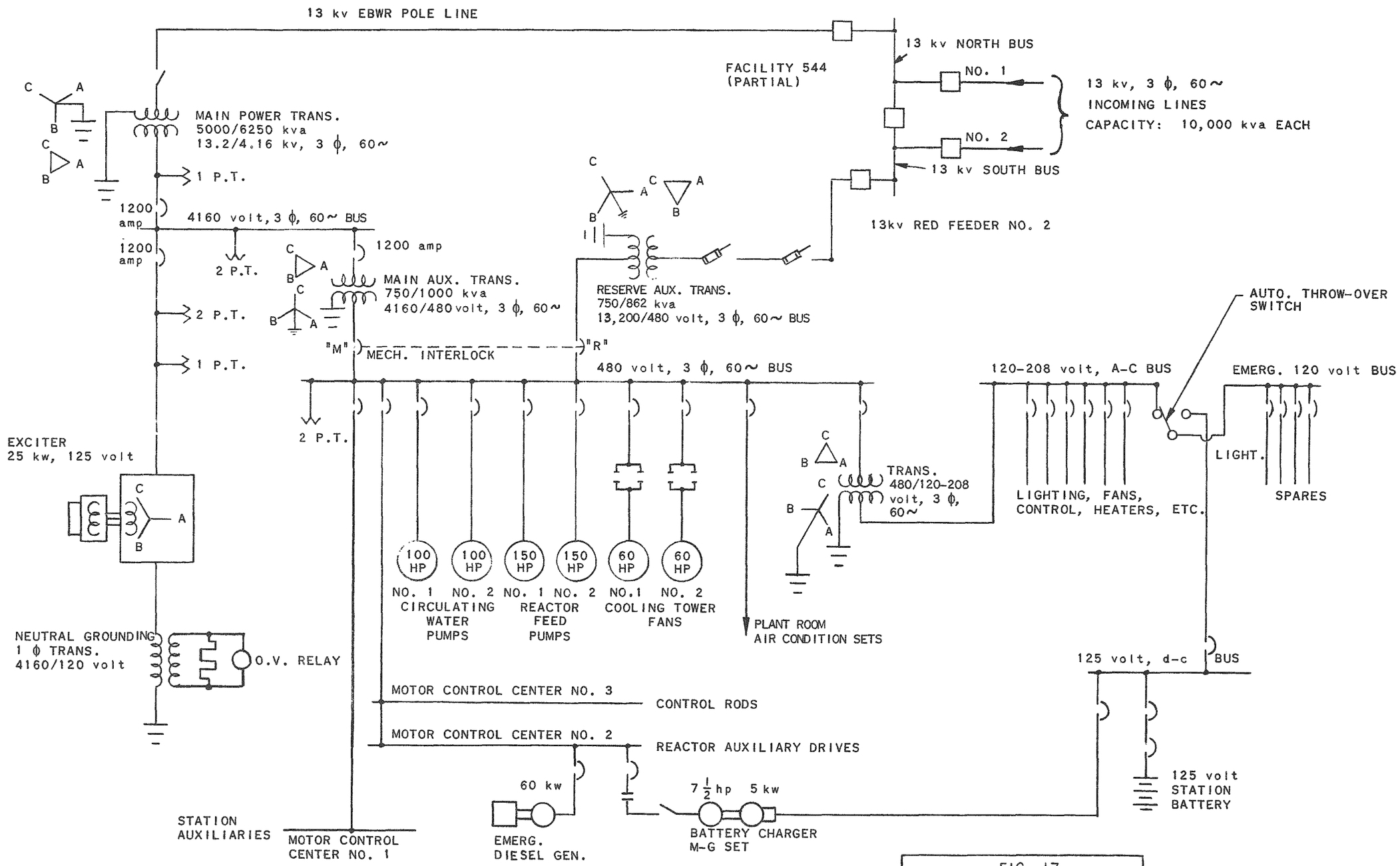

FIG. 17
SIMPLIFIED LINE DIAGRAM OF
EBWR ELECTRICAL SYSTEM

RE-8-17047-B

DECLASSIFIED
DECLASSIFIED

A 60-kw, 480-volt, 3-phase, 60-cycle diesel generator set provides emergency power for the reactor control rod drives, essential system instrumentation, valves, and some auxiliaries, including the fluid recovery system equipment, cooling water system pumps and shield water circulating pumps. Control is arranged to initiate automatic starting of the diesel generator set following approximately 4 seconds of sustained loss of voltage on the 480-volt bus and will restore voltage to motor control centers Nos. 2 and 3 within ten to fifteen seconds.

To provide continuity of emergency lighting, an automatic throw-over switch is included to transfer the emergency lighting circuits to the 125-volt, d-c bus. Transfer will occur immediately upon loss of voltage on the 120-208 volt bus, but will return automatically to the a-c bus position with restoration of power on the same bus.

d. Auxiliary Loads

Figure 18 shows, in block diagram form, the connected h.p. and the 1-hour kw loads for the various distribution centers of the EBWR facility. The values shown include the loads within each block, but do not include loads on the feeders which radiate therefrom. A total demand of 662 kw on the main 480-volt, 3-phase, 60 cycle bus leaves approximately 4300 kw of the power generating capability available for delivery to the Station Facility 544 and from there to the power distribution system and/or the purchased power system. A 662-kw auxiliary demand would represent 13.24% of the generator's kw rating.

D. Building

1. General - A. H. Heineman

The excavation for the power plant building and the service building was completed early during this report period, and all footings were poured. Fabricated material for the power plant steel shell was delivered to the EBWR site during the latter half of August. Actual assembly of the steel shell was started early in September.

Design drawings for all features of the connecting piping, access tunnels, removable shielding, lead shielding, cooling coils, top and bottom shielding, vessel support and containment structure, vessel envelope seals and vent, thermocouple locations, instrument wells, and constituency of the biological shield immediately surrounding the reactor vessel were completed and turned over to the architect-engineers for incorporation into their engineering drawings and specifications.

DECLASSIFIED

NOTE: CONNECTED H.P. AND kw VALUES INCLUDE LOADS ON RADIAL FEEDERS EXCEPT WHERE FEEDERS ARE SHOWN

TOTAL CONN. H.P.:	1080
TOTAL 1 hr kw DEMAND:	662
TOTAL 1 hr kva DEMAND:	746

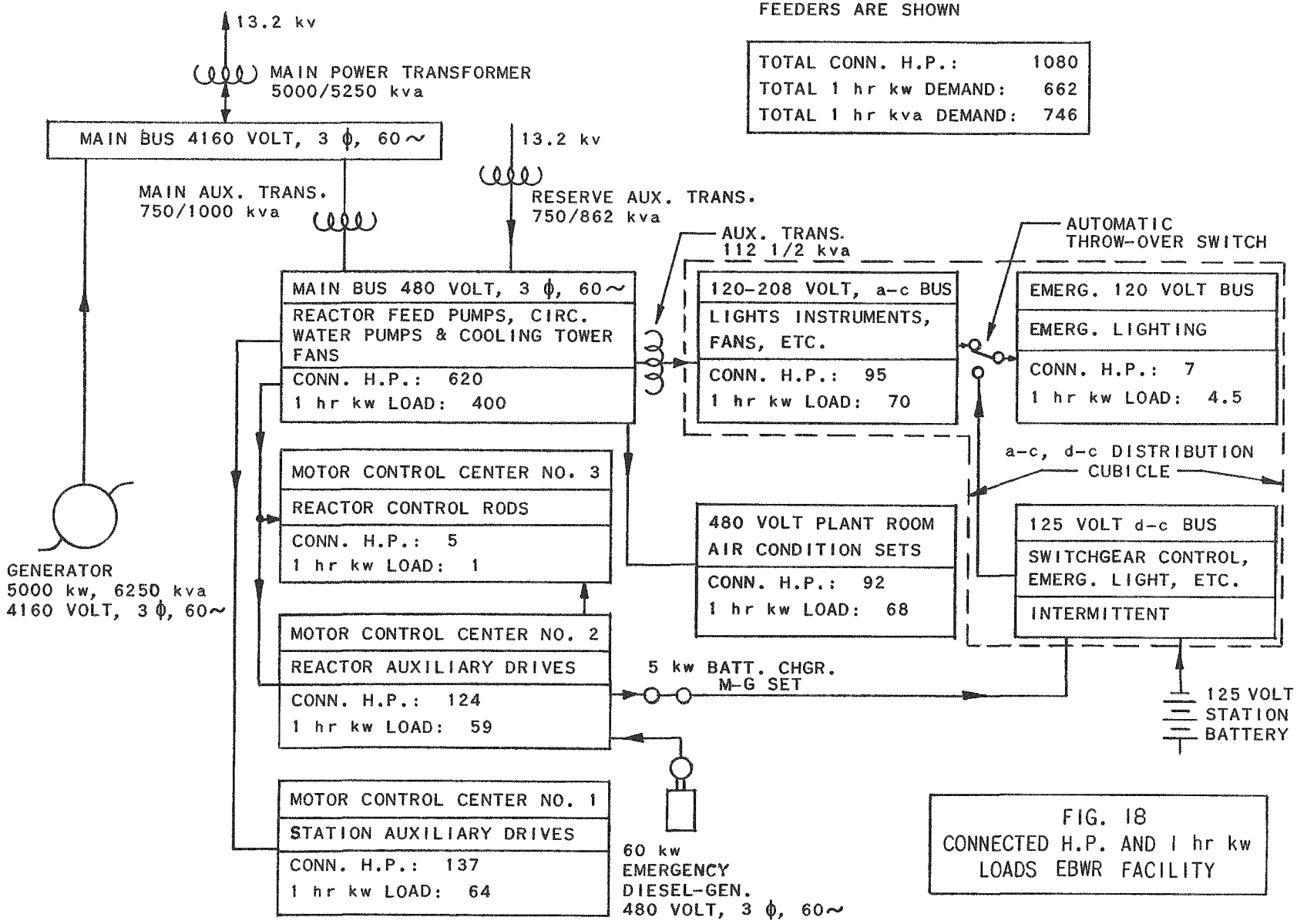

FIG. 18
CONNECTED H.P. AND 1 hr kw LOADS EBWR FACILITY

RE-8-16993-A

2. Emergency Air-Lock Doors - J. N. Young

The design of the emergency air lock has been completed and submitted to the building shell contractor for detailing and fabrication. A schematic drawing of the emergency air lock is shown in Fig. 19.

The operation of the mechanism is completely manual; however, the door and valve interlocks are mechanical and positive acting. Features of operation are listed below:

(1) One door is clamped shut at all times; both doors may be in the clamped shut position at one time.

(2) The pressure-equalizing valve connecting the air lock to the building is closed when the outer door is unclamped, and the valve connecting the air lock to the outside is closed when the inner door is unclamped.

(3) Each door is unclamped from the inside by pulling a lever away from the door. This closes and clamps the other door. The outer door is opened from the outside by a handwheel. The inner door cannot be opened from the outside under ordinary circumstances.

(4) In an emergency a man with a key is able to enter the building through the emergency air-lock door by unlocking the lever inside the air-lock enclosure.

(5) The air lock is air-tight for building pressure of from -0.5 to +15 psig.

(6) A vacuum of more than 2.0 psig inside the air-lock enclosure will be relieved to prevent damage to the mechanism.

(7) The valves and doors have adjustments for tightness.

(8) The mechanism has sealed ball bearings and requires no lubrication.

(9) A uniform clamping pressure of 10 pounds/inch is applied to the door gaskets.

DECLASSIFIED

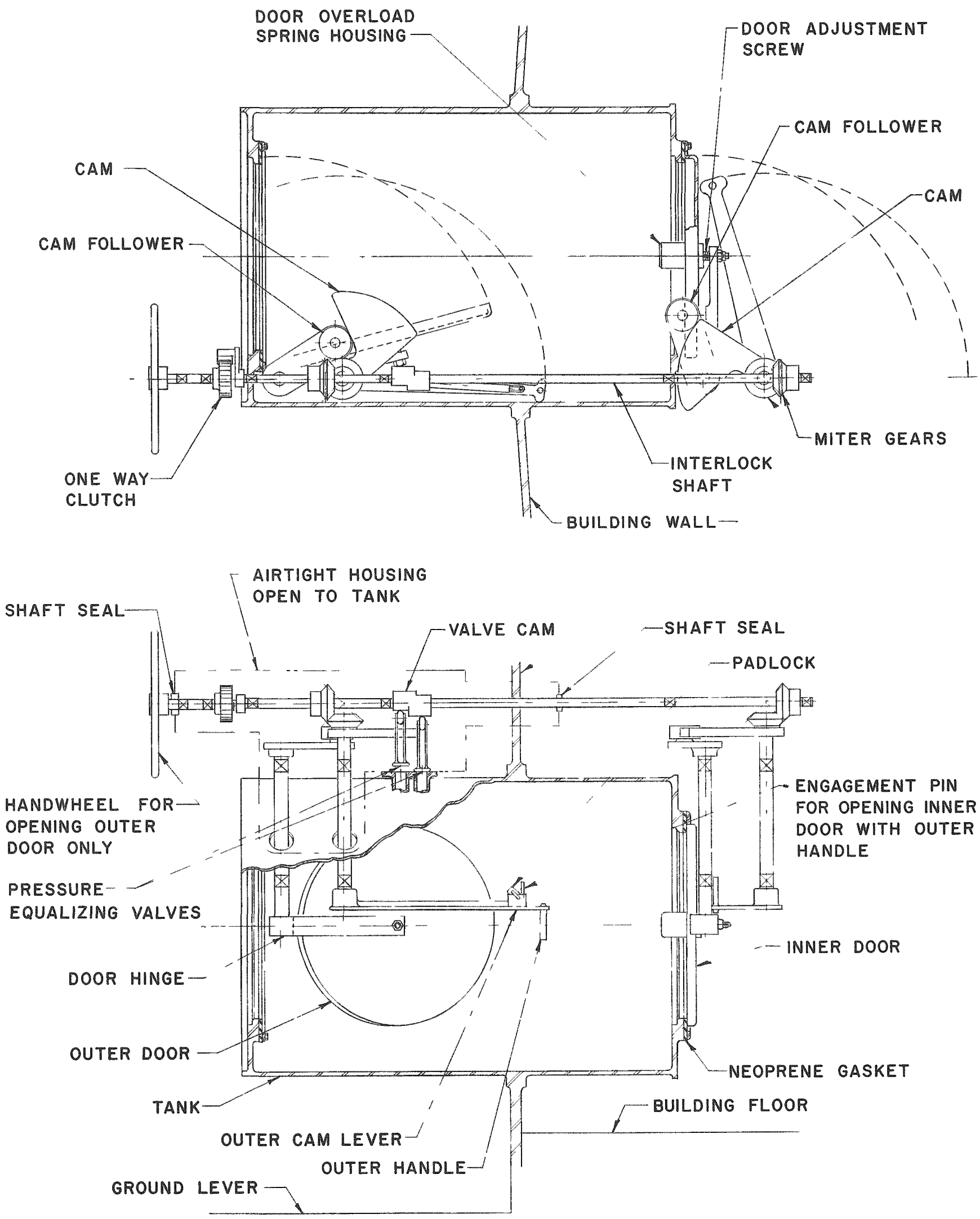

FIG. 19
SCHEMATIC OF EMERGENCY AIR-LOCK DOORS FOR EBWR

II. SUPPORTING AND ALTERNATE DESIGN RESEARCH AND DEVELOPMENT

A. Alternate Methods of Operation of EBWR - S. A. Bernsen, R. J. Rickert

It has become apparent that significant gains in the specific power of boiling reactors might be achieved with forced circulation. It is also felt that greater stability and safety might be reached with a D_2O-moderated and cooled boiling reactor, along with greater economy in the larger sizes planned for eventual central station power plant use. For this reason, the present EBWR, which is primarily a light water natural circulation reactor, has been modified in order to permit future experimentation with both forced circulation and D_2O operation. In order to achieve these goals, components which may not be changed in the system, such as the reactor vessel and shielding, are designed to meet the requirements of all the above types of operation.

The vessel and shielding design necessary for the multipurpose requirements are virtually complete and are described above. However, the nature of the core structure, fuel elements, and control rods (except for rod penetration pattern) have only been pursued far enough to assure that the present system can be adapted to future plans.

1. Forced Circulation - H_2O

The change to forced circulation will be accomplished by placing a circular shroud around the core support plate. This shroud will seat on a machined ring on the bottom head of the vessel and will be bolted down to the support plate to form an inlet plenum chamber. The coolant will enter the chamber through four 6-in. nozzles located outside the control rod nozzles, and will flow up through the core area defined by the dummy fuel elements and possibly by a circular shroud ring around the core. The recirculated water then flows down outside the shroud and out of the vessel through two 12-in. outlet nozzles located opposite each other just above the bottom head of the vessel.

The inlet nozzles penetrate the biological shield vertically and enter the control rod drive area below the reactor vessel, where at present the lines terminate in blind flanges. (Auxiliary use is made of three of the nozzles for connection of the ion-exchange system, high-pressure boron injection system, and startup heater system to the reactor vessel. In this way vessel penetrations are minimized.) When the change to forced circulation is made, the nozzle flanges will be connected by a manifold system and led out of the sub-reactor room to a pump area outside the lower extension of the outer ordinary concrete biological shield. The number and the nature of the pumps have not yet been established; however, the total pumping capacity will be approximately 10,000 gpm with a maximum head of 100 ft.

DECLASSIFIED

A reasonably low NPSH (approx. 5-15 ft) will be required. With these specifications the present EBWR core should deliver about 30-35 mw at the same void fraction as 20-mw natural circulation operation. However, since an improvement in reactor stability should be achieved with forced circulation, the average operating steam void fraction may be increased and a total reactor power in excess of 40 mw may be feasible.

The more significant aspects of forced circulation will be realized in operation with a smaller core diameter. The available pumping head should be sufficient to increase the coolant velocity through the core by a factor of at least 4 with an average steam void fraction in excess of 20%. Under these conditions the reactor power density could be increased possibly five-fold over the natural circulation value of about 26 kw/liter of coolant. At these high power densities the burnout heat flux factor would be limiting for the present fuel elements.

2. Heavy Water Design

Heavy water reactors have always been attractive for large-scale power producers, primarily in the aspect of high neutron economy. Moreover, the large neutron lifetime is attractive from the standpoint of safety and stability, the latter being particularly important for boiling operation. In order to evaluate the effect of D_2O in a boiling reactor, the EBWR system is designed to handle a 40-mw D_2O core of size similar to the present H_2O core. Both the thermal and biological shielding have been designed to meet the more stringent requirements of the D_2O reactor shielding. Present specifications on permissible leakage from the external system are adequate for use of D_2O. The fuel-handling coffin and shielding for fuel element removal have also been designed for the higher power density in the fuel and the lack of a water shield above the core during fuel inspection and unloading.

All items within the reactor vessel in which a change might be required in order to permit revisions in core structure, core position, and fuel assembly, have been designed to be removable and replaceable. Only the locations of control rod penetrations through the lower head of the reactor vessel are unchangeable. The latter does not appear to be a serious limitation, since there are a number of lattice arrays that can be located in the present control rod pattern. Specifically the items that may undergo a change in size, shape and location are:

(1) Lower Support Plate

(2) Fuel Elements and Assemblies

(3) Control Rods and Guides.

DECLASSIFIED

Additions which will be required in any case are:

(1) Process tubes around fuel assemblies to separate the fuel zone from the moderator zone.

(2) An upper support plate (boron-stainless steel in part) to align process tubes and to shield the upper portion of the reactor vessel walls from heating because of thermal neutron capture gammas.

Certain aspects of the heavy water design have been established:

(1) Natural circulation does not appear worthwhile because of the lower resultant core power density in a lumped fuel-type reactor. The D_2O core would have somewhat less than half the volume filled with fuel elements, and hence the core power density may only be 10-15 kw/liter of core with natural circulation. A 500-mw core would require about 33,000 - 50,000 liters of volume, or roughly a core 12 ft in diameter and 12 ft high without reflector, if a 10 - 15 kw/liter power density could be applied to a 12-ft high core. Actually, it is felt that the maximum power output of a natural circulation channel is only slightly dependent on its height once above 2 - 4 ft, and hence the core power density of a 12-ft high core may only be 4 - 6 kw/liter.

(2) In a boiling D_2O reactor, the void fraction for a given steaming rate and the void coefficient in the moderator are high. Therefore, the sudden creation of voids in the moderator (possibly as the result of a small reduction in pressure) can shut the reactor down to such an extent that there is considerable potential for initiation of an excursion when the voids collapse. For this reason it is desirable to operate with the moderator slightly subcooled. This may easily be achieved, in forced circulation operation, by passing a fraction (10% maximum) of the circulated coolant directly into the moderator space, with the fuel element coolant separated from the bulk of moderator. The shroud designed for the H_2O forced circulation will be adequate for separating the moderator zone of the D_2O reactor from the downcomer area.

(3) The present H_2O design has too much stainless steel close to the top and bottom of the active core to utilize the benefits from D_2O as a reflector in these directions. If the axial D_2O reflector is desired, it will be necessary to replace the stainless steel structure with zirconium for at least 1 ft above and below the core, to increase the distance between the support plate and the active core, and to drive the control rods a greater distance out of the top of the core for the "full out" position.

(4) The present fuel assemblies are adequate, but not ideal, for a D_2O design because of plate thickness and excessive metal-to-water ratio. A new fuel element consisting of thinner plates and less metal per unit volume would enhance the performance.

DECLASSIFIED

B. Boiling Heat Transfer Studies

1. Multi-Channel Natural Circulation Boiling Density at 600 psig - W. H. Cook, J. F. Marchaterre

The preceding quarterly report[8] contained a summary of steam void fraction (α) data obtained for variable inlet temperature operation of the 600-psig Boiling Density Test Facility. These data have been extended by a series of variable inlet velocity runs where the flow to the heated channels was restricted and in a series of variable system pressure runs. Data are summarized in this report entirely on the basis of the ratio of steam-to-liquid velocity (C_s/C_ℓ), which is a function of steam void fraction, quality and the steam-to-liquid density ratio.

The following range of variables was covered:

Power density	0 - 50 kw/liter of H_2O
Inlet subcooling	0 - 30 F
Pressure	100 - 600 psia
Steam void fraction (α)	0 - 0.78
Exit steam weight fraction	0 - 0.14
L_B/L, fraction boiling length	0.30 - 1.0

In the previous quarterly report the variable inlet temperature data for voids was characterized by an isometric plot of average voids and the parameters L_B/L, $W_T h_{fg}/Q_T$. Average C_s/C_ℓ values may be plotted with the same parameters as shown in Fig. 20. From this isometric plot constant boiling length lines for possible reactor operating conditions may be obtained. A curve with L_B/L equal to 0.65 (the EBWR boiling length), valid between velocity limits of 1.0 and 1.8 fps, is shown in Fig. 21.

Figures 22, 23, and 24 are plots of exit values of C_s/C_ℓ to show the effects of variable inlet temperature, power, flow and pressure upon the velocity ratio.

Figure 22 shows a curve of C_s/C_ℓ vs velocity for saturated inlet conditions, as well as lines of constant power and inlet temperature. At saturated inlet conditions, data at various power levels and flows plot well on the single saturated curve shown. Maximum spread of data from this curve is ± 20%. Data at lower inlet temperatures show a series of curves

[8] Reactor Engineering Division Quarterly Report - Section II, ANL-5471 (September, 1955) p. 80.

DECLASSIFIED

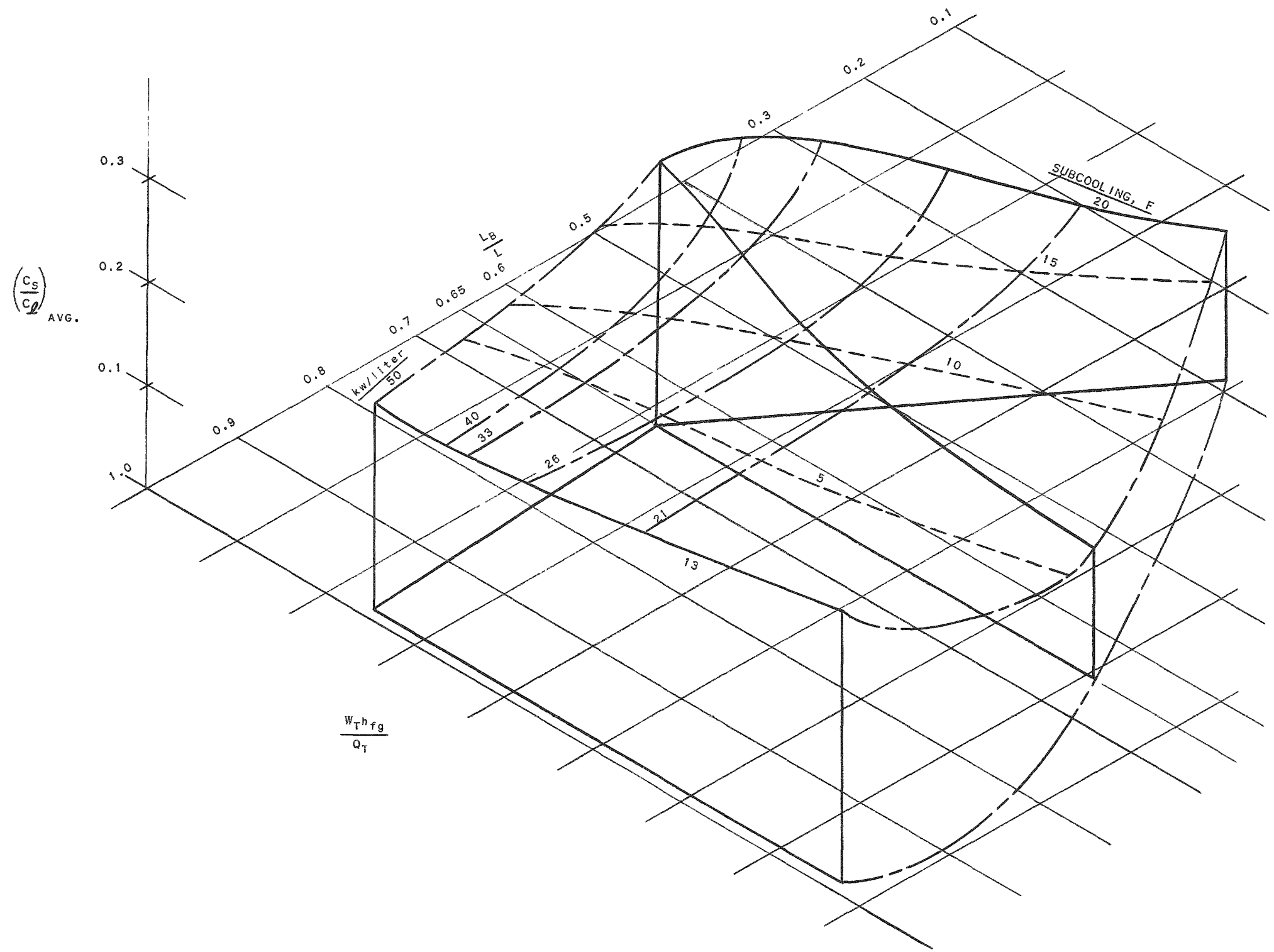

FIG. 20

ISOMETRIC PLOT OF $\left(\frac{C_S}{C_\ell}\right)_{AVG} = \phi\left(\frac{L_B}{L}, \frac{W_T h_{fg}}{Q_T}\right)$ FOR MULTICHANNEL SECTION AT 600 psi

RE-6-17019-C

DECLASSIFIED

DECLASSIFIED

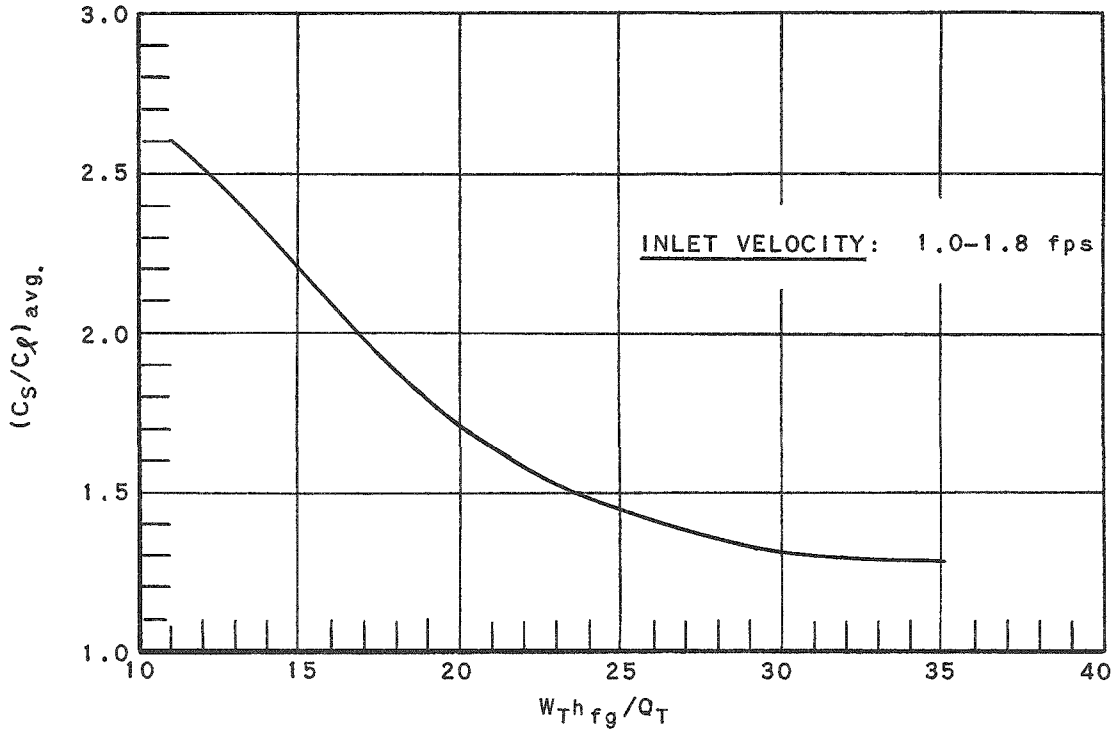

RE-7-16992-A

FIG. 21
$(C_s/C_\ell)_{avg}$ VS $(W_T h_{fg}/Q_T)$ FOR $L_B/L = 0.65$

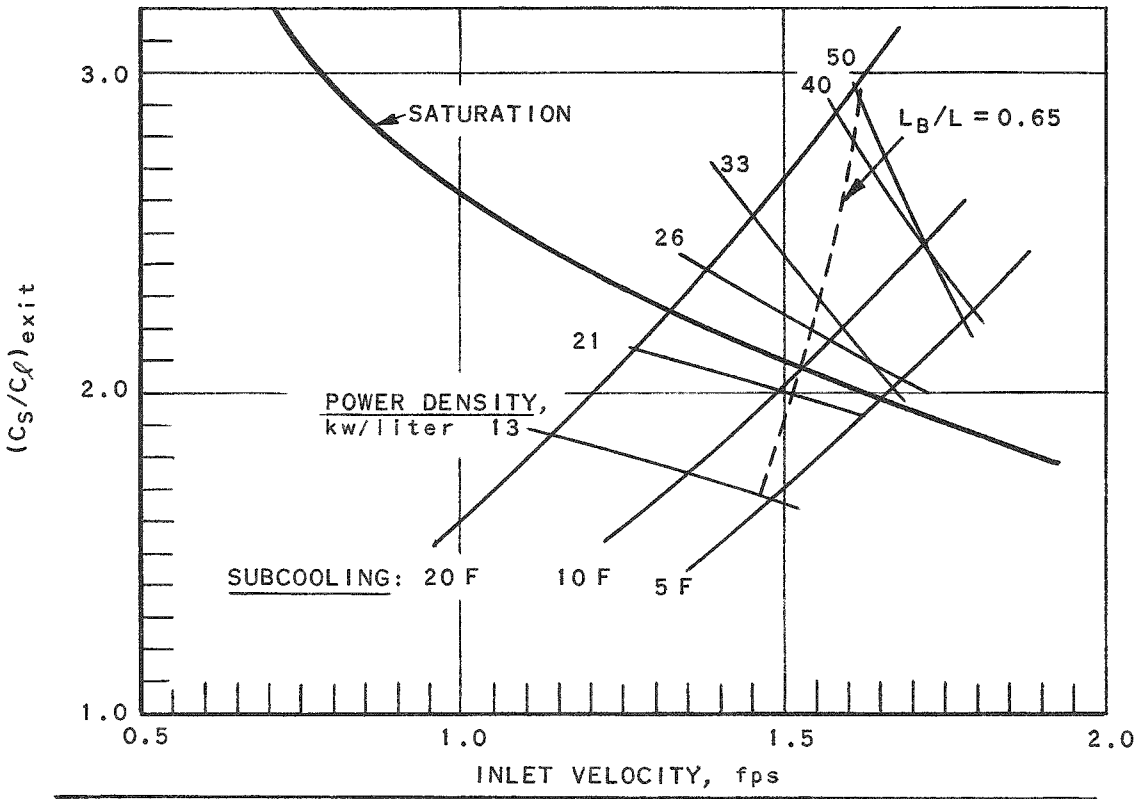

FIG. 22
EFFECT OF SUBCOOLING ON EXIT (C_s/C_ℓ) FOR VARIOUS POWER LEVELS

DECLASSIFIED

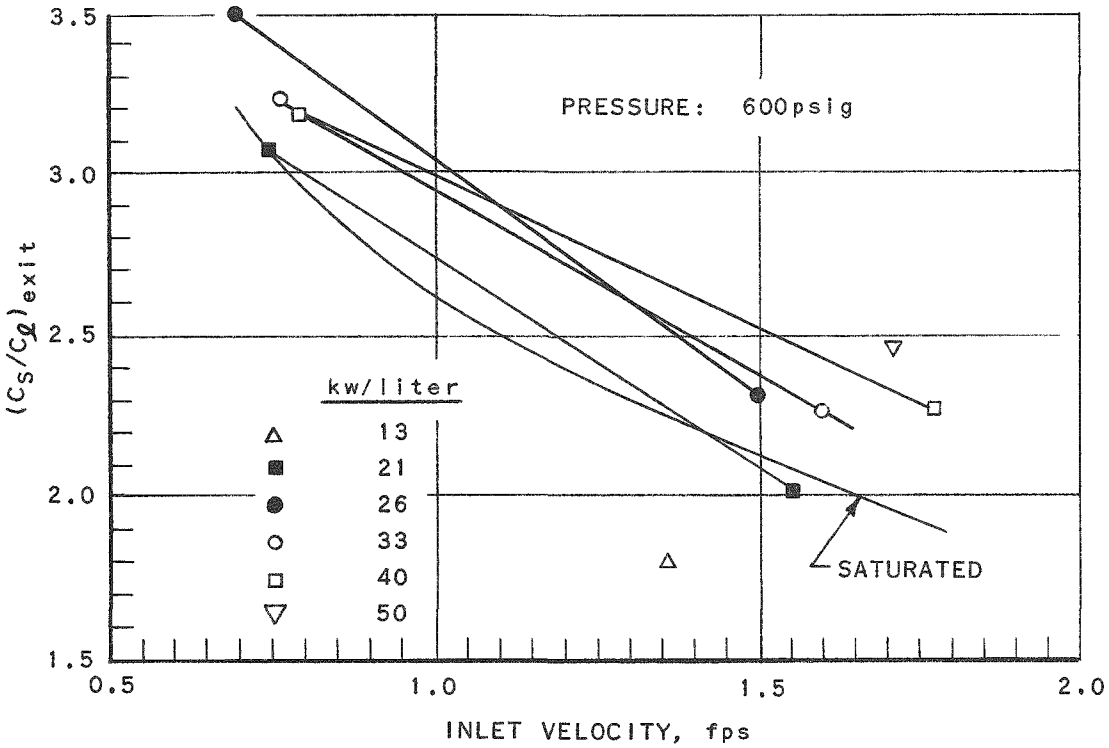

FIG. 23
EFFECT OF INLET VELOCITY ON $(C_s/C_\ell)_{exit}$ FOR 10 F SUBCOOLING WITH CURVE FOR SATURATED DATA

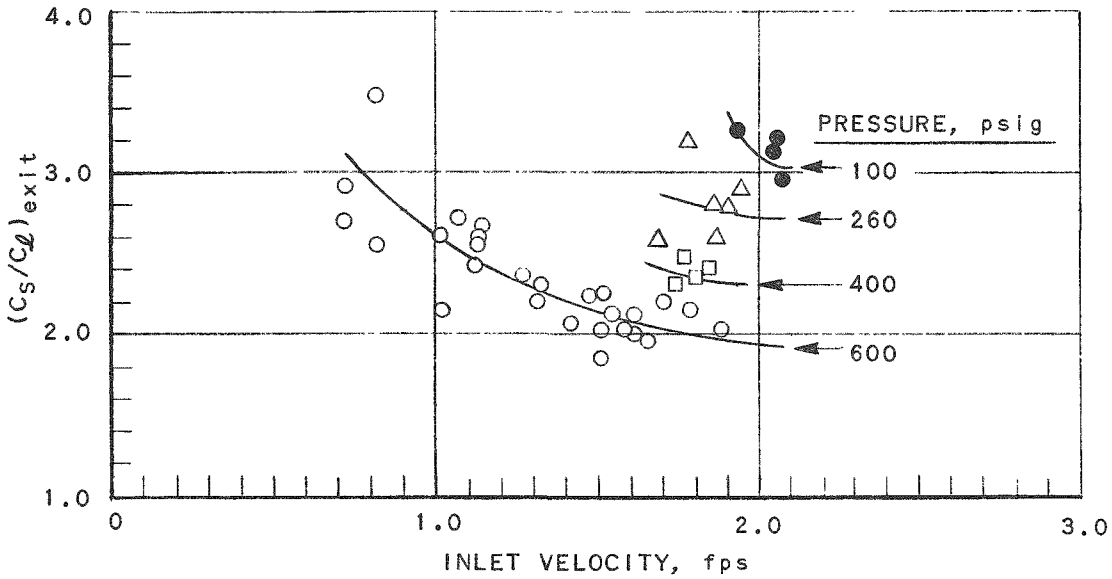

FIG. 24
EFFECT OF PRESSURE ON $(C_s/C_\ell)_{exit}$ AS A FUNCTION OF INLET VELOCITY

DECLASSIFIED

at each power level and at each subcooling which vary from the curve considerably. This effect is shown in plots of local C_s/C_ℓ values vs length of channel. For runs where saturation conditions exist, C_s/C_ℓ is relatively constant along the channel length and the relationship is repeated for any inlet velocity. However, this is not true for runs with lower inlet temperature where local C_s/C_ℓ values change along the length of the channel and rise, depending on the power level, to different values at the channel outlet. It appears that this behavior may be explained on the basis of shortening of the boiling length, giving a different distribution of bubble sizes in each case.

A line of $L_B/L = 0.65$ has also been plotted on Fig. 22; this shows a very rapidly increasing C_s/C_ℓ with very little increase in velocity.

The extent to which lowering the inlet temperature affects exit C_s/C_ℓ values appears to be affected by the inlet velocity. For inlet velocities greater than 1.0 fps the relation shown in Fig. 22 exists with respect to lowered inlet temperature. When the velocity is reduced to 0.75 fps and inlet subcoolings of 10F are compared, it is seen (Fig. 23) that the data at low velocities cluster very close to the saturated curve. When plotting the local values of C_s/C_ℓ against channel length it is seen, for these low velocity runs, that the curves approach the saturated curves both in value of C_s/C_ℓ at exit and in the fact that the variation along the channel length is the same as the saturated values. The difference in results at the two velocity levels is apparently closely related to boiling length, since the boiling lengths of low velocity runs approach those of the saturated data while those for higher velocities are considerably shorter.

The effect of system operating pressure upon exit C_s/C_ℓ values is shown in Fig. 24. The effect of pressure reduction is to increase the value of C_s/C_ℓ.

2. Single Channel Unrestricted Circulation Boiling Studies - W. S. Flinn, P. A. Lottes, R. J. Weatherhead, H. H. Hooker, M. Petrick

Analytical and experimental studies are being made of the 600-psi, unrestricted, single-channel circulation loop (Armadilla) shown in Fig. 25. The purpose of these studies is to determine the effect of channel height (2 to 5 ft), channel spacing (1/2 to 1/8 in.), system pressure (150 to 600 psig), inlet test section velocity (1/2 to over 3-1/4 fps), and power density (16 to about 500 kw/liter) on natural circulation and forced circulation boiling.

DECLASSIFIED

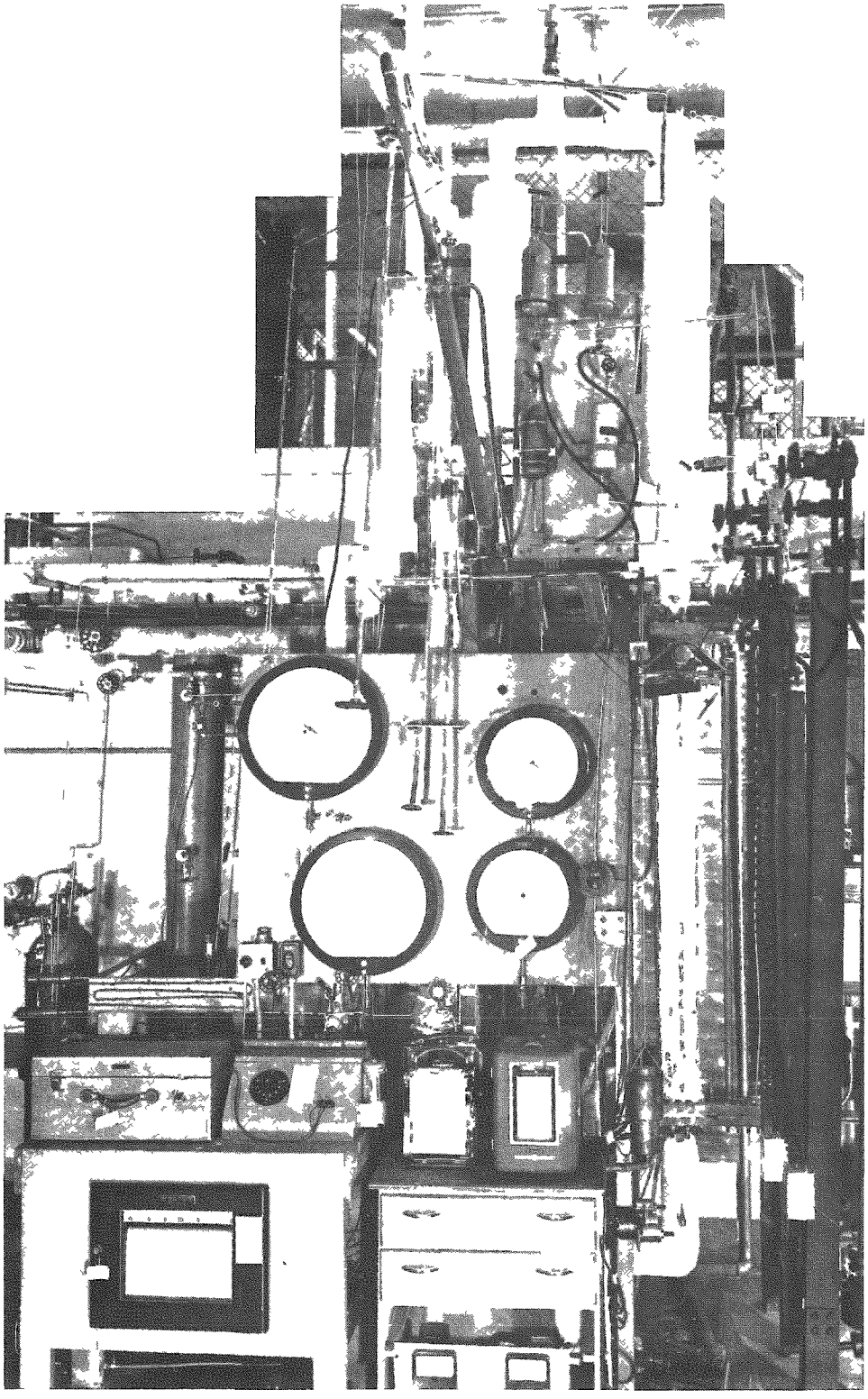

FIG. 25
600 psi UNRESTRICTED SINGLE CHANNEL
CIRCULATION LOOP (ARMADILLA)

DECLASSIFIED

a. Experimental Equipment and Procedure

The relationship of the test section, riser and remainder of the loop is shown schematically in Fig. 26. It can be seen that this open cycle is identical with the type of system that exists in a regular boiling reactor. The most important single feature of this arrangement is that a constant boiling length is automatically maintained for a given system pressure and make-up water temperature regardless of the power density or inlet velocity.

With reference to Fig. 26, the steam discharge and make-up water flows are both measured. Test section flow is measured in the downcomer by means of a venturi section. All of this flow goes through the single 1/2 x 2 in. flow passage in the test section. Voids are measured by means of a thulium oxide source and photomultiplier tube arrangement along the channel length.

Test Section and Riser

The single, rectangular channel test section is 1/2 x 2 in. in flow cross section and 60-1/2 in. long. It is made of stainless steel (1/10 in. thick) and is heated by passing an a-c current through it. Two 5/8-in. thick, insulated back-up plates support the 2-in. span portion under pressure. The test section and support plate arrangement are illustrated below. Heat generation is uniform along the section length and the heat flux at the 1/2-in. edge surfaces is the same as the heat flux over the surface of the 2-in. sides. Higher local heat fluxes exist in the corners of the channel. The cross section of the major portion of the 29-in. riser is approximately that of a halved 2-in. diameter circle.

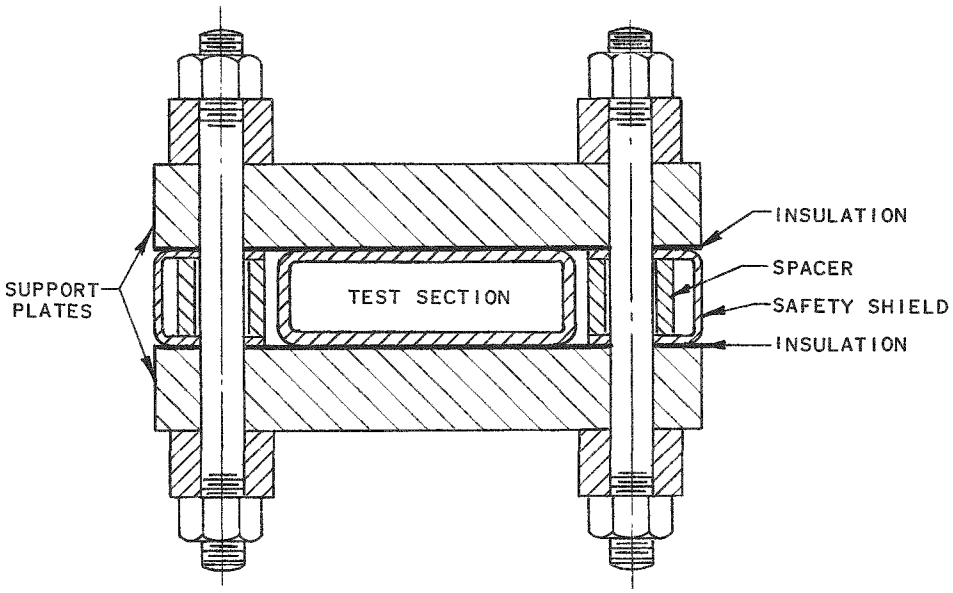

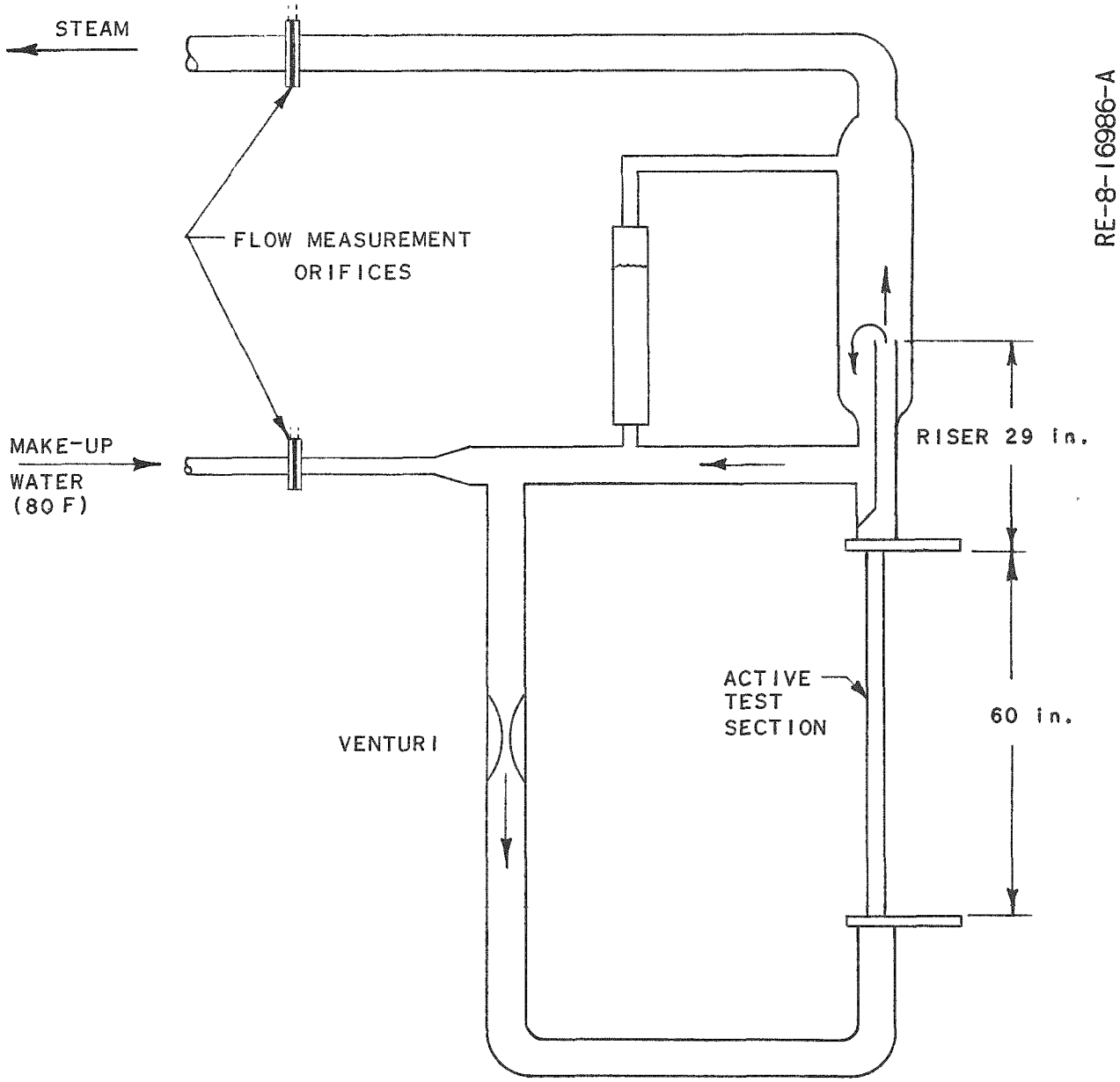

FIG. 26
SCHEMATIC OF ARMADILLA TEST LOOP

DECLASSIFIED

Because all of the venturi-measured flow goes through the section and the riser, velocities and qualities are known quite accurately, since all of the heat goes into this one channel. Another reason that a single channel is quite desirable from an experimental viewpoint is that the test section, support plates, and void measuring device can be integrally connected so that there is less chance of an over-all relative shift that might affect void readings. Also, all void readings are representative of exactly one channel.

Void Measurements

As previously mentioned, void measurements are measured using a radioactive thulium oxide source and a photomultiplier tube pickup. The source-pickup assembly is mounted on a traversing carriage driven along the channel length by a motor.

Recirculating Flow

The recirculating flow piping is 2 in. in diameter, giving a flow area that is 3.14 times the maximum test section (1/2 x 2 in.) flow area. The corresponding pressure drop is quite low.

The calibrated venturi is 1 in. in diameter at its throat. Even though the pressure drop in the recirculating piping is extremely low, there is essentially no increase to this recirculating loss due to the venturi. In all of the runs completed thus far, the maximum venturi pressure drop loss (at a test section velocity of 3.2 fps) was about 1/4 in. H_2O. This was less than 1% of the net driving heat of the system. Venturi readings were made using an inclined manometer and using a fluid with a specific gravity of 1.25. This gave 4 in. of reading for every 1-in. signal from the venturi.

Steam and Make-up Flow

Calibrated orifices are used to measure both the steam discharge flow and the make-up flow. Steady-state conditions of testing exist when, at a constant system pressure, the make-up flow and the steam flow are equal. A steady liquid level reading at the sight glass serves as an additional check for equal flow conditions. These flow readings also give a separate check of the calculated exit quality of the test section.

Temperature and Pressure Measurements

Temperature measurements are made with calibrated iron-constantan thermocouples that have a solid 1-1/4-in. long copper hot junction end mounted on a stainless tube. Calibration of thermocouples is within $\pm$ 0.1F. Pressure measurements are made using calibrated Heise gages. The system pressure is held within about $\pm$ 1/2 psi (max.) during a run.

b. Results

The initial test results on the single channel test section (1/2 x 2 x 60-1/2 in.) are plotted in Fig. 27. Preliminary void data are not included owing to malfunction of some auxiliary equipment of the void-measuring system. The data are based on a constant boiling length approximately the same as the average EBWR boiling length.

c. Analytical

Analyses of the power requirements for arbitrary values of exit void fraction have been made to determine if the Martinelli-Nelson[9] two-phase friction factor ratios, or some variant thereof, can be used to predict the performance of Armadilla at pressures of 150 and 600 psi. Initial assumptions, based on preliminary data from Armadilla and data from previous vertical boiling channel facilities, were slip ratios of 1.5 and 2.0 for 600 and 150 psi, respectively, an isothermal friction factor 20% greater than that for smooth tubes, and chimney void fractions equal to

$$\alpha_c = \frac{1}{\frac{A_c/A_{ex}}{\alpha_{ex}} - \frac{(A_c - A_{ex})}{A_{ex}}}$$

where

α_c = chimney void fraction

α_{ex} = exit void fraction of heated channel

A_c = chimney flow area

A_{ex} = heated channel flow area .

Calculations using the Martinelli-Nelson two-phase friction factor ratios yielded performance predictions approximately 10-30% greater than the data values. Use of a modified Martinelli-Nelson factor, approximately twice the previously used value, resulted in a velocity prediction agreeing closely with the Armadilla data, as shown in Fig. 27.

Plotting of the modified Martinelli-Nelson factors as a function of slip ratio and exit and local void fraction, as shown in Figs. 28 and 29, indicates an insensitivity to pressure, particularly in the 100-1000 psi range. The curves were obtained by cross-plotting from the Martinelli-Nelson curves - the point values of R and $\overline{R}$ are twice the Martinelli-Nelson values, and exit and local void fraction were calculated from exit and local steam quality for slip ratios applicable to the 150-600 psi range. (It should be emphasized that the points shown are the results of cross-plotting and

[9]R. C. Martinelli and D. B. Nelson, "Prediction of Pressure Drop During Forced-Circulation Boiling of Water," Trans. ASME 70, 695-702 (1948).

DECLASSIFIED

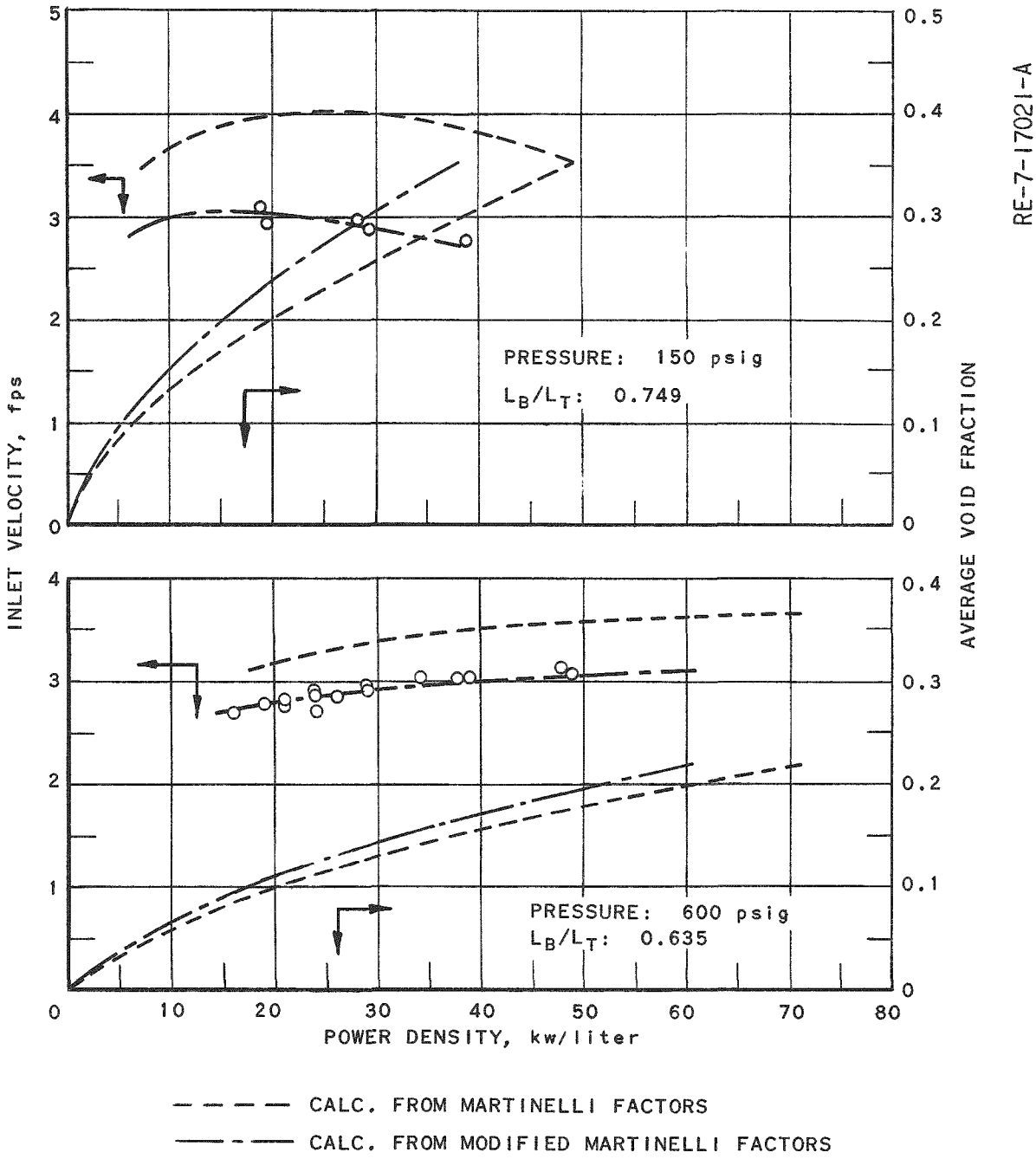

RE-7-17021-A

FIG. 27
COMPARISON OF CALCULATED WITH
ACTUAL PERFORMANCE OF ARMADILLA

DECLASSIFIED

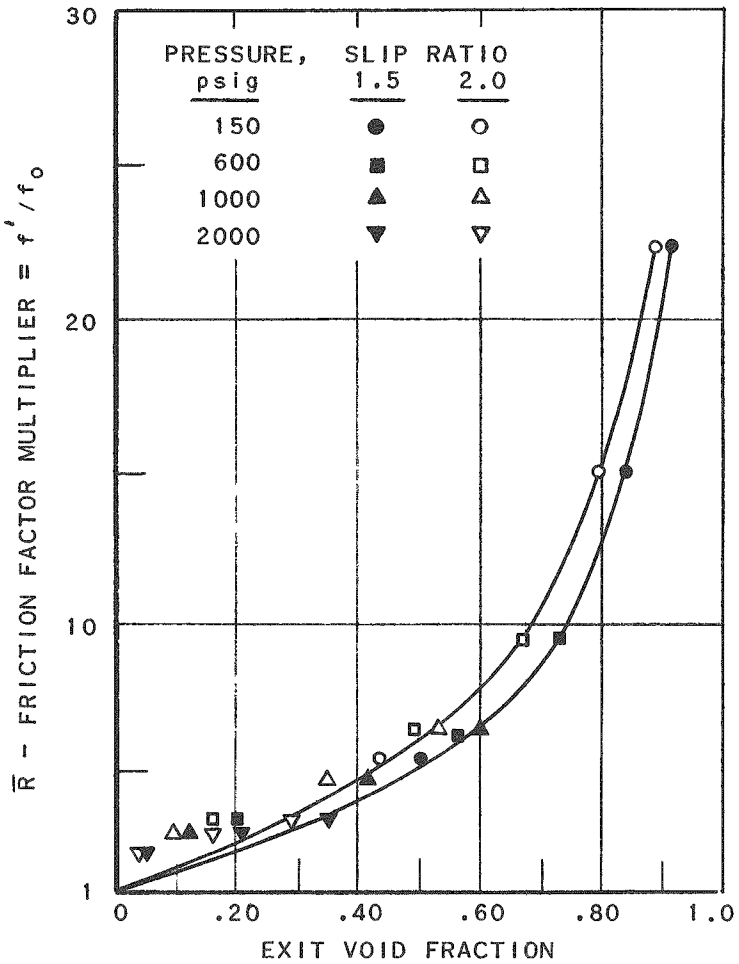

FIG. 28
MODIFIED MARTINELLI-NELSON BOILING FRICTION FACTOR RATIO AS A FUNCTION OF EXIT VOIDS AND SLIP RATIO

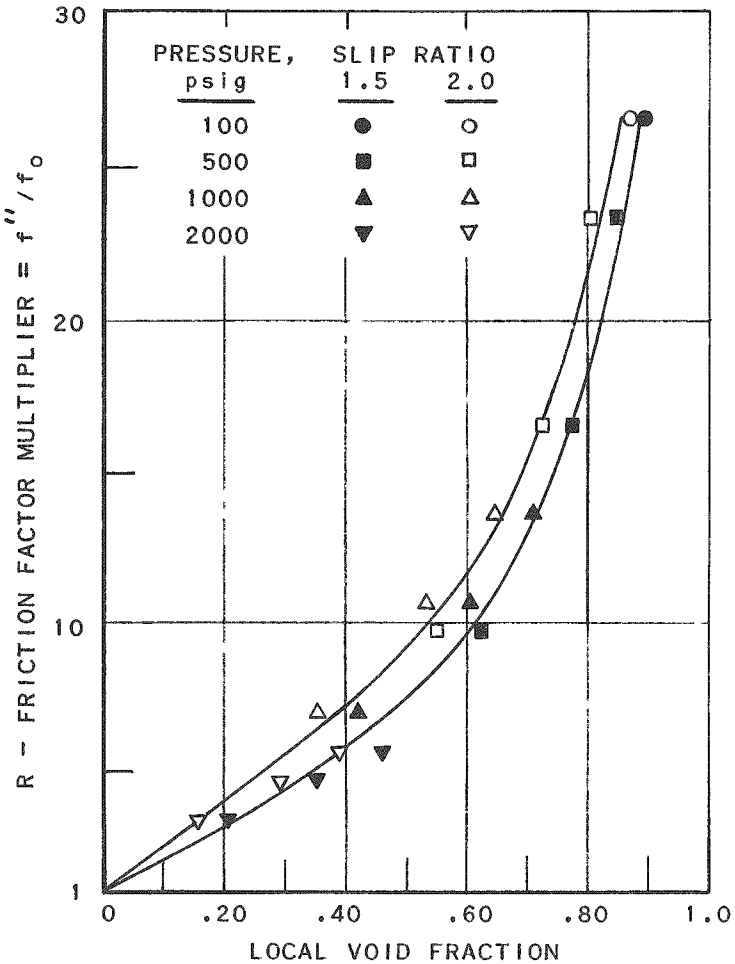

FIG. 29
MODIFIED MARTINELLI-NELSON TWO-PHASE FRICTION FACTOR RATIO AS A FUNCTION OF LOCAL VOIDS AND SLIP RATIO

RE-7-17022-A

calculations and are not experimental data points.) Pressure taps have recently been installed across the Armadilla test section and rough preliminary checks of the first two-phase pressure drop data indicate fairly good agreement with the curves of Figs. 28 and 29.

3. Single Channel Forced and Natural Circulation Boiling Density at 150 and 250 psig - E. A. Wimunc, W. S. Flinn, P. A. Lottes, R. J. Weatherhead, M. Petrick

The single channel tests conducted with the 250-psi pressure shell have been completed. The purpose of the tests was to determine the dependence of slip ratio on voids, steam quality, channel height, mass velocity, and power density.

Void data at the channel exit[10] have been re-run since it was found that a seal leak had allowed an indeterminate portion of the flow to bypass the test section during some of the earlier tests.

Additional forced circulation tests were made at natural circulation velocities, and void data have also been obtained at the three-quarter and one-half points up the channel.

As in the previous tests, the runs were made on a 1/2 x 3-1/2 x 60 in. channel test section and covered a velocity range from 1.3 to 11 fps and power densities ranging from 20 to 60 kw/liter. Data were obtained at 150 and 250 psig.

The results are summarized in Tables VII and VIII. The slip ratios are plotted in Figs. 30 and 31.

The effect of leakage was not sufficient to alter appreciably the conclusions that were drawn from the earlier data:

(1) Slip ratio can be represented as a function of inlet velocity only; the effects of the other variables - point along the section length, quality, voids, power density, subcooling - are negligible.

(2) As shown in Figs. 30 and 31, there is no significant pressure effect on the slip ratio pattern in going from 150 to 250 psig.

(3) In the velocity range from 2-1/2 to 3-1/2 fps, there is a sudden change in the mechanism of boiling and/or flow. Forced circulation runs were made at velocities from 4 to 1-1/2 fps to check the natural circulation data in the velocity range where the slip ratio unexplainably changes trend suddenly.

---

[10] Reactor Engineering Division Quarterly Report, ANL-5371 (January 15, 1955) p. 149.

Table VII

SUMMARY OF SINGLE CHANNEL FORCED AND NATURAL CIRCULATION
BOILING DENSITY TESTS AT 150 psig

Channel Size: 1/2 x 3-1/2 x 60 in.

Run No.	Power Density, kw/liter	Inlet Water Velocity, fps	Inlet Subcooling, F	Steam Wt. Fraction, X	Steam Vol. Fraction, $\alpha(x10^2)$	Slip Ratio, C_s/C_ℓ
			Exit Conditions			
271	20.1	2.07	9.0	0.01665	47	2.98
272	30.0	2.44	7.7	0.0255	64	2.30
273	40.0	2.72	6.7	0.0337	73	2.01
275	19.7	1.36	19.7	0.0167	33.5	5.47
276	30.0	2.18	14.0	0.02198	57	2.74
277	31.8	2.55	6.95	0.027	67	2.14
288	19.7	10.3	1.9	0.00329	19	2.195
289	29.8	11.1	5.35	0.001066	16	0.875
290	40.45	11.1	4.9	0.00439	28	1.77
292	40.45	7.26	5.07	0.00967	41	2.19
293	30.0	7.32	6.1	0.00418	20	2.62
295	30.0	5.1	9.3	0.0053	25	2.49
296	40.2	5.1	7.8	0.0129	53	1.81
298	59.7	4.94	10.5	0.0215	68	1.61
299	50.1	7.26	7.5	0.0104	52	1.50
300	40.2	7.4	6.4	0.0076	45	1.46
301	30.0	7.32	6.7	0.00342	22.5	1.85
303	23.85	11.1	5.2	0.00121	3	1.0
305	40.2	11.1	5.2	0.00393	26	1.75
306	50.3	11.8	5.2	0.00655	42	1.42
320	40.1	10.7	3.1	0.00717	34	2.18
357	20.6	2.32	5.9	0.01835	55.0	2.39
358	20.05	2.12	6.4	0.0196	54.0	2.66
359	20.35	1.91	7.3	0.0217	56.0	2.72
360	20.6	1.62	8.8	0.0259	57.5	3.07
361	20.8	1.37	9.9	0.0321	60.0	3.40
362	21.8	1.18	10.7	0.0423	63.0	3.98
363	30.2	2.72	5.0	0.0203	69	1.45
364	30.4	2.49	5.4	0.0296	69	2.04
365	30.4	2.22	6.4	0.0327	66	2.70
366	30.4	1.90	6.5	0.0407	67.5	3.18
367	30.3	1.64	8.2	0.0456	67	3.64
368	30.3	1.42	8.2	0.0543	68.5	4.13
369	30.9	1.33	10.3	0.0573	74.0	3.35
371	41.3	2.88	7.1	0.0349	76.5	1.73
375	40.0	2.24	14.9	0.0361	70	2.51
376	34.9	1.84	16.7	0.0373	66	3.11
378	40.5	3.8	3.45	0.0267	0.65	2.32
379	39.97	3.48	2.97	0.0292	0.65	2.52
380	40.0	2.90	6.20	0.0320	0.71	2.10
381	30.4	3.88	3.69	0.0179	0.555	2.27
382	30.1	3.42	3.67	0.0206	0.590	2.27
383	30.1	2.92	4.35	0.0241	0.64	2.15
384	30.3	2.92	4.27	0.0244	0.670	1.92
385	30.1	3.91	3.42	0.0177	0.60	1.87
386	30.1	3.3	5.05	0.0199	0.60	2.11
387	29.6	2.44	5.57	0.0277	0.650	2.39
388	40.4	4.12	2.00	0.0255	0.68	1.91
389	39.54	4.35	2.40	0.0229	0.66	1.82

DECLASSIFIED

Table VII (Cont'd)

Run No.	Power Density, kw/liter	Inlet Water Velocity, fps	Inlet Subcooling, F	Steam Wt. Fraction, X	Steam Vol. Fraction, $\alpha(x10^2)$	Slip Ratio, C_s/C_ℓ
			Exit Conditions (Cont'd)			
390	39.97	3.25	4.1	0.0302	0.715	1.93
391	39.77	3.1	3.0	0.0330	0.74	1.87
392	39.54	2.75	2.95	0.3725	0.74	2.11
393	39.77	2.28	4.30	0.0443	0.77	2.16
394	39.77	1.30	7.1	0.0577	0.815	2.17
395	29.6	4.35	2.4	0.0159	0.565	1.93
396	29.8	4.1	3.9	0.0160	0.55	2.07
397	29.4	3.7	3.8	0.0179	0.59	1.97
398	30.3	3.25	4.0	0.0219	0.63	2.04
399	30.5	3.1	3.7	0.0236	0.64	2.11
400	29.8	2.02	6.2	0.0346	0.70	2.39
401	30.7	1.47	9.4	0.0482	0.725	2.99
402	30.1	1.95	5.2	0.0377	0.75	2.03
404	30.3	1.58	8.0	0.0445	0.75	2.41
405	28.67	1.33	8.9	0.0503	0.72	3.21
406	29.22	1.47	7.9	0.0468	0.72	2.97
			Three-Quarter Point Conditions			
216	29.7	11.02	3.0	0.00207	13.5	2.07
219	40	11.1	4.24	0.00248	24	1.23
221	50.4	11.1	6.7	0.00146	22.5	0.785
223	29.8	10.5	2.35	0.00315	17	2.4
224	29.3	7.24	2.43	0.00567	29	2.18
225	30.35	5.1	3.5	0.0084	41	1.9
226	40.8	4.88	3.0	0.0142	58	1.63
228	40	11.1	4.84	0.00174	14	1.67
230	40	4.93	8.54	0.00676	43.5	1.38
231	29.85	4.88	8.53	0.00254	17.5	1.87
232	29.86	7.11	6.3	0.0012	10	1.69
234	50	11.0	5.04	0.00356	27	1.5
235	49.6	7.15	4.93	0.00872	41	1.98
236	50.6	5.4	7.47	0.0108	50	1.71
239	50.6	10.9	4.6	0.00425	28	1.71
241	40.4	7.24	5.8	0.00479	25.5	2.19
242	50.6	7.1	5.1	0.00891	45	1.71
244	40.6	4.8	7.9	0.0084	41	1.9
245	51.7	4.8	7.6	0.0137	55	1.78
246	30.5	4.8	2.4	0.0107	44	2.13
247	40.8	4.93	3.6	0.0133	56	1.65
248	30	10.7	2.6	0.00277	21	1.63
249	30	7.31	2.3	0.00592	35	1.73
250	40.15	7.31	1.7	0.00963	44.5	1.89
251	29	2.65	6.4	0.0156	56	1.91
252	40.2	2.73	6.6	0.0234	66.5	1.88
254	20.9	2.34	7.1	0.0104	41	2.32
256	29.8	2.05	16.3	0.00898	32	2.97
257	39.3	2.5	14.5	0.0157	52	2.3
258	51.2	2.84	13.6	0.0219	66.5	1.76
			One-Half Point Conditions			
324	40.9	2.67	6.1	0.0131	50.5	2.03
334	40.8	2.56	13.4	0.00623	34	1.90
338	30	2.63	6.7	0.00798	37	2.13
340	40.5	2.41	13.7	0.0061	31.5	2.08

DECLASSIFIED

Table VIII

SUMMARY OF SINGLE CHANNEL FORCED AND NATURAL CIRCULATION BOILING DENSITY TESTS AT 250 psig

Channel Size: 1/2 x 3-1/2 x 60 in.

Run No.	Power Density, kw/liter	Inlet Water Velocity, fps	Inlet Subcooling, F	Steam Wt. Fraction, X	Steam Vol. Fraction, $\alpha(x10^2)$	Slip Ratio, C_s/C_ℓ
			Exit Conditions			
280	20.35	2.06	8.7	0.0189	45	2.44
281	30.0	2.52	10.85	0.0222	62	1.325
282	40.1	2.96	5.9	0.0338	70	1.39
284	29.7	2.06	15.4	0.0228	49	2.26
285	39.4	2.35	16.0	0.0304	57.5	2.21
307	30	11.3	4.7	0.00198	11	1.52
308	40	11.2	3.85	0.00590	23	1.89
309	50.2	11.15	4.3	0.00816	31.5	1.69
310	60.2	11.15	4.3	0.0109	42	1.42
312	40	7.23	4.9	0.0105	34	1.93
313	50.2	7.5	4.0	0.01522	41.5	2.08
314	60.2	7.5	5.24	0.0177	51.5	1.58
316	39.5	5.2	6.8	0.0139	42	1.85
317	50.4	5.26	7.0	0.0202	50	1.96
			Three-Quarter Point Conditions			
259	27.6	1.87	19.4	0.00841	21.5	2.94
260	40.1	2.38	15	0.0191	45.5	2.22
261	51.7	2.63	14.2	0.0266	57	1.96
263	30.5	1.87	18.6	0.0132	27	3.43
264	41.0	2.38	16.1	0.0185	44	2.27
265	50.3	2.56	14	0.027	56	2.07
266	20.3	2.22	7.1	0.0117	32	2.38
267	30.0	2.58	5.5	0.0196	49	1.97
268	41.0	2.75	5.8	0.0267	60	1.74
269	41.0	2.75	5.2	0.0275	60	1.79
270	41.0	2.75	5.4	0.0272	60	1.77
			One-Half Point Conditions			
327	7.5	2.59	30	0.00805	30.2	1.8
329	13	2.44	26	0.00953	42.4	2.61
330	13.5	2.63	33.5	0.0115	50.05	2.2
342	10.35	2.50	30	0.00501	30.4	1.12
345	15.25	2.38	27.5	0.00620	40.8	1.57

DECLASSIFIED

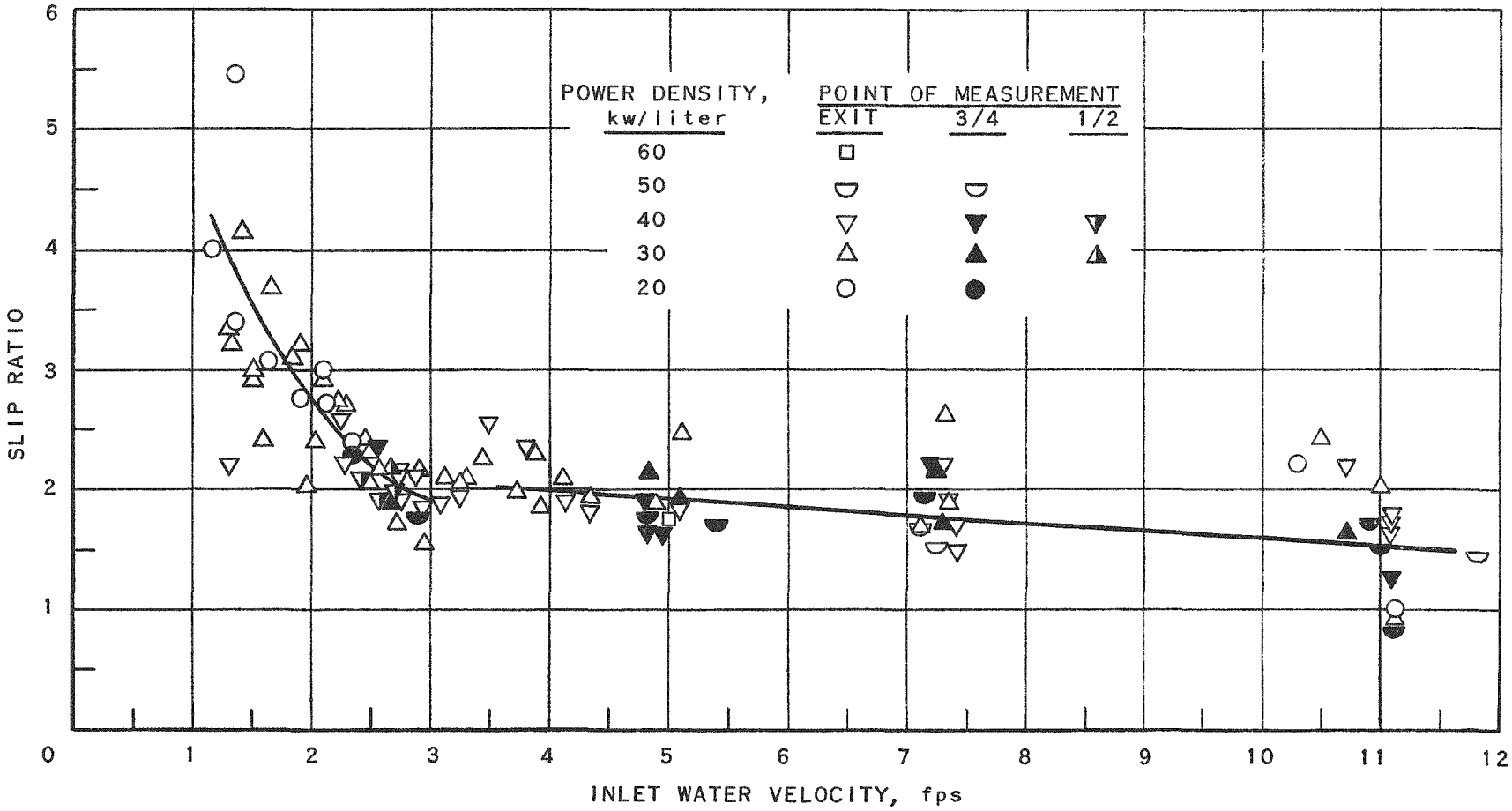

FIG. 30
SLIP RATIO AS A FUNCTION OF INLET WATER VELOCITY AT 150 psig.
(1/2 x 3 1/2 x 60 in. VERTICAL CHANNEL)

RE-7-17063-A

UNCLASSIFIED

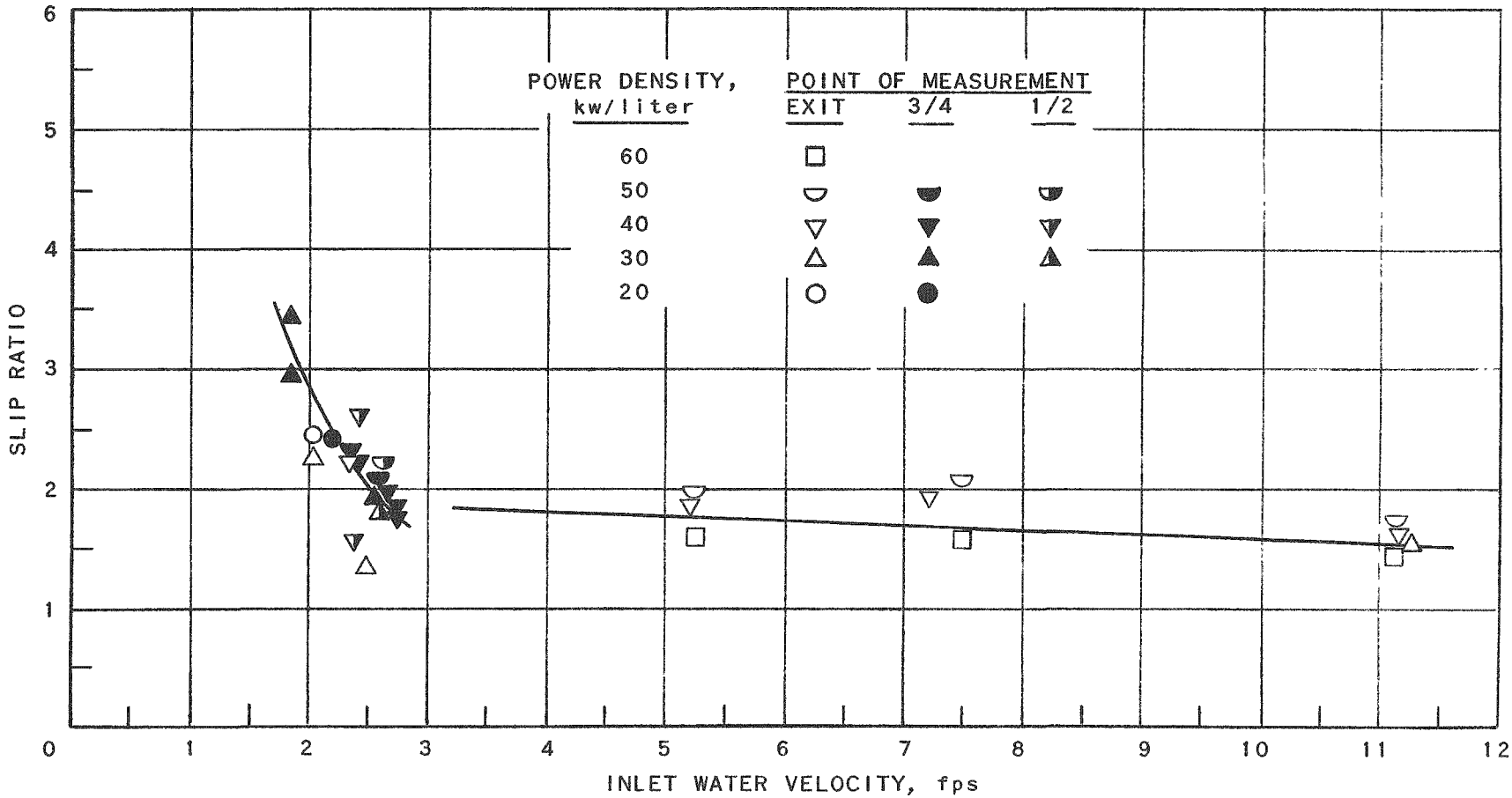

FIG. 31
SLIP RATIO AS A FUNCTION OF INLET WATER VELOCITY AT 250 psig.
(1/2 x 3 1/2 x 60 in. VERTICAL CHANNEL)

RE-7-17062-A

Thus far, slip ratio vs inlet velocity appears to be the most practical and convenient way of plotting slip data. Possibly, Reynolds Numbers should replace the inlet velocity coordinates. Plots of slip ratio vs powers of velocity are smoother than those of Figs. 30 and 31; however, the discontinuity in the 2-1/2 to 3-1/2 fps range still exists.

C. Fuel Elements

1. Corrosion Tests on Fuel and Cladding Materials

a. Zircaloy 2-Clad Uranium-5% Zirconium Plates - C. R. Breden

Since heat treatment for stability and heat treatment for corrosion resistance were found to be incompatible, it was decided to heat treat for stability and to depend on the clad for corrosion resistance. Because the niobium had been added in the first place to improve corrosion resistance, elimination of corrosion resistance as a specification of the core alloy apparently eliminated the need for niobium, a very expensive ingredient. To test this hypothesis, some plates were made up by the Argonne Metallurgy Division with uranium-5% zirconium core clad with Zircaloy 2. The alloy was found to be much more difficult to fabricate than the uranium-1-1/2% niobium-5% zirconium reference alloy.

Four of these plates (Nos. 153T, 154T, 155T, and 158T) were tested in 550F degassed water. After 70 hr a pressure buildup (hydrogen) indicated a rupture, and the test was stopped. As shown in Fig. 32, Plate 158T had ruptured; Plate 153T had developed a large blister on one end above the Zircaloy 2 bond area; and Plates 154T and 155T showed warping.

Plates 153T, 154T and 155T were returned to the Metallurgy Division for further examination. Visual examination showed that the shrinkage pattern delineating the picture frame area had been emphasized as a result of the corrosion test. Ultrasonic tests indicated that the corrosion test had aggravated some defects in the core and bond areas. The blister on Plate 153T was attributed to the use of an end plug of zirconium, instead of Zircaloy 2, which resulted in a non-corrosion resistant bond that permitted water to enter and produce the blister.

The poor behavior of these plates, both during fabrication and in corrosion test, indicates that the uranium-5% zirconium core alloy is not as good as the reference alloy. The difference between the corrosion behavior of Plate 158T with an unintentionally added defect and a reference alloy plate with an intentionally added defect (see Fig. 33) is striking.

DECLASSIFIED

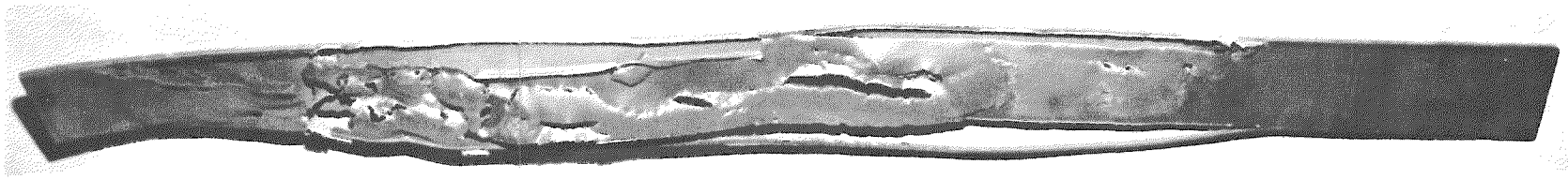

PLATE NO. 158T

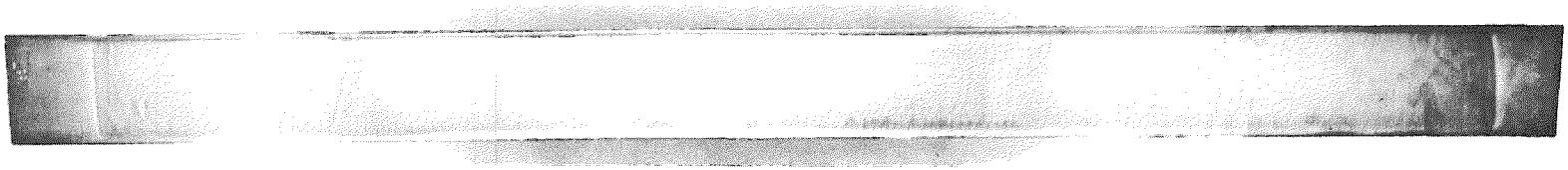

PLATE NO. 154T

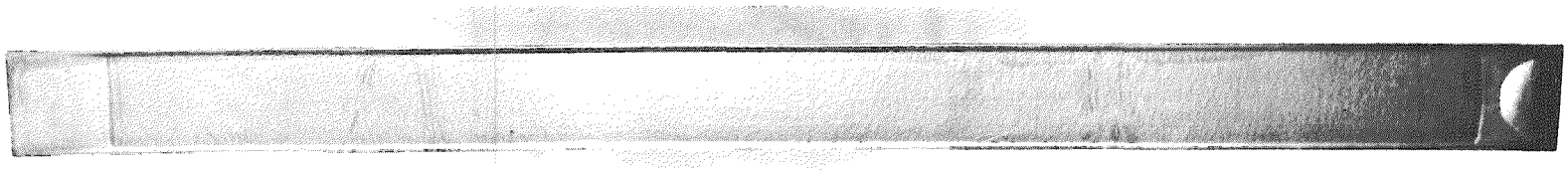

PLATE NO. 153T

PLATE NO. 155T

FIG. 32
ZIRCALOY 2-CLAD, URANIUM-5% ZIRCONIUM ALLOY PLATES
TESTED FOR 70 hr IN 550 F DEGASSED WATER

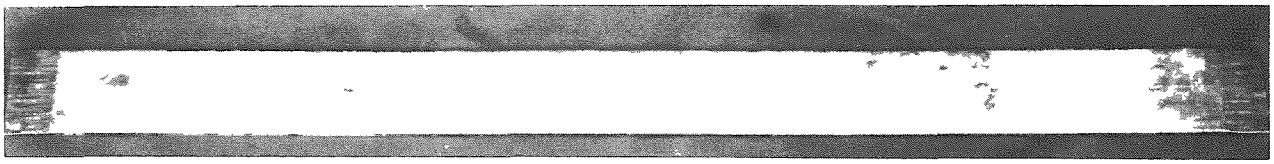

PRE-TEST APPEARANCE

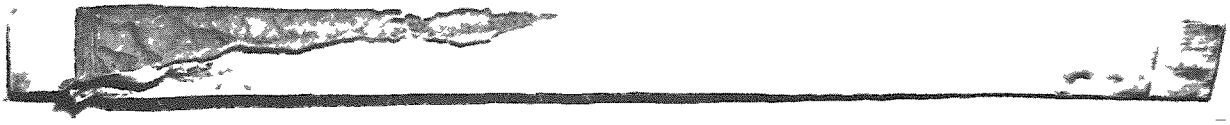

2 hr

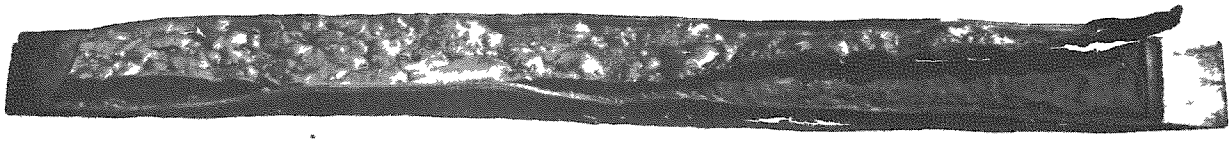

24 hr

ALUMINUM-CLAD NATURAL URANIUM PLATE
TESTED IN 400 F DEGASSED WATER

BOTTOM

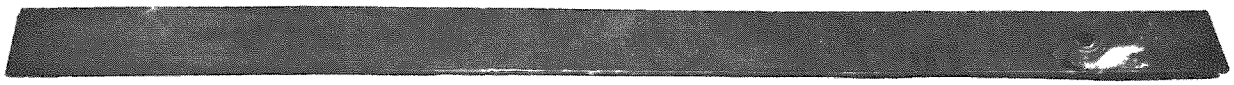

TOP

EBWR REFERENCE ALLOY PLATE TESTED
FOR 24 hrs IN 550 F DEGASSED WATER

FIG. 33
CORROSION BEHAVIOR OF EBWR REFERENCE ALLOY PLATE AND ALUMINUM-CLAD NATURAL URANIUM PLATE AFTER ADDITION OF KNOWN DEFECT

DECLASSIFIED

b. Aluminum-Clad Natural Uranium Plates - C. R. Breden

Tests were made to compare the corrosion behavior (in the presence of a known defect) between aluminum-clad, natural uranium plates and EBWR reference alloy plates.

Two typical aluminum-clad, natural uranium plates, fabricated by the step-pressing technique, were supplied by the Savannah River Laboratory. The plates received were not given unqualified bond approval.

A preliminary corrosion test for 24 hr in 400F showed no clad defects. One plate was provided with a 3/32-in. diameter hole drilled through the clad near one end and then tested for 2 hr in 400F water.

Due to the size of the autoclave, it required about four hours to reach temperature and 24 hr to cool down after test. Increased pressure suggested a rupture and this was confirmed on opening the vessel. The presence of hydrides was indicated by the spontaneous ignition of a cloth used to dry the plate and by the higher-than-ambient temperature of the plate. As a precautionary measure, the plate was returned to the pressure vessel and heated in water for 24 hr to decompose the hydrides. The appearance of the plate before the test, after the 2-hour test, and after the 24-hour test is shown in Fig. 33.

The EBWR reference alloy plate shown for purposes of comparison was tested at an earlier date.[11]

c. Fuel Plate End Closures

Samples of reference alloy fuel plate end closures fabricated by the Argonne Metallurgy Division have been continued in corrosion test. The fabrication history and earlier test results are given in ANL-5471.[12]

The third induction-welded sample ruptured after 967 hr in 550F degassed water. The three samples with the heliarc-welded head added after induction welding are still intact after 1731 hr.

d. Aluminum Alloys

Approximately 120 specimens of aluminum-nickel alloy M-388 and aluminum-copper alloy X-2219 have been tested under varying conditions of pH, velocity, H_2 gas and temperature. The total test time is

[11] Reactor Engineering Division Quarterly Report, ANL-5471 (September, 1955) p. 98.

[12] Ibid., p. 104.

DECLASSIFIED

8 weeks with loop shut-down and specimen withdrawal every two weeks. In general, the aluminum-nickel material is better than aluminum-copper from the viewpoints of total corrosion and uniformity of corrosion in comparative testing of only four weeks' time. Aluminum-copper is prone to pitting attack, and its scale is more easily damaged by mechanical and thermal shock.

Test results on aluminum alloys have been somewhat confusing because of a consistent difference in corrosion of originally loaded samples and replacement samples. In all cases of normal loop operation, replacement samples show more corrosion. This phenomenon is being investigated and is currently believed to be due to the difference in hydrogen gas content of the water in contact with originally loaded and replacement samples.

It should be noted that 90% of the aluminum-nickel alloy M-388 samples as received for test contained inclusions of dirt and foreign matter at the surface, and it is questionable whether these inclusions extend throughout the metal. Results of individual tests follow.

Loop No. 1 (500F, pH 5.0) - Original Samples:

This loop, maintained at pH 5.0 by means of a cation resin bed regenerated with H_2SO_4, has completed the 8-week total test period for aluminum-nickel M-388 alloy. The results are plotted in Fig. 34; each point represents an average of at least three stripped samples, and variations from this average are not greater than 3%. The corrosion rates from this plot are as follows:

Water Velocity, fps	Penetration Rate, mils/yr
21	2.5
7	1.4
Semi-Static	1.2

In all cases the samples corroded uniformly, with no pitting or erosion-corrosion areas. Figure 35 shows the appearance of the aluminum-nickel scale at the end of two weeks of corrosion test.

Loop No. 3 (500F, pH 6.5) - Originally Loaded Samples:

This loop, with the water continuously by-passed through a mixed-bed demineralizer, has completed 6 weeks of the scheduled 8-week test period on aluminum-nickel alloy. The weight losses of the stripped samples (at least three samples per point) are plotted in Fig. 36. The points do not line up too well and extrapolation of a corrosion rate at the end of six weeks is difficult. The approximate corrosion rates are:

DECLASSIFIED

RE-7-16989-A

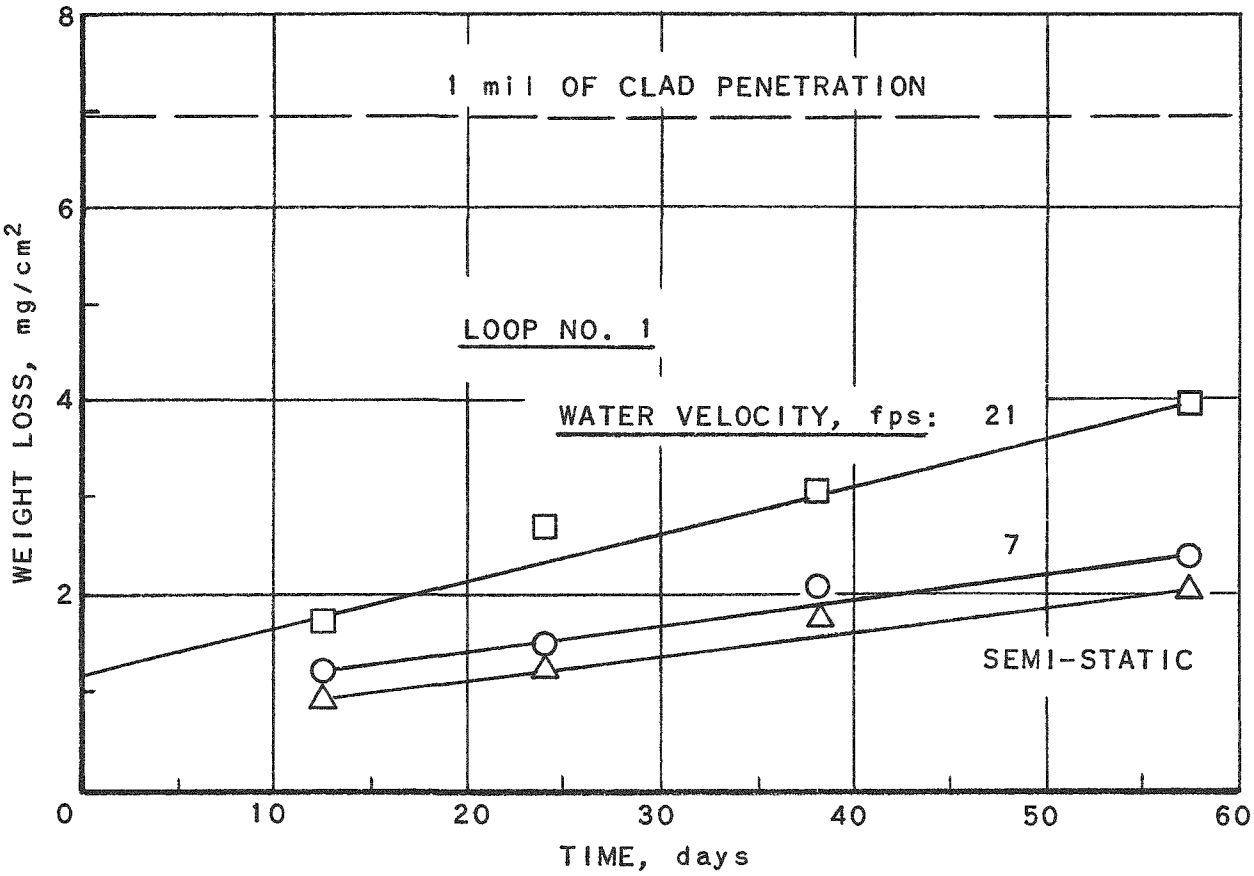

FIG. 34
CORROSION OF ALUMINUM-NICKEL ALLOY (M-388) IN 500 F WATER (pH = 5.0)

DECLASSIFIED

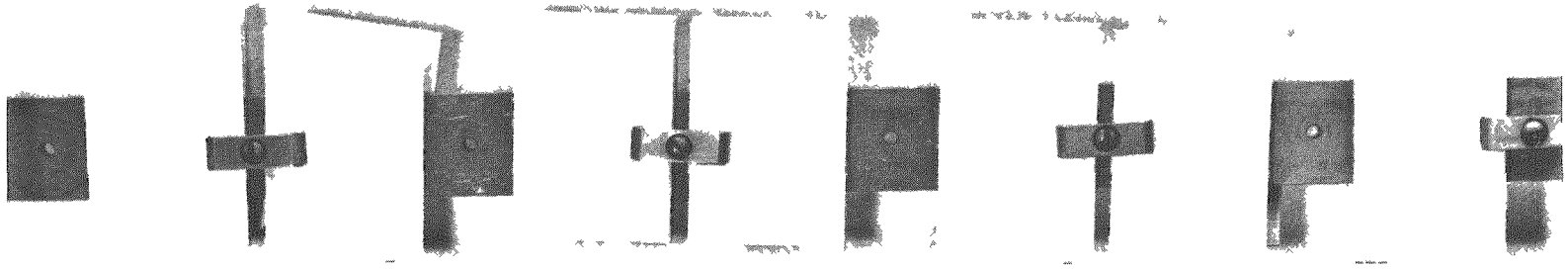

SEMI-STATIC WATER

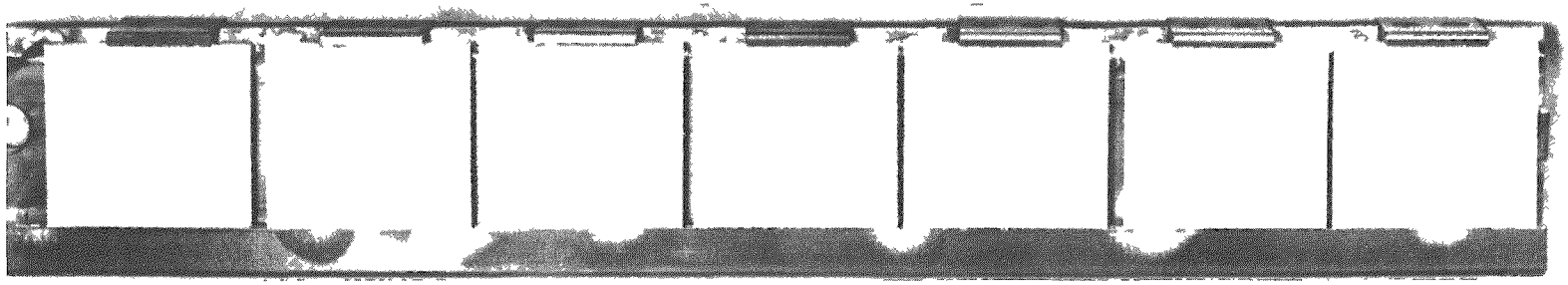

SST

WATER VELOCITY: 21 fps

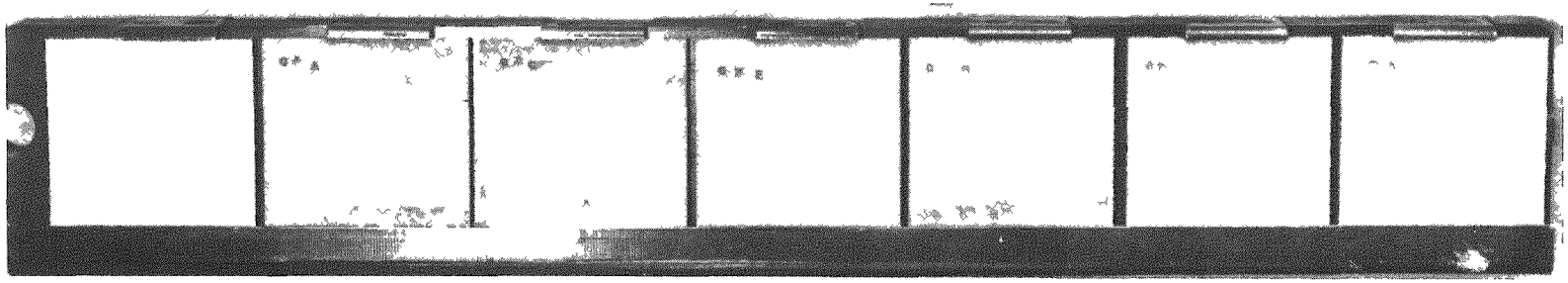

SST

WATER VELOCITY: 7 fps

FIG. 35
AS-REMOVED SAMPLES OF STAINLESS STEEL AND ALUMINUM-NICKEL ALLOY M-388 AFTER EXPOSURE FOR 2 WEEKS IN 500 F WATER
(pH = 5.0; RESISTIVITY = 300,000 ohm-cm)

0121232

RE-7-16990-A

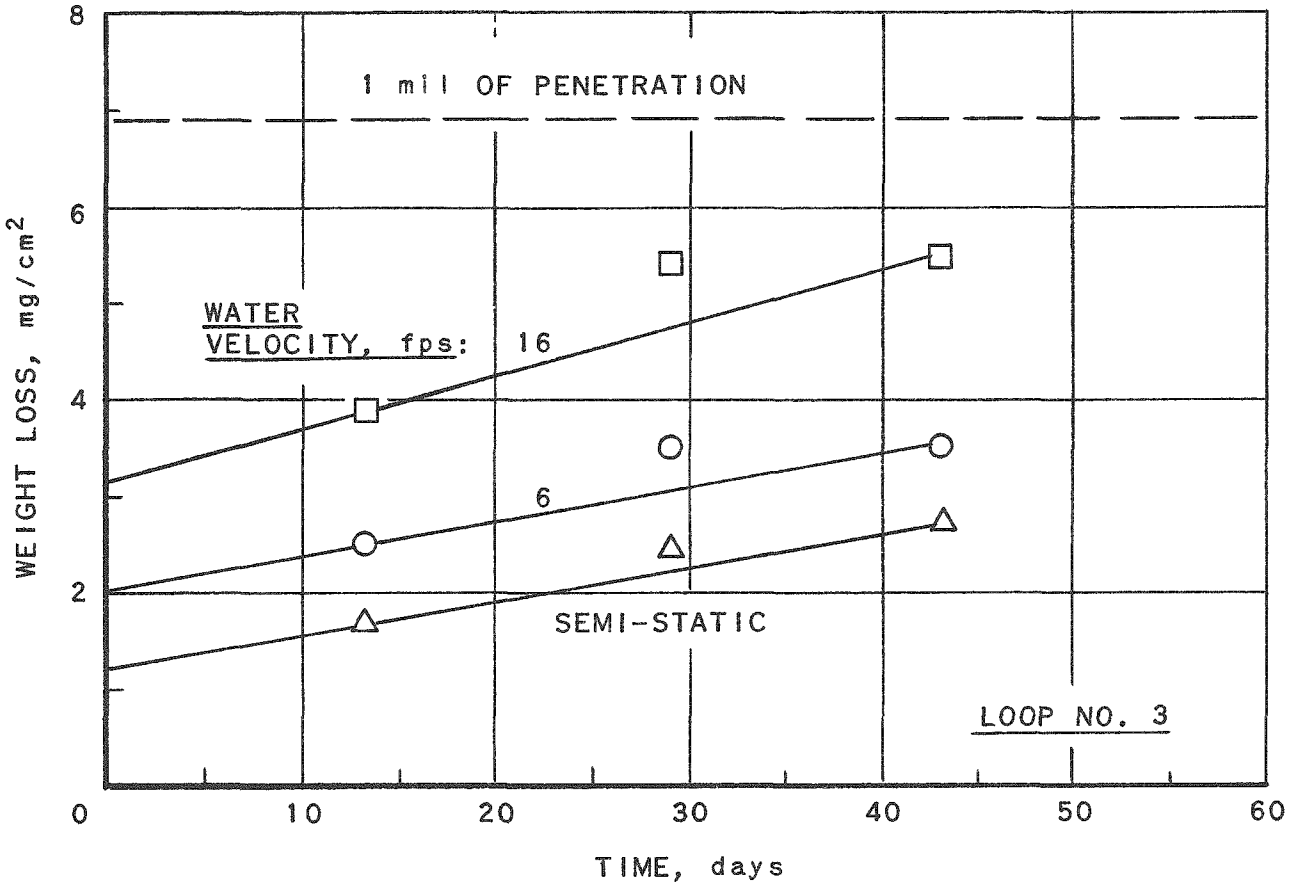

FIG. 36
CORROSION OF ALUMINUM-NICKEL ALLOY (M-388)
IN 500 F DEMINERALIZED WATER (pH = 6.5)

DECLASSIFIED

Water Velocity, fps	Penetration Rate, mils/yr
16	2.8
6	2.0
Semi-Static	2.0

Examination of the 16-fps samples showed erosion-corrosion areas at leading edges and around the holding combs. The 6-fps and static samples showed uniform corrosion. Figure 37 shows the samples upon removal after 2 weeks of test. It appears that at pH 6.5 the total corrosion is higher than at pH 5.0; however, the corrosion rate may not be too much higher.

Replacement Samples of Aluminum-Nickel Alloy

Samples used in dynamic loops as replacements to hold the area configuration have shown considerably higher corrosion [at least as concerns intercept (ordinate)] than originally loaded samples. The problem first arose in the boric acid loop and was attributed at that time to a varying pH. The difference in corrosion rate is considerable and may vary as high as a factor of 4. The higher the velocity the more pronounced was the acceleration of replacement sample corrosion. Figure 38 shows the difference between smooth adherent protective scale and ruptured scale with subsequent accelerated corrosion.

The accelerated corrosion of replacement dynamic stream samples continued to some degree in Loop No. 1 (pH 5) and Loop 3 (pH 6.5). There appears to be a connection between increased replacement sample corrosion and the hydrogen gas content of the flowing loop. Data at present show that aluminum-nickel corrosion has been less in the presence of higher hydrogen content, and this could account for the replacement sample corrosion problem, since the hydrogen content of the loops is highest in the initial two-week periods. A test has been started to investigate the effect of hydrogen as an inhibitor in aluminum-nickel corrosion.

Aluminum-Copper Alloy X-2219

Aluminum-copper alloy X-2219 shows a greater stripped weight loss than aluminum-nickel under the same water conditions. The alloy exhibited small surface pits and localized erosion-corrosion attack in 16 fps, 6.5 pH water. It was more sensitive to velocity than aluminum-nickel. (See Fig. 39.) The stripped weight loss at the end of four weeks at pH 5.0 for aluminum-copper was 6.70 mg/cm^2 at 21 fps, and 3.75 mg/cm^2 at 7 fps.

Aluminum-copper, like aluminum-nickel, does not show erosion-corrosion attack in high-velocity water at pH 5.0; however, surface pitting of aluminum-copper still occurs at this reduced pH.

DECLASSIFIED

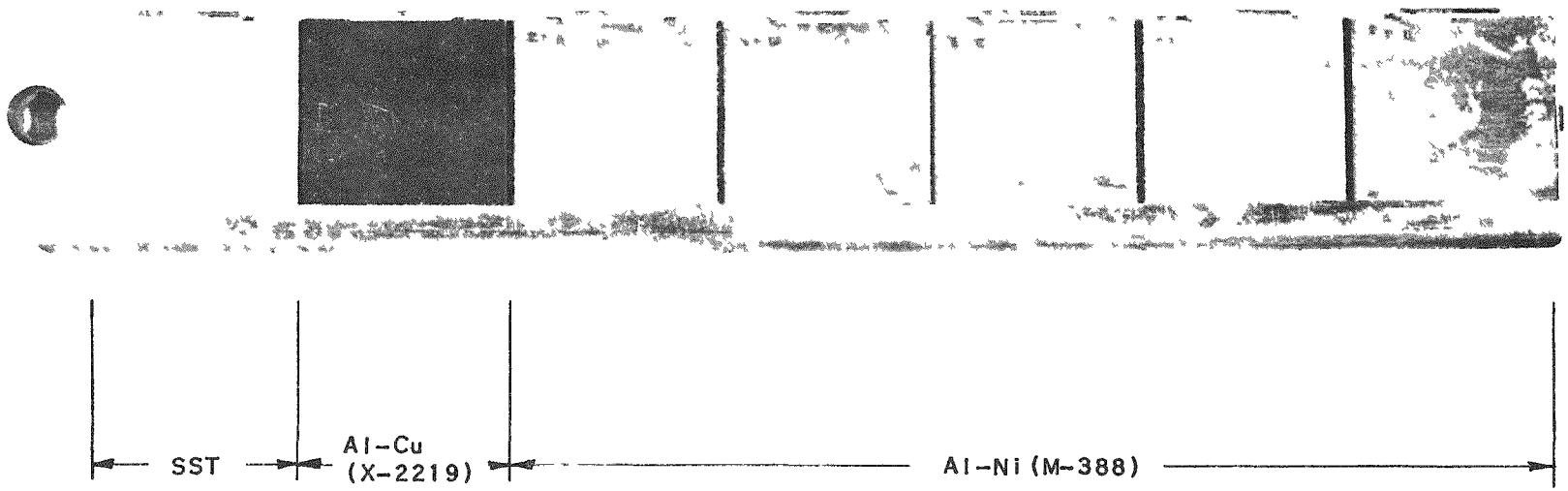

FIG. 37
AS-REMOVED SAMPLES AFTER EXPOSURE
FOR 2 WEEKS IN 500 F WATER AT 16 fps
(pH = 6.5; RESISTIVITY = 1,500,000 ohm-cm)

ORIGINAL SAMPLES

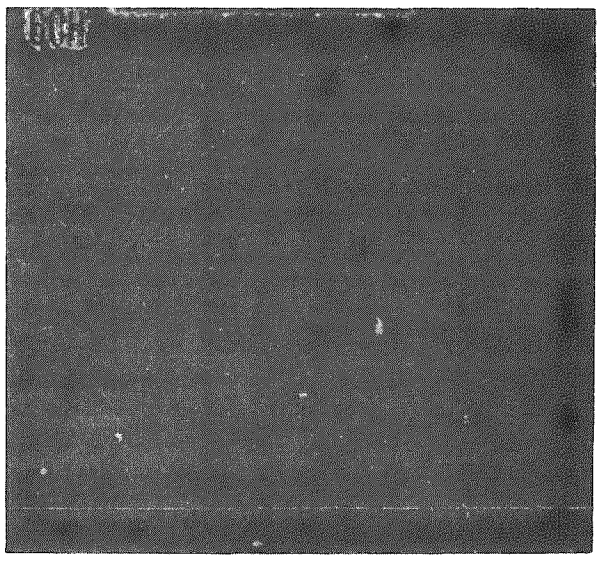

SAMPLE:	A-4360-F	A-4360-H
TEST TIME:	8 weeks	8 weeks
WT. LOSS:	6.14 mg / cm^2	7.08 mg / cm^2

REPLACEMENT SAMPLES

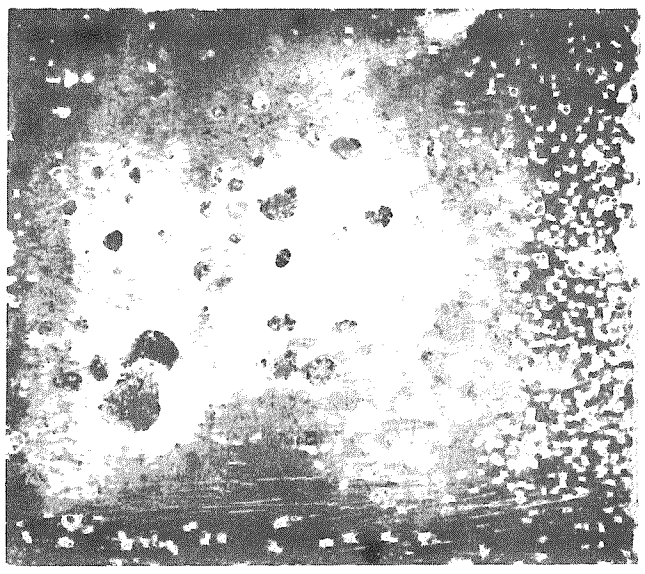

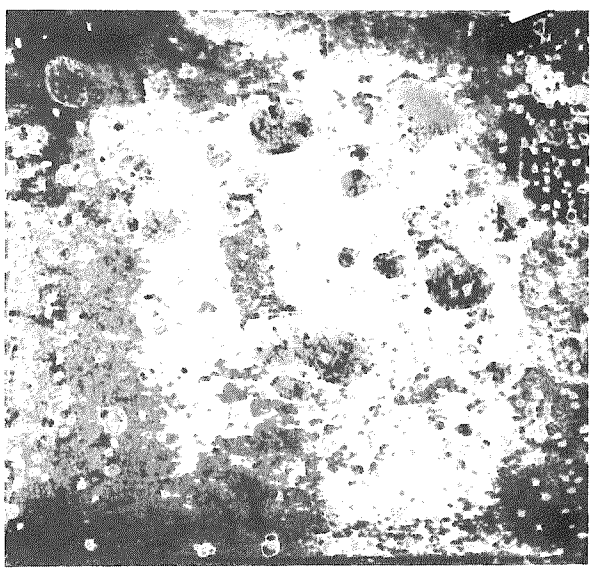

SAMPLE:	A-4361-G	A-4361-H
TEST TIME:	6 weeks	6 weeks
WT. LOSS:	19.2 mg / cm^2	18.4 mg / cm^2

REPLACEMENT SAMPLES

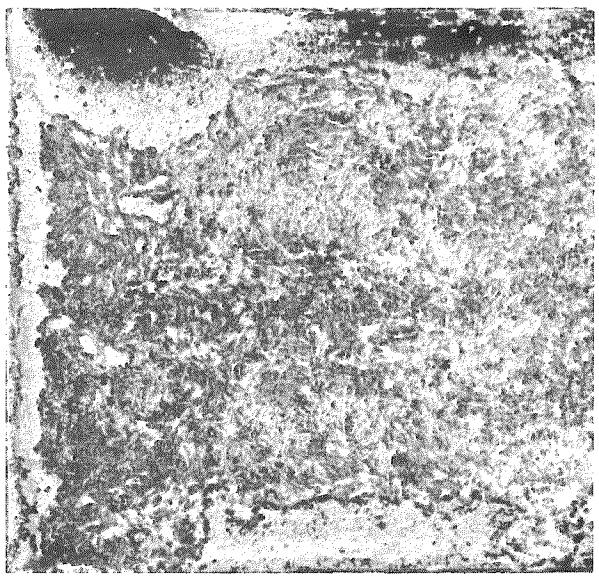

SAMPLE:	A-4361-J	A-4361-K
TEST TIME:	4 weeks	4 weeks
WT. LOSS	18.7 mg / cm^2	21.0 mg / cm^2

FIG. 38

VARIATION IN CORROSION RATES OF ALUMINUM-NICKEL ALLOYS

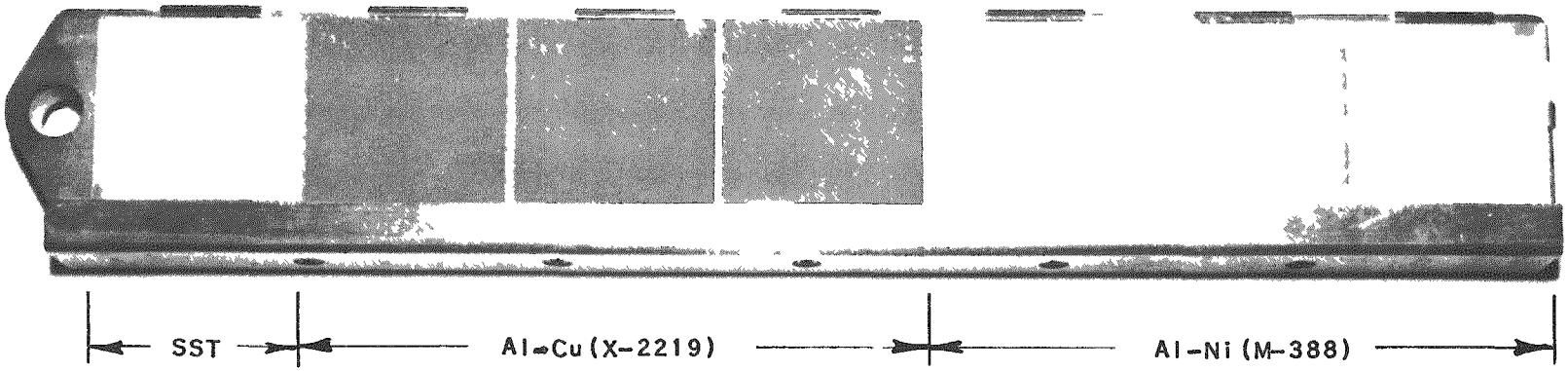

WATER VELOCITY: 21 fps

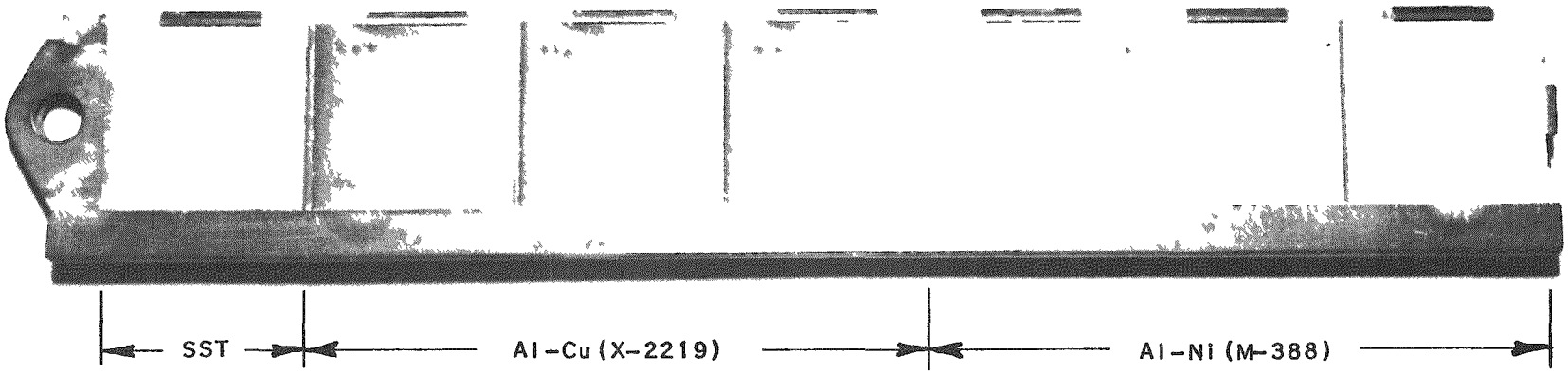

WATER VELOCITY: 7 fps

FIG. 39
AS-REMOVED SAMPLES AFTER EXPOSURE
FOR 4 WEEKS IN 500 F WATER
(pH = 5.0; RESISTIVITY = 300,000 ohm-cm)

Stainless Steel Corrosion at 500F and pH 5.0 and 6.5

Austenitic stainless steel samples were corrosion tested in Loop No. 1 and Loop No. 3 along with the aluminum alloy samples. The weight changes are plotted in Fig. 40. It appears that stainless steel gains weight in pH 6.5 water and loses weight in pH 5.0 water, with about equal weight change rates. Rates are somewhat variable as a result of a varying amount of hydrogen gas from period to period. Figure 40 shows that the weight change rate in pH 5.0 water is approximately 0.05 mg/(cm^2)(mo), in close agreement with the normal rate. The stainless steel samples are shown in Figs. 35, 37, and 39.

Crevice Corrosion Between Aluminum-Nickel and Stainless Steel

Autoclave work had indicated that aluminum-nickel when coupled to stainless steel Type 304 washers tended to seize together and required hammering to separate. An autoclave experiment was run to evaluate the problem of sticking of fuel element end box cones into a bottom support plate of stainless steel Type 304. A test cone is shown in Fig. 41 after its removal from autoclave corrosion at 414F. Three miniature cones were tested and withdrawn at the end of 7, 33, and 44 days, respectively. In no case was any force required for withdrawal. The unit loading pressure of the cone during corrosion test was 3 psi. The aluminum-nickel cones showed evidence of crevice corrosion pitting, and this occurred consistently when aluminum-nickel was coupled to stainless steel in a static system. It has never been observed in dynamic systems.

e. Urania-Thoria Bodies - R. A. Granacki, R. J. Schiltz

(1) Water Solubility

The following bare urania-thoria specimens have been continued in test in static, degassed and deionized water at 600F without any significant changes:

Sample	Composition
A-4282-13	Norton thoria
A-4291	10% urania-thoria
A-4311	10% urania-thoria
A-4335c	2.5% urania (fully enriched)-thoria

The fabrication history and earlier test results are reported in ANL-5471.[13]

[13] Reactor Engineering Division Quarterly Report, ANL-5471 (September, 1955) p. 115.

DECLASSIFIED

RE-7-16991-A

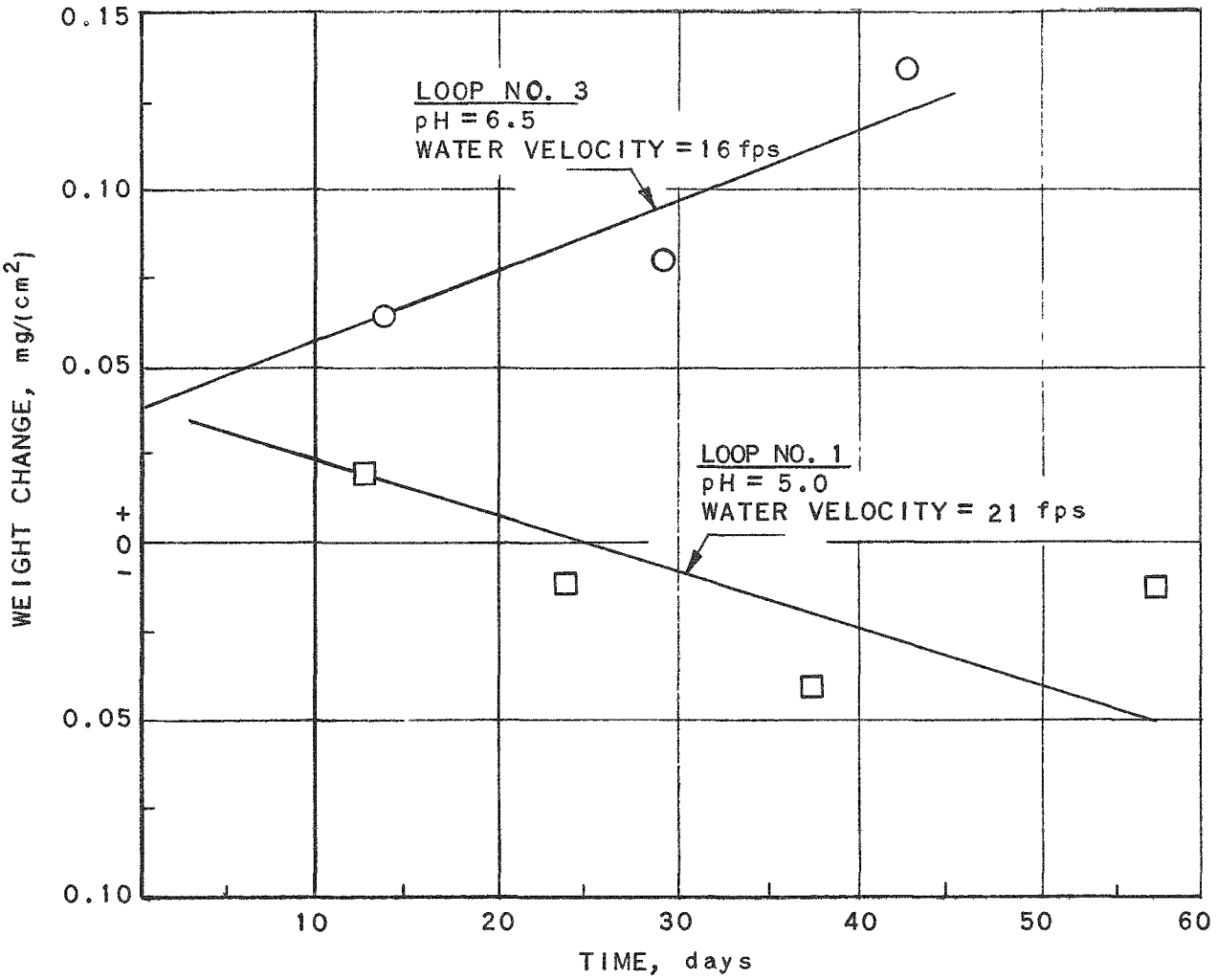

FIG. 40
CORROSION OF AUSTENITIC STAINLESS STEEL
AS A FUNCTION OF TEST CONDITIONS

DECLASSIFIED

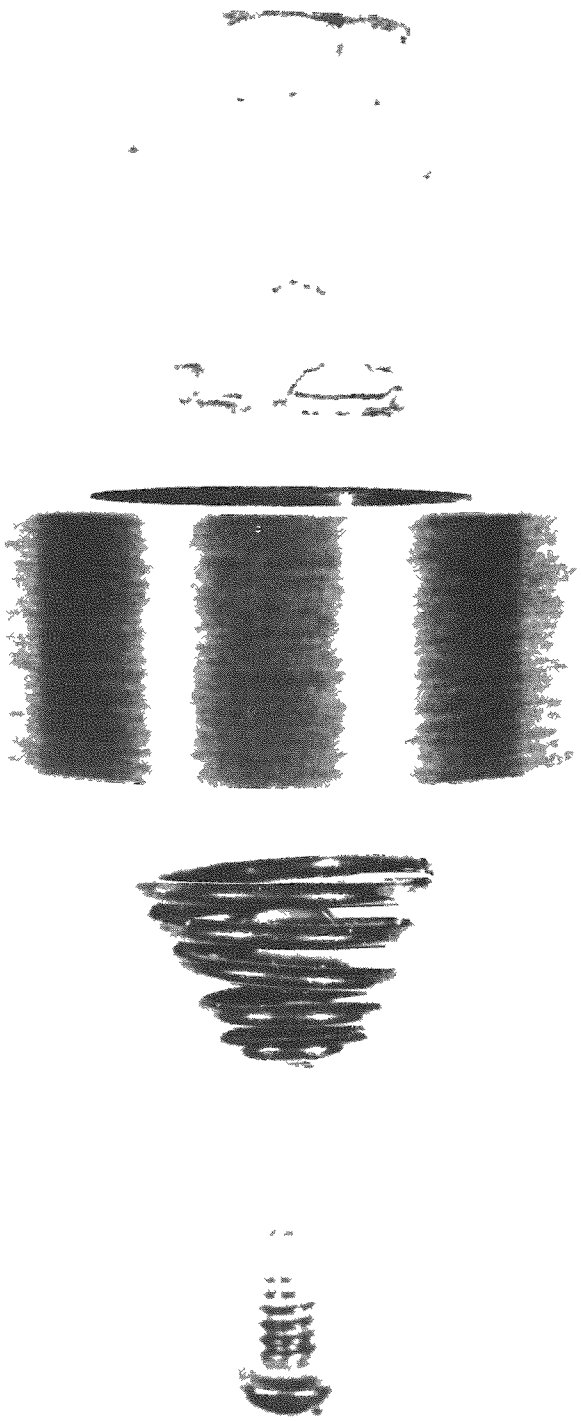

FIG. 41
MINIATURE END BOX FUEL ELEMENT CORE AFTER
EXPOSURE FOR 7 DAYS IN STATIC WATER AT 414 F

DECLASSIFIED

(2) Irradiation

Three irradiation runs have been completed in the CP-5 autoclave facility. Sample descriptions and test conditions are given in Table IX.

Table IX

IRRADIATION TESTS ON URANIA-THORIA BODIES

Autoclave Run No.	Sample No.	Description	Time, hr	Burnup, % Total U Atoms	Burnup, % Total Core Atoms	Operating Characteristics
16	A-4383a	90% ThO_2-10% UO_2 (93% enriched). Four pellets in Zircaloy-2 capsule. Wt U^{235} = 0.910 gm.	1042	1.92	0.063	500-515F; 750-810 psi. System leakage: 5 lb/day
17	A-4383c	90% ThO_2-10% UO_2 (93% enriched). Four pellets in Zircaloy-2 capsule. Wt U^{235} = 0.910 gm.	1592	2.94	0.096	500-515F; 750-785 psi. System developed leak during last day of operation.
18	A-4397-5	90% ThO_2-10% UO_2 (93% enriched). Four pellets in 1% Ni-Al alloy tube. Wt U^{235} = 0.905 gm.	260	0.48	0.016	490-520F; 725-800 psi. System developed leak and had to be removed.

All specimens were 90% ThO_2 and 10% UO_2 with U^{235} enrichment of 93.22%. The constituents were mixed by ball milling, then dry pressed at 500 psi and fired at 3360F (1850C). The samples had a density of 9.58 gm/cc and an average porosity of 9.57%. X-ray examination indicated complete solid solution of the urania in the thoria.

The specimen in each autoclave consisted of four 0.25 in. diameter by 0.50 in. long ceramic pellets jacketed with Zircaloy 2 or 1% nickel-aluminum alloy. There was an annulus of 0.005 in. of lead between pellets and cladding in order to facilitate heat transfer during irradiation. Air-cooled, pressurized water surrounding the specimen in the autoclave acted as a temperature control medium.

DECLASSIFIED

The specimens were irradiated in distilled and demineralized degassed water at 500-515F for 260 to 1590 hr at full CP-5 power, which resulted in calculated burnups of 0.48% to 2.94% of total uranium atoms.

Post-irradiation examination of the autoclaves and specimens was performed in a high-level activity cave. After opening the autoclaves, the water was found to be only faintly discolored; the discoloration was attributed to corrosion products from the autoclave. Activity levels of the water showed mild contamination (approximately 300 mr/hr at 2 in.).

The pellets were removed from the specimen containers by filing the weld off the closure, melting the heat transfer medium, and allowing the pellets to spill out of the tube. The following discussion is made with reference to Fig. 42.

Run 16: Three of the pellets suffered end fractures but the main body remained intact. Pellet No. 3 broke into smaller pieces of fairly uniform size (1/8 in. by 1/8 in.). The fractures have definite cleavage-type planes, the breaks being angular and sharp. A preponderance of fractures seems to occur radially, as can be seen from pellets No. 1 and 2. This same type of radial fissure can be seen occurring in pellet No. 4, thus indicating that the internal thermal stresses were sufficient to rupture the pellets.

Run 17: The four pellets had completely shattered. The pieces were all of uniform size (approximately 1/8 in. by 1/8 in.) with only an estimated 15% of the material either above or below this size.

Run 18: Pellet No. 2 was the only one recovered intact; the others had disintegrated to chips and powder. Examination of this specimen showed, as in the case of the others, angular breaks and radial fractures.

Contamination of the cave following removal of the water from the autoclaves was negligible; however, when the capsules were first opened, the cave became highly contaminated. One-cubic meter air samples showed unusual amounts of activity which were slow to decay. The following tabulation is typical of the measured activity levels.

Decay Time	Beta Activity Level	Alpha Activity Level
1-2 min	9 mr/1 in.	29 x MPL*
18 hr-31 min	1.3 mr/1 in.	-
6 days	70.4 x MPL*	23 x MPL
15 days	37.8 x MPL	22.7 x MPL

* Maximum permissible level for working cave.

UNCLASSIFIED

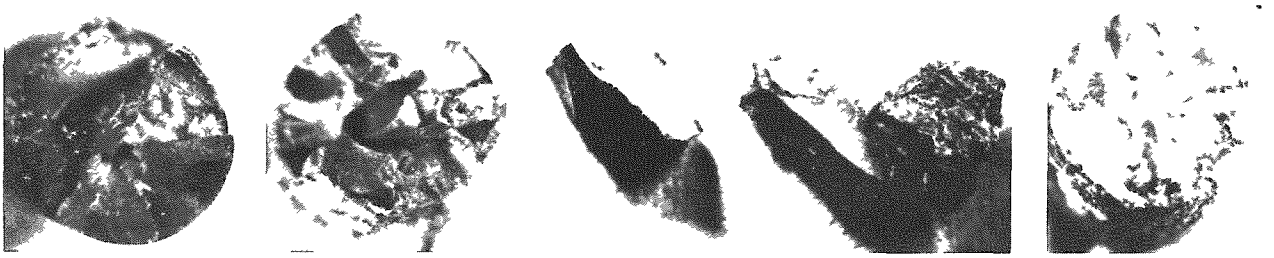

PELLET NO. 1 NO. 2 NO. 3 NO. 4

RUN NO. 16 - 1042 hr

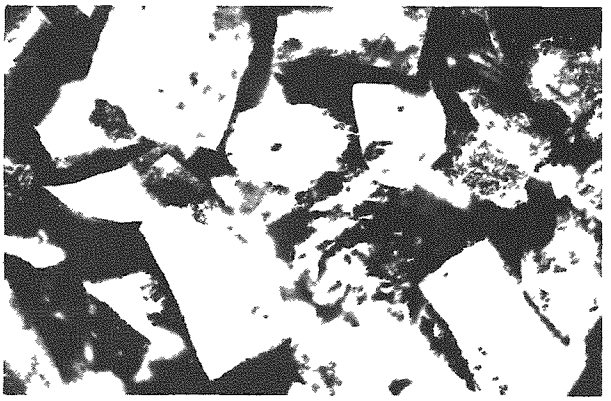

TYPICAL SHATTERED PELLET SHOWING CHARACTERISTIC RADIAL FRACTURES.

RUN NO. 17 - 1592 hr

PELLET NO. 2 - SINGLE INTACT SPECIMEN

RUN NO. 18 - 260 hr

FIG. 42
URANIA-THORIA BODIES IRRADIATED IN CP-5 AUTOCLAVE TEST FACILITY

DECLASSIFIED

Tests of two more thoria-urania specimens with lead bonds between pellets and the aluminum-1% nickel alloy can are in progress.

2. Detection and Location of Fuel Element Ruptures - W. G. Marburger, J. H. Monaweck

An experiment was carried out to test possible methods of locating ruptured fuel elements in the core of a reactor after cladding failure detection and subsequent shutdown. The methods tested were:

(1) Comparing gross gamma activities of fission product materials depositing on the surfaces of sampling devices placed at different points in the circulating water system.

(2) Comparing gross gamma activities of water samples from different parts of the system under different conditions.

A stainless steel, 3-plate subassembly of simulated EBWR fuel plates was placed within a stainless steel standpipe (6 in. dia. x 10 ft long). Boiling water at 400F and 250 psi was pumped through the standpipe with a velocity of 4 fps past the simulated elements.

A failure or hole in the cladding of the fuel plate was simulated by tapping a hole in one of the stainless steel plates perpendicular to the surface and screwing rods of slightly irradiated reference fuel alloy into the tapped holes until the surface of the alloy was flush with the surface of the fuel plate. The hot water and steam passing up the channel over the exposed surface of the fuel corroded the reference alloy and transported the uranium throughout the system. The other channel contained no fuel and therefore generated no contamination.

Grit-blasted stainless steel coupons were placed at various points in the standpipe to act as sampling surfaces. In addition, one unglazed ceramic tube (1/2 in. dia. x 4 in. long) was placed in the flow stream from the channel which had the corroding reference fuel alloy. A similar tube was placed in the flow stream from the channel containing no reference alloy.

The loop was operated with forced circulation at temperature and pressure for 8 to 10 hr, and then cooled to room temperature in approximately 16 hr. The ceramic cylinders and coupons were removed from the standpipe and the contaminating deposit on each was dissolved in acid. The concentration of contamination was determined by measuring the gamma activity of the acid.

DECLASSIFIED

The data from two runs show no difference in activity between material collected by the ceramic cylinder over the channel containing exposed fuel and the cylinder over the channel containing no fuel. The activity was greater on those coupons near the bottom of the standpipe. This was expected, since the coupon near the bottom collected large settled particles of contamination plus the very fine particles carried in the flow stream, while the top coupon collected only those particles distributed by the flow stream.

In addition to the collection of contamination on surfaces, samples of water were taken from the bottom of the standpipe, from the top of the standpipe, and from the stream flowing over the fuel alloys. A sample of water was also taken from the channel while brushing the surfaces of the channel, including the fuel insert. Another sample of water was taken from the channel containing no fuel while that channel was being brushed. Subsequent analyses showed the water at the bottom of the column contained more contaminating particles than the top water, but the contamination in the clear and loaded channels was approximately the same.

It is concluded that after only a few hours of operation with a ruptured fuel plate, a reactor system would be thoroughly contaminated throughout, and samples withdrawn from any part of the container would depend only on the settling characteristics of solid particles in that particular part of the reactor. Neither of the methods tested could be used for determining the location of a fuel element rupture in the system.

D. Control and Thermal Shield Materials

1. Alternate Control Rods for EBWR - J. H. Monaweck

An alternate control rod proposed for EBWR consists of three sections: (a) a welded stainless steel can made up in the form of a cross, approximately 3 ft long with 10-in. blades; (b) a gadolinium-samarium powdered oxide mixture to fill the can; and (c) a second cross, approximately 10 in. long with 10-in. blades, composed of rolled sheet hafnium metal and riveted to the stainless steel can. This composite cross has two distinct advantages in that: (a) it uses hafnium only at the tip of the rod which is closest to the core with the rod in the "full out" position; and (b) it can be constructed at considerably less cost than a complete rod made solely of hafnium.

A model of this rod has been fabricated. The can is blanked from stainless steel sheet (0.050 in. thick). With simple bending and welding it is made to form a container cross with two empty channels, 3 ft long by 10 in. wide by 0.150 in. thick. Added support is supplied by spotwelding 30 evenly spaced blind support studs between the walls of each blade of the cross. After filling with the loose oxides, four stainless steel plugs are welded into the arms of the cross to seal the container and also to allow attachment of the hafnium plates.

DECLASSIFIED

The proposed filler powder, known as 920 mixture, is composed of 50% (min.) samarium oxide and 25% (min.) gadolinium oxide. The balance of the material is composed of member oxides of the rare earth group. The powder as received has an apparent density of 1.3 which, at a layer thickness of 0.150 in. in the cross, is not sufficient for long-time use in EBWR. The Argonne Metallurgy Division has densified these powders by pressing them with 1/2% B_2O_3 added and sintering at 1600C. The sintered mass was crushed and screened. The bulk density of the powder screened to - 100 + 200 mesh was 3.58, whereas that of the powder screened to - 325 mesh was 2.72. The sintered oxides used to fill the above-described cross were screened to have a bulk density of 4.4. The packed density in the cross is 4.1.

The filled cross control rod is to be subjected to the following tests:

(1) thermal cycle between 550F and room temperature to check the amount of warping and change of physical dimensions;

(2) heat in water at EBWR temperature and pressure to determine any tendency for the can walls to collapse upon application of external pressure.

Another alternate control rod consists of powdered B_4C incorporated into a stainless steel matrix. The boron may remain either as solid boron carbide particles incorporated into the stainless steel or the boron, as metal, may dissolve in the stainless steel. Attempts are being made to cast crosses containing high percentages of boron. The present limit is approximately 2%. The cross is cast oversize and is machined to acceptable dimensions. Efforts at developing boron stainless steels are described below.

2. Boron-Stainless Steel Development

a. Fabrication - N. Balai

Stainless steel compositions containing high weight percentages of boron (1.0% and above) show promise as: (1) thermal shielding materials to reduce thermal stresses in reactor pressure vessel shells, and (2) as control rod materials. Conversations were held with a number of producers who have had previous experience in this alloy field for the production of 1-in. thick plate for the EBWR thermal shield. The conversations showed that alloys are obtainable by three different processes: (1) castings, (2) conventional induction furnace air melted alloys, and (3) vacuum melted alloys. A summary of the alloy melting (and production) processes are:

DECLASSIFIED

Source	Process	Boron Range, (Wt - %)	Comments
Electric Steel Foundry Co., Portland, Ore.	Steel castings	over 2.0	Two 1 x 14 x 14 in. experimental castings shipped to ANL Two 1 x 14 x 48 in. castings shipped (2% B) 3600 lbs, castings on order in 5, 6, 7, 8, 9 and 10% boron by weight
Republic Steel Corp.	Air-melted, rolled plate	1.5	One 600-lb experimental ingot on order; to be rolled into 1, 1/2, and 1/4-in. plate
Crucible Steel Corp., Syracuse, N.Y.	Vacuum-melted, rolled plate	1.5 and 2.0	One 600-lb experimental ingot in each alloy on order to be rolled into 1, 1/2, and 1/4-in. plate. Production of laboratory heats in 1.2% B claimed satisfactorily rolled
Universal-Cyclops Steel Corp., Bridgeville, Pa.	Vacuum-melted, rolled plate	to 2.2	Plates to 1/8 in. claimed satisfactorily rolled. In position to bid EBWR requirements in 1 x 18 x 60 in. rolled plate
Superior Steel Corp., Pittsburgh, Pa.	Air-melted, rolled plate	1.0	Strip to 0.015 in. cold rolled from 300-lb ingot. Scaling up process to 2000-lb ingot in 1.2% B content. In position to bid EBWR 1-in. plate requirements.

Electric Steel Foundry Company Alloy

ESCO cast two experimental 1 x 14 x 14 in. plates in a nominal 2% boron (by weight) modification of the CF-8 alloy - one plate in the horizontal position and the other in the vertical position. The casting qualities were good, as evidenced by the 2-in. as-cast "shiplap" edge joints. Accompanying radiographs of the two plates indicated many voids which

DECLASSIFIED

could be interpreted as gas pockets. However, since many machining operations failed to confirm the presence of the varying voids, density of the radiographs may indicate gross segregations of the boron phase.

The horizontally cast plate was cut in half and machined for weldability tests. Planer chips were curly, indicating some ductility. A single vee-butt weld, approximately 10 in. in length, was completed, using a stainless steel Type 308-coated electrode without preheating the base material. An estimated over-correction (for weld pull) and heavy restraint by C-clamps resulted in a badly pulled plate on cooling (approximately 200 degrees from the expected horizontal plane). The fluidity of the melted base alloy was too great for "undercutting." An attempt to cold straighten a section of the welded plate resulted in a sudden and brittle fracture in the base alloy approximately 1/2 in. away from the weld fusion line.

Other samples of the welded plate were hot straightened at 1950 and 2200F without difficulty. The hardness of the hot-straightened base metal ranged from Rockwell B-85 to B-95; the Type 308 welds were found to be slightly embrittled; Rockwell hardness readings of C-12 to C-15 were obtained.

Four 1 x 14 x 48 in. edge cast plates were ordered for: (1) shielding tests in CP-5 (three plates), and (2) further material evaluation tests. In the gate-cutting operations prior to shipment, all four plates were cracked along one edge by flame cutting. Two of the best plates were ordered shipped for the shielding tests.

Cast material in a boron-modified CF-8 alloy, totaling approximately 3600 lb is on order for material evaluation tests. Samples have been ordered in round bar, square plates, and cross shapes.

Superior Steel Corporation Alloys

Superior Steel Corporation has succeeded in air-melting a 300-lb, 1 wt-% B (nominal) ingot and rolling it to a bar 0.340 in. ga. x 5-1/2 in. x 260 in. Pieces of the bar have been cold rolled down to 0.015 in. ga. strip in about 8 passes with intermediate anneals. A chemical analysis of the alloy was reported to be: C-0.06, Mn-1.58, P-0.028, S-0.016, Si-0.53, Cr-18.27, Ni-11.03, B-0.90/0.94%. The alloy in the 0.340 in. ga. is reported to possess the following mechanical properties:

Tensile Strength: 100,000 psi

Yield Point: 50,000 psi

Elongation: 28%

DECLASSIFIED

A 2000-lb ingot with 1.2% B content is to be melted for plate mill rolling experience for the production of 1 in. ga. plate. A further scale-up to a 3500-lb ingot is planned before the end of the year. Material is being made available for evaluation tests.

Crucible Steel Corporation Alloys

Two 600-lb vacuum melted ingots, containing 1-1/2 and 2 wt-% B, respectively, to be rolled into 1 in., 1/2 in., and 1/4 in. plate products, are on order. Crucible claims to have rolled small experimental heats down to 1/8 in. strip in the 1% boron range. The alloy is in the 18% Cr-15% Ni composition.

b. Corrosion - C. R. Breden

The corrosion properties of boron stainless steels of various compositions and from various sources are being investigated. Results to date are summarized in Table X. It will be noted that all of the alloys tested, ranging from 1 to 3% boron, showed good corrosion resistance. In most of the static tests the weight changes were positive, while in the dynamic tests they were negative.

3. Corrosion of Aluminum-Boron-Nickel Alloy - C. R. Breden

Corrosion evaluation tests on samples of aluminum-1% boron-0.5% nickel alloy, used in BORAX III as a burnable poison, have been continued.[14] In general, there was no significant change in appearance except for the weld areas, which showed black glossy slag, holes, and spalling.

Samples of Boral, one as received and the other rolled to a thin sheet about 0.020 in. thick, were tested in 420F degassed water. After test periods of 64 and 160 hr both samples showed high positive weight changes, pits and blisters.

4. Soluble Poisons - N. R. Grant

a. Capacity of Amberlite IRA-400 Resin for Boric Acid

Boric acid is used in BORAX III for control purposes; it is removed by an anion resin bed followed by a mixed-bed ion exchanger. Since available information on anion resin capacities for boric acid is limited, some capacity determinations were made on Amberlite IRA-400.*

[14]Reactor Engineering Division Quarterly Report, ANL-5471 (September, 1955) p. 128.

*Manufactured by Rohm and Haas, Philadelphia, Pennsylvania.

DECLASSIFIED

Table X

BORON-STAINLESS STEEL CORROSION TESTS

Sample No.	Nominal Composition, % Cr	Ni	B	Source	Test Condition	Temp, F	Test Period, hr	Rate of Wt Change, $mg/cm^2/mo$	Comments
A-495	18	8	1	ESCO*	Static**	600	134	+0.34	
							376	+0.145	Adherent black coating.
					Static (air satd.)	600	134	+0.424	
							376	0.0	Adherent dark brown tarnish.
A-496	18	8	2	ESCO	Static	600	134	+0.34	
							376	+0.073	Adherent black coating.
					Static (air satd.)	600	134	+0.068	
							376	+0.048	Adherent brown-black tarnish.
A-497	18	8	3	ESCO	Static	600	134	+0.142	
							376	+0.076	Adherent brown-black tarnish.
A-4403-a	18	14	1.6	KAPL	Dynamic	600	644	-0.152	Adherent black coating.
							721	-0.072	Adherent black coating.
A-4403-b	18	14	2.5	KAPL	Dynamic	600	644	-0.130	Adherent black film.
							721	-0.093	Adherent black film.
A-4473a-1	18	14	2.2	ESCO	Static	550	160	-0.415	Adherent black film.
A-4473a-2	18	14	2.2	ESCO	Static	550	160	+0.382	Adherent black film.
A-4473b-1	18	14	2.8	ESCO	Static	550	160	+0.316	Adherent black film.
A-4473b-2	18	14	2.8	ESCO	Static	550	160	+0.254	Adherent black film.

*Electric Steel Foundry Company, Portland, Oregon.

**Degassed water used unless otherwise noted.

Solutions containing 200 and 500 ppm boric acid were passed through various sized resins beds supported on stainless steel screen in Pyrex glass columns. The resins were used in a completely regenerated form. Procedures were carried out in accordance with the manufacturer's published recommendations for the resin.

Boric acid concentrations were determined by a modification of the Young[15] method, based on initial neutralization followed by titration in the presence of mannitol. Solutions were protected from atmospheric CO_2; resistivity and pH measurements were taken at regular intervals.

Results are summarized in Table XI and in Figs. 43 and 44. It appears that under the test conditions employed, the unit capacity (milliequivalents of boric acid/cc of resin) increases with increased bed volume for a given concentration of boric acid in the influent solution. However, at a bed volume of 865 cc (1-1/2 in. ID by 33 in. high) the unit capacity appears to be approaching a maximum. For a given bed volume, a higher unit capacity was obtained with an influent solution containing 500 ppm of boric acid than with a 200-ppm influent.

During the portion of a typical run prior to the break point (defined as the point at which large concentrations of boric acid begin to pass completely through the bed), the pH of the effluent was above 7 and the specific resistance was low, since boric acid was displacing sodium hydroxide from the bed. At the break point, the pH decreased to 7 and the specific resistance reached a maximum because of a deficiency of both boric acid and sodium hydroxide at this point. After the break point, the pH decreased to the acid side (below 7) and the specific resistance dropped because of increased boric acid content. These effects may be seen in Fig. 43.

A comparison of the boric acid concentration in the effluent as a function of the quantities of boric acid added during the five runs completed may be seen in Fig. 44.

Under the conditions of the experiment, i.e., small scale apparatus and absence of irradiation, the unit capacity of Amberlite IRA-400 anion resin for boric acid ranged from 1.1 to 1.4 meq/cc of resin (4.2 to 5.4 lb boric acid/cu ft).

b. Irradiation of Boric Acid Solution

In a recent BORAX III experiment, pH values as low as 2.7 and as high as 9.1 were observed in the coolant-moderator water containing added boric acid for control purposes. In an effort to resolve this

---

[15]Roland S. Young, Industrial Inorganic Analysis, (New York: John Wiley, 1953), p. 36.

DECLASSIFIED

Table XI

REMOVAL OF BORIC ACID USING AMBERLITE IRA-400 RESIN - SUMMARY OF RESULTS

All Resin Beds 100% Converted or Regenerated

Flow Rate: 0.2 ml Boric Acid Solution/min/cc of Resin

Run No.	Column ID, in.	Resin Bed Height, in.	Resin Bed Vol., cc	Over-all Average Flow Rate, ml/min	Vol. 4% NaOH for Conversion or Regeneration, liters		Vol. Distilled Water for Washing, liters	Avg. Conc. Boric Acid Influent, ppm	Vol. Boric Acid Influent to Breakpoint, liters	Total Vol. Boric Acid Influent, liters	Total Capacity, meq	Unit Capacity, meq/cc Resin
1	1/2	31-1/2	98.5	20.3	Conversion	2.4	13	206	33	37.5	110	1.117
2	1/2	21-3/4	68	15.2	Regeneration	1.0	6	202	21	26.5	68.6	1.009
3	1/2	21-3/4	68	15.2	Regeneration	1.0	9	514	10	15.0	83.3	1.225
4	3/4	30-1/2	220	45.2	Conversion	5.3	24	518	36	47.0	302	1.374
5	1-1/2	33	865	174.4	Conversion	21.0	46	514	144	185.5	1196	1.382

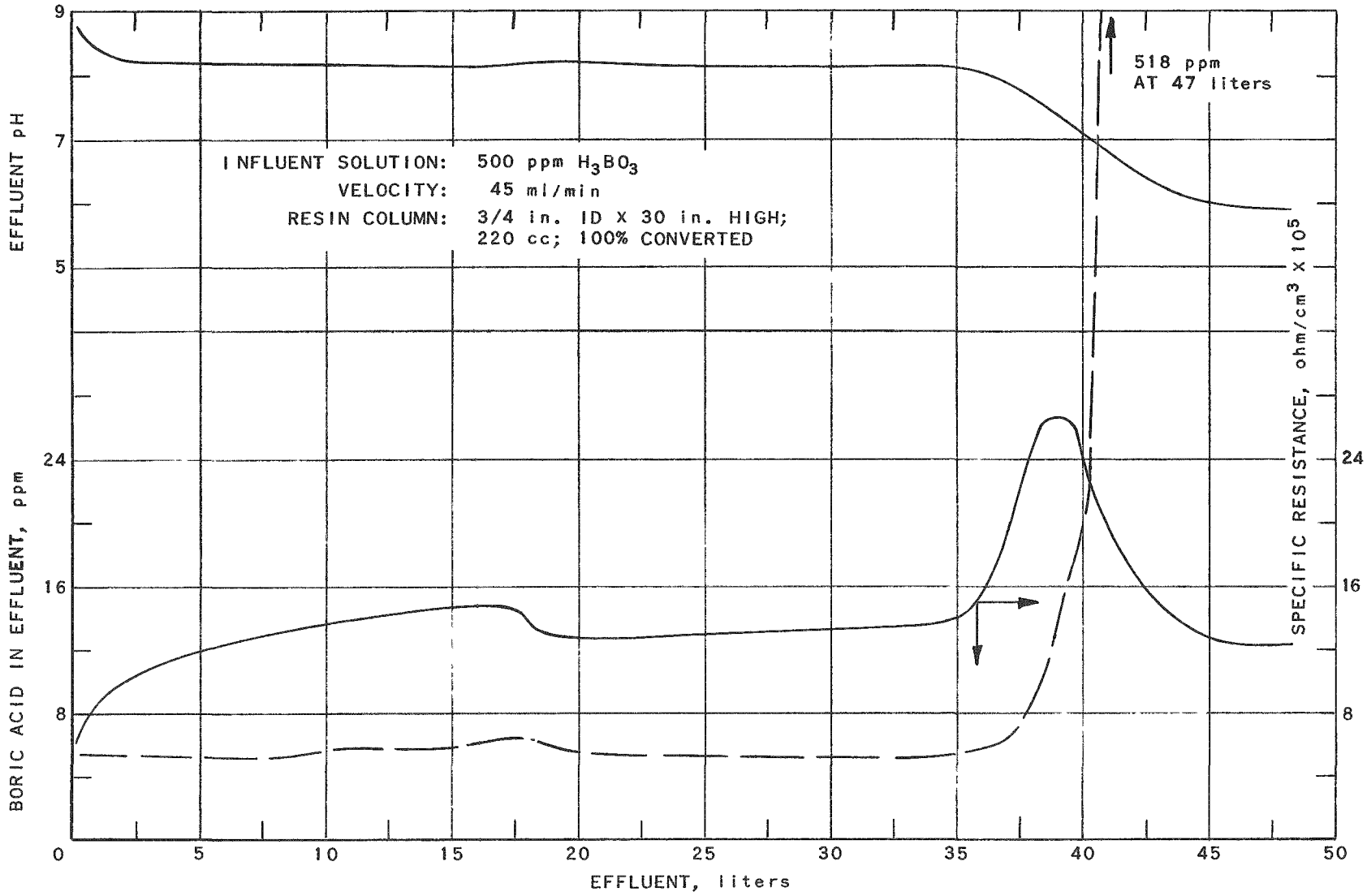

FIG. 43
REMOVAL OF H_3BO_3 USING AMBERLITE IRA-400 RESIN
(RUN NO. 4)

RE-7-16563-A

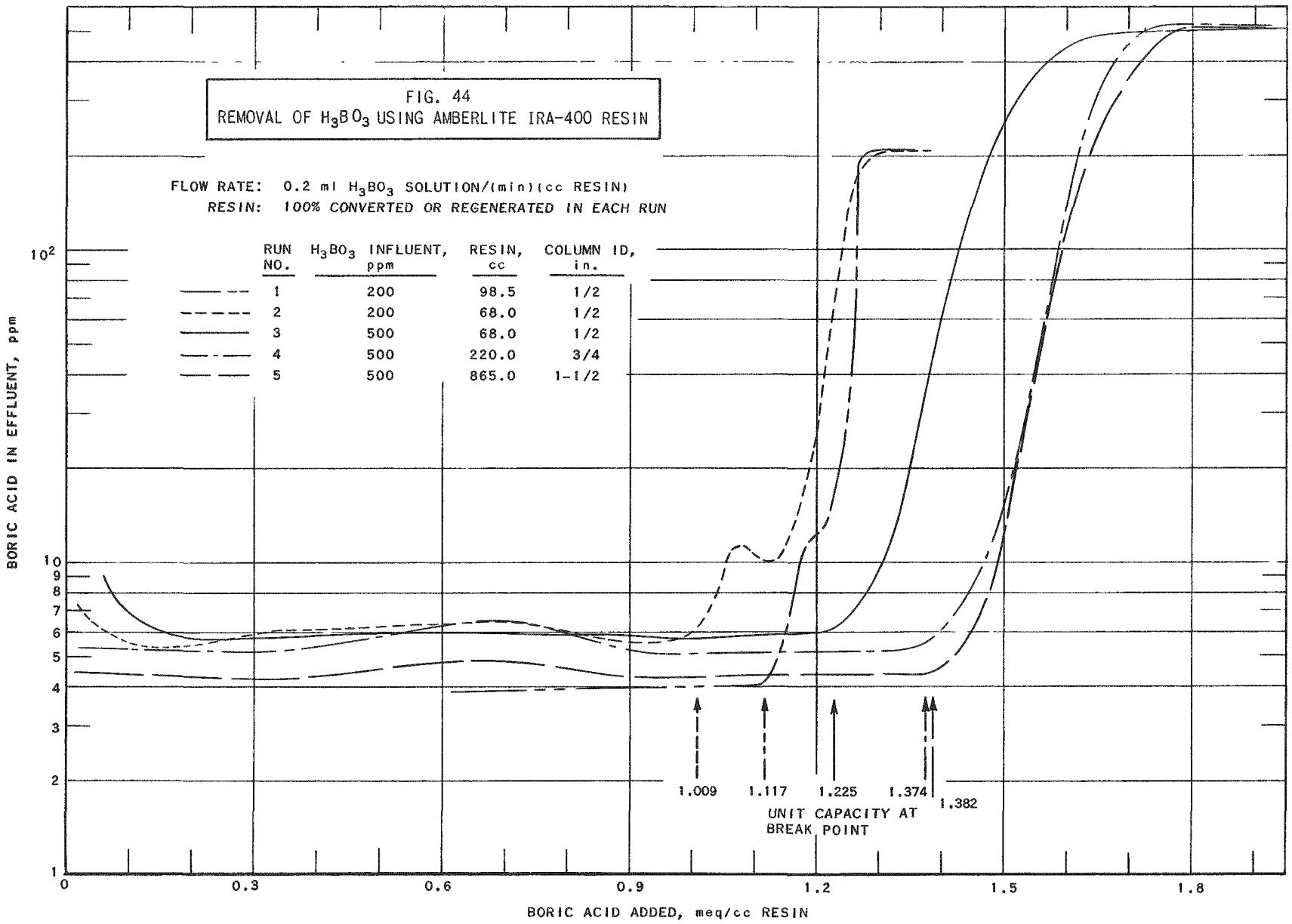

FIG. 44
REMOVAL OF H_3BO_3 USING AMBERLITE IRA-400 RESIN

RE-7-16562-B

behavior, a 50-ml sample of 500 ppm boric acid solution with an original pH of 6.2, in contact with 2S aluminum, was irradiated for 110 hr at 450F in a stainless steel autoclave pressurized with helium in a CP-5 facility. Examination of the resultant solution showed a pH of 2.53 and a nitric acid concentration of 200 to 250 micrograms/ml of solution. Also noted were small red particles of iron oxide suspended in the solution.

To simulate BORAX III conditions, the remainder of the sample was run (downward) through a small resin column (1/2-in. dia.) containing 6 in. of Amberlite anion resin XE-78 and 2 in. of Amberlite mixed-bed resin XE-150 in the order of solution passage. The pH of the effluent for the first half of the solution was 6.7; for the last half it was 8.1. The change in pH during the run may have been caused by channeling through the resin bed. It is believed that the low pH resulted from the presence of nitric acid produced by irradiation of atmospheric nitrogen incompletely purged from the autoclave, and that these factors: ion exchanger characteristics, and nitric acid formation from atmospheric nitrogen, could have accounted for the observations noted in BORAX III.

E. Control Rod Drive Mechanisms

1. Hydraulically Operated Drive Mechanism - C. F. Bullinger

The development of the hydraulic drive mechanism, as an alternate safety rod drive for the EBWR, continues. As a safety rod drive, the unit has only two operating positions, in or out; therefore, continuous position indication, which is difficult with a sealed drive, is not so important, and two-position indication is easily achieved. The unit described in ANL-5461[16] has proved quite stable and easily controllable through all system pressure ranges from 50 to 650 psig. Artificially induced surges of 200 psi in 30 seconds have not disturbed the rod position.

Scram tests utilizing a 4-inch, quick-opening, sleeve-type valve were unsatisfactory. The best time achieved was 1.5 seconds for a 48-inch scram travel. Opening time for the valve was 0.4 to 0.5 second. The high-velocity of the water through the large valve imposed high stresses on the system when stopping the scram if full rate of flow was allowed; therefore, it was necessary to restrain the rate of flow by valving down the outlet line and partially filling the buffer tank.

A 1-inch swing check-type valve with a 3-way solenoid operator has given satisfactory performance to date. This valve opens in approximately 0.20 to 0.25 second from the time the scram signal is initiated. Scram times measured in initial tests varied from approximately 0.7 second for 200-psig operation to 0.45 second for 600-psig operation, for 48-in. travel. Further tests are in progress.

---

[16] Reactor Engineering Division Quarterly Report, ANL-5461 (April 15, 1955) p. 29

DECLASSIFIED

2. Magnetic Jack Drive Mechanism - J. N. Young

Testing has continued on the magnetic jack (No. 16).[17] After completion of 500 cycles (4 ft up and 4 ft down at forty 0.010-in. steps per minute) with a 155-pound load, a new set of coils of an improved design was installed to give the jack more strength and to reduce the heating problem. With the new coils, the jack was operated through 230 cycles with a 400-pound load, when excessive gripper wear necessitated shutting down. During the tests, operation was satisfactory; there was some slippage during running; however, the mechanism never failed to scram or to hold.

To overcome the wear problem, new grippers with more wear surface and with self-aligning pads were fabricated. This unit (No. 17) was tested to 330 cycles with a 155-pound load and 105 cycles with a 400-pound load. There was practically no wear, but during the last few hours of test the rod began to stick and fail to scram. It was found that the self-aligning gripper pads were stuck because of corrosion of the Armco iron gripper bodies.

To eliminate both the wear problem of Unit No. 16 and the sticking problem of Unit No. 17, Unit No. 18 was constructed and has operated very well with loads up to 120 pounds, at 1300 watts input. Testing is continuing on this unit. A modification is in progress to increase strength and decrease input power.

---

[17] Reactor Engineering Division Quarterly Report, ANL-5371 (January 15, 1955) p. 214.

DECLASSIFIED

PART B. FAST POWER BREEDER REACTOR PROGRAM

SUMMARY - L. J. Koch

The EBR-II Working Model was filled with sodium and placed in working order. The system was filled directly from the storage tank and the sodium cold trapped as described previously.[18] After the system was filled, the sodium surface was covered by an unbroken, dull film. The sodium temperature was raised and, after cold trapping for several days, the film disappeared. No difficulty was encountered in pumping the 5,000 gallons of sodium into the model tank or in the process of cold trapping. Very clean sodium (0.002 wt-% oxide) was obtained in this large system with no difficulty.

The ambient temperature of the sodium was progressively raised approximately 50 or 100 degrees per day up to a maximum of 700F. Some difficulty was experienced with sticking of the control and fuel-handling mechanisms. These conditions were improved by removing the units and increasing clearances between moving parts. Another difficulty arose due to differential expansion of the tank in which the system components are mounted. Misalignment was detected between the stations in the fuel element transfer mechanisms. This could not be corrected because sufficient clearance was not available between the tank and the mounting plugs. Fuel element transfers were successfully carried out by compensating for the misalignment. This condition is being corrected by increasing clearances to permit adjustment of equipment at operating temperatures.

The 1,000-gpm, d-c, electromagnetic pump operated very satisfactorily submerged in sodium. The performance of the pump was somewhat better than previous operation in a closed loop. This improvement was probably due to decreased gas entrainment in the sodium.

The second irradiation test was removed from CP-5 after an estimated 0.4% burnup. A section at the top of the fuel element had melted through the element tube. This failure is believed to be due to a void in the sodium bond between the fuel element and the finned-tube capsule. A void may be caused by the repeated melting and freezing of this bond each time the reactor is shut down. These conditions will be duplicated in an external experiment simulating the irradiation conditions to determine if a void can be created in this manner.

---

[18] Reactor Engineering Division Quarterly Report, ANL-5471 (September, 1955) p. 161

DECLASSIFIED

An electrically heated model of the EBR-II fuel subassembly has been constructed to simulate decay heating after various periods of cooling. The fuel subassembly will not cool in air after two weeks of cooling in the primary system. Forced convection of approximately 10 cfm of air is sufficient to remove the 2300 watts of heat which will be generated in the hottest subassembly after two weeks cooling. Additional tests are planned to determine the cooling requirements during the process of removing the hexagonal subassembly container tube and disassembling the individual fuel elements. It appears that forced convection cooling will be required until the fuel elements can be individually separated from the close-packed geometry.

Water pressure drop tests were run on a complete EBR-II fuel subassembly. In addition, the pressure drop loop was arranged to permit the measurement of the hydraulic "hold-down" force exerted by the water. The results, when converted to anticipated conditions in the reactor with sodium, indicate that the subassembly will be held in position hydraulically under all projected conditions of operation.

The conversion ratio for EBR-I second loading was measured by "physical methods" and found to be 1.03 ± 0.05 as compared to a value of 1.01 ± 0.05 measured on the first EBR loading.[19]

Activation measurements have been made at various locations in the outer blanket of EBR. Calculations were performed to compare the experimental measurements with diffusion theory.

---

[19] C. D. Curtis, et al., "A Physical Determination of the Conversion Ratio of The Experimental Breeder Reactor," ANL-5222 (August, 1954.)

I. EXPERIMENTAL BREEDER REACTOR I (EBR-I)

A. Conversion Ratio Measurements - W. Y. Kato, F. S. Kirn, W. F. Mann, D. Metta, G. Main

The conversion ratio has been measured in the second uranium fuel loading of the Experimental Breeder Reactor I. It is a measure of the production of Pu^{239} from the natural uranium blanket per atom of U^{235} destroyed in the reactor. The ratio is determined by a knowledge of the relative amounts of fuel and blanket material and the measurement of the spatial neutron capture and fission distributions in U^{238} and U^{235}, respectively, together with a determination of the effective alpha for U^{235} throughout the reactor.

1. Experimental Procedure

The capture distribution of U^{238} was determined by the irradiation of the depleted U^{238} foils throughout the reactor. In the core and inner blanket, vertical distribution measurements were obtained by sandwiching U^{238} foils between slugs of enriched U^{235} or natural uranium to simulate fuel or blanket rod assemblies. The vertical distribution traverses were made along a radial direction to one corner of the hexagonal core. Another series of traverses was also made toward the flat of a hexagonal side. Normalization between successive traverses was accomplished by irradiating depleted U^{238} foils in the thermal column and using the foil's capture rate activity as standard. The principal reaction in the depleted foils which took place during the irradiation was:

$$n + U^{238} \longrightarrow U^{239} \xrightarrow[23.5\ \text{min}]{\beta,\gamma} Np^{239} \xrightarrow[56.6\ \text{hr}]{\beta,\gamma} Pu^{239} .$$

The capture rate was obtained by observing the 100-kev radiation in the decay of Np^{239} with a thin, NaI scintillation counter using a conventional single-channel pulse height analyzer, as in a procedure developed by Axtmann and Stutheit.[20] The discriminator and window of the analyzer were set to observe just the maximum of the 100-kev photoelectric peak of the Np^{239} radiation.

Following irradiation of the foils the procedure was to measure the thermal column foil activity before and after measuring the activity of a set of foils irradiated in the fast spectrum. Thus in each

---

[20] R. C. Axtmann and J. S. Stutheit, "Scintillation Counting of Natural Uranium Foils," Nucleonics, 12, 52 (July, 1954).

DECLASSIFIED

vertical traverse there was obtained a distribution of fast captures per thermal column capture by taking a ratio of the counting rate of the foil in the fast spectrum to the counting rate of the foil irradiated in the thermal column. Since the thermal column foil was irradiated at the same time as those in the core or blanket, this method of normalization automatically accounted for any variations in reactor power, as well as the decay time of the Np^{239}. Since the same shape and size foil was used for the thermal column as for the core, it was not necessary to introduce corrections for geometry in the counting rate obtained by the analyzer. It was, however, necessary to irradiate the normalization foil in the same place in the thermal column each time. The usual corrections for small variations in foil weight and background were made before computing the fast captures per thermal column capture.

Sufficient activity for analysis was obtained in an irradiation of about 20 kwh, which corresponds to an integrated flux of about 7×10^{15} neutrons/cm^2. Typical vertical traverses are shown in Fig. 45 for various parts of the reactor. A plot of the radial fast capture rate distribution is shown in Fig. 46. Since each fuel element has three sections, lower blanket, central enriched core, upper blanket, it was necessary to obtain the average fast captures per thermal column capture in each section. The total captures or plutonium production throughout the reactor was obtained by integrating the product of the amount of U^{238} material and the average fast captures per thermal column capture over the entire reactor volume.

The relative fission distribution of U^{235} was measured by irradiations of enriched U^{235} foils throughout the reactor. The integrated gamma-ray activity of the fission products produced in the foils was measured with a NaI scintillation counter. The discriminator of the amplifier was set so that only gamma rays of energies greater than 0.5 Mev were detected. This decreased the background correction due to U^{238} capture activity and natural activity of the uranium.

A series of vertical traverses along two radial directions from the center of the reactor were made. The U^{235} foils were sandwiched between slugs of enriched U^{235} or natural uranium to simulate fuel or blanket elements similar to the depleted U^{238} case. Simultaneously with the irradiation in the core or blanket, a foil was irradiated in the same standard thermal column position. The ratio of the activities of the fast spectrum foils to the thermal column foil gave a distribution of the fast fissions per thermal column fission . The total number of U^{235} fissions was obtained by integrating the product of the number of U^{235} atoms and the fast fissions per thermal column fission over the entire reactor volume. A typical distribution of fast fissions per thermal column fission for a vertical traverse is shown in Fig. 47. A radial traverse of fission rates is shown in Fig. 48.

DECLASSIFIED

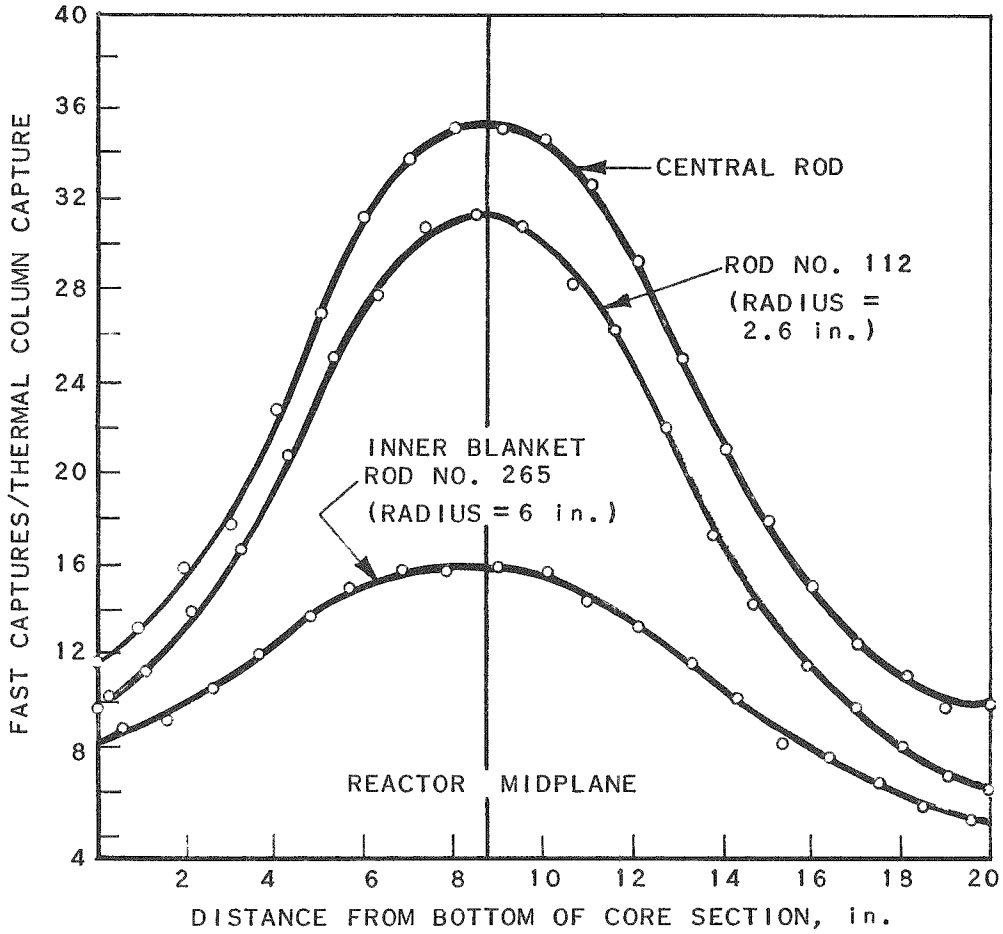

FIG. 45
U^{238} CAPTURE DISTRIBUTION ALONG VERTICAL AXIS OF THE EBR

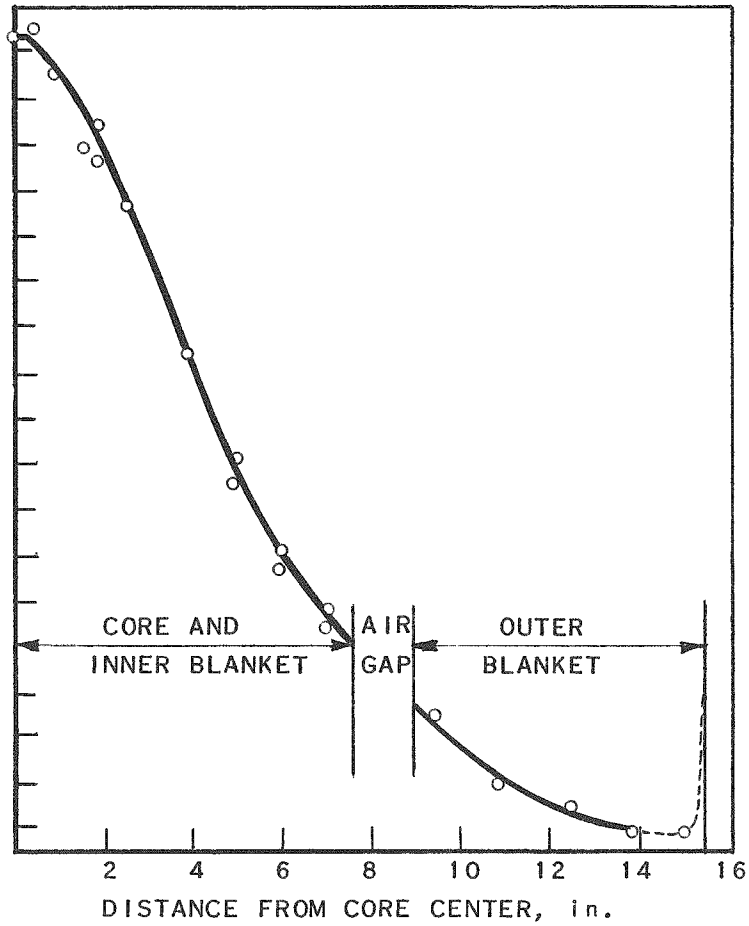

FIG. 46
U^{238} CAPTURE DISTRIBUTION ALONG MIDPLANE OF THE EBR

RE-7-16877-A

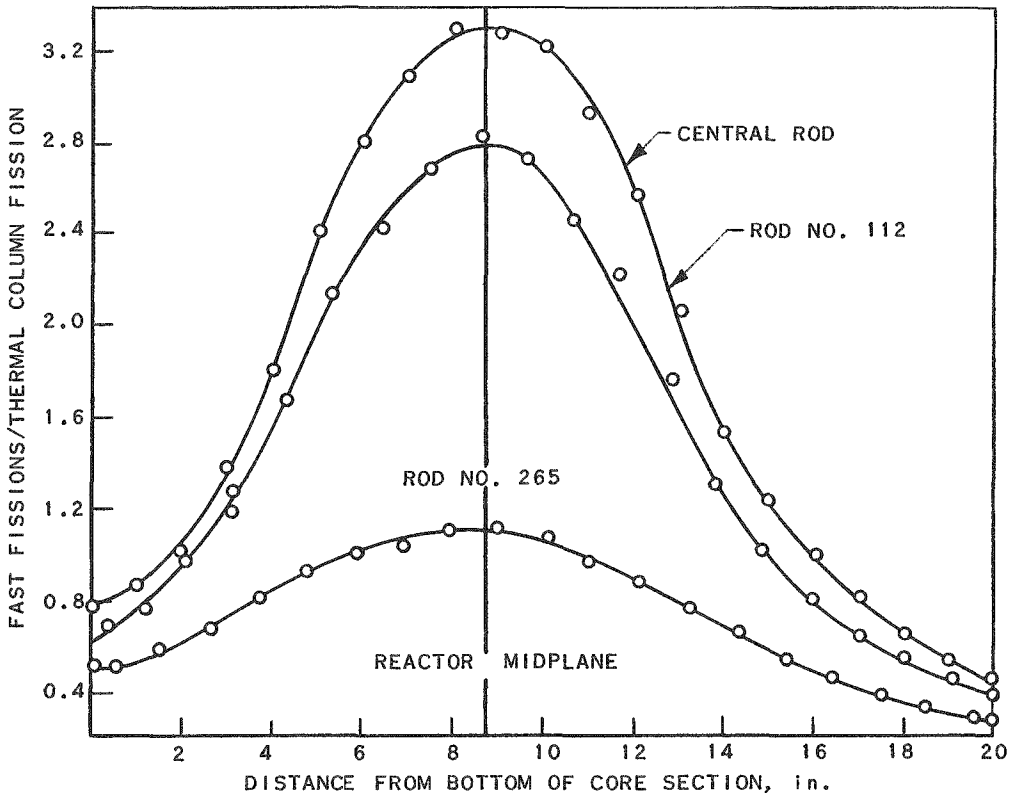

FIG. 47
U^{235} FISSION DISTRIBUTION ALONG VERTICAL AXIS OF THE EBR

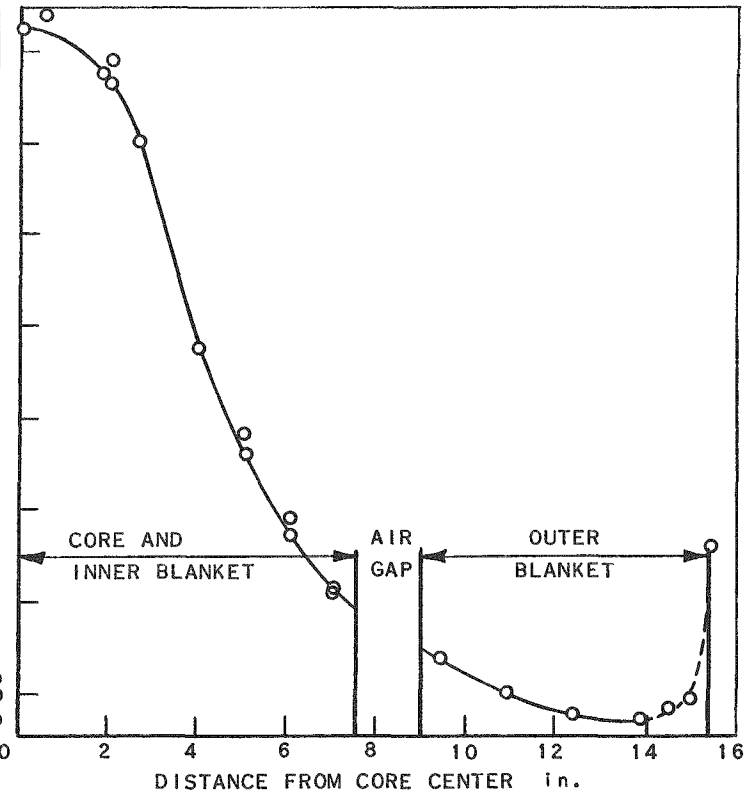

FIG. 48
U^{235} FISSION DISTRIBUTION ALONG MIDPLANE OF THE EBR

The measurements of the U^{238} capture activity and the U^{235} fission activity with the foils resulted in unnormalized capture and fission distribution throughout the reactor. The normalization of the total captures and fissions was made using two independent methods. A vertical distribution of captures and fissions was obtained in the central rod of EBR using duplicate sets of foils. There were thus two foils for each position and the thermal column for the capture rate as well as for the fission rate determinations. A cadmium ratio measurement was also made for the depleted U^{238} and enriched U^{235} foils in the thermal column foil position.

With one set of vertical traverse and thermal column foils the capture and fission distributions were obtained as before. Using the measured capture and fission distributions with the cadmium ratios, and the thermal capture cross section of U^{238} and fission cross section of U^{235}, the conversion ratio (CR) was calculated from:

$$CR = \left(\frac{\sigma_c^{th}}{\sigma_f^{th}}\right) \left(\frac{1 - \frac{1}{CR_f}}{1 - \frac{1}{CR_c}}\right) \left(\frac{\int N^{U^{238}} \frac{C_c^f}{C_c^s} dV}{\int N^{U^{235}} \frac{C_f^f}{C_f^s} dV}\right) \left(\frac{1}{1 + \overline{\alpha}}\right)$$

where

σ_c^{th} = thermal capture cross section of U^{238}, 2.8 barns

σ_f^{th} = thermal fission cross section of U^{235}, 590 barns

C_c^f = specific activity of depleted U^{238} foils irradiated in fast flux

C_c^s = specific activity of depleted U^{238} foils irradiated in thermal column

C_f^f = specific activity of enriched U^{235} foil irradiated in fast flux

C_f^s = specific activity of enriched U^{235} foils irradiated in thermal column

DECLASSIFIED

CR_f = cadmium ratio of U^{235} foil in thermal column

CR_c = cadmium ratio of U^{238} foil in thermal column

$\overline{\alpha}$ = effective alpha of U^{235} in core = 0.143

The effective alpha, $\overline{\alpha}$, of U^{235} in the core was obtained by a mass spectrometric measurement of the U^{236}/U^{235} mass ratio in a number of irradiated U^{235} samples in EBR. The fraction of U^{235} fissioned in the samples was obtained from a radiochemical separation of Cs^{137} using its mass fission yield to determine the total fissions.

The second method of normalization involved the determination of the total number of captures in the second set of depleted U^{238} foils and the total number of fissions in the enriched U^{235} foils using radiochemical techniques. The technique for capture rate determinations is essentially to separate the Np^{239} from the irradiated uranium foil and count the Np^{239} betas with a proportional gas flow counter.

The determination of the absolute disintegration rate of Np^{239} is based on a standardization measurement in which the number of Np^{239} atoms in a large sample was determined from the growth of the Pu^{239} in the sample. A smaller known fraction of Np^{239} atoms is beta counted to determine the efficiency of the beta counter. The absolute disintegration rate of Np^{239} is determined on the basis of the Pu^{239} alpha activity of the larger sample. The specific activity of the Np^{239} was also checked by careful 4π counting the Np^{239} betas. The fraction of Np^{239} separated from an irradiated uranium foil is determined by introducing a known quantity based on the alpha activity of Np^{237} as a tracer before separation. After the Np is separated from the uranium and fission products the Np^{237} alpha activity determines the chemical yield.

The total number of fissions occurring in a U^{235} sample is determined by separating, radiochemically, the Mo^{99} fission product and measuring its disintegration rate by beta counting. The Mo^{99} is separated by using the solvent extraction procedure. The fraction of Mo^{99} separated from the uranium and fission products is determined by weighing the Mo carrier which is introduced into the irradiated uranium solution before separation of the Mo. The absolute beta disintegration rate is obtained from a standardization run by 4π counting a small known fraction of Mo^{99} without carrier obtained from an irradiated sample of Mo. The total fission rate is obtained from the observed disintegration rate of the separated Mo^{99} assuming a mass fission yield of 6.2% for Mo^{99}.

DECLASSIFIED

2. Results

The contributions of the various parts of the reactor to the conversion ratio are given in the following tabulation:

	Fast Fissions Per Thermal Column Fission ($\times 10^3$)	%	Fast Captures Per Thermal Column Capture ($\times 10^4$)	%
Outer Blanket	6.86	5.1	1228	58.1
Inner Blanket	2.26	1.7	570	27.0
Core	123.8	92.5	115.7	5.5
Control Rods	0.41	0.3	79.2	3.7
Lower Cup	0.54	0.4	120.5	5.7
Total	133.87		2113.4	

The conversion ratio for the second uranium loading of EBR-I with the cup about 1/4 in. below its uppermost position was found to be 1.03 ± 0.05, based on the radiochemical normalization. The same conversion ratio was found using the thermal capture and fission cross section normalization.

B. Activation Cross Sections in the Outer Blanket - S. G. Kaufmann, W. B. Loewenstein, L. Pahis, F. S. Kirn

Activation cross section ratios at various locations in the outer blanket of the EBR have been surveyed.

1. Procedure

Experimental bricks were prepared to permit the exposure of foils along the direction radially outward from the vertical center line of the reactor, or to accommodate foils in positions corresponding to those where measurements of the capture to fission ratios of some isotopes had been made previously. Perturbations due to the presence of the foils or containers was held to a minimum. A reference foil exposed in a reproducible position in the thermal column, 70 in. away from the tank wall, accompanied every exposure and was used for normalization purposes whenever the activity was sufficient to permit measurement.

All foils were protected by thin aluminum during the exposure. The plutonium foils were covered by somewhat heavier aluminum sheet which was cold welded along the edges. No alpha contamination was detected on the outside of the encapsuled plutonium after a number of necessary manipulations during and after the exposure.

DECLASSIFIED

Exposed foils were sent back to Argonne and counted after a delay of several days. Each foil was counted over a period of days. The constancy of the ratio of activation of foils exposed during the same run at different points was used as the criterion for reliability of the data. Thermal column measurements by means of a monitor foil proved unreliable for gold and cadmium-covered plutonium because the activation was low. The cobalt monitor foil, however, appeared to have been activated sufficiently so that the discrepancy between the observed and calculated points on the cobalt curves can hardly be relegated to inaccuracies of the measured values.

Captures in U^{238} were detected in a single-channel analyzer circuit. A distinct 100-kev line with the expected time decay was visible. The intensity of this line was assumed to be proportional to the number of captures in U^{238}. Fission rates were determined from the number of pulses whose height was 6 or more times that of the pulses originating in U^{238} capture. Activation of all other foils was measured by counting gamma-ray pulses which appeared distinctly above noise. The decay of the activation was followed and the expected half-lives were verified whenever this seemed practicable.

2. Experiment vs Theory

Calculations were performed to compare the experimental measurements with diffusion theory. The basis of the calculations was UNIVAC Problem 21D01, a cylindrical description of EBR. The predicted values are indicated by the solid curves and the experimental values as discrete points in Figs. 49 and 50.

The solution of Problem 21D01 gives the group fluxes as $\phi_j(R, P)$, where j refers to the energy group, R to the spatial region, and P to a point in the region. Hence the activation, a, of a sample, s, at a given point would be proportional to

$$\sum_{j=1}^{j=20} \sigma_{a,j}^{s} \, \phi_j(R, P) \quad .$$

This quantity was evaluated at various points in the brick. It was then possible to compare the shape of the curve predicted by diffusion theory with that of the experimental data. In general, the agreement is perhaps as good as can be expected. The rather striking disagreement near the brick-graphite interface is due to a limited representation of the thermal neutrons in the multigroup structure.

DECLASSIFIED

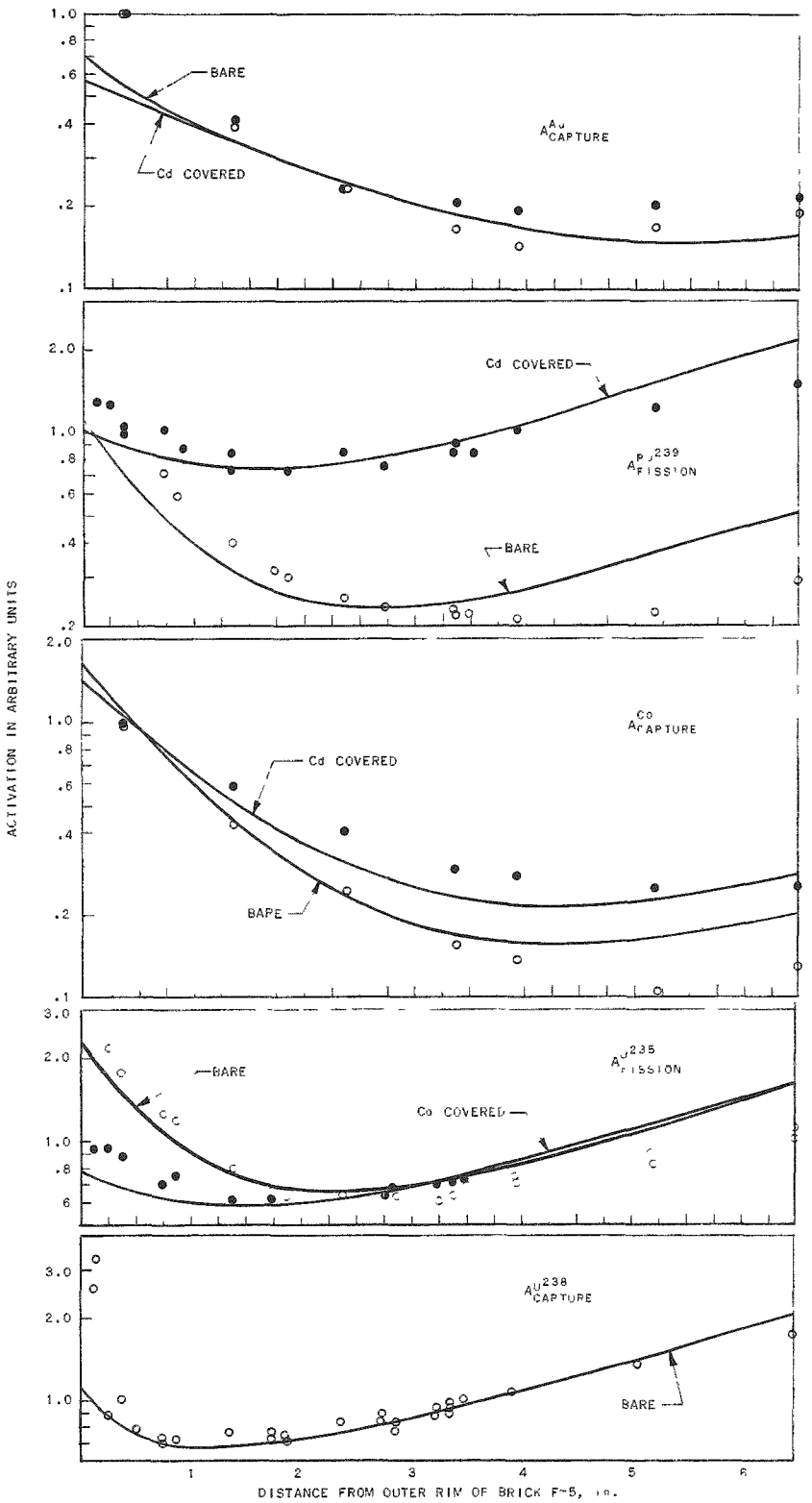

RE-7-16869-B

FIG. 49
COMPUTED VS MEASURED FOIL ACTIVATIONS
IN THE OUTER BLANKET OF THE EBR

DECLASSIFIED

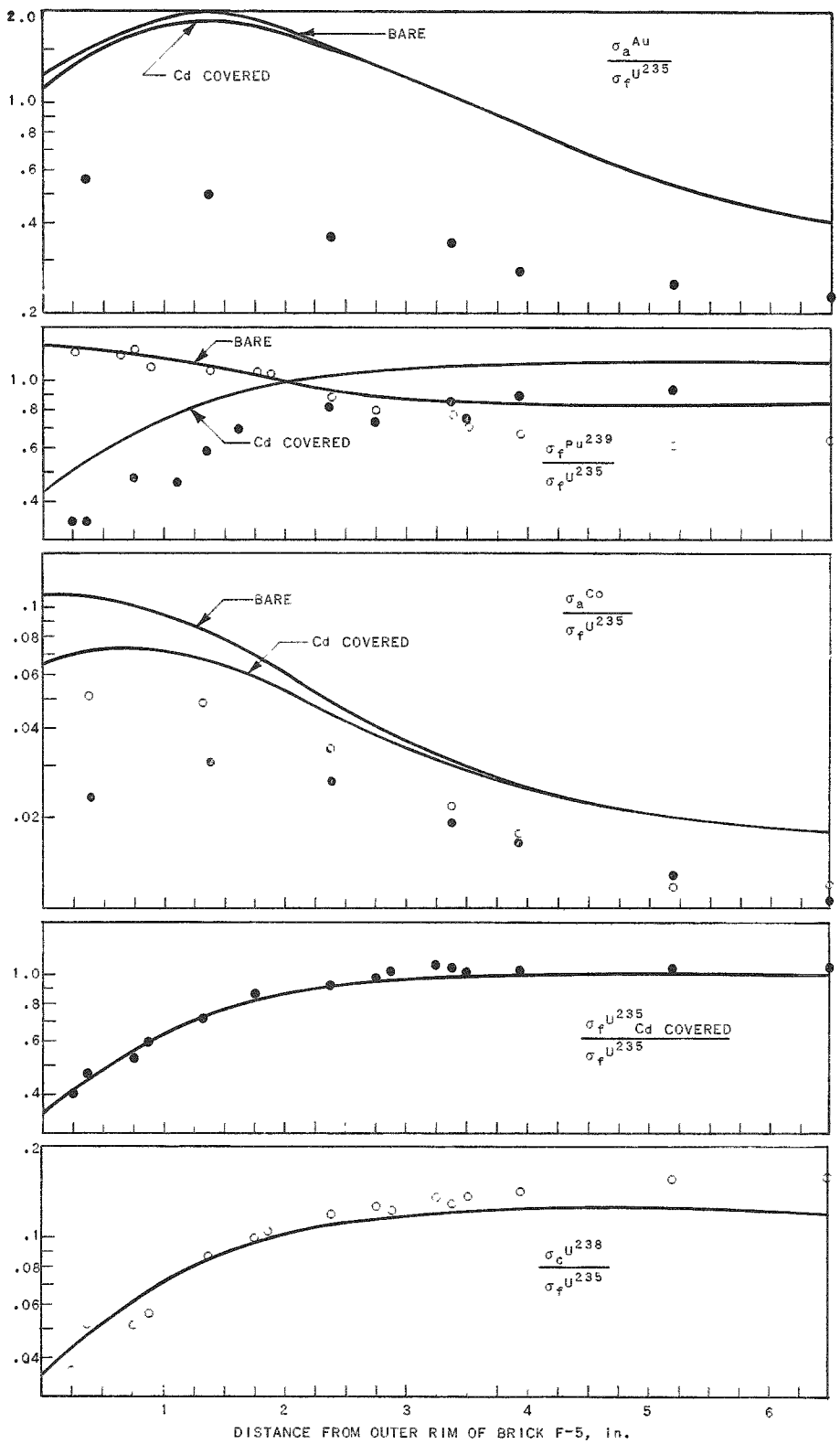

RE-7-16865-B

FIG. 50
MEASURED VS COMPUTED CROSS SECTION RATIOS IN OUTER BLANKET OF EBR

UNCLASSIFIED

A more demanding comparison between experiment and theory is obtained by calculating activation ratios at various points in the brick. These give an absolute comparison between theory and experiment. The predicted ratio of an activation, a, of a sample, s, to the fission in U^{235} at a point, P, in a region, R. is expressed as:

$$\frac{\sigma_a^s(R,P)}{\sigma_f^{U^{235}}(R,P)} = \frac{\sum_{j=1}^{j=20} \sigma_{a,j}^s \, \Phi_j(R,P)}{\sum_{j=1}^{j=20} \sigma_{f,j}^{U^{235}} \, \Phi_j(R,P)} .$$

These ratios can also be calculated from the available experimental data. For each sample, s, the activation $A_a^s(x)$ has been obtained at various points, x. In addition, the ratio of the activations at points, X, in the brick to a point in the thermal column, TC, has been obtained. Hence the activation ratio of interest at point x is simply:

$$\frac{\sigma_a^s(x)}{\sigma_f^{U^{235}}(x)} = \frac{\sigma_a^s(TC)}{\sigma_f^{U^{235}}(TC)} \left[\frac{A_a^s(X_2)}{A_a^s(TC)}\right] \left[\frac{A_f^{U^{235}}(TC)}{A_f^{U^{235}}(X_1)}\right] \left[\frac{A_f^{U^{235}}(X_1)}{A_f^{U^{235}}(x)}\right] \left[\frac{A_a^s(x)}{A_a^s(X_2)}\right] .$$

For those materials where the cross sections are known as a function of energy the agreement is quite good. The apparent disagreement between theory and experiment of

$$\frac{\sigma_f^{Pu^{239}}}{\sigma_f^{U^{235}}}$$

indicates that the value for

$$\frac{A_f^{Pu^{239}}(0.375 \text{ in.})}{A_f^{Pu^{239}}(TC)}$$

is not reliable, since the shape of the calculated curve is quite similar to that indicated by the experimental data.

There are large gaps in the energy spectrum where the activation cross sections of cobalt and gold are not well known; hence it is not surprising that the calculated and experimental ratios do not agree.

DECLASSIFIED

II. EXPERIMENTAL BREEDER REACTOR-II (EBR-II)

A. Decay Heat Cooling Requirements of Spent EBR-II Fuel Subassemblies - C. H. Scheibelhut

After full-power operation of the EBR-II reactor to 1% burnup of the fuel, the spent fuel subassemblies will be allowed to decay in the reactor storage racks for two weeks. At this time the subassemblies that received the highest burnup will be generating about 2300 watts of decay heat.

An electrically heated model of a reference design fuel subassembly was constructed to simulate the decay heat after removal from the storage rack. The blanket sections were omitted since their decay heat is insignificant. A ceramic-insulated, nichrome resistance wire was inserted 14-1/4 in. (the length of the fuel) into a fuel tube that had one end closure and a spiral rib welded on. Groups of 18 tubes were wired in series and constituted a single circuit. There were five such circuits, each controlled by an auto-transformer and monitored by an ammeter and voltmeter. This arrangement left one tube which was controlled by its own auto-transformer. A total of 21 thermocouples was welded to various tubes to facilitate vertical and transverse temperature surveys of the tube surface temperatures. The 91 elements were inserted in a reference hexagonal subassembly tube and mounted in a vertical position. Provision was made so that a blast of cooling air or argon gas could be metered into the bottom of the assembly.

The first test consisted of a determination of the heat dissipation from the assembly in air without forced cooling. At a power of 261 watts (11% of expected power), the hottest element reached a temperature of 530C (986F). A 30-in. high stack was attached to the top of the assembly to determine if the chimney effect would enhance the cooling; no detectable difference.

Air at the rate of 9.41 standard cubic feet per minute (scfm) was introduced into the bottom of the assembly and the power adjusted to 2330 watts. Under these conditions, a maximum fuel tube surface temperature of 563C (1045F) was recorded. The air outlet temperature was 444C (831F), indicating an air temperature rise of 422C (760F). This amount of air and temperature rise accounted for 90% of the heat input.

With a heat input of 2265 watts and an argon gas flow of 12.2 scfm, a maximum temperature of 536C (997F) was recorded. The argon outlet temperature was 453C (847F), indicating an argon temperature rise of 443C (797F). This amount of argon and temperature rise accounted for 96.5% of the heat input.

DECLASSIFIED

The temperature distributions effected by the cooling methods employed are shown in Fig. 51.

Cooling of the subassembly after removal from the reactor will be necessary but can be easily accomplished by blowing about 12 cfm of argon through the subassembly. Further work is in progress to determine cooling requirements during disassembly of the subassembly and head requirements for the blowers.

B. Water Pressure Drop Tests of EBR-II Core Subassembly - E. L. Currier, W. H. Bond

Water pressure drop tests have been conducted on the complete core subassembly for the EBR-II reactor. Pressure drop test results for the major individual sections of the core subassembly (upper blanket, core, and lower blanket) have been reported earlier.[21] The data which are now shown cover the over-all pressure drop in 120F water of the complete design No. 1 core subassembly, which is composed of the lower end piece, lower blanket, core, upper blanket, and upper end piece. In addition, test results are given for the pressure drop through a modified complete subassembly in which the upper and lower blanket rods were installed with no spacer ribs. The results of these tests are shown in Fig. 52 (a). The design core sodium coolant flow rate is 27 fps. At this flow, the subassembly pressure drops in 120F water for Design No. 1 and the modified design are 80 psi and 45 psi, respectively.

A series of low flow pressure drop tests were run to obtain data for analysis of emergency shutdown convection cooling of the EBR-II reactor. The results are shown in Fig. 52 (b).

Since the coolant flow is upward through the subassembly, the coolant imparts a lifting force on the subassembly. The EBR-II lower plenum arrangement provides an opposing downward hydraulic force against the lower end of the subassembly, which acts as a piston in the grid. Tests were made to determine the resultant hydraulic hold-down force.

The experimental setup of the hold-down test (Fig. 53) shows the subassembly positioned in a simulated lower grid contained in a 4-in. piping system. The resultant hold-down forces are measured by means of a lever linkage pinned to the lower end piece of the subassembly and to a fulcrum in the leakage tank under the test section.

The results (Fig. 54) indicate that in 120F water, with entrance pump pressure of 103 psig and standard flow rate of 27 fps, the EBR-II modified subassembly exerts a force of 245 lb on the seat of the lower plenum.

[21] Reactor Engineering Division Quarterly Report, ANL-5471 (September, 1955) p. 166.

DECLASSIFIED

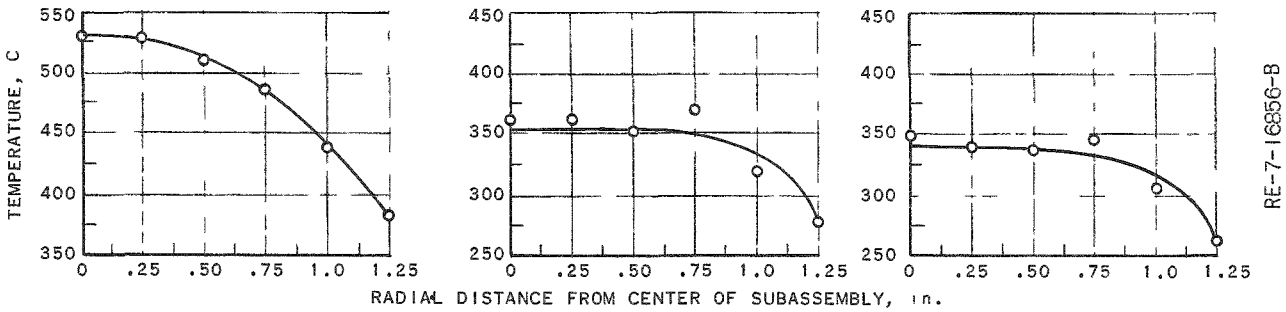

TEMPERATURE TRAVERSE ONE INCH ABOVE SUBASSEMBLY MIDPLANE

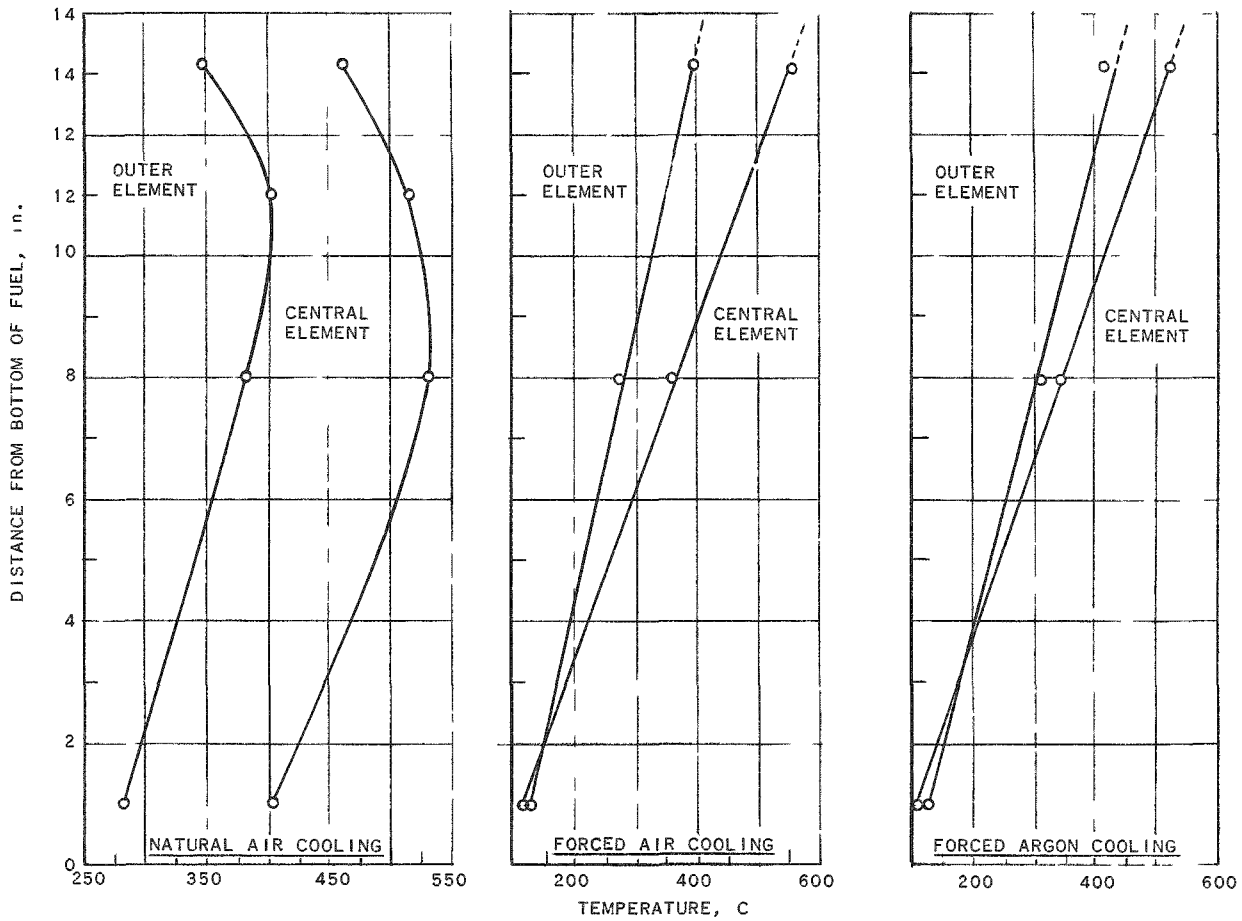

SURFACE TEMPERATURE OF HOTTEST AND COOLEST ELEMENT

FIG. 51
DISSIPATION OF SIMULATED DECAY HEAT
GENERATED IN EBR-II CORE SUBASSEMBLY

DECLASSIFIED

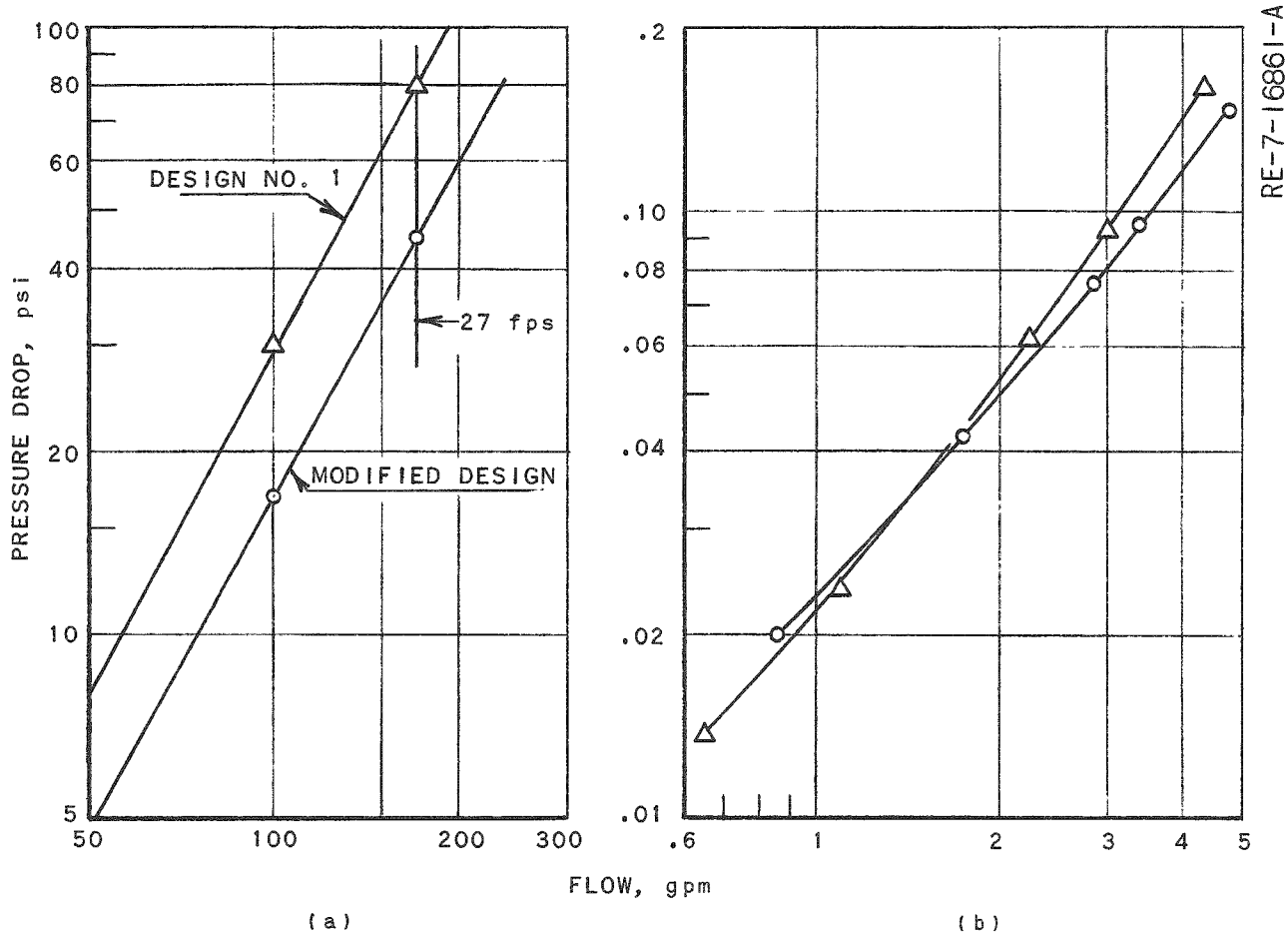

FIG. 52
WATER PRESSURE DROP IN EBR-II CORE SUBASSEMBLY
(120 F WATER)

DECLASSIFIED

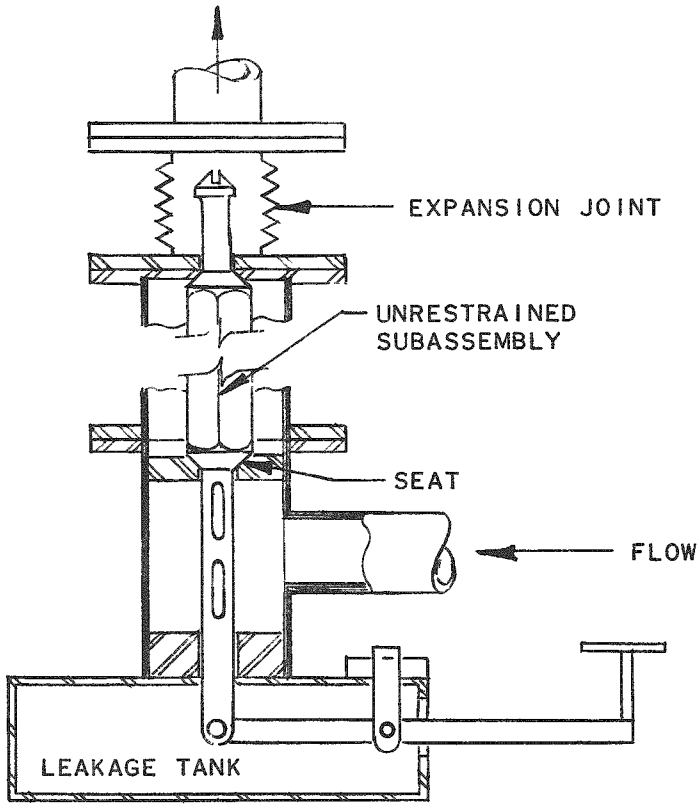

RE-7-16862-A

FIG. 53
SCHEMATIC OF HOLD-DOWN TEST FACILITY

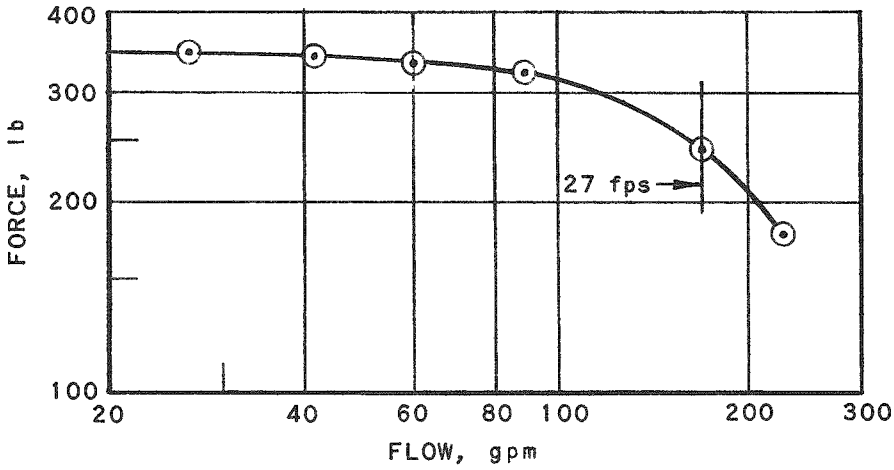

FIG. 54
RESULTANT HOLD-DOWN FORCES FOR MODIFIED EBR-II CORE SUBASSEMBLY IN WATER AT 120 F AND 103 psig

DECLASSIFIED

It is recognized that the pressure drop values and the hold-down forces have been determined for 120F water under non-idealized test conditions. In the pressure drop tests, the flow of the system was controlled by a throttle valve after the orifice, before the pump. This provides a nearly constant pump head pressure on the test assembly. In the actual reactor, however, the flow rate of the coolant will be controlled by a variable pump pressure. The pump head pressure would equal the sum of the subassembly pressure drop and the pressure drop of the remainder of the system, both of which are functions of the flow rate. Therefore, it was necessary to devise a method of calculation whereby the results obtained by the water tests could be projected to a sodium reactor system.

The prominent hydrodynamic features of the idealized model fuel subassembly used in the analysis are shown in the accompanying illustration. Positive values are defined as downward forces. Analysis of this model shows that

$$\Sigma_{iF} = mV_e + P_e A_e$$

$$= (w/g)V_e + P_e A_e \quad , \qquad (1)$$

where

Σ_{iF} = resultant internal thrust, lb

m = mass flow rate, slugs/sec

V_e = exit velocity, fps

P_e = exit pressure, psig

A_e = flow area of exit, sq in.

w/g = slugs of water/sec ,

and

$$\Sigma_{eF} = -P_0A_0 - P_iA_1 - P_eA_3 + P_eA_B \quad (2)$$

where

Σ_{eF} = resultant external thrust, lb

P = as illustrated, psig

A = as illustrated, sq in.

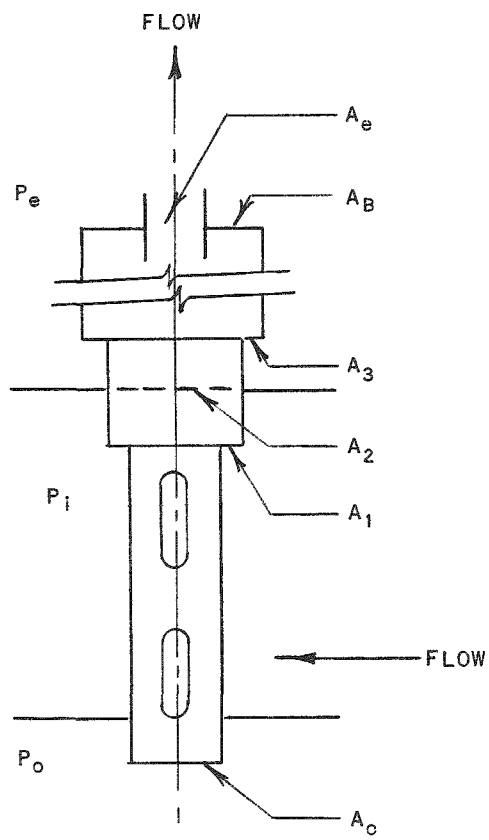

DECLASSIFIED

Adding Eqs. (1) and (2) and including the buoyed weight of the subassembly in water, Wg, yields the following equation:

$$(w/g)\,(V_e) + P_eA_e - P_iA_1 - P_eA_3 + P_eA_B + Wg - P_0A_0 = F \quad , \tag{3}$$

where

F = hold-down force, lb

Combining terms, since

$$P_eA_e - P_eA_3 + P_eA_B = P_eA_2$$

and in this instance $P_0 = 0$,

$$(w/g)(V_e) + P_eA_2 - P_iA_1 + Wg = F \tag{4}$$

Using Eq. (4), a typical calculation of the hold-down forces at 230 gpm flow illustrates the various forces:

$$\left(\frac{w}{g}\right) = \frac{(230\ \text{gpm})(0.1337\ \text{ft}^3/\text{gal})(61.7\ \text{lb/ft}^3)}{(60\ \text{sec/min})(32.2)} = 0.982\ \text{slugs/sec} \quad .$$

$$V_e = \frac{\text{ft}^3}{(\text{sec})(\text{ft}^2)} = \frac{(230\ \text{gpm})(0.1337\ \text{ft}^3/\text{gal})}{(60\ \text{sec/min})\ (0.016)} = 32.0\ \text{fps} \quad .$$

$$\left(\frac{w}{g}\right)(V_e) = (0.982)(32.0) = 31\ \text{lb} \quad . \tag{5}$$

$$P_eA_2 = (103\ \text{psi} - 77\ \text{psi})(\pi/4)(2.1)^2 = 90\ \text{lb} \quad . \tag{6}$$

$$-P_iA_1 = -P_i(A_2 - A_0) = -(103\ \text{psi})(\pi/4)\ [(2.1)^2 - (1.885)^2] = -69 \quad . \tag{7}$$

Substitution of the values obtained in Eqs. (5) through (7) inclusive into Eq. (4) yields the unknown value, F:

31 + 90 - 69 + 85 = 137 lb force.

Table XII shows both the results of the experimental tests and the calculated results based on the model analysis. Except for the region of flow represented by test No. 1, the calculations show good agreement with the experimental results.

Table XII

COMPARISON OF CALCULATED AND EXPERIMENTAL HOLD-DOWN FORCES

		EXPERIMENTAL		CALCULATED					
Test No.	Flow, gpm	Pressure Drop, psi	Force, lb	$(W/g)(V_e)$	P_eA_2	P_iA_1	Wg	Force, lb	$\frac{F_{ex} - F_{calc}}{F_{ex}}$
1	230	77	182	31	90	-69	85	137	0.25
2	178	47	237	19	194	-69	85	229	0.03
3	123	25	296	9	270	-69	85	295	0.00
4	90	14	322	5	308	-69	85	329	0.02
5	60	7	335	2	333	-69	85	351	-0.05
6	42	3.5	346	1	345	-69	85	361	-0.05
7	27	1.5	354	1	352	-69	85	369	-0.04

Based on the foregoing considerations, an estimate was made of the expected pressure drop and hold-down forces during normal reactor operation. The estimated pressure drop values, Δp, were based on the relationship

$$\frac{\Delta p\ (Na)}{\Delta p\ (H_2O)} = \frac{[f\,(Na)]\ \ [\rho\,(Na)\,]}{[f\,(H_2O)]\ [\rho\,(H_2O)]}$$

where

f = friction factor
ρ = density .

In addition, an estimate was made of the pressure drop for the balance of the primary sodium coolant system. The combination of the two pressure drop values constitutes the total estimated Δp of the system and is equal to the pump pressure. The results are given in Table XIII.

Table XIII

CALCULATED PRESSURE DROPS AND HOLD-DOWN FORCES IN EBR-II PRIMARY SYSTEM

		Δp, psi							
Test No.	Flow, gpm	Sub-assembly	System	Total	$(w/g)(V_e)$	P_eA_2	P_iA_1	Wg	Force, lb
1	230	62	22	84	27	76	-56	85	132
2	178	34	14	48	16	48	-32	85	117
3	123	18	7	25	8	24	-17	85	100
4	90	10	4	14	4	14	- 9	85	94
5	60	5	2	7	2	7	- 5	85	89
6	42	2.5	1	3.5	1	3	- 2	85	87
7	27	1	0.5	1.5	1	2	- 1	85	87

An assumption was made that the reactor cover had been left off and the main pump started. This assumption creates an "open system" with zero pressure in the upper plenum. In this case

$$\Sigma_{iF} = \left(\frac{w}{g}\right)(V_e)$$

$$\Sigma_{eF} = -P_i A_1 + Wg$$

$$F = \left(\frac{w}{g}\right)(V_e) - P_iA_1 + Wg \quad . \tag{8}$$

DECLASSIFIED

The results are given in Table XIV and Fig. 55. The estimated pressure drop of the modified design No. 1 EBR-II core subassembly was 33 psi at a sodium temperature of 900F and standard flow of 27 fps. The estimated pressure drop of the balance of the system was 13 psi. The estimated hold-down force exerted by the subassembly on the lower grid seat was calculated to be 115 lb. In an "open system" - zero pressure in the upper plenum - the calculated hold-down force which the subassembly would exert on the lower grid seat was 78 lb. The extrapolated flow rate of sodium at which the subassembly would lift in an "open system" is seen to be well above the capability of the pump.

Table XIV

CALCULATION OF HOLD-DOWN FORCES FOR EBR-II CORE SUBASSEMBLY IN "OPEN SYSTEM" OPERATION

Test No.	Flow, gpm	Subassembly Δp, psi	$\left(\frac{w}{g}\right)(V_e)$	$P_i A_1$	Wg	Force, lb
1	230	62	27	-42	85	70
2	178	34	16	-23	85	78
3	123	18	8	-12	85	81
4	90	10	4	- 7	85	82
5	60	5	2	- 3	85	84
6	42	2.5	1	- 2	85	84
7	27	1	1	- 1	85	85

C. Irradiation of EBR-II Pin Type Fuel Elements - J. E. Kemme, E. S. Sowa

Three facilities are now available in the CP-5 reactor for the irradiation of EBR-II pin-type fuel elements. A description of a typical facility and test assembly is given in ANL-5371.[22] To date five elements have been placed under irradiation.

Irradiation Test No. 1 is complete; test conditions and results of post-irradiation inspection are given in ANL-5371 and ANL-5471.[23] Recent analyses indicate an average burnup of 0.38 fuel alloy atom per cent, which is in good agreement with the estimated burnup for this element.

---

[22] Reactor Engineering Division Quarterly Report, ANL-5371 (January 15, 1955) p. 184

[23] Reactor Engineering Division Quarterly Report - Section II, ANL-5471 (September, 1955) p. 130

DECLASSIFIED

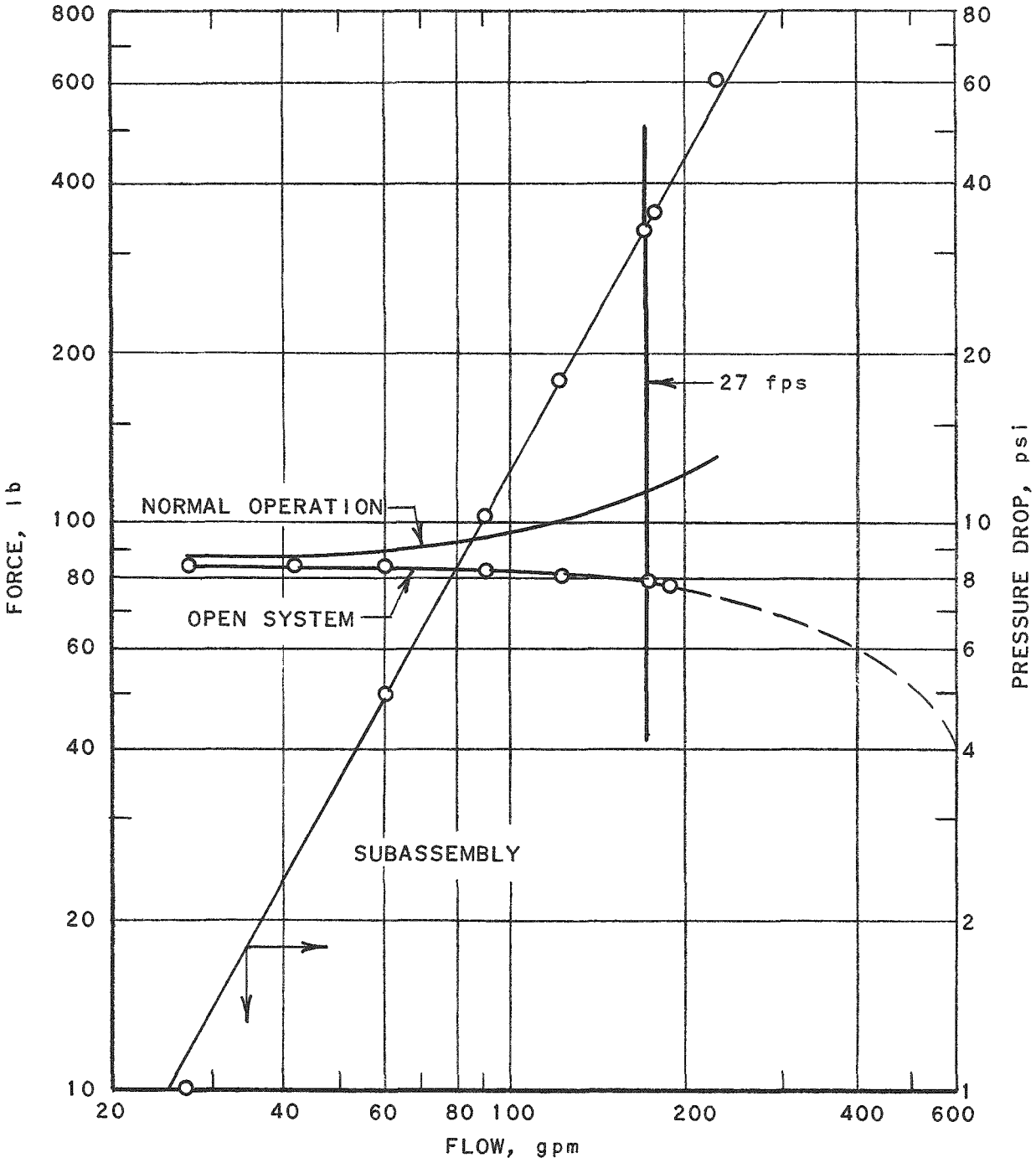

RE-7-16860-A

FIG. 55
CALCULATED HOLD-DOWN FORCES AND PRESSURE DROPS FOR MODIFIED DESIGN EBR-II CORE SUBASSEMBLY IN SODIUM AT 900 F

DECLASSIFIED

Test No. 2 was terminated after a total irradiation time (at full power) of 1316 hr, corresponding to an estimated average burnup of 0.40 fuel alloy atom per cent. The approximate maximum fuel temperatures at reactor operating power and at higher power reactor safety checks were 1000F and 1150F, respectively. The element accumulated 195 thermal cycles.

Post-irradiation inspection showed the fuel to have melted in the uppermost region, damage being greatest at the top and extending downward approximately two inches. The remainder of the fuel appeared to be in excellent condition, showing some surface roughening only at the bottom section. Figure 56(a) shows the various sections described; a typical undamaged portion is included for comparison.

Figure 56(b) shows sections of the fuel tube before removal of the fuel. Complete penetration of the stainless steel tubing is shown throughout much of the damaged region. The penetration was probably hastened by the formation of eutectics of uranium and elements of the stainless steel. Removal of this tubing disclosed a clean, white Na surface extending from below the damaged section to the bottom of the fuel.

The type of damage noted does not necessarily indicate a poor fuel element. The assembled element was placed in a finned capsule for irradiation. A 20-mil annulus of Na was provided for heat transfer. In Test No. 2 only enough Na was provided to place the level at the top of the fuel element. When the finned capsule was opened considerable Na was found in a region two to three inches above this point. Since cooling air entered at the top of the test assembly, there was a region where freezing of Na was probable. Enough Na in this position could have prevented complete bonding in the annulus around the fuel, giving a most reasonable explanation for the type of damage received.

Test No. 3 was terminated during the present period and is cooling prior to post-irradiation inspection.

Two more elements are now under test. A sixth element is being assembled using NaK in the annulus between the element and its finned capsule to prevent any possibility of affecting the test by formation of voids during freezing of sodium during shutdown.

DECLASSIFIED

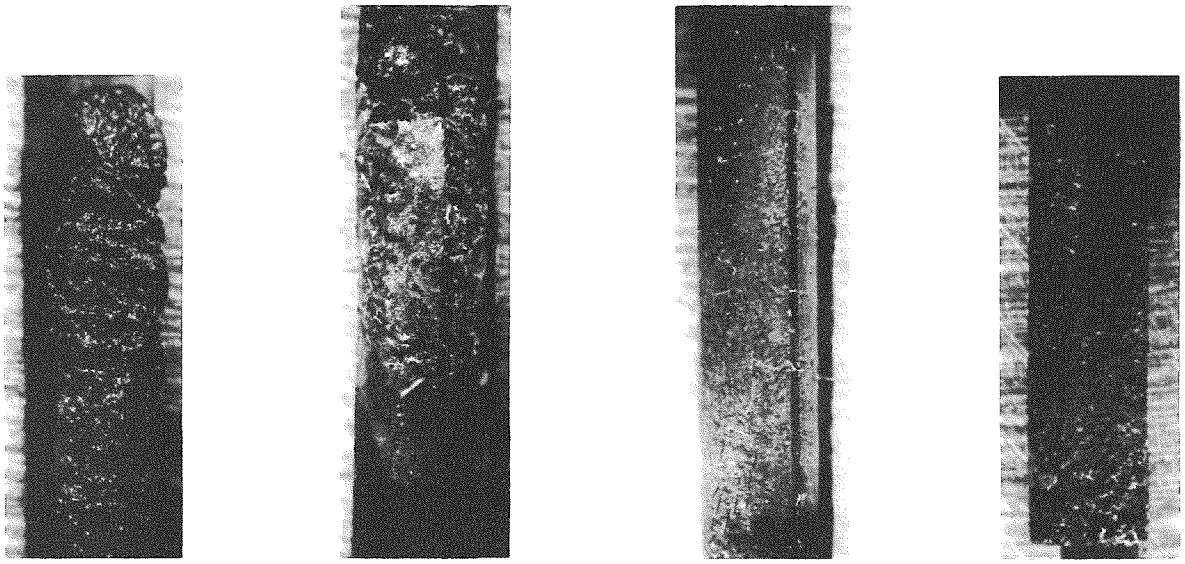

(a) FUEL

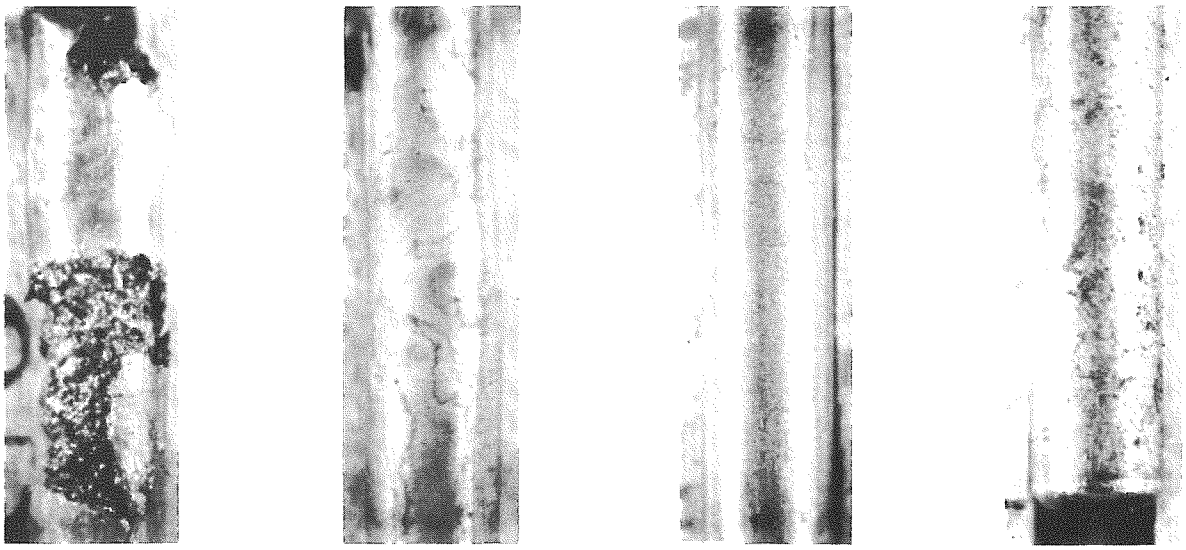

TOP 2 in. FROM TOP UNDAMAGED BOTTOM

(b) STAINLESS STEEL TUBE

FIG. 56
ENLARGED SECTIONS OF EBR-II PIN-TYPE FUEL
ELEMENT IRRADIATED IN CP-5 TEST NO. 2.
MAGNIFICATION: 4X

DECLASSIFIED

III. EBR-II WORKING MODEL

System Performance Tests

1. Control Rod and the Cover Raising and Rotating Mechanisms - D. Nicoll

These units were installed and initially tested inside the empty and unheated primary tank. The tank was then filled with helium, and the temperature of the tank was increased periodically until the temperature of the gas was raised to 565F. All mechanisms performed satisfactorily under these conditions.

The primary tank was then filled with sodium, leaving about an 18-in. gas blanket. Performance tests were then conducted concurrently with periodic increases in temperature until a sodium temperature of 700F was reached.

The control rod operating mechanism performed satisfactorily, with the exception of the sensing device which began to stick at 400F. At this temperature the dial pointer could be moved by exerting a slight pressure on the pointer. Movement of the sensing device became more difficult with increased temperature and it finally stuck completely at 500F. The cause for this difficulty is believed to be insufficient clearance between the sensing shaft and graphite bushing.

Upon dismantling the mechanism, the sensing shaft was found to be colored a dark blue by the temperature, and the presence of oil was detected on the shaft. There was also an accumulation of oil and broken particles of graphite from one of the bushings. The shaft showed no signs of galling or roughening of the surface. It is assumed that the wedging of graphite particles between the shaft and bushing, coupled with the burning of the oil on the shaft by the high temperature, caused the sensing shaft to stick.

The sensing device mechanism was sealed by gasketed flanges and bellows; however, there were no indications of sodium leakage into the unit.

The unit is being cleaned and the graphite bushing machined to permit greater operating clearance prior to installation for further testing.

The cover raising and rotating mechanism performed satisfactorily throughout the test.

DECLASSIFIED

2. Fuel Unloading System - E. Hutter

The operation of the unloading system (Fig. 57) in the empty and unheated primary tank was checked first and then the tank temperature was raised step-wise up to 565F. It was observed that the components worked progressively harder as the temperature increased, and galling occurred between several stainless steel surfaces. To improve these conditions, clearances on the gripper, transfer arm, and the bottom parts of the fuel elements were increased. The hold-down tubes extending downward from the reactor shield cover were removed also. After these adjustments were made the primary tank was filled with sodium, leaving about an 18-in. gas blanket. Performance tests were conducted while the sodium temperature was gradually increased to 700F.

The equipment worked through the whole temperature range in sodium for 30 unloading cycles.

Reactor Vessel (1): After reaching 700F, misalignment with the rotating plugs was noticed.

Gripper Mechanism (2): The open jaws did not always release the fuel rod, due to misalignment.

Hold-Down Mechanism (3): Sodium was siphoned inside the bellows of the shaft seal.

Transfer Arm and Storage Rack (4): Difficulties occurred in transferring fuel rods because of differential thermal expansion.

Rotating Shield Plugs (5): Increased friction on the sealing surface of the large rotating plug stalled the drive motor.

It was then decided to lower the sodium temperature to allow for removal and readjustment of some of the plugs and mechanisms before continuation of the performance tests.

3. d-c Electromagnetic Pump - A. H. Barnes, R. A. Jaross

The d-c electromagnetic pump designed to test the feasibility of operating a pump completely submerged in the primary sodium coolant has been operated in the EBR-II Working Model.

The pump is located in the tank[24] in a circuit which includes an electromagnetic flowmeter, pressure transmitter, and throttling valve. The current to the pump is obtained from a rectifier installation capable of supplying up to 30,000 amperes.

[24]Reactor Engineering Division Quarterly Report, ANL-5471, Section II, (September, 1955) Fig. 59.

DECLASSIFIED

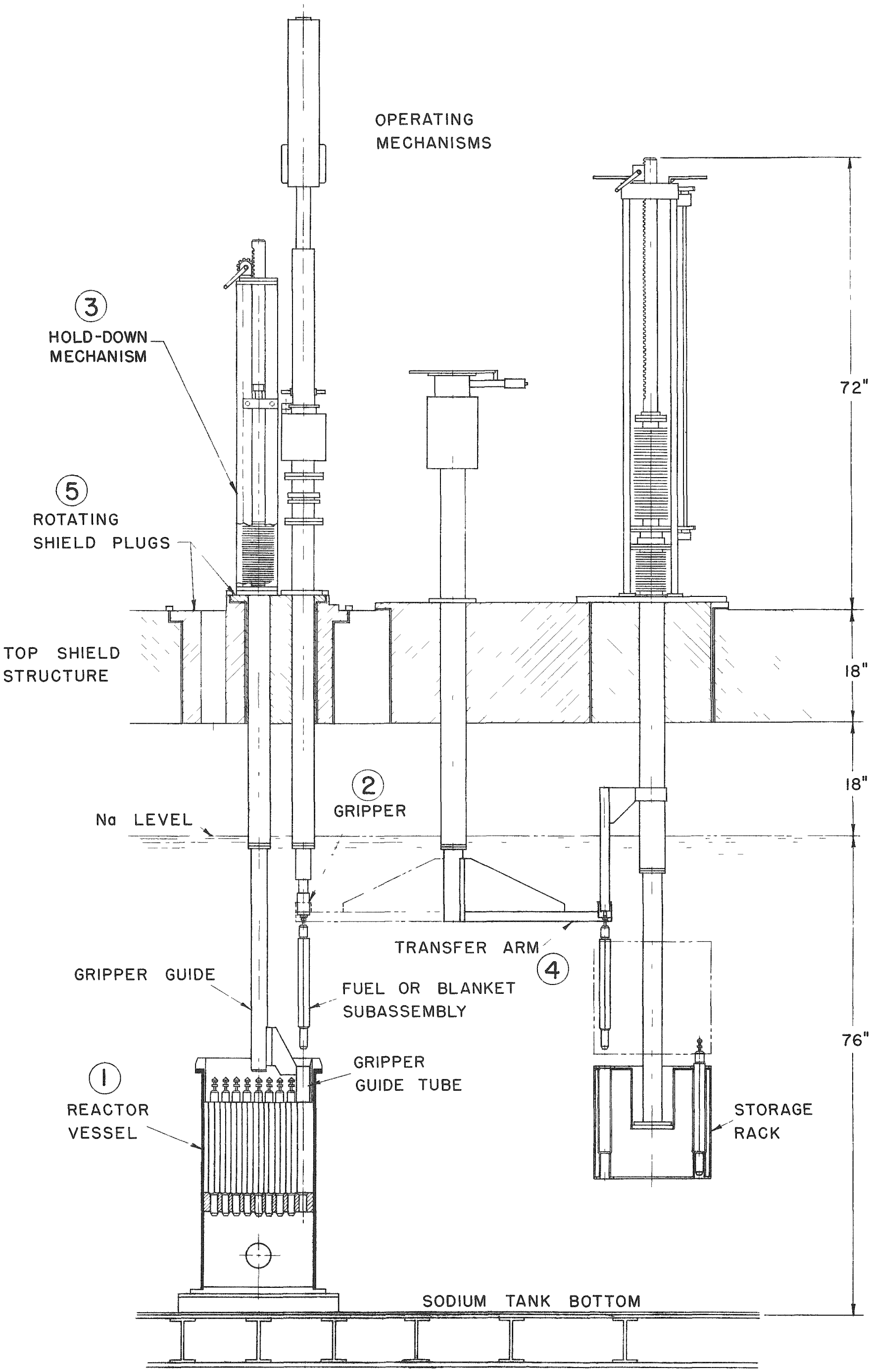

FIG. 57
FUEL UNLOADING SYSTEM
EBR II WORKING MODEL

The pump has been operated at 30,000 amperes (design current is 50,000 amperes) with an ambient sodium temperature of 370C. Figure 58 shows the head-capacity characteristics at input currents of 20,000 and 30,000 amperes. It was observed that the performance of the pump when submerged in sodium was somewhat better than that obtained when the pump was tested in a closed pipe loop.[25] The increase in capacity (at a given head) is believed to be due to lower gas entrainment in the sodium in the tank circuit.

The efficiency of the pump was determined by measuring the potential difference at the pump terminals at the top of the tank cover plate and computing the d-c power input to the pump. Efficiency was taken to be

$$\frac{0.435\ (\text{gpm})\ (\text{pressure rise through pump, psi})}{(\text{current})\ (\text{terminal pressure drop})}\ .$$

Figure 58 also shows the variation of efficiency with flow at two input currents and at a variable head. Maximum efficiency occurred at a flow of 900 gpm against a 26-psi head.

4. Sodium Purification - J. R. Humphreys

The model tank was first degreased and, following field installation of the test components, particulate matter was removed from all metal surfaces with a vacuum cleaner. No attempt was made to chemically clean the metal surfaces of the tank to remove adsorbed gases and oxides before filling. It was decided to use only those cleaning techniques which could practically be employed in a large field installation and to observe the magnitude of added impurities to clean sodium.

After filling (approximately 5,000 gal), the sodium surface was covered by an unbroken, dull grey coating. The sodium temperature was then raised from the filling temperature of 300F to 550F, and cold-trapping operations were begun. After ten hours of cold trap operation the dissolved oxygen content of the tank sodium was 0.002 wt-%. At this time the sodium surface still retained the grey coating. After 75 hr the sodium surface was mirror bright and the dissolved oxygen concentration was 0.001 wt-%.

It is believed that the initial grey coating on the sodium was in the form of oxide. The two probable sources of this oxide were oxygen impurities in the argon atmosphere and sodium reaction with adsorbed gases and oxides on the metal surfaces. The experimental evidence indicates that the rate of solution of this oxide film is the rate-limiting process in system clean-up, in that the dissolved oxygen concentration was reduced to less than 0.002 wt-% by cold trapping while the oxide surface film still existed. It is

[25] Ibid., Fig. 58.

DECLASSIFIED

RE-7-16855-A

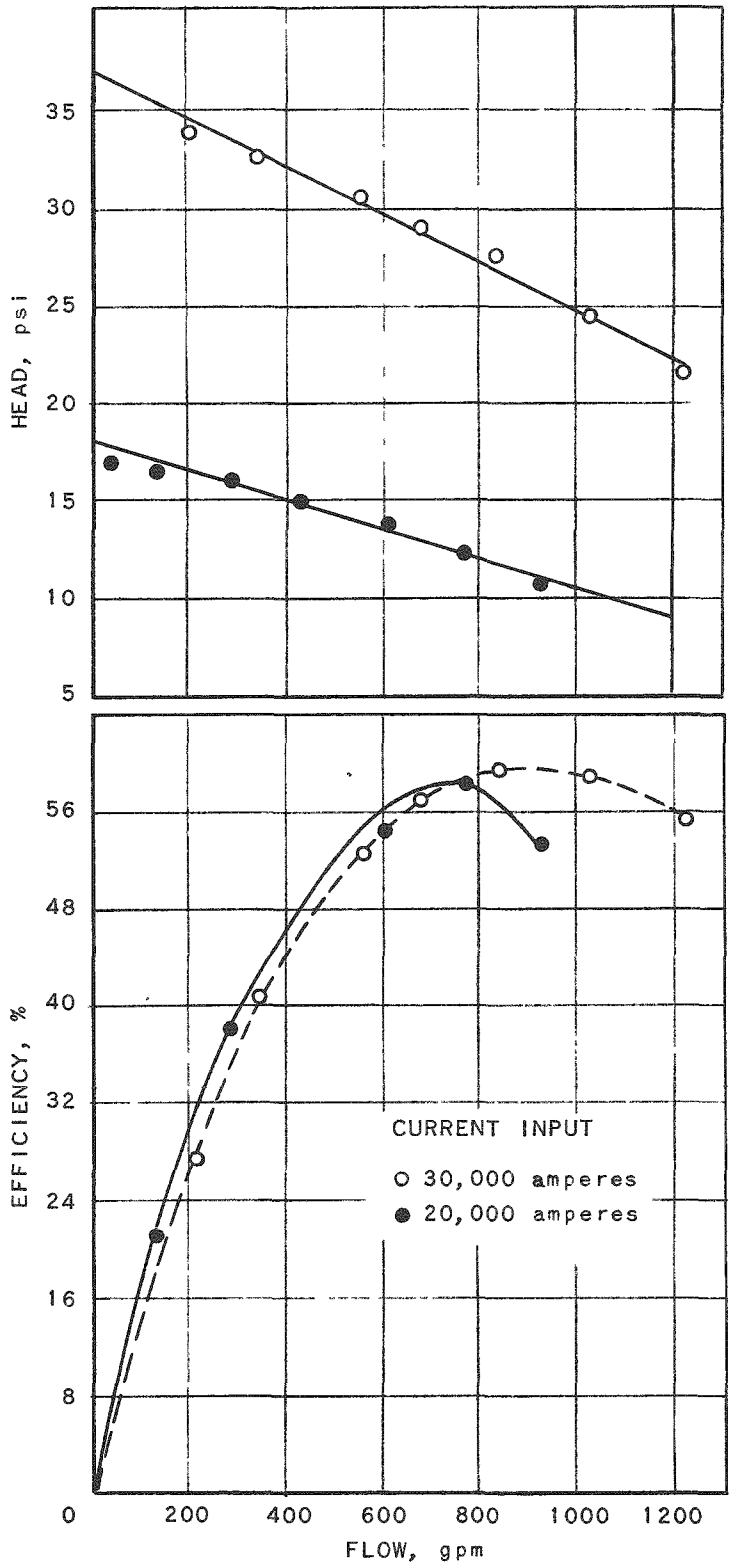

FIG. 58
PERFORMANCE CHARACTERISTICS OF
MODEL TANK PUMP IN SODIUM AT 370 C

DECLASSIFIED

probable that higher operational temperatures would result in more complete wetting of the oxide by sodium, thus increasing its rate of solution. This, with the increase in saturation concentration of oxide in sodium at high temperatures, would reduce considerably the cold-trapping time necessary to clean up a closed sodium system.

DECLASSIFIED

IV. SUPPORTING AND ALTERNATE DESIGN RESEARCH AND DEVELOPMENT

A. Thermal Cycling of Molybdenum-Uranium and Zirconium-Uranium Alloys - J. E. Kemme, H. O. Monson

A group of powdered metallurgy specimens, fabricated by Sylvania Electric Products, were thermally cycled in NaK to determine the relative stability of molybdenum-uranium and zirconium-uranium alloys. Some wrought and heat treated 2% zirconium-uranium specimens, fabricated by the Argonne Metallurgy Division, were included as a further basis for comparison. Of particular interest was the effect produced by cycling above the alpha-beta transformation temperature of unalloyed uranium.

All specimens were 2.3 in. long by 0.144 in. in diameter. The powdered metallurgy specimens were in the as-sintered condition. The samples prepared at Argonne were swaged to size and heat treated. The stabilizing heat treatment consisted of heating the swaged specimens at 800-810C for 8 min. and furnace cooling in vacuo (5×10^{-5} mm Hg). Time lapse in cooling from 800C to room temperature was 11.3 hr.

To obtain the information desired, four specimens of each type were used. Two specimens from each set were given 200 cycles from 150F to 1150F (the high alpha region). The remaining specimens were given 200 cycles from 200F to 1320F (the beta region). Holding time at each temperature was three minutes, with a ten-second transition between temperatures. All specimens of a given group were cycled together to obtain identical cycling conditions.

Figure 59 shows the composition, grain size, and appearance of one alpha- and one beta-cycled specimen of each type, along with the average per cent change of length, weight, and density for each set of specimens. Magnified views of the surface condition of all specimens are shown in Fig. 60.

As expected, all alpha-cycled specimens showed little distortion. The beta-cycled zirconium alloys exhibited considerable distortion, whereas the molybdenum alloys appeared to be unaffected. There was some change in the surface condition of these alloys with decreasing molybdenum content, as shown in Fig. 60; however, no cracking or surface bumping was evident. The thermal-cycling stability of the low molybdenum alloys make them attractive for applications where operation, or cycling, of the fuel in the beta region is contemplated, provided their irradiation damage resistance is satisfactory.

DECLASSIFIED

A - ALPHA CYCLED. 200 CYCLES FROM 150 F TO 1150 F
B - BETA CYCLED. 200 CYCLES FROM 200 F TO 1320 F

SPECIMEN	1A	1B	2A	2B	3A	3B	4A	4B	5A	5B	6A	6B
ANALYSIS	2.5% Mo-U		2% Mo-U		1.4% Mo-U		2% Zr-U		2% Zr-U		2% Zr-U	
GRAIN SIZE, microns	18-50		13-70		13-70		UP TO 1200		17-35		WROUGHT & HEAT TREAT.	
ELONG., %	0.61	0.80	0.98	1.02	1.70	0.89	1.24	**	1.02	**	*	*
WT. CHG., %	+0.10	+0.01	+0.31	-0.71	-0.32	-4.20	-0.26	-3.40	-0.48	-3.96	*	*
DENSITY DECREASE, %	1.13	0.80	1.07	1.02	1.55	0.89	1.60	**	1.78	**	0.83	*

* CUT FROM SINGLE PIN WHOSE DENSITY HAD BEEN MEASURED. INDIVIDUAL LENGTHS AND WEIGHTS NOT MEASURED PRIOR TO CYCLING.

** COULD NOT BE MEASURED ACCURATELY BECAUSE OF DISTORTION

FIG. 59
MOLYBDENUM-URANIUM AND ZIRCONIUM-URANIUM ALLOY PINS THERMALCYCLED IN NaK

ALPHA CYCLED. 200 CYCLES FROM 150 F TO 1150 F

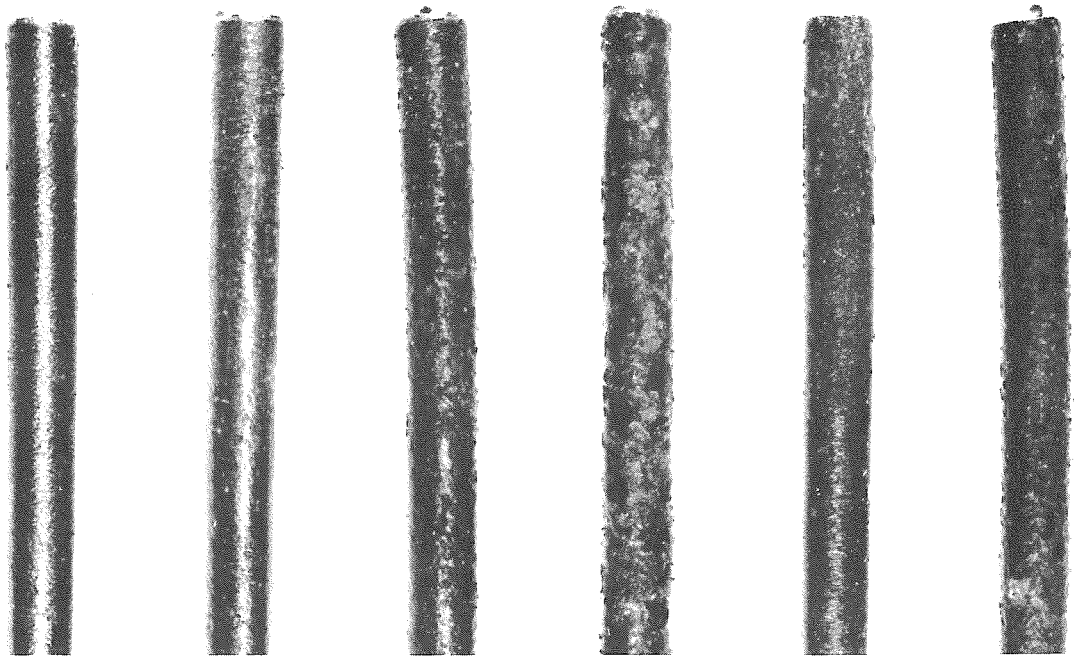

BETA CYCLED. 200 CYCLES FROM 200 F TO 1320 F

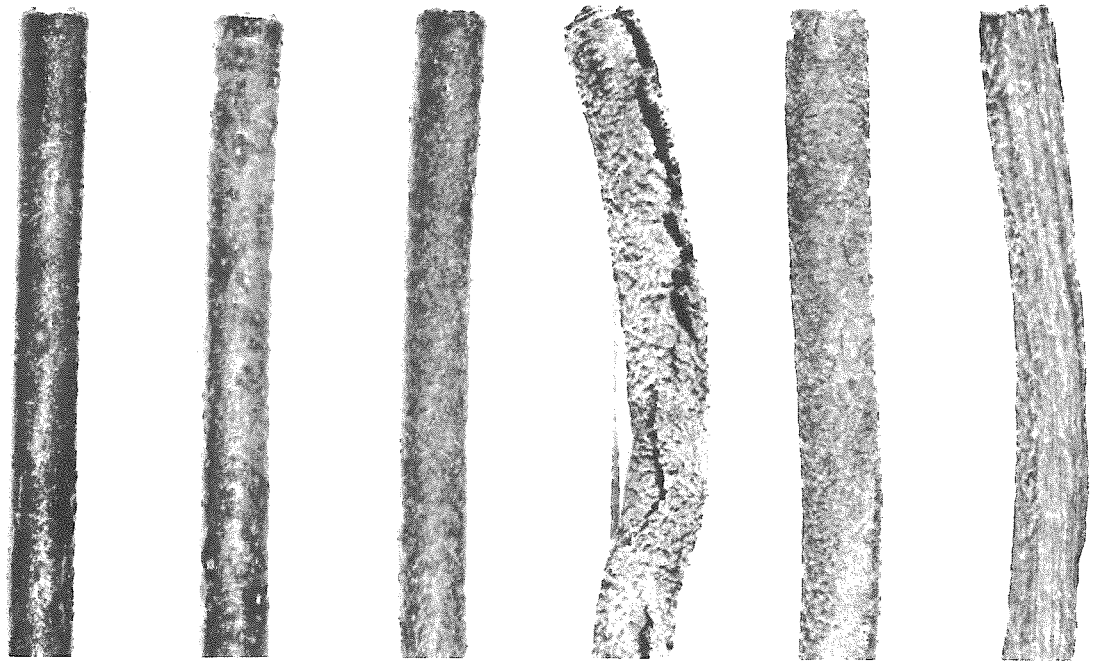

2.5% Mo-U	2% Mo-U	1.4% Mo-U	2% Zr-U	2% Zr-U	2% Zr-U
(18-50)	(13-70)	(13-70)	(UP TO 1200)	(17-35)	WROUGHT & HEAT TREAT.

PARENTHESIZED NUMBERS INDICATE GRAIN SIZE IN MICRONS

FIG. 60
SURFACE CONDITION OF MOLYBDENUM-URANIUM AND ZIRCONIUM-URANIUM ALLOY PINS THERMALCYCLED IN NaK. MAGNIFICATION: X4

DECLASSIFIED

B. Induction Heating of a Four-Inch IPS Sodium Test Loop - R. A. Jaross

Previous experience[26, 27] has shown that it is possible to raise the temperature of an insulated, magnetic steel pipe by winding a simple copper conductor continuously around the pipe and applying a 60-cycle current to the coil. The coil may be wound over the insulation and hence remain in a region of low ambient temperature.

Since the 18-8 stainless steels used extensively in sodium coolant work are non-magnetic, a pipe of this material cannot be heated directly by 60-cycle induction heating. It is necessary to provide a magnetic material in close proximity to the 18-8 stainless steel so that the heat produced in the magnetic material can be conducted to the stainless steel and hence to the sodium.

A previously constructed Type 347 stainless steel test loop was revised to test this method of heating. The old armoured nichrome wire heaters were removed along with the pipe insulation. Since the loop had been previously operated it was known to be leaktight. The entire loop was now covered with S.A.E. 1020 H.R. steel with a thickness of 3/16 in. This magnetic steel was fitted as closely to the stainless steel as possible and tack welded in place. Figure 61 (a) shows the loop covered in this manner. It will be noted that the mild steel does not cover the pipe in the region of the electromagnetic pump. The major portion of the steel covering was formed in the shape of half-round shells of suitable diameter and length. No effort was made to obtain a close fit between each adjacent piece of steel.

As shown schematically in Fig. 61 (b), the loop was thermally insulated with Kaylo pipe insulation (3 in. wall thickness for 4-1/2 in. IPS pipe) which, in turn, was covered with canvas. An induction coil consisting of 2600 ft of Type AA insulated, 10-gage copper wire was wound around the insulation (42 turns per ft). It would have been desirable to wind this coil over the entire loop, but, due to the difficulty in winding over valves and elbows, the coil was placed only on the straight sections of pipe.

The completed test loop is shown in Fig. 61 (c). It will be noted that the electromagnetic pump is completely without any source of heat. The pump tube has a 2 in. by 2 in. cross section and is 30 in. long. It was found in subsequent tests that sufficient heat was conducted from hotter regions to bring the sodium temperature to 275F in the pump tube.

---

[26] Reactor Engineering Division Quarterly Report, ANL-5461, (April 15, 1955) p. 89.

[27] Reactor Engineering Division Quarterly Report, ANL-5471, (September, 1955) Section II, p. 147.

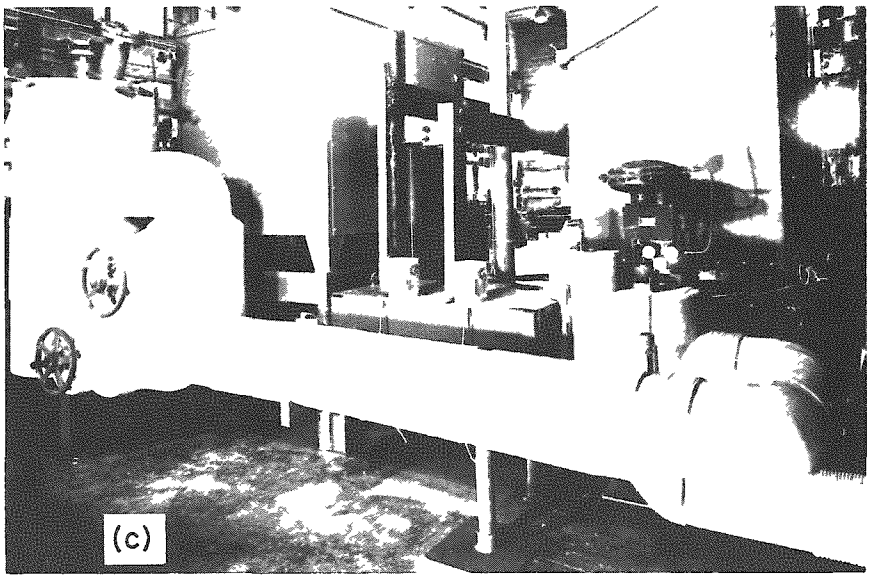

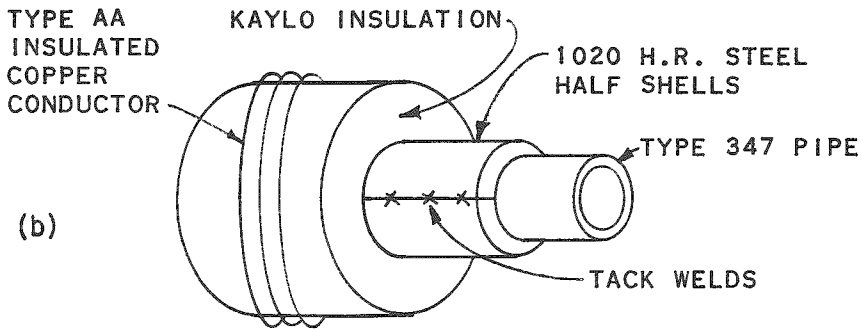

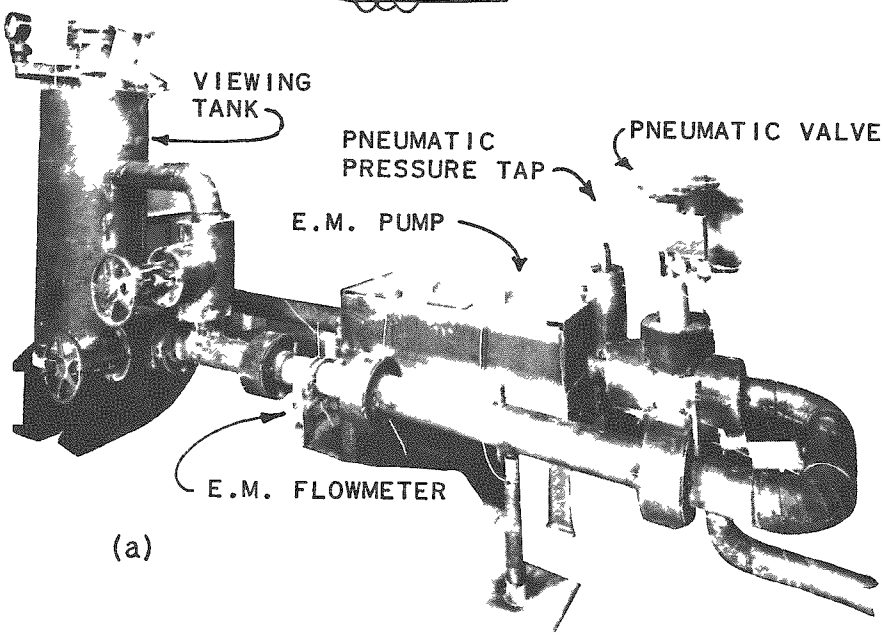

FIG. 61
SEQUENCE OF INSULATING INDUCTION
HEATED SODIUM TEST LOOP

DECLASSIFIED

With frozen sodium in the loop the induction coil was energized at 235 volts, single phase, 60 cycles. The coil current was 20 amp and had an input of 3600 watts with a power factor of 77%. Figure 62 shows the resultant time versus temperature curve obtained. At the end of this 72-hour heat-up period the sodium was circulated and no difficulty was experienced in the operation of the valves, pressure taps or pump. It must be remembered that the purpose of induction heating a sodium system is merely to melt the sodium and allow circulation. Once this is achieved further heating is easily obtained by various methods.

C. Inspection of 1472F Sodium Loop Welds - F. A. Smith, J. H. Monaweck, R. A. Stella

Metallographic examination of weld samples cut from Type 347 stainless steel piping of a recirculating 1472F sodium loop reveal typical spheroidization of ferrite and carbides with limited sigma phase formation (Fig. 63). Although the sigma phase forms fastest at temperatures between 1350 and 1500F, general weld embrittlement was not serious since the loop operated at temperature only 160 hr. However, extensive cracking in a field weld which lacked proper weld preparation was evident.

The nature of these cracks, root cracking, heat-affected zone cracking (Fig. 64), and cracking along grain boundary carbides (Fig. 65), emphasizes the need for strict observance of the welding procedures currently used in fabricating sodium loops. The welding procedure minimizes root cracking by making the first pass with an inert arc weld rod. Some control of heat-affected zone cracking is possible by using small-size grain boundaries where carbide and sigma phase formation occurs and is delayed by using low-ferrite, extra low-carbon weld rod.

Table XV compares recommended weld metal composition with the chemical analysis of the cracked field weld described above.

The relatively large amount of carbon in the cracked weld results in a weakened metal structure as diffusion of carbides to the grain boundaries occurs. Figure 66 shows decarburization of the pipe inner surface to a depth of 0.001 in.

DECLASSIFIED

RE-7-16866-A

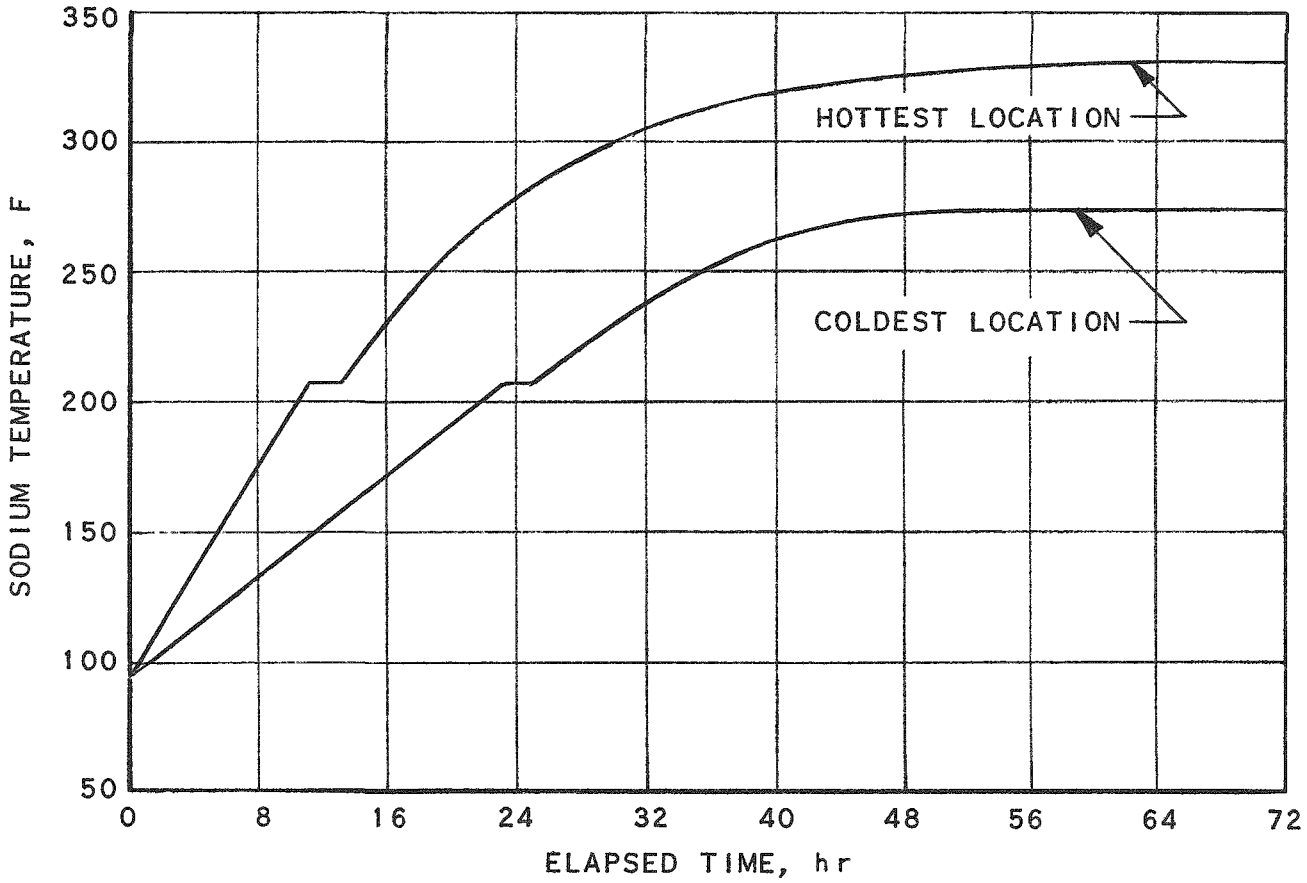

FIG. 62
INDUCTION HEATING TIME FOR
4-inch SODIUM LOOP

DECLASSIFIED

FIG. 63
SPHEROIDIZED CARBIDE AND SIGMA PHASE FORMATION

AUSTENITE: LIGHT BACKGROUND. CARBIDE: DARK STAIN.
SIGMA: LIGHT BORDERED AREAS ADJACENT TO CARBIDES.
ETCH: 10 NORMAL KOH. STAIN: HNO_3 (~2000)

FIG. 64
HEAT-AFFECTED ZONE CRACK

ETCH: OXALIC ACID (~200)

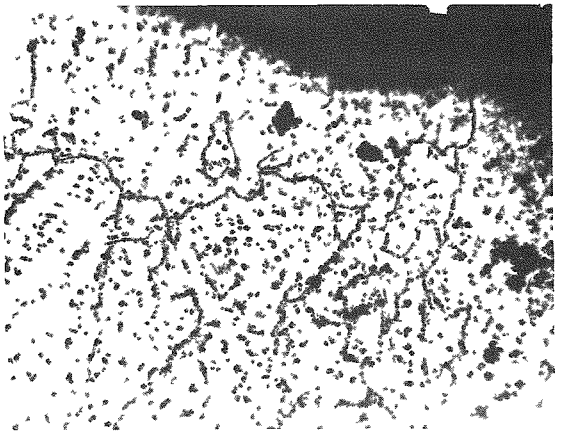

FIG. 65
CRACKING ALONG CARBIDES AT GRAIN BOUNDARIES

ETCH: OXALIC ACID (~200)

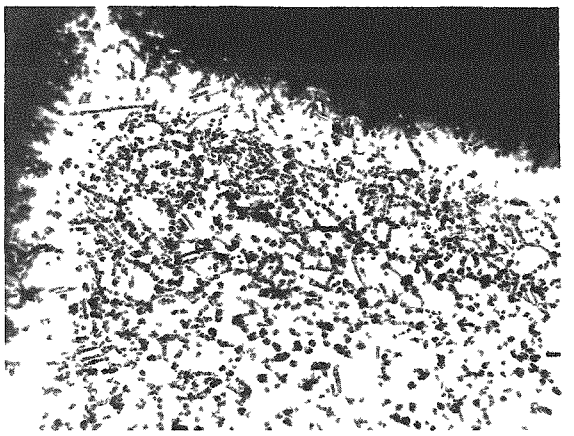

FIG. 66
DECARBURIZATION OF SODIUM-WETTED SURFACE

ETCH: HCl-ETHYL ALCOHOL (~300)

DECLASSIFIED

Table XV

CHEMICAL COMPOSITION OF DEPOSITED WELD METAL

(in per cent)

	Recommended*	Cracked Weld
Carbon	0.07-0.10	0.24
Manganese	1.50-2.50	1.11
Silicon	0.50	0.63
Chromium	18.4-20.5	20.40
Nickel	9.0-10.5	10.96
Columbium	0.60-0.90	0.66
Molybdenum	-	0.13
Silicon/carbon ratio, max.	5/1	2.6/1

*Specification Limits for Special Low-Ferrite, Type 347 Welding Electrodes.[28]

[28]R. M. Curran, A. W. Rankin, "Welding Type 347 Stainless Steel for 1100F Turbine Operation," The Welding Journal 34 (3), pp. 205-213 (March, 1955).

DECLASSIFIED

PART C REACTOR TECHNOLOGY - RESEARCH AND DEVELOPMENT

1. REACTOR SAFETY AND KINETICS - R. O. Brittan

A. ZPR-III

The report on ZPR-III (Fast Reactor Zero Power Assembly) to the AEC Advisory Committee on Reactor Safeguards was prepared and submitted. The work was reviewed with the Committee in Washington, D.C., on June 30, 1955. Permission to operate under the restrictions imposed by the report (with one stipulation) was obtained by letter from the AEC on August 3, 1955.

B. Machine Solution of Kinetics Equation

The AVIDAC RE-13[29] routine for solution of the kinetics equations proved to be of limited usefulness in dealing with fast reactors having lifetimes of the order of 10^{-7} sec because of the small time intervals required. Only problems in which k_{ex} is a step function or k_{ex} is very large can be solved in reasonable times. To get around this limitation, a new approach was made by first integrating the equations, then working only with changes in the parameters, using trapezoidal integration where necessary. The solution by R. O. Brittan was programmed and coded as RE-29 for AVIDAC by E. C. Jutzi and B. Garbow.

In addition to the problem of obtaining the time variation of neutron flux for a prescribed mode of variation in reactivity, it was decided that the converse problem of obtaining the time variation of reactivity consistent with a given time variation in neutron flux would be a useful tool. Attempts to arrange a program which would accomplish this were stimulated by a need for analyzing the data obtained in the BORAX series of experiments. The solution by H. J. Wheeler was programmed and coded as RE-22 for AVIDAC by L. Kramer and M. L. Butler.

One further tool of limited usefulness is the solution of the inhour equation yielding asymptotic periods corresponding to certain excess reactivities, and conversely. This problem has been programmed for AVIDAC as RE-19 and RE-23 by J. Hall, L. Kassel, and E. McNulty.

There follows here in some detail the development of the two solutions to the kinetics equations.

---

[29] Reactor Engineering Division Quarterly Report, ANL-5371 (January 15, 1955) p. 66.

DECLASSIFIED

1. Solution of the Kinetics Equations, Given k_{ex} (RE-29)

Because of the severe limitation on interval size encountered in earlier solutions for AVIDAC, an attempt was made to manage the computations with an interval size which need be only small enough that n, k_{ex} and c_i may be reasonably assumed to vary linearly from point to point. The general approach used was to integrate the usual kinetics equations over the interval size to obtain the change in the variables. By working only with the changes in the variables, many of the steps involving small differences between large numbers are eliminated. The formal procedure is:

Consider the usual set of eight kinetic equation for a one-group, space-independent model:

$$\left.\begin{aligned} \frac{dn}{dt} &= \frac{k_{ex}}{\ell} n - \sum_i \frac{dc_i}{dt} + S \\ \frac{dc_i}{dt} &= (1 + k_{ex})\frac{\beta a_i}{\ell} n - \lambda_i c_i \end{aligned}\right\} \quad i = 1,2,\ldots.6$$

$$\frac{dk_{ex}}{dt} = f(n,t)$$

where

- n = neutron density
- c_i = density of i'th delayed neutron precursor
- β = fraction of neutrons that are delayed
- a_i = fraction of delayed neutrons of the i'th group ($\Sigma a_i = 1$)
- λ_i = decay constant for the i'th group
- S = constant source term
- k_{ex} = excess reactivity = $k_{effective} - 1$
- t = time variable
- ℓ = effective lifetime

The change in n between two points, j and j+1, can be obtained by integrating the first equation:

$$n_{j+1} - n_j = \int_{t_j}^{t_{j+1}} dn = \frac{1}{\ell}\int_{t_j}^{t_{j+1}} k_{ex}\, n\, dt - \sum_i (c_{i_{j+1}} - c_{i_j}) + S(t_{j+1} - t_j) \quad .$$

DECLASSIFIED

Using the notation $n_{j+1} = n_j + \Delta n$; $k_{ex_{j+1}} = k_{ex_j} + \Delta k$; $c_{i_{j+1}} = c_{i_j} + \Delta c_i$ and $t_{j+1} = t_j + \Delta t$, this becomes

$$\Delta n = \frac{1}{\ell}\int_{t_j}^{t_j + \Delta t} k_{ex}\, n\, dt - \sum_i \Delta c_i + S\Delta t \quad .$$

If k_{ex} and n are assumed to vary linearly over the interval Δt, then

$$k_{ex} = k_{ex_j} + \Delta k\left(\frac{t - t_j}{\Delta t}\right) \text{ and } n = n_j + \Delta n\left(\frac{t - t_j}{\Delta t}\right) \text{ for } t_j < t < t_{j+1} \quad .$$

The product $k_{ex}n$ is formed from these and integrated to yield

$$\Delta n = \frac{1}{\ell}\left[n_j\left(k_{ex_j} + \frac{\Delta k}{2}\right) + \frac{\Delta n}{2}\left(k_{ex_j} + \frac{2\Delta k}{3}\right)\right]\Delta t - \sum_i \Delta c_i + S\Delta t \quad .$$

Similarly, the change in c_i between two points, j and j + 1, is obtained by integrating the second equation:

$$c_{i_{j+1}} - c_{i_j} = \int_{t_j}^{t_{j+1}} dc_i = \frac{\beta a_i}{\ell}\int_{t_j}^{t_{j+1}} n\,dt + \frac{\beta a_i}{\ell}\int_{t_j}^{t_{j+1}} k_{ex} n\,dt - \lambda_i \int_{t_j}^{t_{j+1}} c_i\,dt \quad .$$

Again changing the notation, replacing k_{ex} by $k_{ex} + \Delta k\frac{(t - t_j)}{\Delta t}$; n by $n_j + \Delta n\frac{(t - t_j)}{\Delta t}$; and c_i by $c_{i_j} + \Delta c_i\frac{(t - t_j)}{\Delta t}$, performing the integrations and replacing

$$\left[\frac{\beta a_i}{\ell}(1 + k_{ex_j})n_j - \lambda_i c_i\right] \text{ by } \left(\frac{dc_i}{dt}\right)_j \quad ,$$

there is obtained

$$\Delta c_i = \frac{\frac{\beta a_i}{\ell}\left[n_j\,\Delta k + \Delta n\left(1 + k_{ex_j} + \frac{2\Delta k}{3}\right)\right]\frac{\Delta t}{2} + \left(\frac{dc_i}{dt}\right)_j \Delta t}{\left(1 + \lambda_i\frac{\Delta t}{2}\right)}$$

These Δc_i can be summed over all i's and inserted in the expression for Δn to finally yield

$$\Delta n = \frac{\frac{\Delta t}{\ell}n_j\left[k_{ex_j} + \frac{\Delta k}{2}\left(1 - \beta\sum_i \frac{a_i}{1 + \lambda_i\frac{\Delta t}{2}}\right)\right] - \sum_i\left[\frac{\left(\frac{dc_i}{dt}\right)_j \Delta t}{\left(1 + \lambda_i\frac{\Delta t}{2}\right)}\right] + S\Delta t}{1 - \frac{\Delta t}{2\ell}\left[\left(k_{ex_j} + \frac{2\Delta k}{3}\right)\left(1 - \beta\sum_i \frac{a_i}{1 + \lambda_i\frac{\Delta t}{2}}\right) - \beta\sum_i \frac{a_i}{1 + \lambda_i\frac{\Delta t}{2}}\right]}$$

UNCLASSIFIED

The values for Δk can be obtained directly from the third equation if k_{ex} is dependent on t only, and by iteration between Δk and Δn if k_{ex} is also dependent on n. In the latter case, the order of procedure should be:

Compute $\Delta k^{(0)}$ assuming Δn has the value between j-1 and j points.

Compute $\Delta n^{(1)}$ using this $\Delta k^{(0)}$.

Compute $\Delta k^{(1)}$ using $\Delta n^{(1)}$.

Compute $\Delta n^{(2)}$ using $\Delta k^{(1)}$.

Continue to convergence.

Compute Δc_i.

Compute $(dc_i/dt)_{j+1} = \frac{2\Delta c_i}{\Delta t} - (dc_i/dt)_j$.

The two forms of (dk_{ex}/dt) coded to date are

$$(dk_{ex}/dt) = A + Bn$$

and

$$(dk_{ex}/dt) = \frac{\Omega}{\omega}\cos\omega t \quad .$$

For these,

$$\Delta k = A\Delta t + B(n_j + \frac{\Delta n}{2})\Delta t$$

and

$$\Delta k = \Omega\left[\sin\omega(t_j + \Delta t) - \sin\omega t_j\right] \quad .$$

In the program for AVIDAC, computation of Δk is divorced from the main body of the code so that any number of forms for expressing k_{ex} may be utilized with little additional coding time.

It is of interest to note that these solutions may be obtained by hand computation in about 15 to 20 minutes per point. The interval size is restricted to that interval in which k_{ex}, n, and c_i can reasonably be considered linear and which will not cause the numerator of the Δn expression to go to zero for $k_{ex} > \beta$.

2. Solution of the Kinetics Equations, Given n (RE-22)

There has been increasing demand for means of analyzing time-dependent neutron flux data obtained on reactors with a view to determining the time variation of reactivity required to produce such flux data.

DECLASSIFIED

The means has been provided by arranging for a solution of the reactor kinetics equations on AVIDAC for a given input of flux-time data. This is the converse of the solution outlined above for a given excess reactivity variation. The procedure is as follows:

Consider again the first two kinetics equations, which are rewritten here as

$$\frac{dn}{dt} = \frac{k_{ex}(t)(1-\beta) - \beta}{\ell} n(t) + \sum_{i=1}^{6} \lambda_i c_i(t) \tag{1}$$

$$\frac{dc_i}{dt} = \frac{\left[1 + k_{ex}(t)\right] \beta a_i}{\ell} n(t) - \lambda_i c_i(t) \qquad (i=1,2...6) \quad . \tag{2i}$$

The neutron density data for which the associated k_{ex} variation is desired is available for points in time at h-second intervals. Equations (2i) can be integrated to give

$$C_i(t) = \frac{\beta a_i}{\ell} e^{-\lambda_i t} \int_{t_0}^{t} \left[k_{ex}(y) + 1\right] n(y) e^{\lambda_i y} dy + e^{-\lambda_i (t - t_0)} c_i(t_0) \quad ,$$

and at time h later,

$$C_i(t+h) = e^{-\lambda_i h} C_i(t) + \frac{\beta a_i}{\ell} e^{-\lambda_i (t+h)} \int_{t}^{t+h} \left[k_{ex}(y) + 1\right] n(y) e^{\lambda_i y} dy \quad .$$

This equation can be solved for $k_{ex}(t+h)$ in terms of $c_i(t+h)$, $c_i(t)$, $n(t)$ and $k_{ex}(t)$ if the integral is evaluated by trapezoidal integration. The result is to yield six simultaneous equations in seven unknowns where it is assumed that $c_i(t)$, $n(t)$ and $k_{ex}(t)$ are known. This is the case when $t = t_0$. Equation (1) provides the seventh equation if we replace $\frac{dn}{dt}$ by $\frac{n(t+h) - n(t-h)}{2h}$ (which is the three-point derivative of n at t). There are now seven simultaneous equations in seven unknowns if we set $t = t_0$. These can be solved for $c_i(t_0+h)$ and $k_{ex}(t_0+h)$. Now set $t = t_0+h$ and solve for $c_i(t_0+2h)$ and $k_{ex}(t_0+2h)$, and so on.

The order of solution used here is

$$k_{ex}(t+h) = \frac{1}{1 - \beta(1 - \frac{h}{2}\Sigma\lambda_i a_i)} \left\{ \frac{\frac{\ell}{2h}\left[n(t+2h) - n(t)\right] - \sum \lambda_i e^{-\lambda_i h}\left[\ell c_i(t) + \frac{k_{ex}(t)+1}{2}\beta a_i h n(t)\right]}{n(t+h)} + 1 \right\} - 1$$

DECLASSIFIED

$$c_i(t+h) = e^{-\lambda_i h}\left\{c_i(t) + \frac{h}{2}\frac{k_{ex}(t)+1}{\ell}\beta\, a_i\, n(t)\right\} + \frac{h}{2}\frac{k_{ex}(t+h)+1}{\ell}\beta a_i\, n(t+h) \quad .$$

The initial conditions are that k_{ex} has been constant (k_{ex_c}) long enough so that the concentration of delayed emitters have the asymptotic form; that is, it is assumed that the flux has the form $n(t) = n_0\, e^{t/\tau}$ (where τ is the asymptotic period) and that t is large enough so that the expression for the delayed emitters

$$c_i(t) = \frac{\beta a_i n_0}{\ell}\left[\frac{(k_{ex_c}+1)\lambda_i e^{t/\tau} + (1/\tau - \lambda_i k_{ex_c})\, e^{-\lambda_i t}}{\lambda_i(\lambda_i + 1/\tau)}\right]$$

can be replaced by

$$c_i(t_0) = \frac{\beta a_i\,(k_{ex_c}+1)\,n(t_0)}{\lambda_i + 1/\tau} \quad .$$

Because of the use of trapezoidal rule for integrating the expression

$$\int_{t_0}^{t}\left[k_{ex}(y)+1\right] n(y)\, e^{\lambda_i y}\, dy \quad ,$$

errors have been introduced which depend on the interval size h independently of how the flux and reactivity change over this interval. These errors are of the order of magnitude of

$$-\frac{\beta h^3}{12}\sum a_i \lambda_i^3 \quad ,$$

and for Hughes' data,[30] when $h \simeq 0.1$, this is roughly -4×10^{-5}. For $h \leq 0.01$ the only limit imposed on interval size arises from the assumption that n is linear over the interval, essentially.

This method has been used successfully to analyze data from the BORAX experiments, EBR oscillation tests, and to do control rod calibrations by the rod drop method.

---

[30] D. J. Hughes, et al, "Delayed Neutrons from Fission of U^{235}," Phys. Rev., 73, 111 (1948)

DECLASSIFIED

C. Analytical Solutions of Kinetics Equations

Stimulated by a need to analyze some pile oscillation experiments, Harold Greenspan has succeeded in obtaining analytical solutions of the kinetics equations for limited inputs of n or k_{ex} which parallel both the synthesis scheme of RE-29 and the analysis scheme of RE-22 described above. Specifically, the problem of obtaining the flux at any time resulting from a sinusoidal reactivity input plus a reactivity response proportional to the flux (with a time delay) was solved, along with that of obtaining the reactivity necessary to produce a sinusoidally varying flux. Greenspan's solutions are presented here in some detail.

1. Solution for n, Given k_{ex}

An analytical solution for the variation of neutron density with time in a one-group, space-independent model has been obtained when the reactivity is a function of time and a functional of the neutron density involving a delay time, Γ. Specifically,

$$k = 1 + a\left[n(t) - n_0\right] + b\,H(t-\Gamma)\left[n(t-\Gamma) - n_0\right] + c\sin\omega t \quad .$$

The linearized solution is obtained as follows, using the primary definitions above:

Let

$$n = n_0 + n_1(t) \qquad\qquad n_1 \ll n_0$$

and

$$c_i = c_{i_0} + c_{i_1}(t) \qquad\qquad c_{i_0} = \frac{\beta_i n_0}{\lambda_i \ell}$$

with zero (0) subscripts denoting steady-state values.

$$H(t-\Gamma) = 0 \qquad\qquad t < \Gamma$$

$$H(t-\Gamma) = 1 \qquad\qquad t \geq \Gamma$$

and

$$n_1(t-\Gamma) = \bar{n}_1 \quad .$$

Also

$$k = 1 + k_{ex} \quad .$$

Using these relationships, the basic kinetics equations set forth previously can be written (ignoring all squared terms in n_1):

DECLASSIFIED

$$\ell\frac{dn}{dt} = \ell\frac{dn_1}{dt} = -\rho n_1 + an_0n_1(1-\beta) + bn_0H\bar{n}_1(1-\beta) + n_0(1-\beta)\,c\sin\omega t + \ell\sum_i \lambda_i c_i$$

and

$$\frac{dc_i}{dt} = \frac{dc_{i_1}}{dt} = -\lambda_i c_i + \frac{\beta_i}{\ell}\left[n_1 + an_0n_1 + bn_0H\bar{n}_1 + n_0c\sin\omega t\right] \quad .$$

Using the information that $n_1(0) = 0$ and $c_{i_1}(0) = 0$, one writes the Laplace transforms of these equations, where

$$\mathcal{L}\left\{n_1(t)\right\} = N(s)$$

and

$$\mathcal{L}\left\{c_{i_1}(t)\right\} = C_i(s) \quad ,$$

as follows:

$$\ell sN(s) = -\beta N(s) + an_0N(s)(1-\beta) + bn_0e^{-s\Gamma}(1-\beta)N(s) + \frac{n_0c(1-\beta)\omega}{s^2+\omega^2} + \ell\sum_i \lambda_i C_i(s)$$

and

$$(s+\lambda_i)C_i(s) = \frac{\beta_i}{\ell}\left[N(s) + an_0N(s) + bn_0e^{-s\Gamma}N(s) + n_0c\,\frac{\omega}{s^2+\omega^2}\right] \quad .$$

From the latter,

$$\ell\sum_i \lambda_i C_i(s) = \sum_i \beta_i\left(1-\frac{s}{s+\lambda_i}\right)\left[N(s) + an_0N(s) + bn_0e^{-s\Gamma}N(s) + n_0c\,\frac{\omega}{s^2+\omega^2}\right] .$$

This may be substituted into the $\ell\, sN(s)$ equation above, and by proper algebraic manipulations it is found that

$$N(s) = \frac{n_0c\omega}{(s^2+\omega^2)\,W(s)} \quad ,$$

wherein

$$W(s) = \frac{1}{Q(s)} - n_0(a + be^{-s\Gamma})$$

$$Q(s) = \left[\frac{s\left(\ell + \sum_i \frac{\beta_i}{s+\lambda_i}\right)}{\left(1 - s\sum_i \frac{\beta_i}{s+\lambda_i}\right)}\right] .$$

Then $n_1(t)$ is obtained from the transform as

$$n_1(t) = n_0c\omega \text{ times sum of residues of } \frac{1}{(s^2+\omega^2)\,W(s)}$$

DECLASSIFIED

and is

$$n_1(t) = n_0 c\omega \left[\frac{e^{j\omega t}}{2j\omega W(j\omega)} + \frac{e^{-j\omega t}}{-2j\omega W(-j\omega)} \right] + n_0 c\omega \sum_i \frac{e^{\mu_i t}}{\left(\mu_i^2 + \omega^2\right) \frac{d}{ds} W(s) \Big|_{s=\mu_i}}$$

This may be put in a more convenient form:

$$n_1(t) = \frac{n_0 c}{\left| W(j\omega) \right|} \sin(\omega t + \Psi) + n_0 c\omega \sum_i \frac{e^{\mu_i t}}{(\mu_i^2 + \omega^2) \frac{d}{ds} W(s) \Big|_{s=\mu_i}}$$

where $\Psi = \arctan \frac{\text{Im. } W(j\omega)}{\text{Real } W(j\omega)}$.

Depending on the combination of $n_0 a$, $n_0 b$ and Γ, the roots of $W(s)$ are determined and these determine the character of $n_1(t)$. In many cases $n_0 a$, $n_0 b$ and Γ are such that $W(s)$ has no roots with positive real parts, but $W(s)$ may have roots which are pure imaginary, have a negative real part, or both. The formula above for $n_1(t)$ does not apply for all such values of t, $n_0 a$, $n_0 b$, Γ, and ω which would make $n_1(t) > n_0$, but even with such combinations it can be used to investigate the development of an unstable situation.

2. Solution for k_{ex}, Given n

If the flux can be represented by a function whose Laplace transform exists, then the one-group, space-independent kinetics equations can be solved analytically for excess reactivity. The essential point in the solution is to work with $\mathcal{L}\left\{k_{ex} n\right\}$ rather than with $\mathcal{L}\left\{k_{ex}\right\}$. The solution is developed as follows:

Consider again the basic kinetic equations

$$\frac{dn}{dt} = \frac{1-\beta}{\ell} k_{ex} n - \frac{\beta}{\ell} n + \sum_i \lambda_i c_i \tag{1}$$

and

$$\frac{dc_i}{dt} = \frac{\beta_i}{\ell} k_{ex} n + \frac{\beta_i}{\ell} n - \lambda_i c_i \quad . \tag{2}$$

Now let

$$n(t) = n_0 + n_1(t); \; c_i(t) = c_{i_1}(t) + c_{i_0} \quad ;$$

$$\mathcal{L}\left\{n_1(t)\right\} = N(s) \quad ; \mathcal{L}\left\{c_i(t)\right\} = C_i(s) \quad ; \mathcal{L}\left\{k_{ex}(t)\,n(t)\right\} = G(s) \quad .$$

At $t = 0$ assume $n_1(0) = c_{i_1}(0) = k_{ex}(0) = 0$ so that

$$C_{i_0} = \frac{\beta_i n_0}{\lambda_i \ell} \quad . \tag{3}$$

The transformed equations for dn/dt and dc_i/dt are then

$$sN(s) = \frac{1-\beta}{\ell} G(s) - \frac{\beta}{\ell} N(s) + \sum_i \lambda_i C_i(s) \quad ;$$

$$sC_i(s) = \frac{\beta_i}{\ell} G(s) + \frac{\beta_i}{\ell} N(s) - \lambda_i C_i(s) \quad .$$

Combining these,

$$sN(s) = \frac{1-\beta}{\ell} G(s) - \frac{\beta}{\ell} N(s) + \frac{1}{\ell}\left[N(s) + G(s)\right] \sum_i \frac{\lambda_i \beta_i}{s+\lambda_i} \quad .$$

Solving for $G(s)$, the final result is

$$G(s) = N(s) \left[\frac{s\left(\ell + \sum_i \frac{\beta_i}{s+\lambda_i}\right)}{1 - s \sum_i \frac{\beta_i}{s+\lambda_i}} \right] . \tag{4}$$

The expression

$$\frac{s\left(\ell + \sum_i \frac{\beta_i}{s+\lambda_i}\right)}{1 - s \sum_i \frac{\beta_i}{s+\lambda_i}} = Q(s)$$

appearing here and in the solution previously treated is of the same form as the inhour equation if the asymptotic pile period is substituted for s. It can be written as the ratio of two polynomials in s:

$$Q(s) = \frac{P_1(s)}{P_2(s)} \quad .$$

The coefficients of $P_1(s)$ depend only on the lifetime of the pile and on the β_i's and λ_i's, and the coefficients of P_2 depend only on the β_i's and λ_i's. Here

$$P_1(s) = \left[a_7 s^7 + a_6 s^6 + a_5 s^5 + a_4 s^4 + a_3 s^3 + a_2 s^2 + a_1 s \right]$$

DECLASSIFIED

and

$$P_2(s) = (s - \mu_1)(s - \mu_2)(s - \mu_3)(s - \mu_4)(s - \mu_5)(s - \mu_6) \quad .$$

The problem has been worked for the case where $n_1(t) = c \sin\omega t$.
Then

$$k_{ex}n = c\omega\left\{\frac{e^{j\omega t} P_1(j\omega)}{2j\omega\, P_2(j\omega)} + \frac{e^{-j\omega t} P_1(-j\omega)}{-2j\omega\, P_2(-j\omega)} + \sum_i \frac{e^{\mu_i t} P_1(\mu_i)}{(\mu_i^2 + \omega^2)\frac{d}{ds} P_2(s)\Big|_{s=\mu_i}}\right\}$$

or, more conveniently,

$$k_{ex}n = cR\sin(\omega t + \Psi) + c\omega \sum_i \frac{e^{\mu_i t} P_1(\mu_i)}{(\mu_i^2 + \omega^2)\frac{d}{ds} P_2(s)\Big|_{s=\mu_i}} \quad ,$$

where

$$R = \sqrt{\frac{(\text{Real } P_1)^2 + (\text{Im } P_1)^2}{(\text{Real } P_2)^2 + (\text{Im } P_2)^2}}$$

$$\Psi = \arctan\frac{\text{Im } P_1}{\text{Real } P_1} - \arctan\frac{\text{Im } P_2}{\text{Real } P_2} \quad .$$

Since $\mu_i < 0$, the summation drops out for large enough t. The asymptotic form for $k_{ex}n$ then is

$$k_{ex}n = cR\sin(\omega t + \Psi) \quad .$$

For the Hughes six-delay group data,[30] the values of the a's and μ's in the polynomials above are:

$a_1 = (6.24021\,\ell + .576232) \times 10^{-4}$	$\mu_1 = -\ .012506$
$a_2 = (7.55841\,\ell + .487508) \times 10^{-2}$	$\mu_2 = -\ .031546$
$a_3 = (2.25144\,\ell + .0662658)$	$\mu_3 = -\ .154319$
$a_4 = (16.2843\,\ell + .196642)$	$\mu_4 = -\ .457148$
$a_5 = (32.8757\,\ell + .116456)$	$\mu_5 = -\ 1.61315$
$a_6 = (16.266\,\ell + .00755)$	$\mu_6 = -14.005$
$a_7 = \ell$	

DECLASSIFIED

D. Kinetic Studies

The calculation methods above have been used in investigating oscillatory behavior of the kinetic system for a reactor with a lifetime, like EBR-I, of 4×10^{-8} sec. As a correlation check among the methods, the response of the flux to a sinusoidal input of reactivity was determined for a model in which reactivity was independent of flux, such as would correspond to "zero power" operation in the reactor. Three sets of calculations were performed:

(1) Using RE-29, the reactivity was allowed to oscillate according to

$$k_{ex} = \Delta k \sin \omega t \quad .$$

A value of $\Delta k = 0.0002$ and $n_0 = 1$ was used throughout, while various values of the frequency, ω, between 0.05 and 10 radians/sec were assumed. The response of n for each ω is shown plotted in Fig. 67. From these response curves the values $\frac{n_{max} - n_{min}}{2} = \Delta n$ were obtained and the quantity $n_0 \Delta k/\Delta n$ was calculated. In addition, the phase shift, Ψ, represented by the angular displacement of peaks on the n curve from peaks on the k_{ex} curve, was measured. These quantities represent together the "transfer function" for the model.

(2) Using the linearized analytical method with the coefficients of reactivity dependence on flux equal to zero, the quantities $n_0 \Delta k/\Delta n$ and the phase angle Ψ were calculated directly for the same range of values of ω. These two quantities were plotted vs ω in Fig. 68. The corresponding quantities obtained with RE-29 were plotted as points on the analytical curve.

(3) Flux response curves obtained experimentally on EBR-I by use of an oscillating control rod were used to prepare input data for RE-22, and the reactivity vs time relation was obtained for a number of frequencies. Here $n_0/\Delta n$ was known, and Δk was determined from the AVIDAC output using the relation

$$\Delta k = \frac{k_{ex_{max}} - k_{ex_{min}}}{2} \quad .$$

Again $n_0 \Delta k/\Delta n$ and Ψ were obtained and these also have been superimposed on the analytical curves of Fig. 68.

The excellent agreement gives assurance that the several methods are compatible, and that linearization has resulted in no practical loss in accuracy. Further computations are in progress to examine the importance

DECLASSIFIED

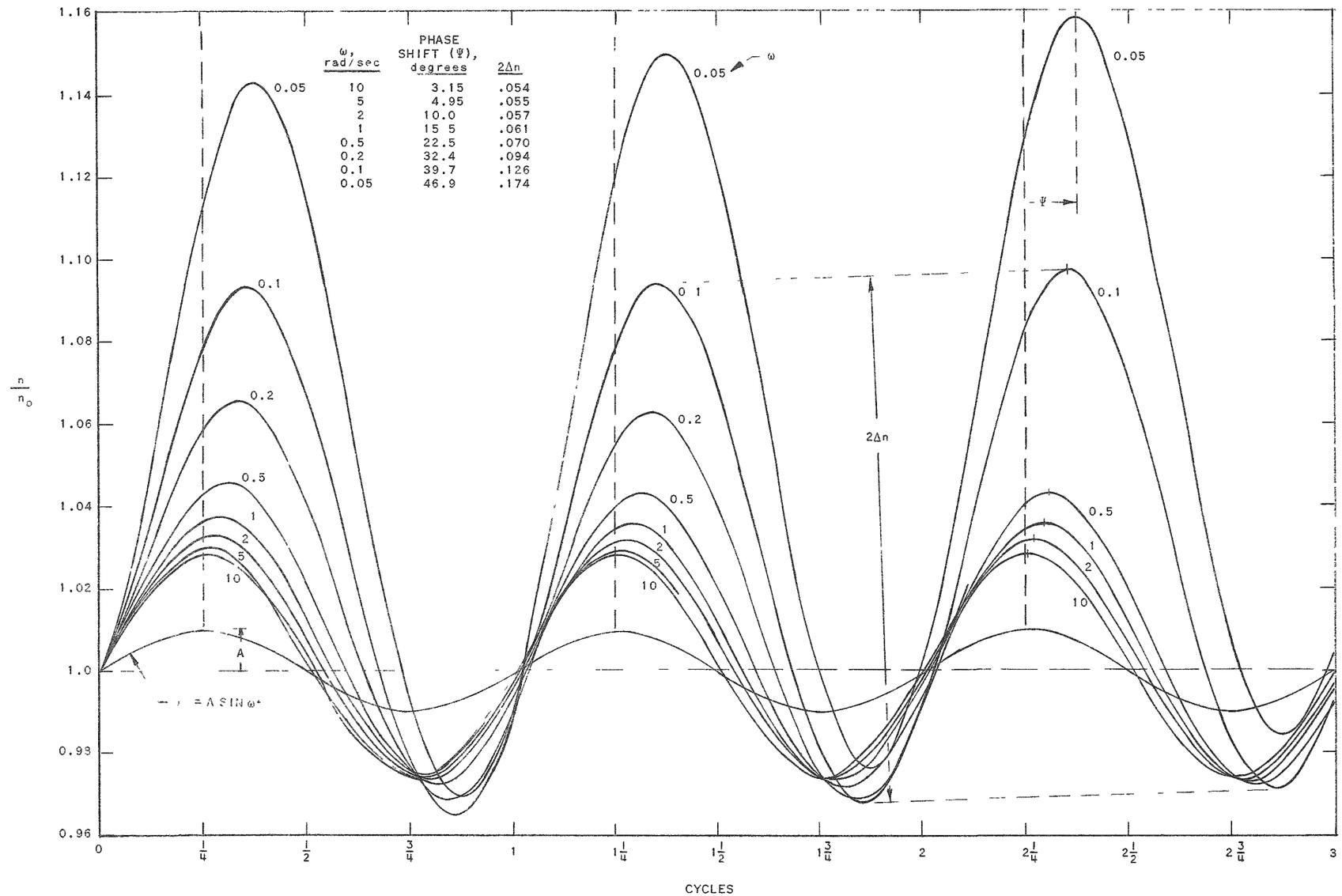

FIG. 67
OSCILLATORY RESPONSE OF NEUTRON POPULATION
TO SINUSOIDAL REACTIVITY INPUT AT ~ ZERO POWER
A = 0.0002
$\ell = 4 \times 10^{-8}$ seconds
(AVIDAC RESULTS FROM RE-29 PROGRAM)

RE-7-17042-C

DECLASSIFIED
DECLASSIFIED

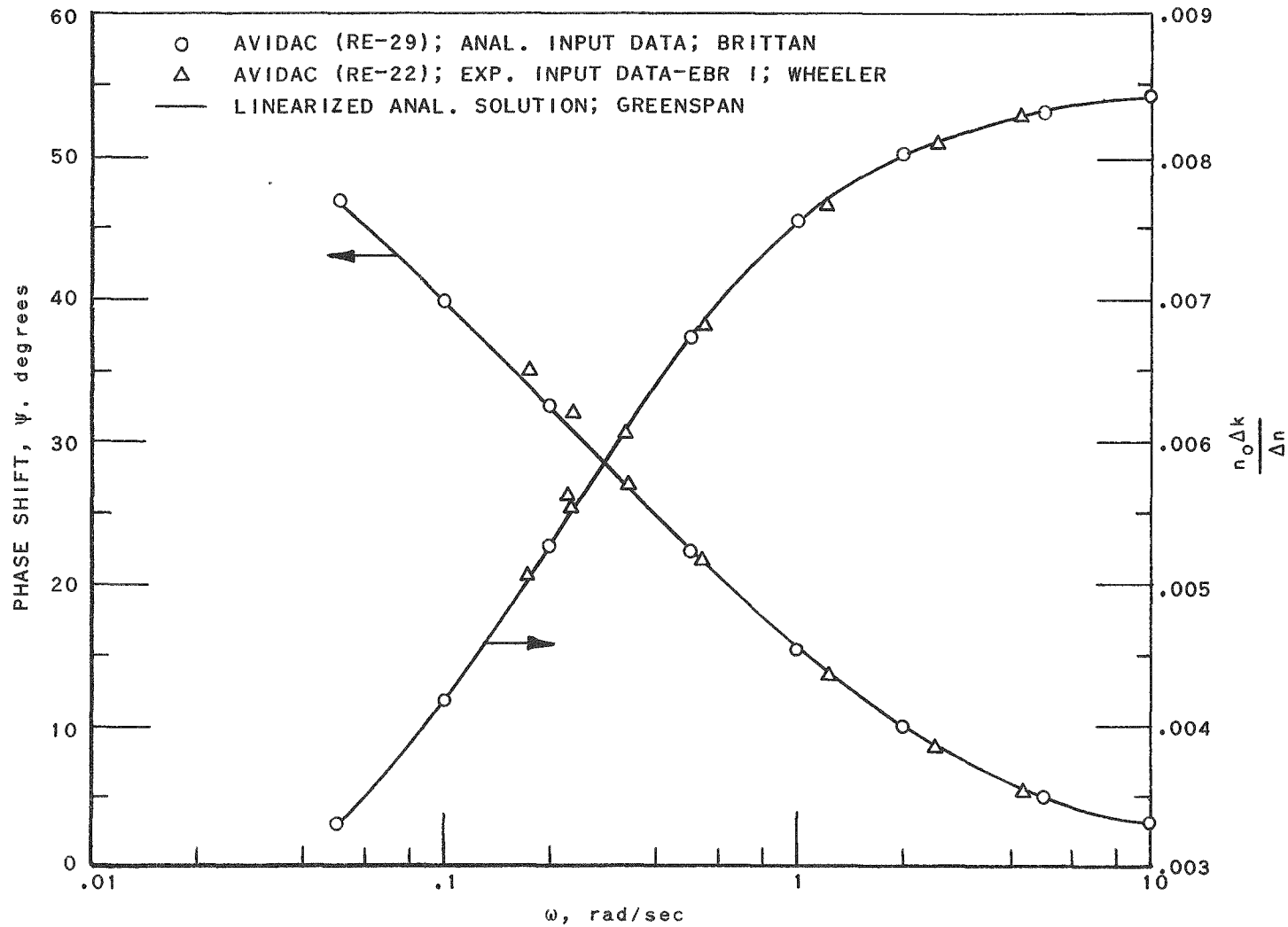

FIG. 68
RESPONSE TO AN IMPRESSED PERIODIC VARIATION
IN REACTIVITY ON A REACTOR AT ZERO POWER
HAVING AN EFFECTIVE LIFETIME OF 4×10^{-8} seconds

RE-7-17071-A

of departure of input information from a true sine curve, and to determine the point at which linearizing assumptions in the analytical method render it unusable. It is also planned to use RE-29 with a reactivity dependence like

$$k_{ex} = \Omega \sin \omega t + \xi \left[n(t) - n_0 \right] + \Lambda \left[n(t - \Gamma) - n_0 \right]$$

and compare with the analytical solution of Greenspan and oscillating power runs on EBR-I analyzed by use of RE-22.

E. Thermal Inertia

The thermal inertia of a uranium rod in sodium was last reported in ANL-5371, p. 90. The solution to the general problem of obtaining temperature distributions in two-region cylindrical geometry for an exponentially rising source in the central region was made by Greenspan, but never published. It complements the slab and spherical geometry solutions by Greenspan appearing in ANL-4951, p. 13. For the sake of completeness and to make it useful, the solution is presented here. In addition, application of the solution to the thermal inertia problem was expanded over that previously reported for large αt to include small values of αt. The scheme used and the results obtained are presented.

1. Temperature Distribution in Two-Region Cylindrical Geometry with Exponentially Rising Heat Source in Control Region

Solutions to the time-dependent heat conduction and temperature-distribution problems in fuel elements have been previously reported for the cases of plates and spheres. Since then there has been a demand for a solution for the case of cylinders in some safety studies. The problem has been solved in two-region cylindrical geometry for an exponentially rising heat source in the central region, as follows:

Consider a composite cylinder made up of a central cylinder of heat source material surrounded by a cylinder of non-source material. The source material occupies the region 1 ($0 \leq r \leq r_1$). Its density is ρ_1, specific heat c_1, conductivity k_1, and source strength $Q_1 e^{\alpha t}$. Here α is the inverse of the e-folding time or period of the source whose strength increases exponentially with time. The non-source material occupies the region $r_1 \leq r \leq r_2$ and has the properties ρ_2, c_2, k_2 with $Q_2 = 0$.

The space-time dependent equations defining the temperatures $T_i(r, t)$ are, as usual,

$$\frac{\partial T_i}{\partial t} = \kappa_i^2 \left[\frac{\partial^2 T_i}{\partial r^2} + \frac{1}{r} \frac{\partial T_i}{\partial r} \right] + q_i e^{\alpha t} \qquad (i = 1, 2) \quad ,$$

DECLASSIFIED

where

$$\kappa_i^2 = \frac{k_i}{\rho_i c_i}$$

and

$$q_i = \frac{Q_i}{\rho_i c_i} \quad ,$$

and

$$q_2 = 0 \;;\; \frac{\partial T_2}{\partial r} = 0 \text{ at } r = r_2 \;;\; \left.\begin{array}{l} T_1 = T_2 \\ k_1 \dfrac{\partial T_1}{\partial r} = k_2 \dfrac{\partial T_2}{\partial r} \end{array}\right\} \text{ at } r = r_1 \quad .$$

T_1 is finite at $r = 0$; $T_i(r,0) = 0$.

(Such a condition would exist, for example, if this composite cylinder were formed as a representative cell in an array of cells. This would correspond closely to a group of uranium rods in sodium.)

The method of Laplace transformations is applied to the equation above to obtain the transform of T_i, thus:

$$V_i(r,s) = A_i(s) I_0(\mu_i r) + B_i(s) K_0(\mu_i r) + \frac{q_i}{s(s-\alpha)} \quad \left(\mu_i^2 = \frac{s}{\kappa_i^2}\right) \quad .$$

Applying the conditions above, one obtains

$$V_1(r,s) = \frac{q_1 \rho \left[I_1(\mu_2 r_1) K_1(\mu_2 r_2) - I_1(\mu_2 r_2) K_1(\mu_2 r_1) \right]}{s(s-\alpha)\, D(s)} I_0(\mu_1 r) + \frac{q_1}{s(s-\alpha)}$$

and

$$V_2(r,s) = \frac{q_1 \, I_1(\mu_1 r_1)}{s(s-\alpha)\, D(s)} \left[I_0(\mu_2 r) K_1(\mu_2 r_2) + I_1(\mu_2 r_2) K_0(\mu_2 r) \right] \quad ,$$

where

$$\rho = \frac{k_2 \kappa_1}{k_1 \kappa_2}$$

and

$$D(s) = I_1(\mu_1 r_1) \left[I_0(\mu_2 r_1) K_1(\mu_2 r_2) + I_1(\mu_2 r_2) K_0(\mu_2 r_1) \right] - \rho I_0(\mu_1 r_1) \left[I_1(\mu_2 r_1) K_1(\mu_2 r_2) - I_1(\mu_2 r_2) K_1(\mu_2 r_1) \right] \quad .$$

The inverse transformation is applied to these to obtain the temperature distribution in the two regions:

DECLASSIFIED

$$T_1(r,t) = \frac{q_1}{\alpha}(e^{\alpha t} - 1) + \frac{\rho q_1 e^{\alpha t} I_0\left(\frac{\sqrt{\alpha}}{\kappa_1} r\right)\left[I_1\left(\frac{\sqrt{\alpha}}{\kappa_2} r_1\right) K_1\left(\frac{\sqrt{\alpha}}{\kappa_2} r_2\right) - I_1\left(\frac{\sqrt{\alpha}}{\kappa_2} r_2\right) K_1\left(\frac{\sqrt{\alpha}}{\kappa_2} r_1\right)\right]}{\alpha D(\alpha)}$$

$$- \rho q_1 \pi \sum_{j=1}^{\infty} \frac{J_0\left(\frac{\lambda_j}{\kappa_1} r\right)\left[J_1\left(\frac{\lambda_j}{\kappa_2} r_2\right) Y_1\left(\frac{\lambda_j}{\kappa_2} r_1\right) - J_1\left(\frac{\lambda_j}{\kappa_2} r_1\right) Y_1\left(\frac{\lambda_j}{\kappa_2} r_2\right)\right] e^{-\lambda_j^2 t}}{\lambda_j\left(\lambda_j^2 + \alpha\right) \frac{d}{d\lambda} D\left(-\lambda^2\right)\Big|_{\lambda = \lambda_j}}$$

$$- \frac{\rho q_1}{\alpha}\left[\frac{\kappa_1}{\kappa_2\left(\frac{r_1^2}{r_1^2 - r_2^2}\right) - \rho\kappa_1}\right] ;$$

$$T_2(r,t) = \frac{q_1 e^{\alpha t} I_1\left(\frac{\sqrt{\alpha}}{\kappa_1} r_1\right)\left[I_0\left(\frac{\sqrt{\alpha}}{\kappa_2} r\right) K_1\left(\frac{\sqrt{\alpha}}{\kappa_2} r_2\right) + I_1\left(\frac{\sqrt{\alpha}}{\kappa_2} r_2\right) K_0\left(\frac{\sqrt{\alpha}}{\kappa_2} r\right)\right]}{\alpha D(\alpha)}$$

$$- q_1 \pi \sum_{j=1}^{\infty} \frac{J_1\left(\frac{\lambda_j}{\kappa_1} r_1\right)\left[J_1\left(\frac{\lambda_j}{\kappa_2} r_2\right) Y_0\left(\frac{\lambda_j}{\kappa_2} r\right) - J_0\left(\frac{\lambda_j}{\kappa_2} r\right) Y_1\left(\frac{\lambda_j}{\kappa_2} r_2\right)\right] e^{-\lambda_j^2 t}}{\lambda_j\left(\lambda_j^2 + \alpha\right) \frac{d}{d\lambda} D\left(-\lambda^2\right)\Big|_{\lambda = \lambda_j}}$$

$$- \frac{q_1}{\alpha}\left[\frac{\kappa_2\left(\frac{r_1^2}{r_1^2 - r_2^2}\right)}{\kappa_2\left(\frac{r_1^2}{r_1^2 - r_2^2}\right) - \rho\kappa_1}\right] .$$

In these equations λ_j are the roots of $D(-\lambda^2) = 0$. For large values of αt, i.e., after several periods (say $\alpha t = 6$), the last two terms in each equation above can be neglected. For investigation of the problem near the beginning of the excursion, these terms are important.

2. Time Variation of Stored Heat in Sodium-Cooled Uranium Rod During Transient

The study of thermal inertia effects was meant to determine the maximum reactor periods for which it could be reasonably assumed that heat transfer out of the element could be neglected. The solution of the temperature distribution for an exponentially rising source in a two-region cylindrical cell provided a means of making this study, since one can determine the fraction of total heat produced remaining in the element for various αt and α ($\frac{1}{\alpha}$ = e-folding time). The procedure reported in ANL-5371, p. 90, was to calculate the ratio of heat content in the element (region 1) to total heat in the cell as

DECLASSIFIED

$$R_H = \frac{H_1}{H} = \frac{\rho_1 c_1 \int_0^{r_1} T_1 \, 2\pi r dr}{Q_1 \pi r_1^2 \int_0^{t_1} e^{\alpha t} dt}$$

by substituting Greenspan's expression for T_1, given above. The calculation involved evaluation of the summation terms, except for large αt. At the time of the last reporting the calculation had been made for $\alpha t > 6$, with the summation terms neglected. Since then, calculations have been completed for the range of $0 < \alpha t < 6$, including these terms. In addition, a second scheme was used to obtain the ratio R_H by calculating the heat leaving the region 1, i.e., H_2. Then

$$R_H = \frac{H - H_2}{H} = \frac{Q_1 \pi r_1^2 \int_0^{t_1} e^{\alpha t} dt - \left[-2\pi r_1 k_1 \int_0^{t_1} \left. \frac{\partial T_1}{\partial r} \right|_{r = r_1} dt \right]}{Q_1 \pi r_1^2 \int_0^{t_1} e^{\alpha t} dt} .$$

Both these schemes lead to identical results, the latter less circuitously. The procedure is worth recording in the following detail:

(The same notation and definitions are used as in the above solution for T_i.)

From basic heat flow considerations, the heat leaving region 1 is

$$H_{1\,out} = H_{2in} = -2\pi r_1 k_1 \int_0^{t_1} \left. \frac{\partial T_1}{\partial r} \right|_{r = r_1} dt \quad .$$

Partial differentiation of the expression for $T_1(r,t)$ written previously yields

$$\left. \frac{\partial T_1}{\partial r} \right|_{r = r_1} = \frac{\rho q_1 \frac{\sqrt{\alpha}}{\kappa_1}}{\alpha} M e^{\alpha t} + \frac{\rho q_1 \pi}{\kappa_1} \sum_{j=1}^{\infty} N e^{-\lambda_j^2 t} \quad ,$$

where

$$M = \frac{I_1\left(\frac{\sqrt{\alpha}}{\kappa_1} r_1\right) \left[I_1\left(\frac{\sqrt{\alpha}}{\kappa_2} r_1\right) K_1\left(\frac{\sqrt{\alpha}}{\kappa_2} r_2\right) - I_1\left(\frac{\sqrt{\alpha}}{\kappa_2} r_2\right) K_1\left(\frac{\sqrt{\alpha}}{\kappa_2} r_1\right) \right]}{D(\alpha)}$$

and

DECLASSIFIED

$$N = \frac{J_1\left(\frac{\lambda_j}{\kappa_1}r_1\right)\left[J_1\left(\frac{\lambda_j}{\kappa_2}r_2\right)Y_1\left(\frac{\lambda_j}{\kappa_2}r_1\right) - J_1\left(\frac{\lambda_j}{\kappa_2}r_1\right)Y_1\left(\frac{\lambda_j}{\kappa_2}r_2\right)\right]}{\left(\lambda_j^2 + \alpha\right)\frac{d}{d\lambda}D\left(-\lambda^2\right)\Big|_{\lambda = \lambda_j}} \quad .$$

The total amount of heat produced (see above) is

$$H = Q_1 \pi r_1^2 \int_0^{t_1} e^{\alpha t} dt = Q_1 \pi r_1^2 \left(\frac{e^{\alpha t} - 1}{\alpha}\right) \quad .$$

From these relations the ratio is found to be

$$R_H = \frac{H - H_2}{H} = 1 + \frac{2\rho\kappa_1}{r_1\sqrt{\alpha}} M + \frac{2\rho\kappa_1 \pi \alpha}{(e^{\alpha t} - 1)} \sum_{j=1}^{\infty} \frac{N}{\lambda_j^2}\left(1 - e^{-\lambda_j^2 t}\right) \quad .$$

The calculations involve evaluating $D(\alpha)$ for each α investigated. One must also make sufficient evaluations of $D(-\lambda^2)$ to determine the first several values of λ_j, at which $D(-\lambda^2)$ is zero and the slopes $\frac{d}{d\lambda} D(-\lambda^2)$ at each λ_j. Next, N is evaluated for each λ_j and α and the summation obtained for each α.

The R_H has been obtained over the range $1 < \alpha < 10^5$ and $0 < \alpha t < 6$ for the following specific problem:

Region 1	Region 2
Material: Uranium	Material: Sodium
ρ_1 = 19 gm/cc	ρ_2 = 0.834 gm/cc
c_1 = 0.0432 cal/(gm)(C)	c_2 = 0.3041 cal/(gm)(C)
k_1 = 0.0816 cal/(cm)(sec)(C)	k_2 = 0.1617 cal/(gm)(sec)(C)
r_1 = 0.20828 cm	r_2 = 0.33731 cm

(This is the same problem calculated for large αt neglecting the summation term, and shown in ANL-5371, Fig. 38.)

The results are presented as Fig. 69.

UNCLASSIFIED

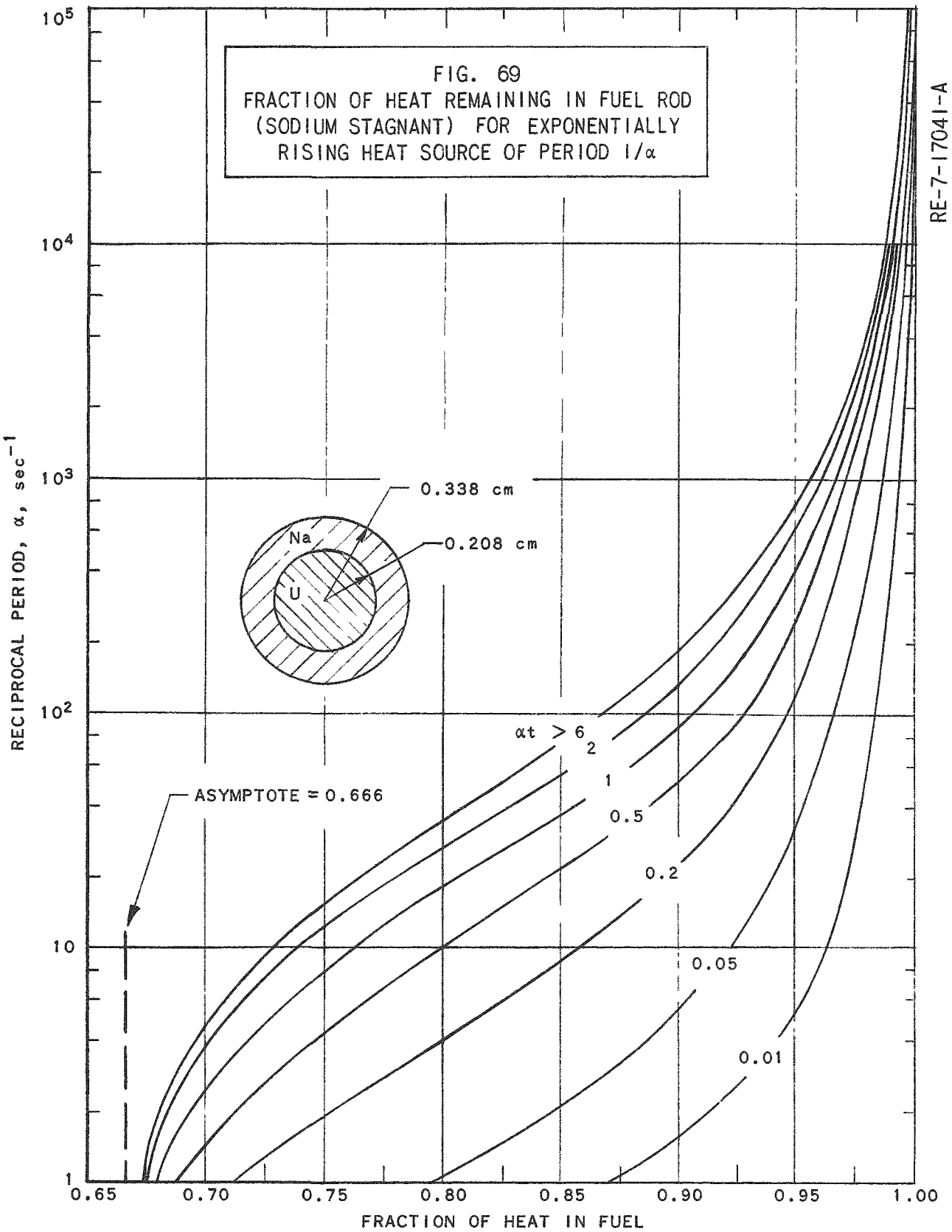

DECLASSIFIED

II. FUEL AND STRUCTURAL MATERIALS

A. Export-Type Fuel Plates - C. R. Breden

Two experimental fuel plates of a type being considered for possible export to foreign nations were submitted for corrosion testing by the Argonne Metallurgy Division. These roll-clad plates had a natural uranium core and were clad with Grade III zirconium. They were about 30 in. long, 4-1/8 in. wide and 1/16 in. thick.

The plates were tested for 203 hr in 420F degassed water and 692 hr in 550F degassed water. After the test the plates were warped, and showed quite heavy white corrosion on the sheared edge surfaces.

B. BORAX III Fuel Plates - C. R. Breden

Three fuel plates of a type being made for BORAX III, with cores of 19% enriched uranium-aluminum alloy, clad with aluminum-1% nickel, were submitted by the Argonne Metallurgy Division for corrosion testing to ascertain whether surface inclusions resulted in accelerated attack. After 147 hr in 420F degassed water, none of the pre-test identified spots showed attack. One small area, not previously identified, on one plate showed pitting.

Samples of 2S aluminum, spot-welded to simulate BORAX III assembly welds, were satisfactory after tests totaling 512 hr in 420F degassed water.

C. Examination of Heat Exchanger from ANL Water Loop at MTR - J. H. Monaweck, R. A. Stella

Examination of some samples from the MTR Water Loop water-to-water heat exchanger revealed that cracking of the tubes carrying primary system pressure (1500 psi) resulted from localized stresses plus chloride stress corrosion. The heat exchanger was removed in April, 1955, after serious cooling water leaks developed.[31] It had inadvertently been operated earlier for some months with raw cooling water containing a high concentration of chloride.

The cross section of one tube assembly is shown in Fig. 70. Twenty-four such tubes, welded into two headers, made up the heat exchanger assembly. Preliminary examination by MTR personnel indicated that five inner pressure tubes had cracked at the weld to the outer sleeve. Apparently the cooling water, which was found to contain 40-50 ppm chloride, had first cracked the annular tube, hydrolyzing the magnesium oxide.

[31] Reactor Engineering Division Quarterly Report, ANL-5471, (September, 1955) p. 137.

DECLASSIFIED

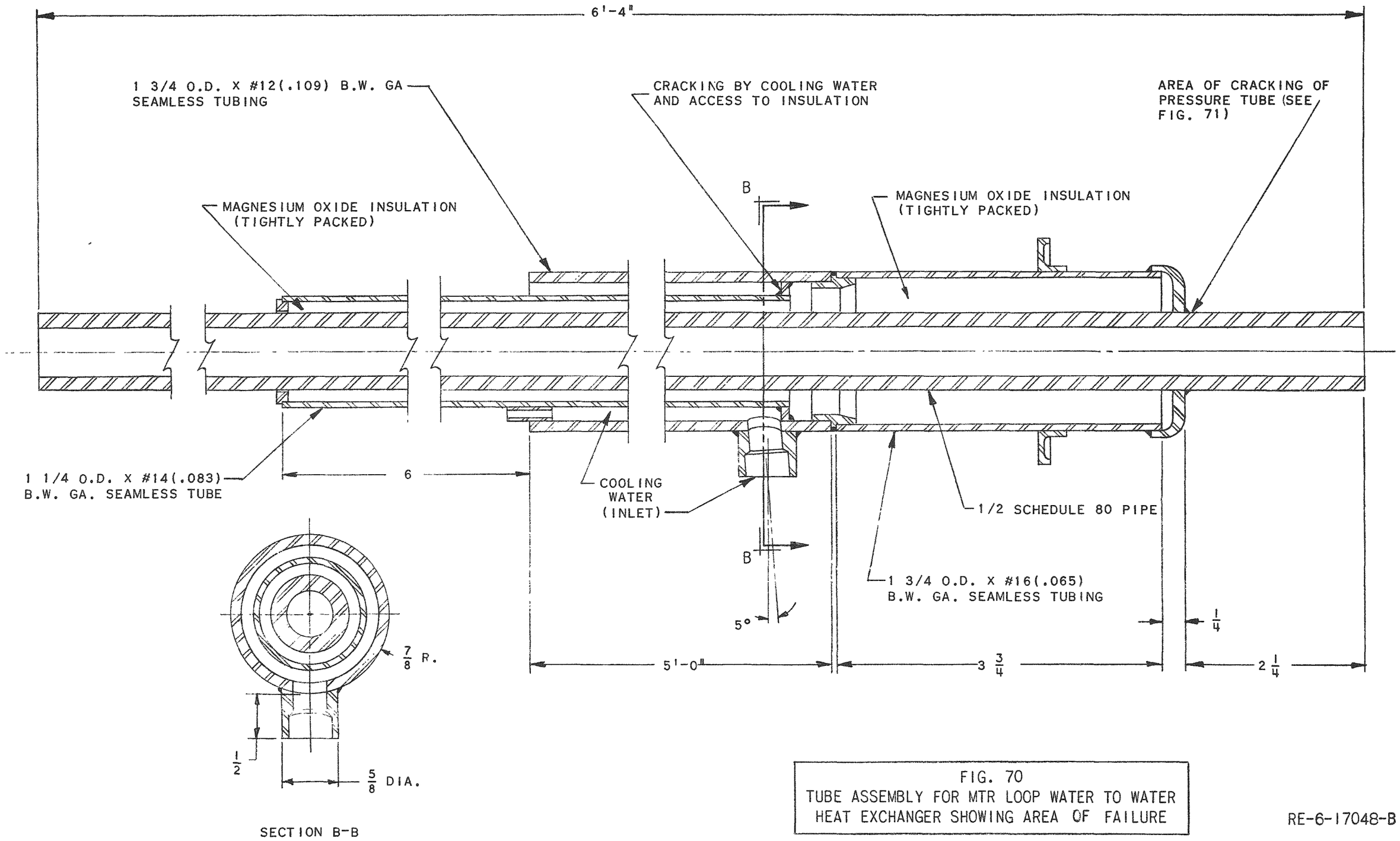

FIG. 70
TUBE ASSEMBLY FOR MTR LOOP WATER TO WATER HEAT EXCHANGER SHOWING AREA OF FAILURE

RE-6-17048-B

DECLASSIFIED

DECLASSIFIED

The combined internal pressure and thermal stresses at the point of failure never exceeded 4000 psi, but the expansion of hydrolyzing magnesium oxide bearing against the outer surface of the tube could have introduced stresses as high as 9300 psi. In all cases, cracking started at the outside of the tube and progressed inward (see Fig. 71), which substantiates that failure was initiated by external forces. Failure at low stress mentioned above can be attributed to corroding chlorides which attack the austenitic tube material in the trangranular manner shown in Fig. 71.

Sectioning of the headers of one of the failed tubes and of other high pressure welds failed to reveal any other cracks in the heat exchanger However, previous failure of three brass fittings at the cooling water inlet had been identified as typical examples of chloride stress corrosion.

Additional samples of the high pressure tube welds are being returned from MTR for further examination.

DECLASSIFIED

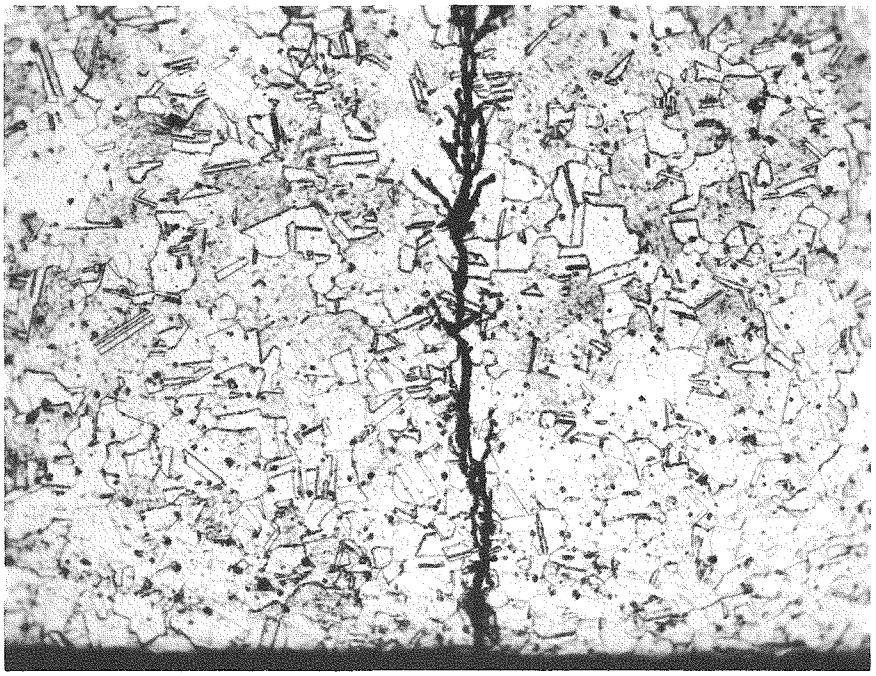

FIG. 71
STRESS CORROSION CRACK STARTING AT OUTSIDE OF HEAT EXCHANGER TUBE.
ETCH: AQUA REGIA. (X250)

DECLASSIFIED

III. INSTRUMENTATION

Neutron-Sensitive Electron Photomultiplier Tubes - G. F. Erickson, S. G. Kaufmann

Experimental evidence on the secondary electron emission from surfaces bombarded with heavy positive ions suggests that photosensitive surfaces of commercial photomultiplier tubes should release a useful number of electrons when fission products or alpha particles pass into, or through, such a surface. An experiment to test the hypothesis and to use the expected secondary yield in the construction of a neutron detector was conducted in cooperation with the Allen B. DuMont Laboratories.

A number of glass covers designed for DuMont 6292 tubes were made available to Argonne. The inner flat surfaces of three covers were coated with a suspension of B^{10} in oil. A small region in the center of each surface was left uncoated to facilitate routine light-sensitivity tests at the factory. The covers were then baked in vacuo at 400F for 24 hr, care being taken that the covers were brought to temperature slowly and uniformly. Subsequently, a thin layer of aluminum was evaporated upon the baked-out boron surfaces. The covers were then returned to DuMont for assembly into standard photomultiplier tubes.

The completed tubes were tested in the thermal beam of the CP-5 reactor. A pulse-height distribution of the observed signals due to the B^{10} (n, α) reaction is shown in Fig. 72(a). The pulses from Co^{60} gamma rays falling upon a 1/4-in. anthracene crystal attached to the tube face for the experiment are shown for comparison.

A second set of tubes was assembled with covers neutron-sensitized through a series of three coatings evaporated onto the inner surface in the succession: aluminum, natural uranium, aluminum. It was estimated that a total of 1 mg of uranium was evaporated on each cover, and that the thickness of the final aluminum coating was of the order of 0.1 mg/cm^2.

The pulse-height distribution of the fission signals is shown and compared with noise and gamma-ray pulses in Fig. 72(b).

Figure 73 shows two covers prior to shipment and two completed tubes.

DECLASSIFIED

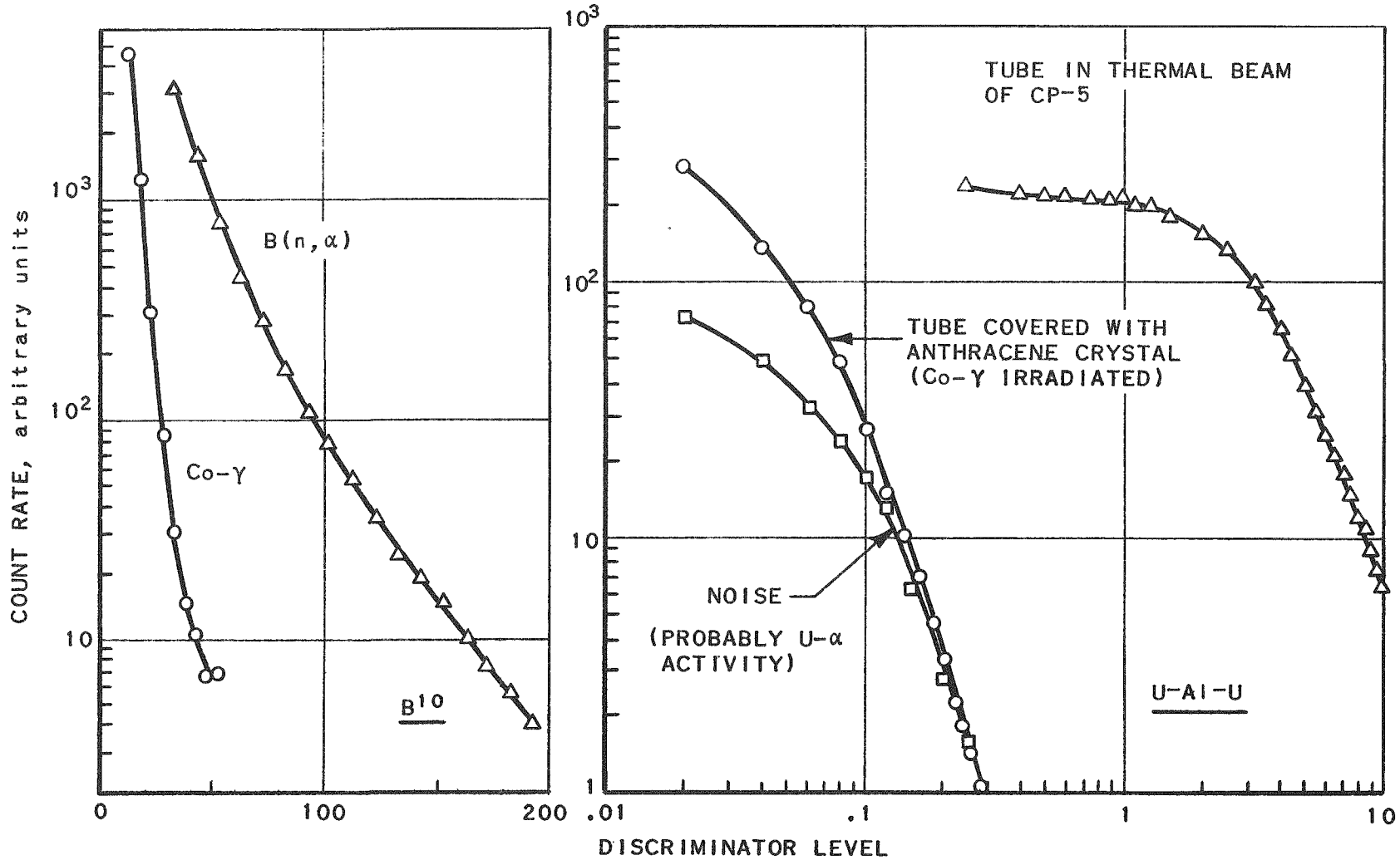

FIG. 72
PULSE HEIGHT DISTRIBUTION IN B^{10} AND IN U-Al-U SENSITIZED PHOTOMULTIPLIER TUBES

RE-7-16868-A

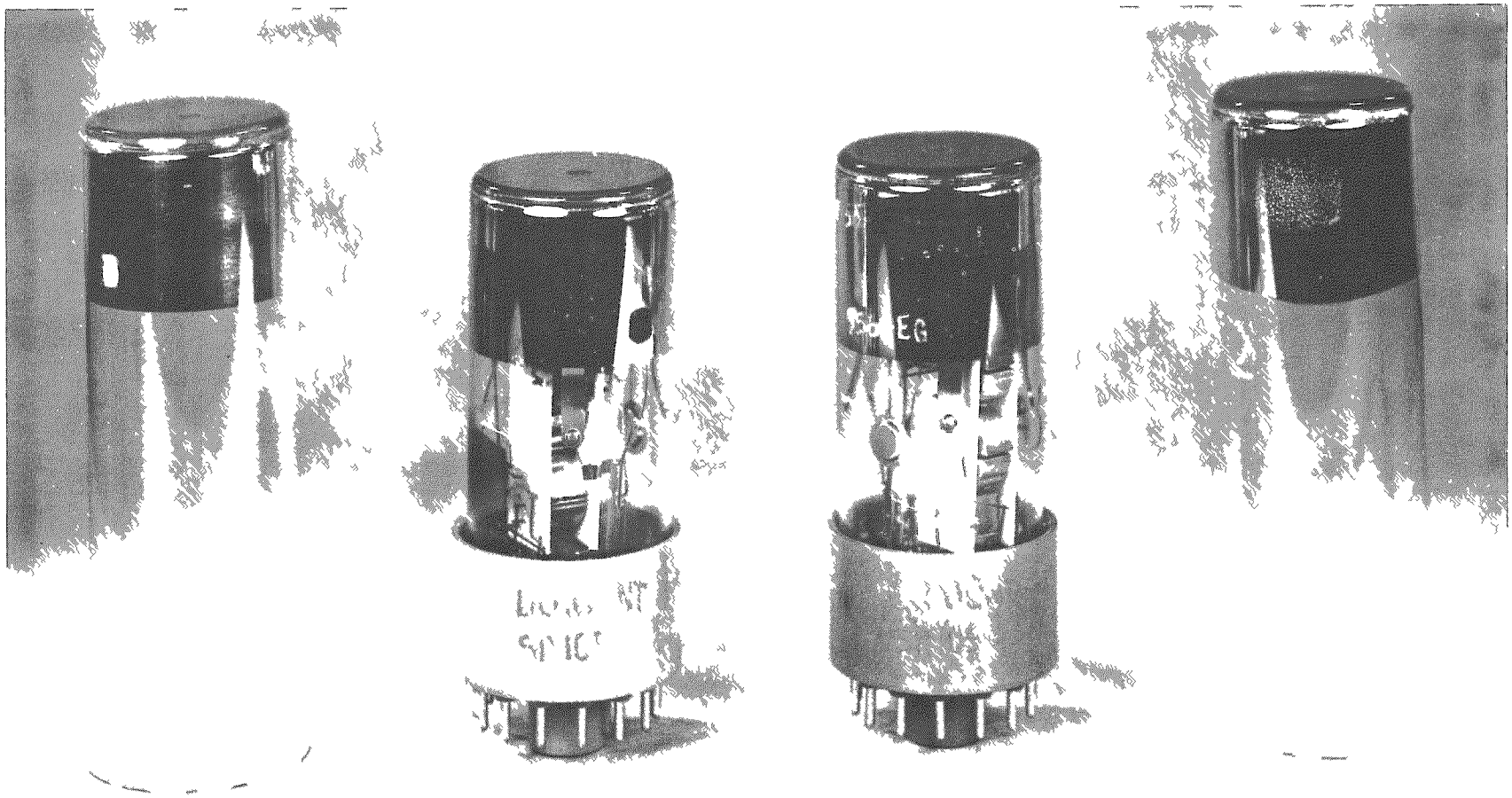

Al-U-Al COATED

B^{10} - Al COATED

FIG. 73
NEUTRON-SENSITIVE ELECTRON PHOTOMULTIPLIER
TUBE COVERS AND ASSEMBLIES

DECLASSIFIED